A GEOCHEMICAL STUDY OF A LAYERED PORTION OF THE HOROMAN PERIDOTITE, SOUTHERN HOKKAIDO, JAPAN

Vol 1

by

Alan Edward Leinbach

B.S., Beloit College
(1982)

SUBMITTED TO THE DEPARTMENT OF
EARTH, ATMOSPHERIC, AND PLANETARY SCIENCES
IN PARTIAL FULFILLMENT
OF THE REQUIREMENTS
FOR THE DEGREE OF

MASTER OF SCIENCE

at the

MASSACHUSETTS INSTITUTE OF TECHNOLOGY

April 1987

Signature of Author _____
Department of Earth and Planetary Sciences
April, 1987

Certified by _____
Fred Frey
Thesis Supervisor

Accepted By _____
W.F. Brace, Department Chairman

Abstract

The Horoman peridotite in southern Hokkaido, Japan is an alpine peridotite providing direct, spatial information about melting processes in the upper mantle. It is conspicuously layered on several scales, and the layering is believed to be produced by processes of partial melting and melt segregation in the upper mantle. A complete geochemical study, consisting of bulk rock major and trace elements, major elements in minerals, and in situ analysis of REE and other trace elements in clinopyroxene by ion microprobe, was performed on a suite of rocks from a layered sequence at Horoman (~300 m thick), with stratigraphic control. The layers are manifested by variations of, modal composition (from plagioclase lherzolite to harzburgite), bulk rock chemistry, and mineral chemistry. These variations are gradual and considerable with modal clinopyroxene varying from 2 to 10%, modal plagioclase from 0 to 10%, bulk MgO from 37 to 45%, bulk Al_2O_3 0.8 to 4.1%, bulk CaO 0.6 to 3.6%, and incompatible element abundances (Sr, Y and REE) by factors of 10 to 20. The variation in chemistry produces wavy patterns with stratigraphy throughout the entire peridotite body and this thesis is a detailed geochemical study of just one of these waves. Linear trends are observed in melt sensitive variation diagrams of bulk rock chemistry for all elements studied. Major element and compatible trace elements are consistent with formation of residual peridotites by various degrees (1 to 25%) of partial melting of a primitive, homogeneous upper mantle composition. However, data for incompatible trace elements are not consistent with this interpretation.

A model of varying degrees of trapped melt from a few percent for the harzburgites to up to 12 to 15% for one sample is allowed by the incompatible element data and does not greatly effect the overall conclusion of a series of residues produced by varying degrees of partial melting. The presence of plagioclase, textural evidence and partitioning evidence of trace elements between clinopyroxene and plagioclase lends support to the idea of trapped melt and suggests that much of the plagioclase is not a primary mantle phase but is produced secondarily from interaction of melt and residual peridotite. However, other melting models were used to try and reproduce the bulk rock REE data. These models show that some sort of disequilibrium melting process may be necessary to explain all of the data and that mantle metasomatic processes cannot be ruled out. Comparison of the Horoman data to other alpine peridotites, and in particular the Ronda peridotite, suggests that the processes operating on a fairly small scale at Horoman and apparently repeated, (owing to the oscillatory, wavy chemical variation observed through the entire massif stratigraphy) may be widespread throughout the upper mantle.

Very complex behavior of trace elements and particularly REE in clinopyroxene was observed. REE patterns for clinopyroxenes tend to mimic the whole rock pattern suggesting that processes affecting the whole rock patterns are doing so by altering the clinopyroxene chemistry. These data are obscured by sub-solidus reequilibration and repartitioning of trace elements, but still provide an opportunity to understand the underlying melting and melt segregation processes in greater detail.

Acknowledgments

A great deal of other peoples' time, advice and concern have gone into this thesis to whom I owe my gratitude. Foremost, is Fred Frey, my advisor, who helped considerably throughout it all. His scientific insight, guidance and patience were invaluable to me. Masaaki Obata deserves some special thanks. He did all the necessary footwork for the project from Japan, as well as providing the rock samples, some preliminary geochemical data and basic working hypotheses.

Many other people have been very helpful, but in particular I would like to thank, in no particular order, those mentioned below. Song Yan has been my analytical cohort, scientific confidente, and office-mate for the 3+ years at MIT. Don Hickmott provided all the expertise for and collected most of the ion probe clinopyroxene data, as well as providing help to reduce the data and general computer help. Nobu Shimizu was greatly appreciated for allowing use of the ion probe and for discussions about the results. Michael Baker helped considerably through a number of discussions and by providing programs and computer guidance. Virginia Mills gave much of her valuable time protecting me from the MIT Bursars and Degree offices and kept me in touch with the MIT machine while out of the country. Tim Grove's advice was helpful on several occasions as was Steve Recca's help with the electron microprobe. Ila P. provided a great deal of help with the

neutron activation lab and with reducing the INAA and RNAA data, while Rosemary Hickey taught Song Yan and myself the RNAA procedure. I must thank those who provided the XRF facilities, J. M. Rhodes and Joel Sparks at UMASS and J. Dostal at St. Mary's University, Halifax. Tom Juster was a great help with computer programming and with compiling the thesis while I was out of the country. Barry Parsons was very gracious in providing the necessities for finishing the thesis while at Oxford University. Many of the people mentioned above I am indebted to also for their friendship, support and good humor. To many others (Allen Kenedy, Tanya Furman, Ro Kinzler, Dan Tormey, Jim Knapp, Vincent Salters and other denizens of the Green Building) I owe much gratitude for their friendship and help. A special note of thanks goes to Beth Robinson for whom I am forever indebted for her immeasurable aid and support (not to mention considerable logistical help).

Table of Contents

List of Figures

List of Tables

List of Plates

Introduction

Knowledge of the geochemistry of the mantle has largely been gathered by study of basaltic magmas erupted at the surface of the earth. This work has shown conclusively that basalts are principally derived by the process of partial melting of the mantle. It is generally believed that these mantle melts are erupted after melt is generated within a larger volume of mantle and segregated into a smaller volume. Understanding of the actual physical processes of melting and segregation in the mantle are very difficult to extract from geochemical study of basalts. The basalts are in a sense the "smoothed" result of these processes. Furthermore, it is known that other processes exist prior to eruption (e.g. fractional crystallization) to complicate matters.

The most direct way to study the geochemistry of the upper mantle is to sample mantle exposed on the surface. Although not nearly as pervasive as basalts, several locations exist for direct mantle investigation. Locations of ultramafic xenoliths in alkalic basalt or kimberlite exist in a variety of tectonic settings around the world. Detailed petrologic and geochemical studies have shown that xenoliths generally have complex petrogeneses. Interpretations of the complicated chemical data, particularly in terms of physical processes, are made more

difficult by their small size and the fact that original spatial relations between inclusions is generally unknown. Ultramafic rocks presumably from the upper mantle are also collected from the sea floor but they are generally dredged with little geologic information to support the sampling, highly altered and difficult to sample.

Alpine peridotites are large exposures of upper mantle ultramafic rocks brought to the surface by tectonic processes. This allows sampling and analysis ranging from a mineral scale (mm) to that of several kilometers, possibly with original spatial relations still intact. The processes of melting and segregation are not well understood in the mantle. Theoretical models have been proposed in recent years for these physical processes (e.g. Maaloe,1981; Maaloe and Schie, 1982; McKenzie, 1985; Turcotte and Ahern, 1978; and Richter and McKenzie,1984) that should not exist in a geochemical vacuum. Detailed study of alpine peridotites can help to describe and quantify mantle variations in space and perhaps elucidate something about physical processes.

A distinctly compositionally layered ultramafic massif at Horoman in southern Hokkaido, Japan is the subject of this study. Bulk rock major and trace element abundance data, as well as some mineral chemical data, were collected with the objective of determining upper mantle composition variability at this location and to gain some understanding of physical processes relating to melting of the mantle. One considerable drawback to studying ultramafic rocks is

the analytic problem of obtaining good trace element data on such depleted rocks. The accuracy of analytic methods and the data produced has been seriously considered in this work (see Appendices).

This work was largely inspired by Masaaki Obata who has worked at Horoman for several years, is currently working there, and who provided the samples and a general petrologic and geologic framework to work in. Similar geochemical work on the Ronda peridotite by people at M.I.T. (Suen, 1978; Obata, 1977 and 1980; Stockman, 1982; and Frey et al, 1985) was also heavily drawn upon for inspiration and guidance.

Regional Geology and Tectonic Setting

Some understanding of the general geologic and tectonic setting is requisite when attempting to use geochemical data to interpret the petrogenesis of a particular rock body and relationships between samples in that body. The geology surrounding the Horoman massif is very complex and several tectonic interpretations have been made in the last decade (e.g. Niida, 1984; Komatsu et al, 1983; Kimura et al, 1983). Hokkaido is a classic region in which collision orogenesis and accretion tectonics are believed to be dominant. The geodynamics of these processes will best be understood from detailed study of the key region of south-central Hokkaido of which Horoman is a part. Not only is it important to keep in mind the geology and tectonics when doing geochemistry but the reverse may be true--geochemical

research may aid the understanding of the tectonic processes.

Hokkaido is generally divided into several N-S trending tectonic provinces or belts. These provinces consist primarily of a pile of tectonic sheets with westward vergence. (The exact delineation, names, and number of these belts varies slightly between authors.) Six tectonic divisions are shown in Figure 1. Descriptions of the belts' generalized geology from west to east follow.

1) Oshima Belt- This region consists primarily of early Mesozoic sediments overlain by Miocene to Quaternary sediments which are predominantly pyroclastics (Okada, 1983). This region is generally considered to be the N extension of NE Honshu geology.

2) Ishikari Belt- This zone of thick, late Mesozoic and Tertiary detrital sedimentary rocks, is believed to correspond to a subsiding basin with sediment supplied from both the west and the east (Cadet and Chavet, 1983).

3)Kamuikotan Belt- A complex region with a variety of rock types all of ophiolitic affinity from late Triassic to early Cretaceous in age. It's characterized chiefly by high-P and -T metamorphic rocks derived from basalts and associated oceanic sediments (Okada, 1983; Cadet and Chavet, 1983).

4) Hidaka Belt- This belt is made up of two subzones, the Western Zone and the Main Zone. The Western Zone ,or Western melange Zone (Komatsu et al, 1983), consists primarily of early Mesozoic rocks similar to parts of the Kamuikotan Belt ophiolite assemblage. The bulk of the Main Zone is made up of a several kilometer thick sequence, largely Jurassic in age, of volcanic rich greywackes, sandstones and schists (Cadet and Chavet, 1983; Okada, 1983). Also in the Main Zone is a group of metamorphic rocks, including the Horoman massif, called the Hidaka Metamorphic Belt. This belt will be described in more detail below.

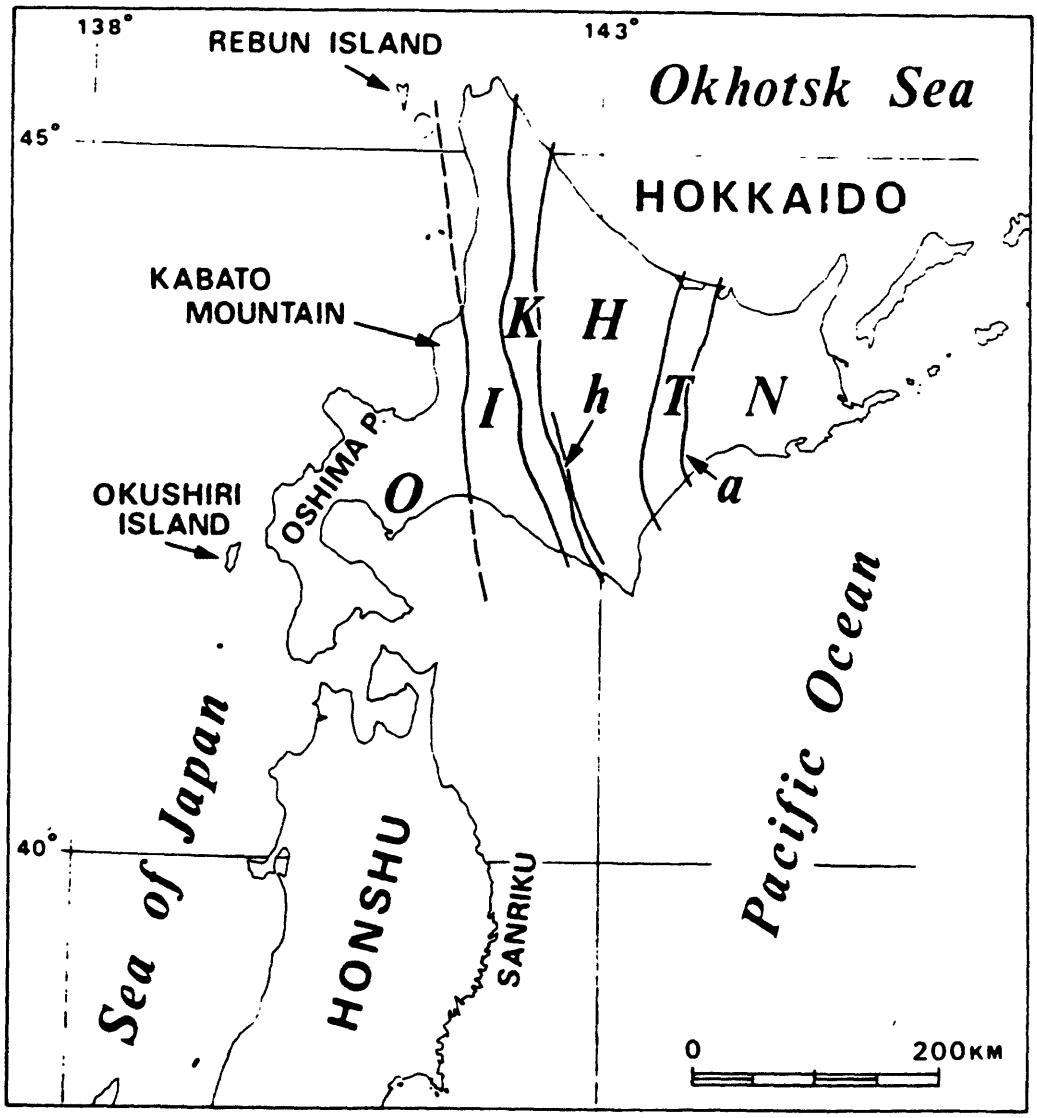

Figure 1. Map of Hokkaido, Japan showing tectonic divisions. O: Oshima Belt; I: Ishikari Belt; K: Kamuikotan Belt; H: Hidaka Belt (h: Hidaka Western melange zone); T: Tokoro Belt; N: Nemuro Belt; a: Abashiri Tectonic Line (tectonic suture) (from Okada, 1983, p. 92).

5) Tokoro Belt- The contact with the Hidaka Belt is hidden by relatively recent volcanism. The bulk of the belt consists of Upper Jurassic sediments of oceanic affinity but a detrital series rich in calc-alkaline debris supplied from the east also exists (Cadet and Chavet, 1983).

6) Nemuro Belt- A tectonic suture line separates this belt from the Tokoro Belt (Kimura, 1981). A sequence of late Cretaceous to early Miocene basalt and andesite lavas, tuffs, cherts, and flysch make up the majority of this belt. These rocks are unconformably overlain by Quaternary east derived volcanics (Okada, 1983; Cadet and Chavet,1983).

The Hidaka Metamorphic Belt (HMB) is a key geologic region of Tertiary rocks in south-central Hokkaido (Fig's. 2 and 3). The HMB is divided into two zones, the Western Zone and the Main Zone. The Western Zone is a meta-ophiolite faulted into slices and overturned. The Main Zone is a varied crustal section of continental or island arc crust. The two zones are separated by a thick mylonite zone from a major thrust fault, the Hidaka main thrust superimposing continental or island arc crust atop oceanic crust of the W Zone (Komatsu et al., 1983; Kimura et al, 1983; Niida, 1984). Seven major "alpine-type" peridotite bodies are exposed along the fault zone (Fig. 3). Each of these peridotites have lherzolite series with conspicuous layering, (particularly the Horoman massif and a peridotite ~100 kilometers to the NW along the Wensaru (or Uenzaru) River (Komatsu, 1975)) while at four locations harzburgite series of ultramafic tectonites exist as well. All the ultramafic bodies appear to be tectonically emplaced

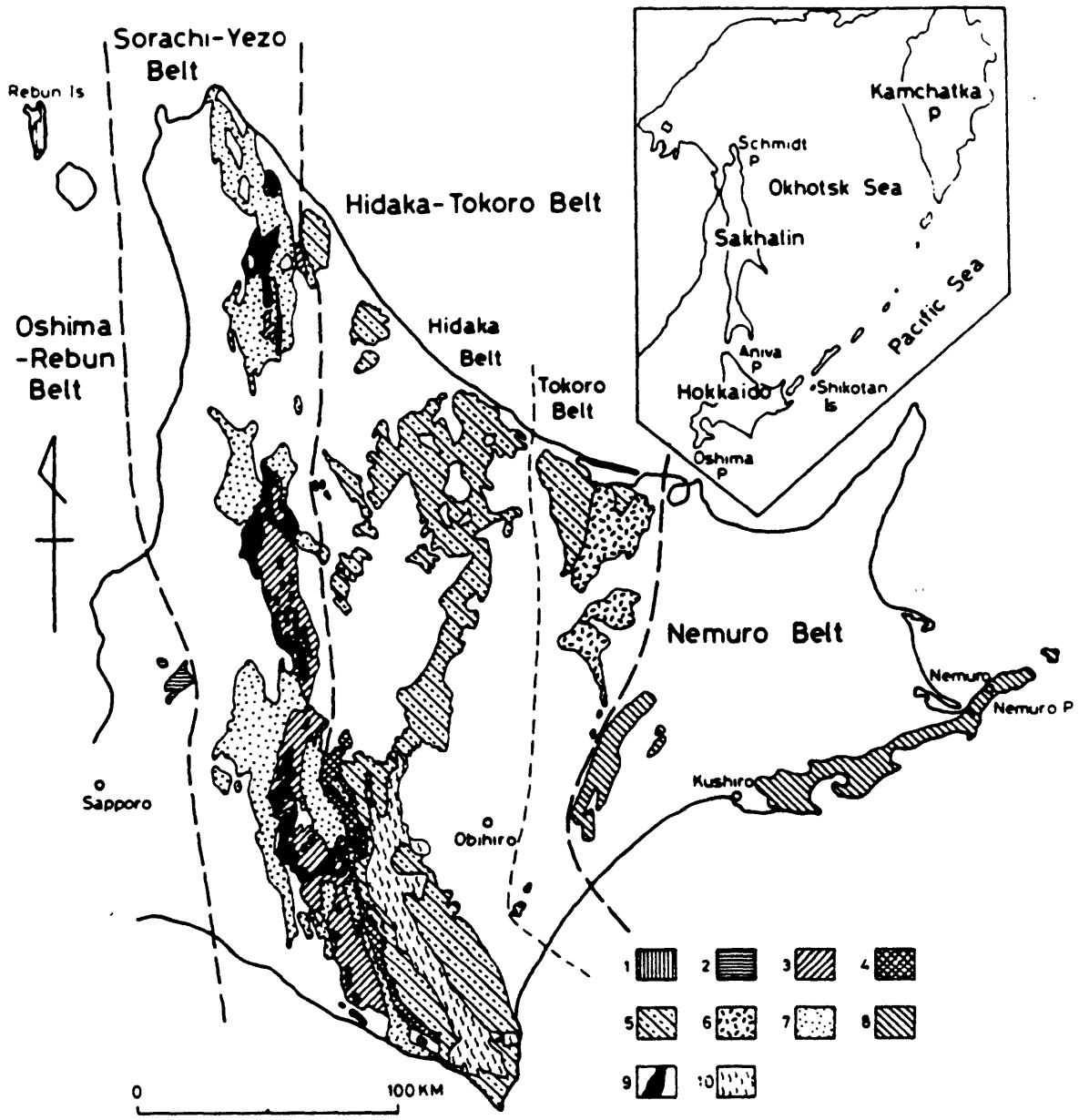

Figure 2. Location map of Hokkaido, Japan (inset) and map showing the distribution of Mesozoic rocks, location of Hidaka metamorphic rocks (Tertiary), and some tectonic divisions. 1: Rebun Group; 2: Kumaneshiri Group; 3: Sorachi Group and Kamuikotan metamorphic rocks; 4-6: Hidaka Supergroup; 7: Yezo Group; 8: Nemuro Group; 9: serpentinites; 10: Hidaka metamorphic rocks (from Kiminami and Kontani, 1983, p. 108).

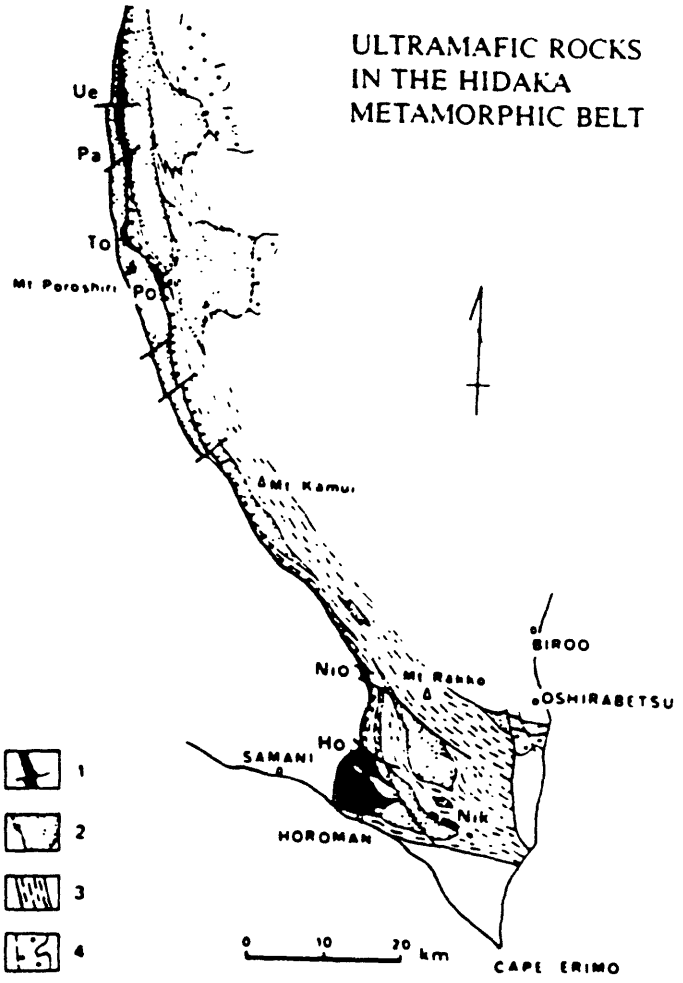

Figure 3. Map showing distribution of ultramafic rocks in the Hidaka Metamorphic Belt. 1: ultramafic rocks; 2: mafic rocks (meta-ophiolite and gabbros); 3: metamorphic rocks (pyx-gneiss, biotite-gneiss and migmatite); 4: granitic rocks. Ue: Uenzaru; Pa: Pankenushi; To: Tottabetsu; Po: Poroshiri; Nio: Niobetsu; Ho: Horoman; Nik: Nikanbetsu (from Niida, 1984, p. 199).

(Hashimoto, 1975) and there is no evidence of contact metamorphism around any of them (Niida, 1984).

Metamorphism and magmatism in the Main Zone are dated from 40-17 m.a.. Minor NW trending thrusts occur and are believed to have been active simultaneously with the metamorphism and magmatism. The Hidaka main thrust in this period (late Eocene to early Miocene) produced dextral strike-slip movement converting to westward thrusting in latest Miocene to Pliocene uplifting the HMB (Kimura et al, 1983; Komatsu et al., 1983).

There are several competing tectonic interpretations for Hokkaido but most agree that the geology is best explained by multiple collisions (Okada, 1983; Kimura et al, 1983; Cadet and Chavet, 1983; Komatsu et al., 1983; and Kiminami and Kontani, 1983). Two fossil subduction zones exist in central Hokkaido: the late Jurassic-early Cretaceous Kamuikotan Belt and the late Triassic-late Jurassic Hidaka Western melange Zone. Volcanic rocks exist in the Oshima Belt interpreted to be the volcanic arc associated with the Kamuikotan trench with west-dipping subduction (Komatsu et al., 1983). This arc corresponds to the northern extension of arc volcanism in NE Honshu. The dip direction of subduction is controversial. The Hidaka subduction zone may have been east-dipping and Kamuikotan west-dipping (Kiminami and Kontani, 1983; Komatsu et al., 1983; Cadet and Chavet, 1983). All subduction may be west-dipping (Dickinson, 1978; Okada, 1980), or both

paleosubduction zones were east-dipping (Miyashiro, 1977). Kiminami and Kontani (1983) even suggest that a third subduction zone existed. Also, two actual suture zones exist: one between the Kamuikotan and Hidaka Belts, believed to represent Oligocene to middle Miocene collision (Okada, 1979, 1980, 1983); and the other between the Tokoro Belt and the Nemuro Belt representing latest Miocene collision. The Kamuikotan subduction/obduction complex and part of the Hidaka complex appear to have been overthrust onto western Hokkaido from convergence of the two arcs and ensuing collision (Komatsu et al., 1983). In central Hokkaido westward vergence of overturned folds and thrust faults active in the Tertiary and Tertiary magmatism and metamorphism suggest east-dipping subduction but the Hidaka Western melange Zone is dated no more recently than late Jurassic. Therefore the Tertiary geologic features must be collision related (Kimura et al, 1983). This later collision, believed to have occurred in latest Miocene, was west-directed between the Kurile arc and south-central Hokkaido. The collision appears to be due to a westward shifting of the Kurile arc from more oblique subduction of the Pacific plate, as evidenced by the change in fault style of the Hidaka main thrust (Kimura et al, 1983). Central Hokkaido seems to be best explained by the superposition of two collisions.

Local Geology

The Horoman massif is situated near the extreme southern tip of the HMB (Fig. 4). A number of Japanese scientists have worked in this region since the early 1900's. For references to previous work the interested reader is referred to two of the few papers published in English (Niida, 1974, 1984). (It is from these two references that much of the following descriptive geology of the Horoman peridotite is taken, as the author has not been to the location.) The massif is approximately eight by ten kilometers and is greater than 3000 meters thick. It is conspicuously layered on several scales and consists of dunite, harzburgite, lherzolite, plagioclase lherzolite, and small amounts of gabbro and pyroxenite. Horoman is bounded to the west by the Hidaka main thrust which occurs in low-grade metamorphic rocks. The eastern margin is irregular from NW-SE trending faults and shear zones. Sometimes banded gneiss and amphibolite are faulted with the ultramafic rocks (Fig. 5). The peridotite is relatively fresh with high degrees of serpentinization occurring predominantly along margins and shear zones.

Structure

From the foliation in the ultramafic rocks Niida (1974) was able to structurally map the massif. He recognized a half dome structure in the southern half opening to the south and an almost monoclinal northern half with E-W strike and moderate dip to the south. The layering sequences can

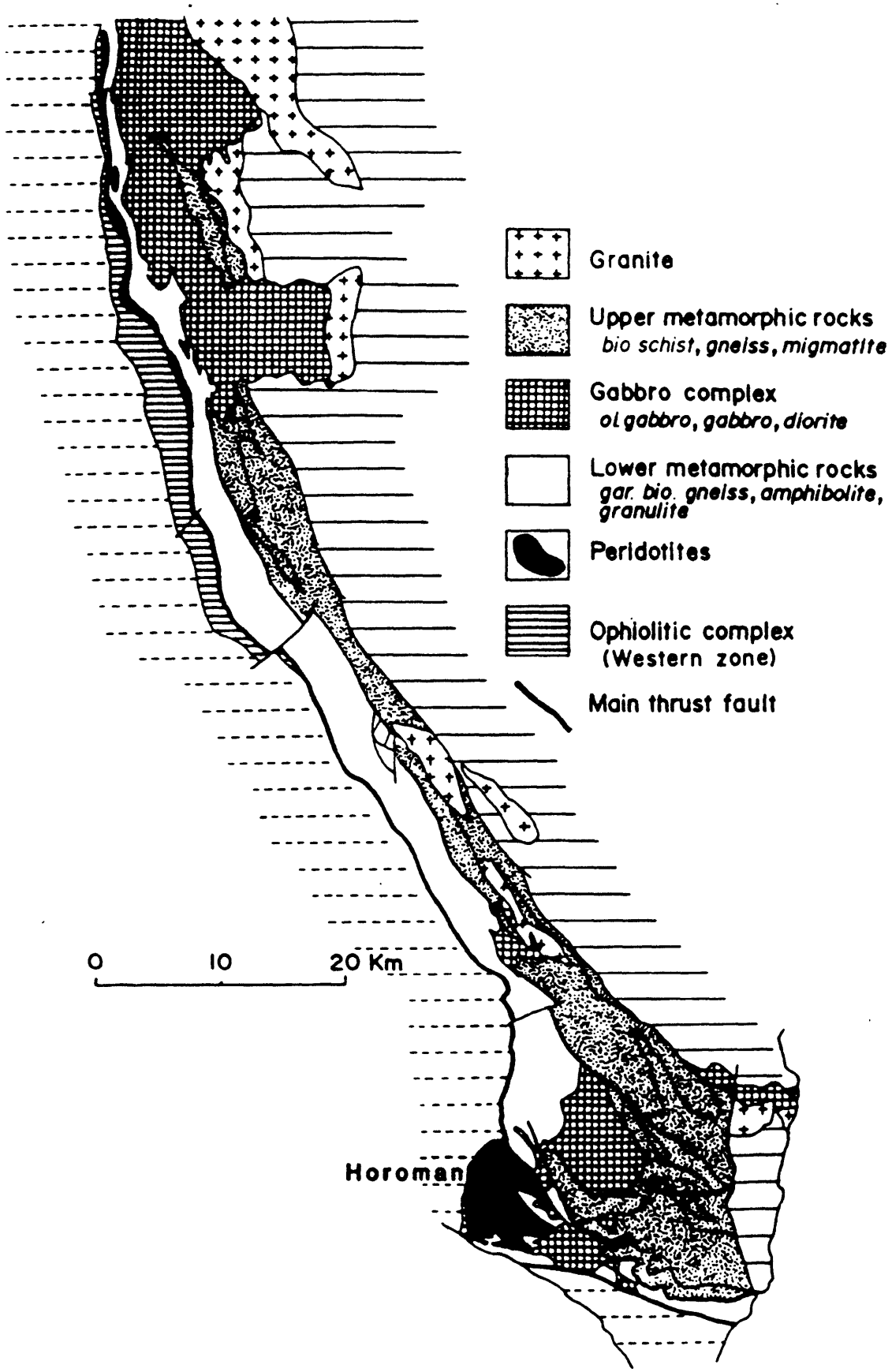

Figure 4. Simplified geologic map of the Hidaka Metamorphic Belt showing Horoman peridotite (from Komatsu et al, 1983, p. 154).

Figure 5. Simplified geologic map of the Horoman region, with location map and cross section. Dunite horizons A to E are also shown in Fig. 7 (from Obata and Nagahara, 1987, Fig. 1).

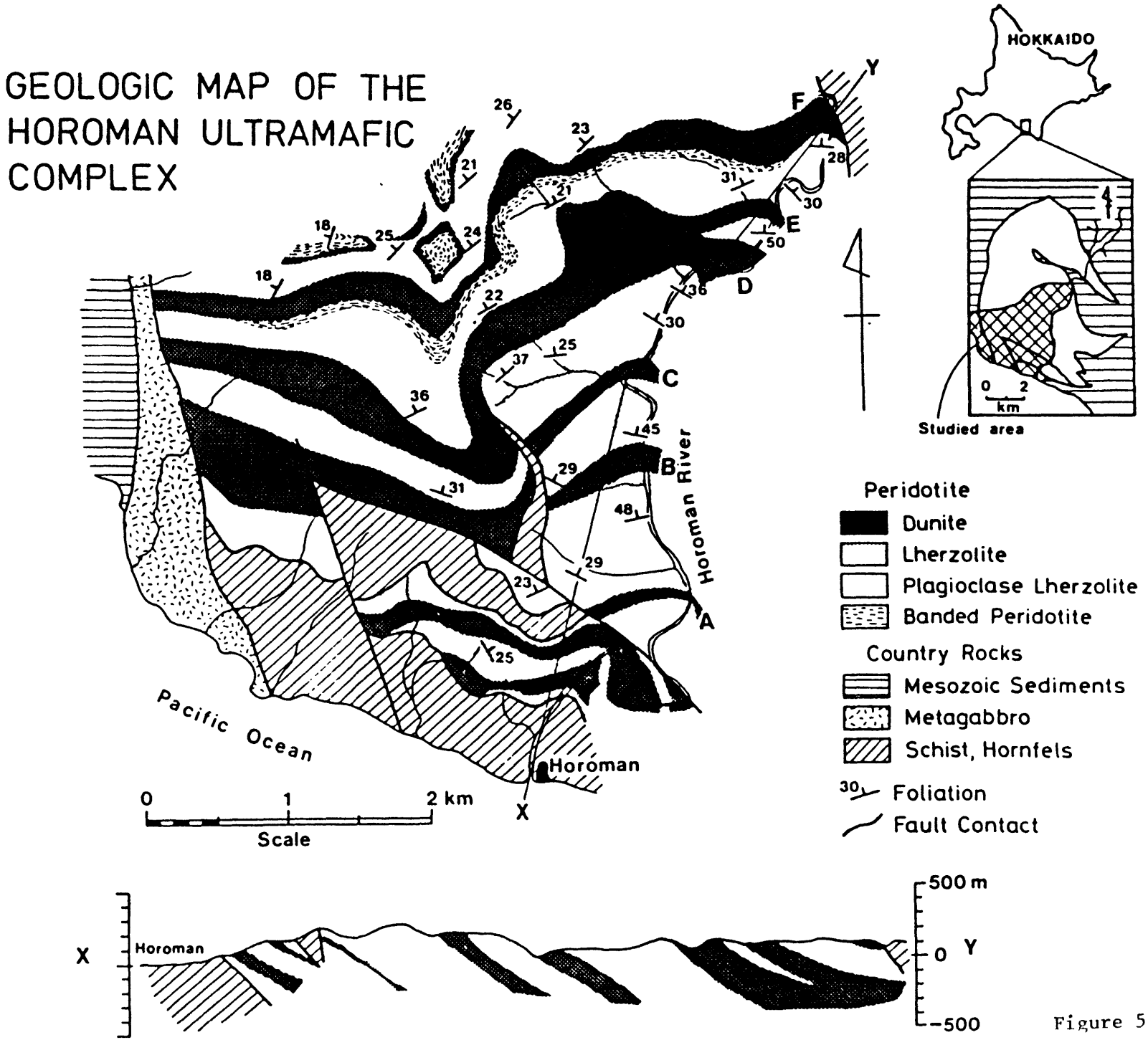
GEOLOGIC MAP OF THE HOROMAN ULTRAMAFIC COMPLEX
HOKKAIDO
Studied area
0 2 km
Peridotite
Dunite
Lherzolite
Plagioclase Lherzolite
Banded Peridotite
Country Rocks
Mesozoic Sediments
Metagabbro
Schist, Hornfels
Foliation
Fault Contact
Horoman River
Pacific Ocean
Horoman
Scale
0 1 2 km
A
B
C
D
E
F
X
Y
500 m
0
-500

Figure 5

be correlated across several sections and lineations show a constant trend. In general the massif takes the form of a warped sheet and probably was emplaced along a deep-seated thrust zone (NW-SE trending). During the last stages the sheet was thrust slightly up to the SW producing structure seen today (Niida, 1974).

Layering

The distinct compositional layering can be seen in the stratigraphic column from Niida (1984) (Fig. 6). There are two types of layering at Horoman.

> 1) Upper part- Well developed compositional layers exist from a few centimeters to several meters thick with distinct contacts between layers. The layers consist primarily of plagioclase lherzolite and dunite with some gabbro and pyroxenite layers. No pattern in the layering is apparent but a general association can be recognized between thicker and more gabbro layers with the thickest dunite layers.
>
> 2) Lower part- This portion is dominated by massive layers generally several hundred meters thick. The contacts are gradational over several meters. Regularity in the layers is well developed, generally with lherzolite between plagioclase lherzolite and dunite. The sequence dunite-lherzolite-plagioclase lherzolite-lherzolite is repeated four times in the Horoman River section (Fig. 6). Thin layers or seams of one or more minerals appear in all thick compositional layers. These thin layers consist of fine-grained monomineralic olivine, orthopyroxene + spinel, plagioclase + spinel, and occasional pyroxenite layers. Gabbro layers appear infrequently.

Layering in the Horoman massif is clearly different from that in layered intrusions and zoned complexes. No gravity stratification or density gradation of constituent minerals is seen as is common in layered intrusions. The layers are greater than 95 percent ultramafic at Horoman

Figure 6. Stratigraphic sections of Horoman peridotite showing rock sequences at several localities. 1: Oomagari-no-sawa in the northern part of the massif; 2: Western ridge of the Apoi-dake; 3: Furukawa-no-sawa in the western part of the Horoman River; 4: Horoman River section, the main part of the massif; 5: Taki-no-sawa in the eastern part of the Horoman River; 6: Kage-no-sawa in the eastern part of the Horoman River (from Niida, 1984, p. 206).

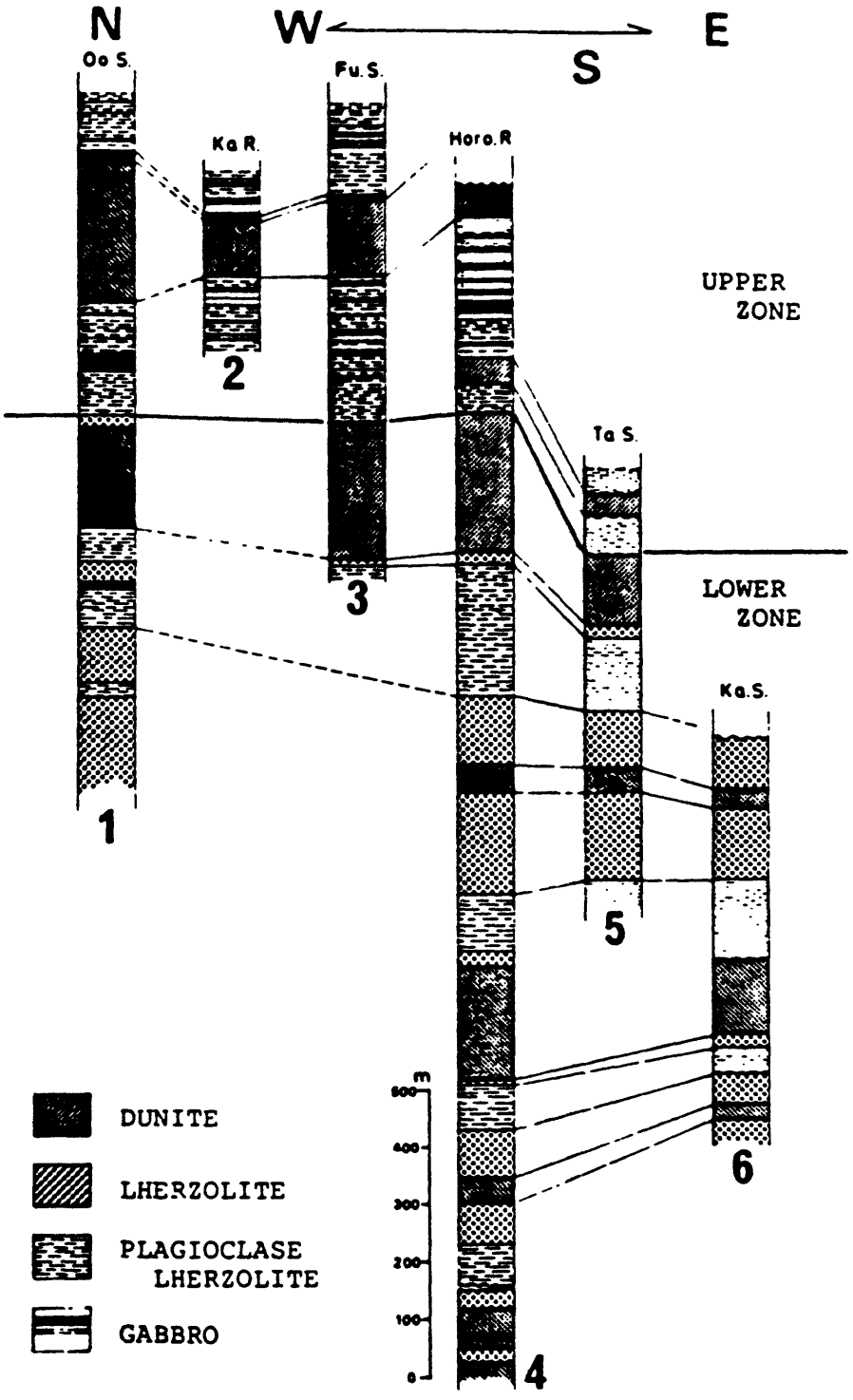
N
W
E
S
Oo S.
Fu.S.
Ka R.
Horo.R
UPPER ZONE
Ta S.
LOWER ZONE
Ka.S.
1
2
3
4
5
6
m
600
400
300
200
100
0
DUNITE
LHERZOLITE
PLAGIOCLASE LHERZOLITE
GABBRO

Figure 6

compared to predominantly mafic in the layered intrusions. Fractional crystallization from a basaltic melt should produce gabbros to ultramafics in 10:1 ratio. However, erosion may reduce this value (e.g. Stillwater, 4:1; Bushveld 6:1) (Dick, 1977). Also, no "rhythmic" layering is found at Horoman as originally described by Wager and Deer (1939) at Skaergaard. The layering at Horoman may be similar to that seen at Lizard (Green, 1964). There are also no igneous textures in the ultramafic rocks of Horoman. This is in marked contrast to layered complexes such as Skaergaard and Stillwater that have cumulate textures of olivine, pyroxene and plagioclase.

Petrologic Framework

The Horoman massif has been studied recently by Obata and Nagahara (1987). From major element chemistry of the ultramafics they recognized patterns in the chemical variation (see Niida, 1984 as well) that could best be explained by a model of partial melting and melt migration. Figure 7 shows how the chemistry varies with respect to stratigraphy in a portion of the Horoman River section remapped by Obata and Nagahara. The rock types in the figure are: dunite, which consists of 90-95 percent olivine, up to 10 percent orthopyroxene and less than a few percent of clinopyroxene and Cr-spinel; lherzolite, which contains more clino- and orthopyroxene but with less than 90 percent olivine; and plagioclase lherzolite, which is defined by the occurrence of plagioclase in the lherzolite assemblage, usually less

Figure 7. Portion of Horoman River stratigraphic section of Horoman peridotite, with dunite horizons labelled as in Fig. 5, showing sub-section of this study, and wavy, repeated pattern of compositional layering, expressed in terms of CaO, Al_2O_3, and olivine forsterite content (from Obata and Nagahara, 1987, Fig. 3). Rock names defined as in text, not IUGS classification.

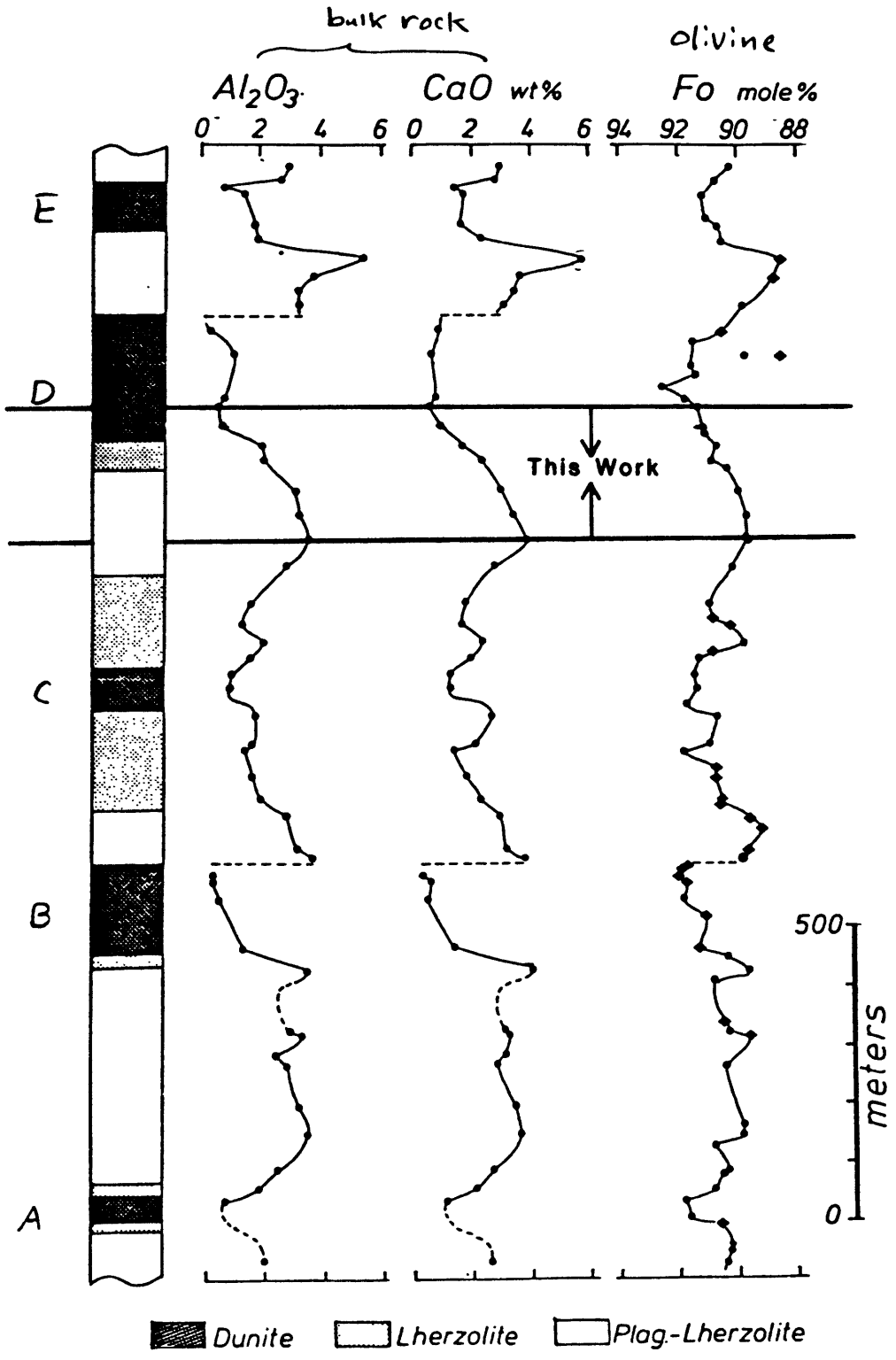
bulk rock
olivine
Al_2O_3
CaO wt%
Fo mole%
0 2 4 6
0 2 4 6
94 92 90 88
E
D
C
B
A
This Work
500
meters
0
Dunite
Lherzolite
Plag.-Lherzolite

Figure 7

than 15 percent (Obata and Nagahara, 1987). For this work the IUGS term harzburgite will be used for an ultramafic rock with less than 90 percent olivine, less than five percent clinopyroxene and greater than five percent orthopyroxene.

Sampling and Petrography

The samples for this study were received from Obata from a portion of the Horoman River section (Fig. 7). The seven samples selected are from the largest and most distinct "wave" of chemical variation. The variations correspond to changes in rock type. The samples are porphyroclastic to granular in texture. Point count analyses of petrographic thin sections were made both by the author and by Obata for several of the same samples. These modal analyses were deemed to be poor due to pervasive disequilibrium texture, inhomogeneous grain size distribution, nonuniform macroscopic mineral layers, and misidentification of very fine-grained mineral aggregates. Table 1 shows the results of a rather painstaking least squares linear regression using electron microprobe analyses of constituent minerals and XRF whole rock analyses (Appen. II). From this reconstituted mode the seven samples include four plagioclase lherzolites, one plagioclase harzburgite and two harzburgites. All samples have less than one percent spinel. Plagioclase always occurs in fine-grained seams usually associated with spinel and olivine.

Table 1: Modes of Horoman Peridotites in Volume Percent, From Linear Regression of Major Elements

	Olivine	opx	cpx	spinel	plag
62210	57.8±0.6	21.6±0.7	10.2±0.2	0.55±.06	9.8±0.3
62212	57.6±0.6	23.6±0.7	8.8±0.2	0.57±.05	9.4±0.3
62213	61.1±2.2	22.5±2.7	7.9±0.9	0.6±0.2	8.0±1.0
62131	68.5±0.5	20.9±0.7	6.5±0.2	0.47±.04	3.7±0.2
62130	70.7±0.8	21.3±1.0	3.9±0.3	0.34±.06	3.8±0.3
62128	73.3±0.6	22.9±0.8	2.9±0.3	0.89±.06	-
62127	77.9±1.9	19.6±0.9	1.9±0.3	0.64±.06	-

Analytical Techniques

For bulk chemical analyses 150 to 200 grams of rock were powdered to insure homogeneous sampling of these coarse-grained rocks. An agate shatterbox was used for powdering to minimize contamination. Major element compositions were determined using X-ray fluorescence at the University of Massachusetts laboratory of J. M. Rhodes. A split was also analyzed by J. Dostal at St. Mary's University, Halifax, Nova Scotia. A separately prepared set of the same samples was analyzed by Obata at Toyama University, Toyama, Japan. The UMASS data is used in this work except for volatiles which were measured at St. Mary's by the loss on ignition technique. Na_2O was analyzed by both XRF and instrumental neutron activation (INAA). The INAA data is used in this study and was collected in F. A. Frey's laboratory at MIT. XRF was also used to analyze for the trace elements Cr, Ni, V, Zn, Sr, Zr, Ga, and Y (only at the UMASS laboratory). INAA was used for the trace elements Cr, Co, Sc and Hf. Neutron activation Cr data is used in this work rather than XRF data. REE data were determined by radiochemical neutron activation analysis (RNAA) using the general procedure outlined by Hickey and Frey (1981). This technique was refined and duplicate analyses were made to estimate precision. REE were also determined using standard INAA with much poorer accuracy as a check to RNAA data. Mineral analyses were obtained with the MIT JEOL 733 electron microprobe, using the on-line data reduction and

matrix reduction procedure of Bence and Albee (1968) with the modifications of Albee and Ray (1970). REE and other trace elements were analyzed in hand-picked clinopyroxenes at M.I.T. with the Cameca IMS 3f ion microprobe. Special gratitude goes to Don Hickmott who collected almost all of the ion probe data. Specifics of the ion probe procedure are in the section on trace elements in clinopyroxenes. (See appendices for more on major element and REE data.)

Results

Table 2 lists major element data in the order of increasing MgO content and increasing stratigraphic elevation for the seven peridotite samples. In terms of modal mineralogy Table 2 is generally in the order of increasing olivine and decreasing clinopyroxene and plagioclase. The sample with lowest MgO content and highest CaO and Al_2O_3 contents (62210) is similar in major element composition to various estimates of "fertile" upper mantle (see Table 15).

Trace element compositions of the seven samples are given in Tables 3 and 4 in the same sample order as for the major elements. Again, the most fertile sample, 62210, is relatively similar to Jagoutz et al (1979) estimate of trace element abundance in the upper mantle (Table 15).

Tables 5-9 show major element analyses of minerals in the seven samples obtained by the electron microprobe. The analyses shown are most often averages of several high quality microprobe analyses and are the ones used for the modal linear regression. Trace element compositions of

Table 2: Major Element Abundances in Horoman Peridotites (volatile-free)

	62210	62212	62213	62131	62130	62128	62127
SiO_2	44.95	45.15	44.56	44.30	43.65	43.95	43.30
TiO_2	0.15	0.14	0.13	0.071	0.073	0.015	0.012
Al_2O_3	4.14	3.90	3.66	2.19	2.14	1.07	0.76
Cr_2O_3	0.376	0.379	0.384	0.400	0.298	0.477	0.457
FeO*	8.04	8.21	8.20	7.96	8.23	7.82	8.02
MnO	0.145	0.140	0.139	0.132	0.131	0.132	0.132
MgO	37.10	37.55	38.66	41.80	42.45	44.51	45.06
CaO	3.59	3.18	2.81	1.95	1.47	0.80	0.60
Na_2O	0.410	0.362	0.296	0.171	0.139	0.021	0.021
K_2O	0.01	0.004	0.006	0.006	0.006	0.003	-
P_2O_5	0.01	0.01	0.01	0.003	0.006	-	-
NiO	0.251	0.252	0.264	0.291	0.297	0.309	0.317
Total	99.172	99.277	99.119	99.274	98.890	99.107	98.679
Mg#[1]	0.892	0.891	0.894	0.904	0.902	0.910	0.910
CaO/Al_2O_3	0.87	0.82	0.78	0.89	0.68	0.75	0.79
LOI[2]	4.5	-	0.8	0.1	0.2	1.0	0.3

[1]Mg# = Mg/Mg+Fe
[2]Volatiles, from loss on ignition

Table 3: Trace Element Abundances in Horoman Peridotites (ppm on as received basis)

	62210	62212	62213	62131	62130	62128	62127
Sc	15.37	15.53	14.56	10.40	9.31	9.06	8.02
V	63	70	61	45	43	34	29
Cr	2457	2590	2608	2733	2038	3228	3120
Co	98	105	107	111	119	115	120
Ni	1883	1981	2062	2284	2331	2401	2485
Zn	49	56	54	54	57	49	51
Ga	4.4	4.3	4.3	3.2	3.2	2.2	2.3
Sr	15.9	13.4	12.4	5.5	5.0	1.1	1.1
Y	3.6	3.6	3.4	1.6	1.7	0.2	0.2
Zr	6.6	7.5	5.9	2.9	3.5	-	-
Hf	0.15	0.17	0.18	-	0.11	-	-

Table 4: Rare-Earth Element Abundances in Horoman Peridotites (ppm on as received basis)

	62210	62212	62213	62131	62130	62128	62127
La	0.179	0.164	0.204	0.093	0.070	0.036	0.033
Ce	0.51	0.47	0.60	0.29	-	-	-
Nd	0.62	0.57	0.58	-	0.34	-	-
Sm	0.310	0.284	0.269	0.130	0.135	0.012	0.019
Eu	0.133	0.126	0.116	0.061	0.058	0.0076	0.010
Tb	0.099	0.095	0.084	0.041	0.044	-	-
Yb	0.439	0.407	0.392	0.191	0.199	0.027	0.022
Lu	0.074	0.069	0.068	0.034	0.0335	0.0063	0.0052

Table 5: Electron Microprobe Analyses for Olivines From the Horoman Peridotite

Sample	62210	62212	62213	62131	62130	62128	62127
SiO_2	41.19	40.56	41.17	40.76	40.77	41.11	41.10
TiO_2	0.04	0.04	0	0.03	0.07	0	0.06
Al_2O_3	0.05	0.06	0	0	0.03	0	0
Cr_2O_3	0.02	0.02	0.05	0	0.02	0	0
FeO*	10.38	10.52	9.91	9.20	9.78	8.88	8.73
MnO	0.16	0.13	0.17	0.10	0.13	0.02	0.08
MgO	48.98	48.43	49.25	49.10	49.38	49.92	49.82
CaO	0.03	0	0.02	0.03	0	0	0.01
NiO	0.28	0.02	0.05	0	0.34	0.34	0.36
Total	101.13	100.04	100.88	99.54	100.52	100.27	100.16
Numbers of cations on the basis of 4 oxygens							
Si	1.001	0.998	1.001	1.002	0.996	1.001	1.001
Al	0.001	0.002	0.000	0.000	0.001	0.000	0.000
Ti	0.001	0.001	0.000	0.000	0.001	0.000	0.001
Cr	0.000	0.000	0.001	0.000	0.000	0.000	0.000
Fe^{2+}	0.211	0.216	0.202	0.189	0.200	0.181	0.178
Mn	0.003	0.003	0.004	0.002	0.003	0.000	0.002
Mg	1.774	1.776	1.786	1.799	1.797	1.812	1.810
Ca	0.001	0.000	0.001	0.001	0.000	0.000	0.000
Ni	0.009	0.009	0.010	0.010	0.011	0.011	0.011
Total	3.002	3.005	3.003	3.003	3.008	3.004	3.003
Fo content	89.4	89.1	89.9	90.5	90.0	90.9	91.0

Table 6: Electron Microprobe Analyses For Orthopyroxenes From the Horoman Peridotite

Sample	62210	62212	62213	62131	62130	62128[1]	62127
SiO_2	54.99	55.28	54.82	55.31	55.40	56.15	56.64
TiO_2	0.22	0.21	0.16	0.12	0.12	0.07	0.05
Al_2O_3	3.75	3.29	4.41	3.65	3.79	2.54	2.53
Cr_2O_3	0.43	0.42	0.47	0.65	0.55	0.49	0.77
FeO*	6.99	7.01	6.77	6.06	6.30	5.42	5.46
MnO	0.10	0.15	0.15	0.09	0.12	0.17	0.06
MgO	33.12	33.17	33.57	33.67	33.52	33.99	23.86
CaO	0.89	0.73	0.57	0.73	0.78	0.62	0.91
Na_2O	0.03	0.02	0.02	0	0	0	0
Total							
Numbers of cations on the basis of 6 oxygens							
Si	1.899	1.912	1.883	1.906	1.905	1.942	1.944
Al^{IV}	0.101	0.088	0.117	0.094	0.095	0.058	0.056
Al^{VI}	0.052	0.047	0.061	0.054	0.058	0.045	0.046
Ti	0.006	0.005	0.004	0.003	0.003	0.002	0.001
Cr	0.012	0.011	0.013	0.018	0.015	0.013	0.021
Fe^{2+}	0.202	0.203	0.194	0.175	0.181	0.157	0.157
Mn	0.003	0.004	0.004	0.003	0.003	0.005	0.002
Mg	1.705	1.711	1.719	1.729	1.718	1.752	1.733
Ca	0.033	0.027	0.021	0.027	0.029	0.023	0.033
Na	0.002	0.001	0.001	0.000	0.000	0.000	0.000
Total	4.014	4.011	4.017	4.008	4.007	3.997	3.993
$Mg\#$[2]	0.894	0.894	0.898	0.908	0.905	0.918	0.917
Wo	1.7	1.4	1.1	1.4	1.5	1.2	1.7
En	87.9	88.2	88.9	89.6	89.1	90.7	90.1

[1]Analysis by Obata
[2]$Mg\# = Mg/Mg+Fe$

Table 7: Electron Microprobe Analyses for Clinopyroxenes From the Horoman Peridotite

	62210	62212	62213	62131	62130	62128	62127
SiO_2	50.88	50.92	51.17	50.91	50.70	53.14	53.17
TiO_2	0.78	0.89	0.72	0.45	0.73	0.06	0.09
Al_2O_3	5.65	5.32	4.99	5.09	5.27	3.20	2.65
Cr_2O_3	0.92	0.95	1.07	1.53	1.12	1.01	1.07
FeO*	3.08	3.12	3.16	2.68	2.66	2.05	1.93
MnO	0.06	0.06	0.08	0.07	0.08	0.07	0.05
MgO	15.50	15.66	16.19	16.00	15.86	17.11	17.37
CaO	22.54	22.57	21.97	21.79	22.54	23.15	22.54
Na_2O	0.68	0.73	0.69	0.72	0.66	0.36	0.49
Total	100.09	100.22	100.04	99.24	99.62	100.15	99.36
Numbers of cations on the basis of 6 oxygens							
Si	1.855	1.856	1.866	1.868	1.856	1.925	1.938
Al^{IV}	0.145	0.144	0.134	0.132	0.144	0.075	0.062
Al^{VI}	0.098	0.085	0.080	0.088	0.084	0.061	0.052
Ti	0.021	0.024	0.020	0.012	0.020	0.002	0.002
Cr	0.027	0.027	0.031	0.044	0.032	0.029	0.031
Fe^{2+}	0.094	0.095	0.096	0.082	0.081	0.062	0.059
Mn	0.002	0.002	0.002	0.002	0.002	0.002	0.002
Mg	0.843	0.851	0.880	0.875	0.866	0.924	0.944
Ca	0.881	0.881	0.858	0.857	0.884	0.898	0.880
Na	0.048	0.052	0.049	0.051	0.047	0.025	0.035
Total	4.013	4.017	4.016	4.013	4.018	4.003	4.004
$Mg\#^1$	0.900	0.899	0.901	0.914	0.914	0.937	0.941
Wo	48.5	48.2	46.8	47.2	48.3	47.7	46.7
En	46.4	46.6	48.0	48.2	47.3	49.0	50.1

$^1Mg\# = Mg/Mg+Fe$

Table 8: Electron Microprobe Analyses for Spinels From the Horoman Peridotite

	62210[1]	62212	62213	62131	62130	62128	62127
SiO_2	0	0.06	0.05	0.15	0.07	0.20	0.03
TiO_2	0.32	0.34	0.31	0.29	0.36	0.03	0.08
Al_2O_3	40.50	38.55	39.91	37.71	39.64	40.07	32.90
Cr_2O_3	24.04	26.58	25.89	29.27	28.61	29.47	37.08
FeO*	19.77	21.62	19.94	18.40	17.65	16.01	17.32
MnO	0.12	0.23	0.17	0.18	0.17	0.16	0.24
MgO	13.98	14.01	14.59	14.63	14.67	15.55	13.67
CaO	0	0.03	0.04	0.03	0.03	0	0
Total	98.73	101.42	100.90	100.66	101.20	101.49	101.32
Numbers of cations on the basis of 4 oxygens (renormalized to 3 cations)							
Si	0.000	0.002	0.001	0.004	0.002	0.006	0.001
Al	1.371	1.286	1.326	1.266	1.316	1.318	1.127
Ti	0.007	0.007	0.007	0.006	0.008	0.001	0.002
Cr	0.546	0.595	0.577	0.659	0.637	0.651	0.852
[2]Fe^{3+}	0.069	0.101	0.081	0.054	0.027	0.019	0.016
Fe^{2+}	0.405	0.411	0.389	0.384	0.389	0.355	0.405
Mn	0.003	0.006	0.004	0.004	0.004	0.004	0.006
Mg	0.599	0.591	0.613	0.621	0.616	0.647	0.592
Ca	0.000	0.001	0.001	0.001	0.001	0.000	0.000
Total	3.000	3.000	3.000	3.000	3.000	3.000	3.000
$Mg^{\#}$[3]	0.596	0.590	0.612	0.618	0.613	0.646	0.59.4
$Cr^{\#}$[4]	0.285	0.316	0.303	0.342	0.326	0.330	0.430

[1]Analysis by Obata
[2]Fe^{3+} was calculated assuming perfect spinel stoichiometry
[3]$Mg^{\#} = Mg/Mg+Fe^{2+}$
[4]$Cr\# = Cr/Cr+Al$

Table 9: Electron Microprobe Analyses For Plagioclases From the Horoman Peridotite

	62210	62212	62213	62131	62130
SiO_2	51.29	52.40	50.15	52.26	50.10
TiO_2	0.03	0.04	0	0	0
Al_2O_3	30.75	30.15	31.16	29.56	31.35
FeO*	0.11	0.18	0.15	0.16	0.09
CaO	13.49	12.90	14.34	12.32	14.30
Na_2O	3.92	4.28	3.41	4.57	3.37
Total	99.83	100.08	99.23	99.92	99.22
An	0.654	0.625	0.699	0.598	0.701

clinopyroxene obtained using the ion microprobe are in Table 10.

Major Elements

Although point counting of petrographic thin sections is not a valid method to quantify mineral proportions in these coarse-grained rocks (grains, up to ten mm across are not uncommon), it can be used to determine relative amounts of serpentine. The samples are generally quite fresh but all of the them have some serpentine. Five samples have less than two percent alteration minerals, one (62128) has four percent and only 62210 has undergone considerable serpentinization (~20 percent). These approximate amounts are supported by the loss on ignition volatile data from Table 2. 62210 is used throughout this study as a model source composition. Since this sample has considerable serpentine it's important to establish whether this hydrous metamorphic mineral affects interpretations of geochemical data. The primary reaction suggested by Komor and others (1985) is,

$$\underset{\text{oliv.}}{2Mg_2SiO_4} + 3H_2O \quad \underset{\text{serp.}}{Mg_3Si_2O_5(OH)_4} + \underset{\text{brucite}}{Mg(OH)_2}.$$

They suggest that most serpentinization occurs at the expense of olivine with clinopyroxene undergoing limited alteration. Small MgO losses and small SiO_2 gains were observed by Komor and others in dunite and wehrlite samples but all within statistical variation. Al_2O_3, FeO, and CaO were not affected at all. Another study, (Coleman and

Table 10: Ion Probe Data For Horoman Clinopyroxene Trace Elements

	62210	62212	62213	62131	62130	62128
La	0.975	0.794	1.26	0.969	0.627	1.06
Ce	4.55	3.61	4.79	2.68	2.67	2.32
Pr	1.32	0.87	1.09	0.619	0.727	0.404
Nd	8.14	6.60	7.09	4.03	4.97	2.15
Sm	3.11	2.51	2.63	1.44	-	-
Eu	1.23	0.923	1.04	0.544	0.787	0.200
Dy	6.08	2.99	3.05	0.910	3.40	0.522
Er	3.85	1.77	1.52	0.500	2.00	0.331
Sc	33.1	29.1	36.0	17.9	59.2	52.5
Ti	3501	3506	3405	2633	4452	371
V	360	353	367	450	386	238
Cr	5788	6424	6955	13,771	7921	6844
Sr	11.4	11.3	11.5	75.6	7.6	44.0
Zr	34.1	45.0	30.3	16.4	59.6	16.1

Keith, 1971) showed no chemical variation except for very small CaO losses. Figure 8a, of whole rock CaO versus MgO, should reflect any effect of serpentinization because the samples vary from zero to twenty percent serpentine. The trends have quite good correlation and the serpentinized samples do not appear to be offset. Frey and others, (1985), found similar lack of effect with a larger data set and even greater variation in serpentine content. The rocks are in a closed chemical system with respect to major elements despite serpentinization. More proof for this conclusion is that reconstituted modes using linear regression fit no worse in samples with more serpentine even though serpentine analyses were not used in the regression (Appen. II).

Modal proportions change gradually with respect to stratigraphic height of the peridotite (Fig. 9). The modes are reconstituted into only pyroxene and olivine components (Obata, 1977) and plotted with the Ronda peridotites for comparison (Fig. 10). This removes the effect of varying amounts of plagioclase and allows one to compare rocks from Ronda which have aluminous phases from different stability fields (Obata, 1977). A clear correlation exists between modal pyroxene and bulk rock magnesium content (Fig. 11). This inverse relationship, and those between CaO, Al_2O_3, TiO_2, SiO_2, FeO, Na_2O and MgO (Fig. 8), correspond to trends defined by upper mantle peridotite xenoliths in alkalic basalts from around the world (Maaloe and Aoki, 1977; Reid and Woods, 1979; and Kurat et al, 1980). The modal and

Figure 8a-f. Anhydrous MgO variation diagrams for CaO, Al_2O_3, TiO_2, SiO_2, FeO*, and Na_2O in 7 Horoman peridotite samples (circles) and 16 samples from the Ronda peridotite (crosses) for comparison (Frey et al, 1985).

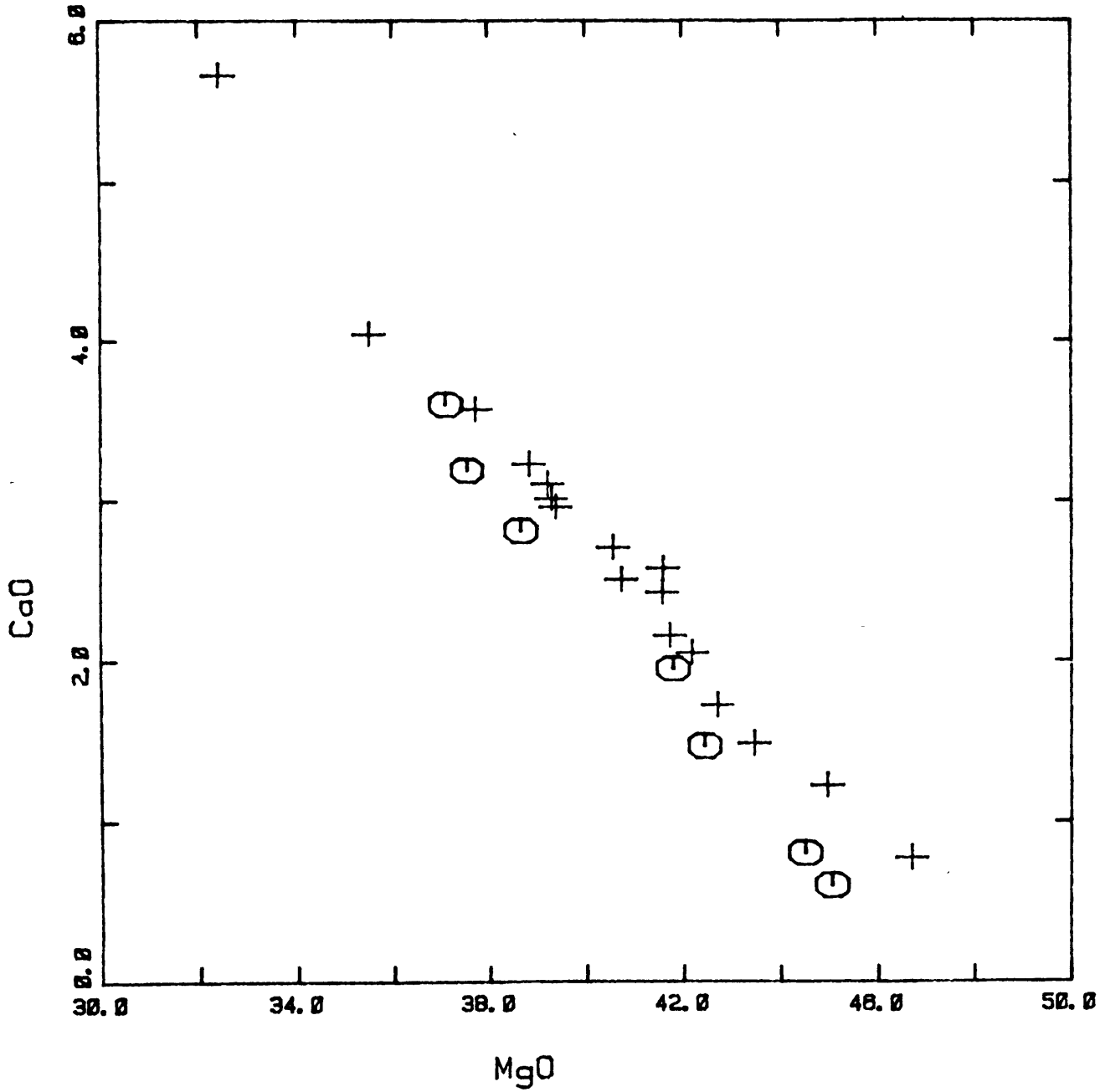

Figure 8(a)

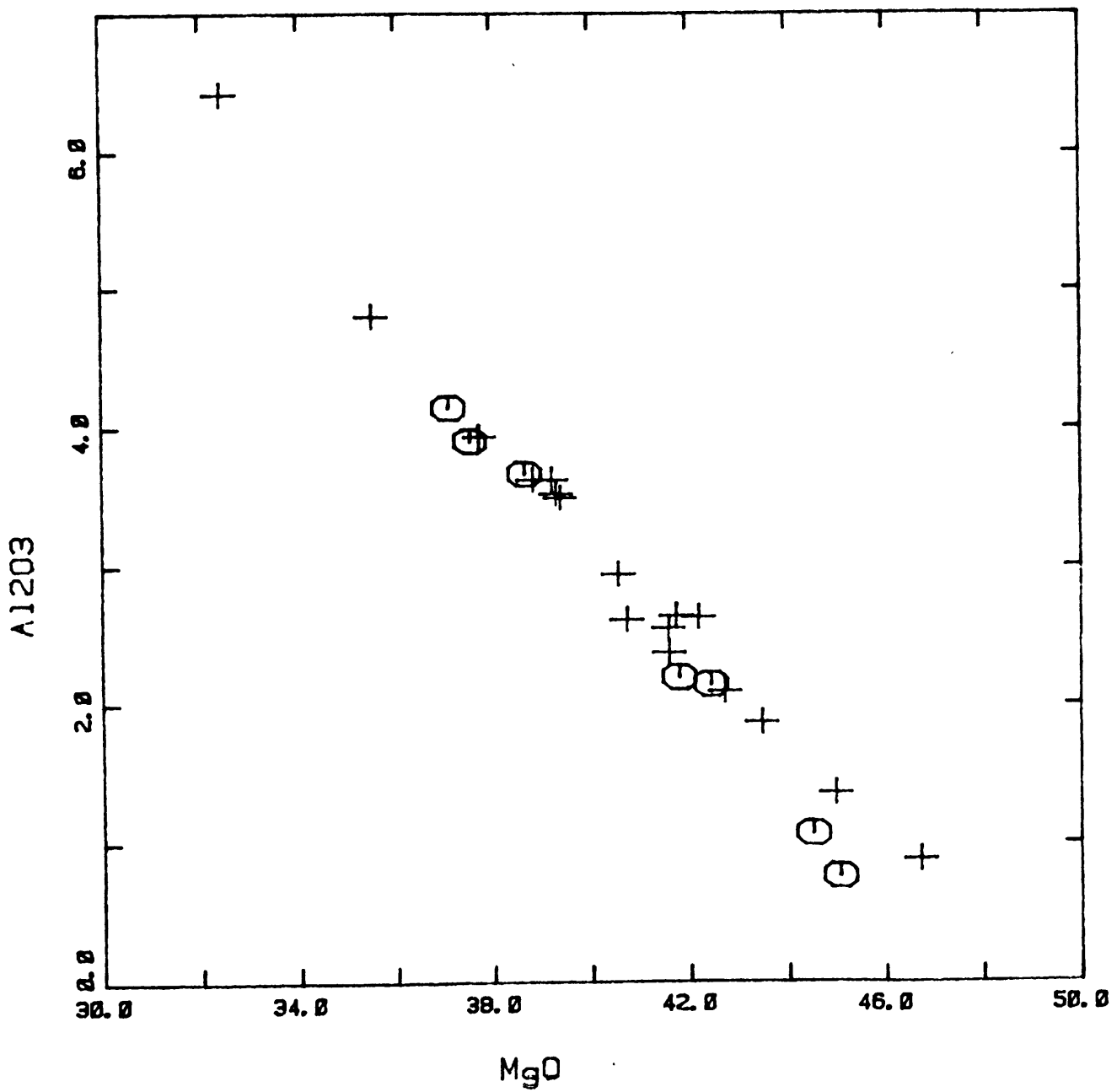

Figure 8(b)

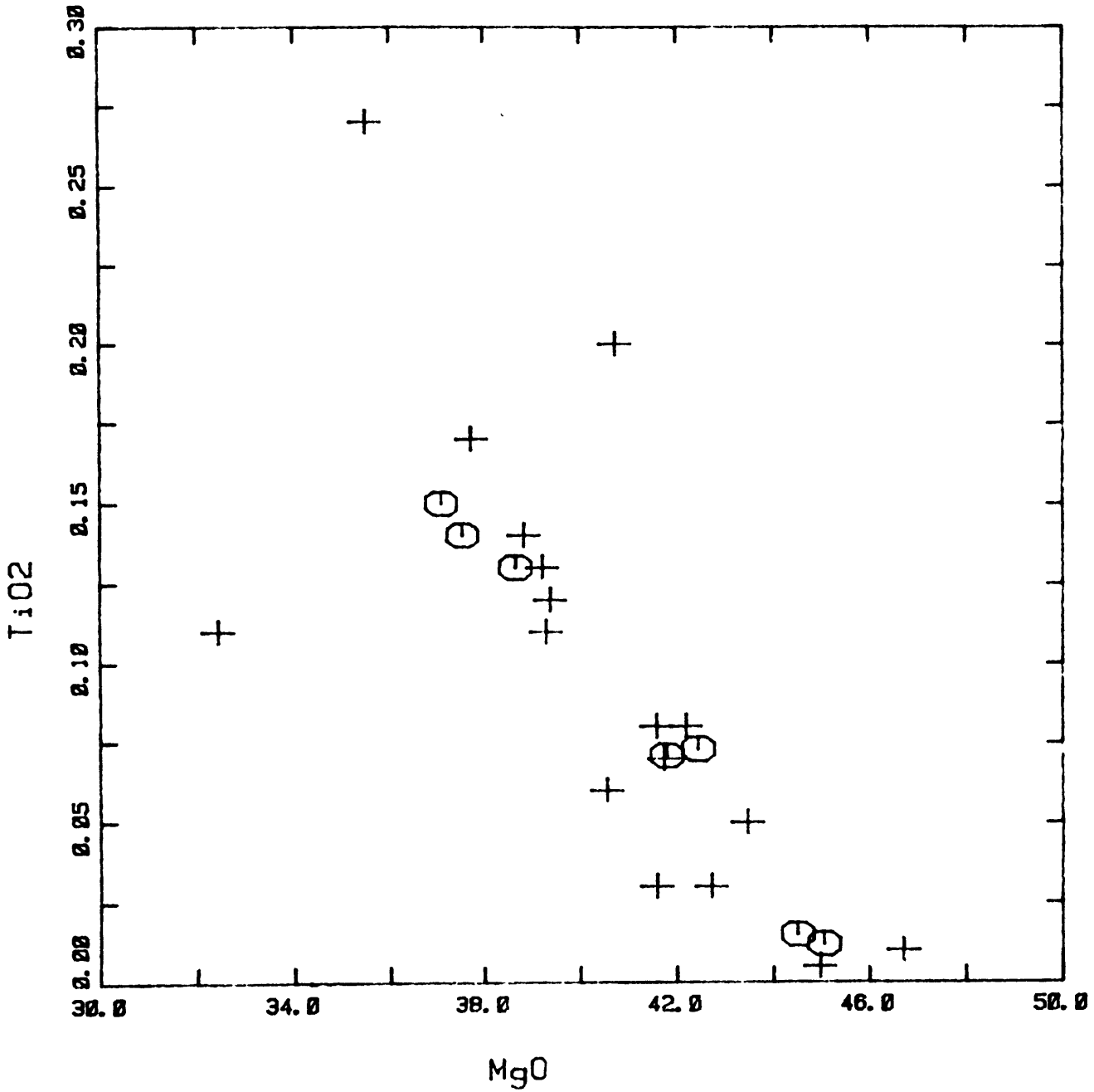

Figure 8(c)

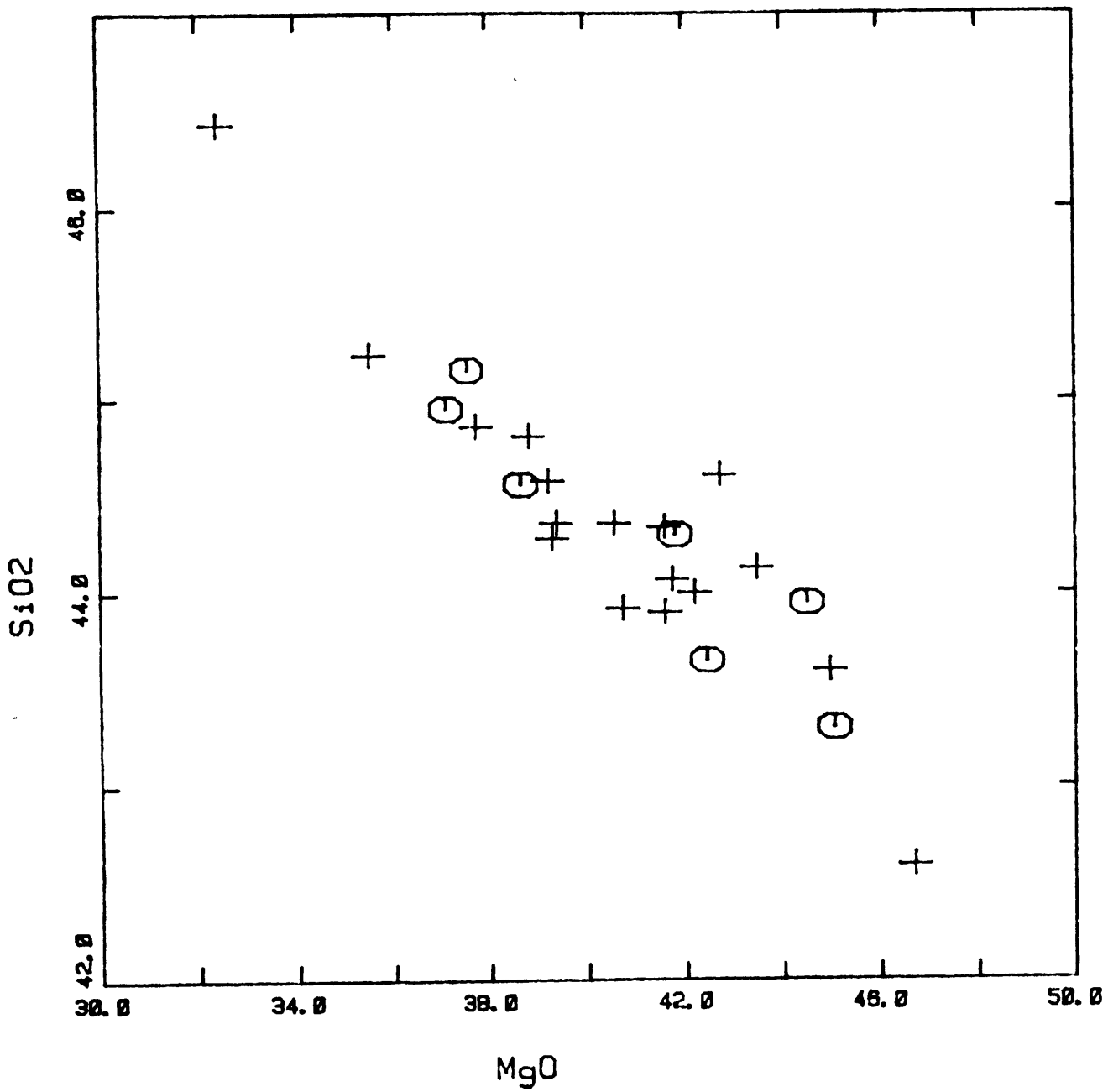

Figure 8(d)

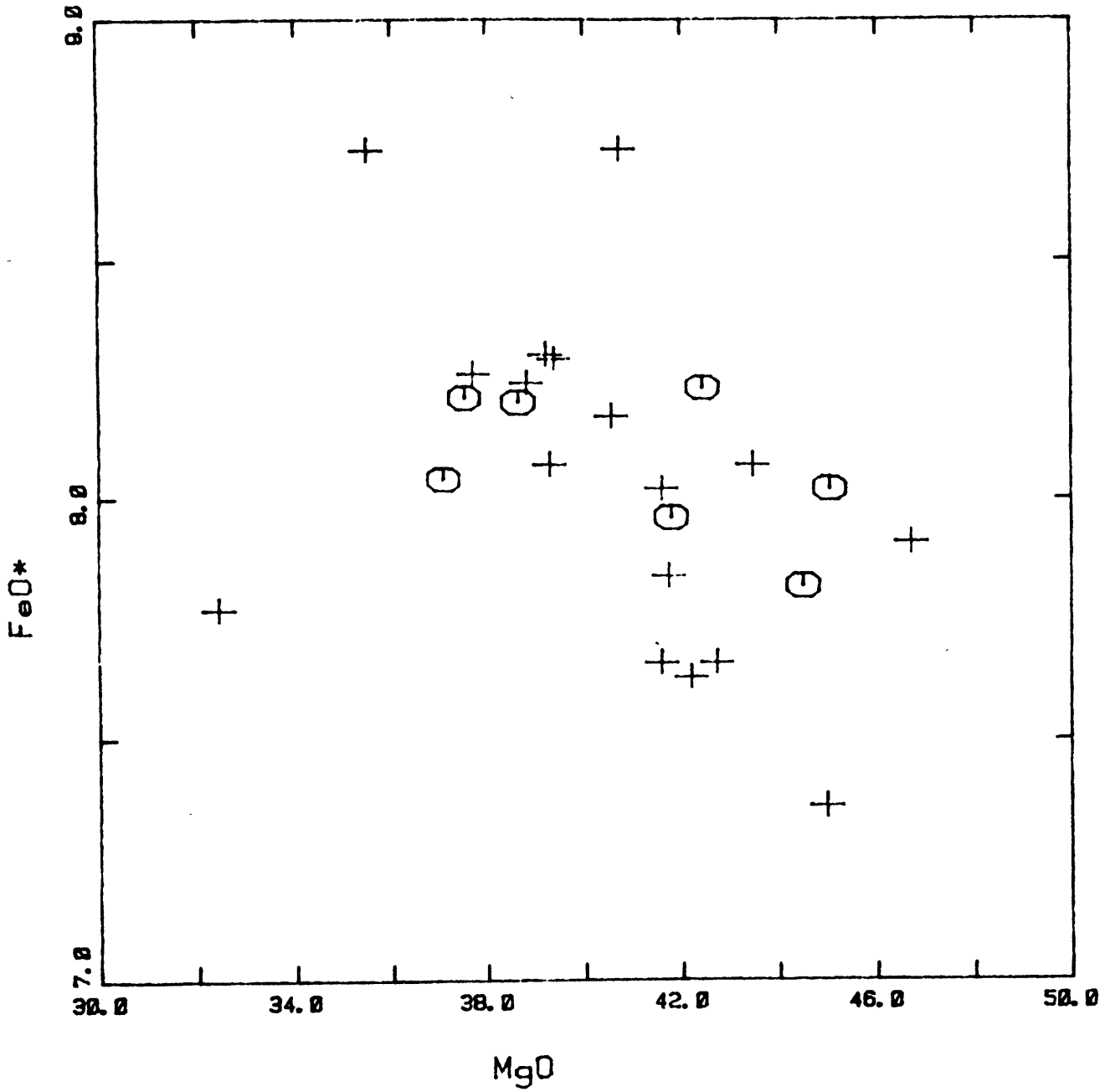

Figure 8(e)

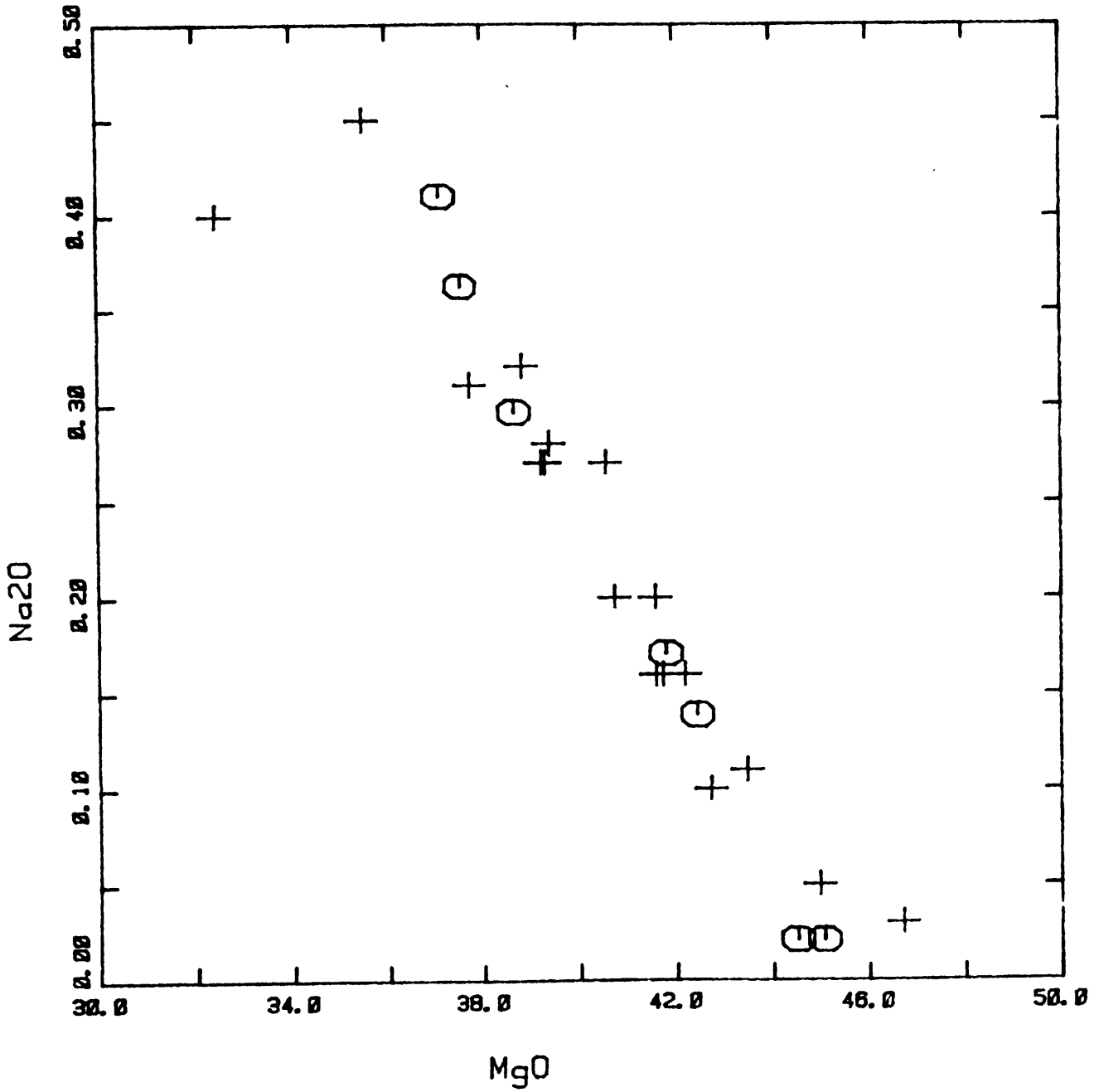

Figure 8(f)

Figure 9. Modal variations with respect to stratigraphic height (in meters) for the Horoman peridotite. The samples, arranged from top to bottom, are: two harzburgites (62127 and 62128) with no plagioclase; one plagioclase harzburgite (62130); and four plagioclase lherzolites (62131, 62213, 62212 and 62210).

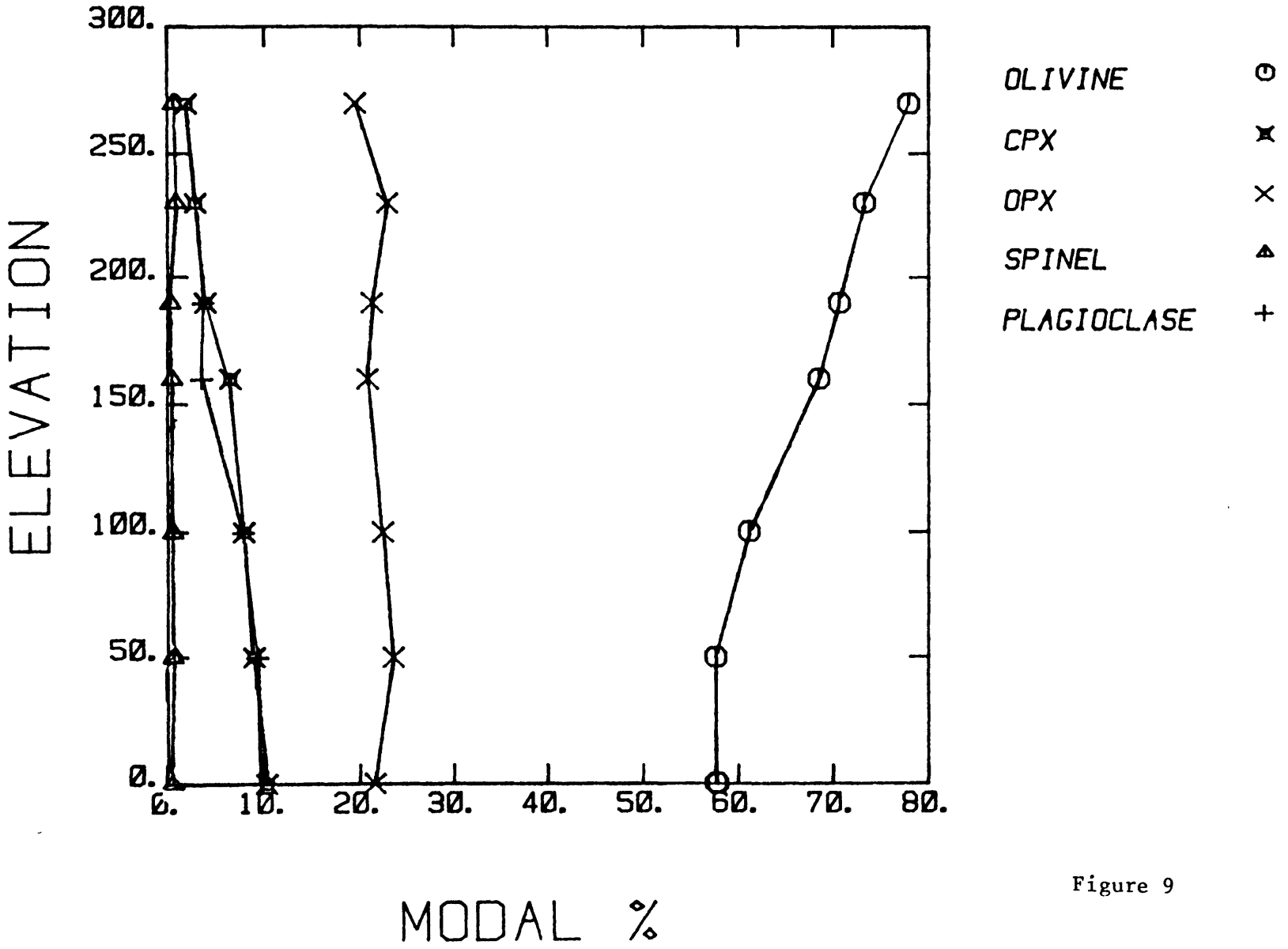
ELEVATION
300.
250.
200.
150.
100.
50.
0.
0.
10.
20.
30.
40.
50.
60.
70.
80.
MODAL %
OLIVINE
CPX
OPX
SPINEL
PLAGIOCLASE

Figure 9

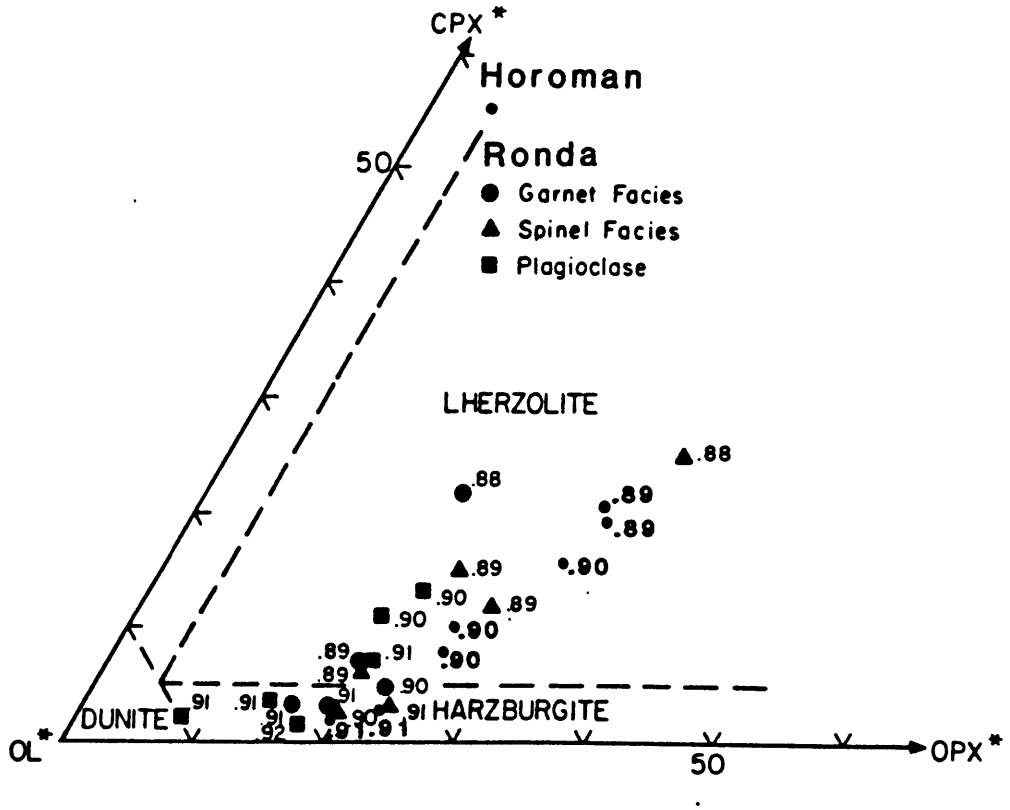

Figure 10. Reconstituted modal proportions (*a la* Obata, 1977) of Horoman peridotites and Ronda peridotites (Frey et al, 1985) for comparison, *i.e.* aluminous phases are recast as modal olivine and pyroxene (indicated by * superscript). The numbers adjacent to each point are forsterite content of olivine which increases from 0.88 to 0.92 as modal cpx* increases.

Figure 11. MgO content versus total reconstituted modal pyroxene (as in Fig. 10) for the Horoman peridotite.

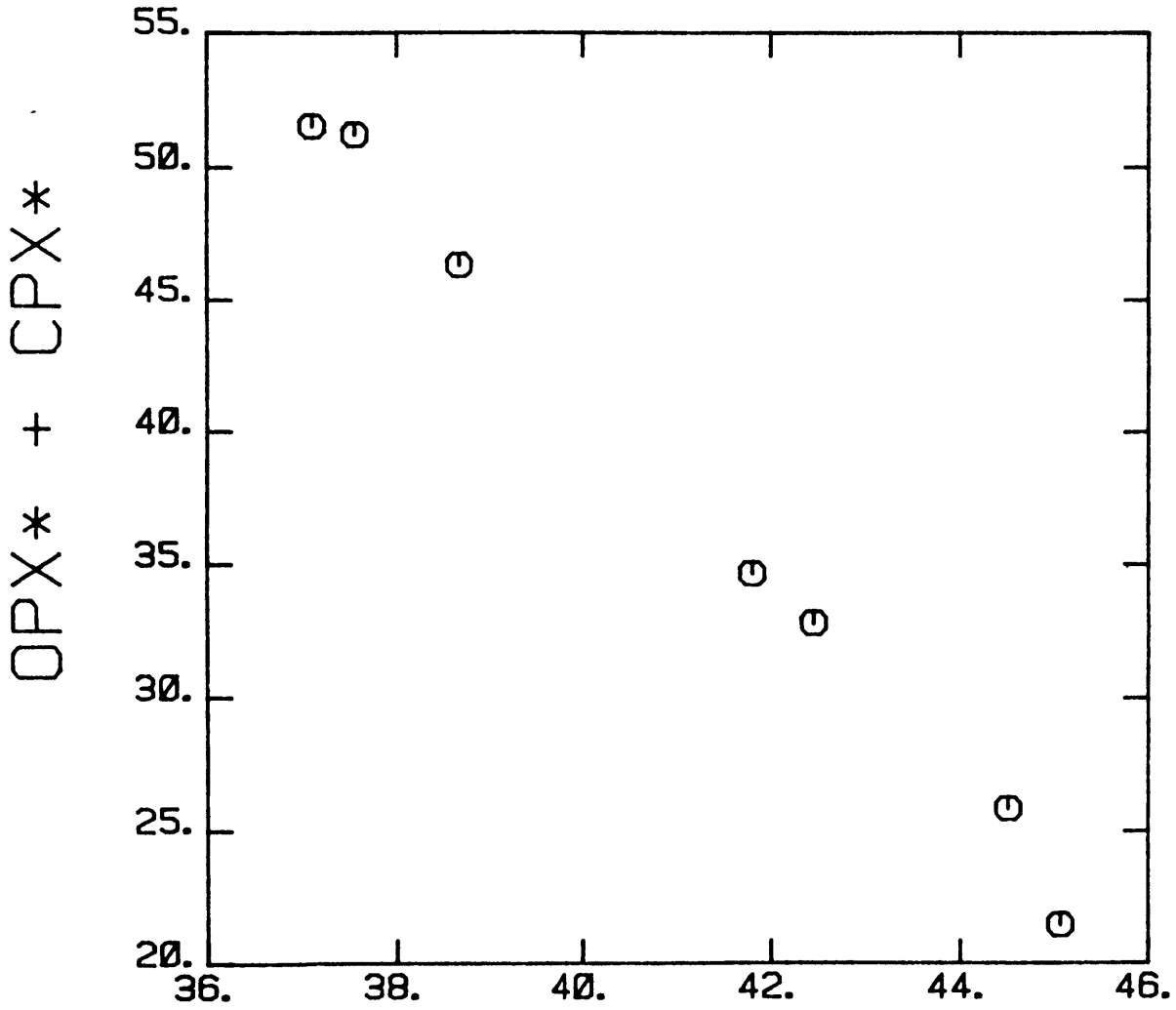

Figure 11

major element chemical variations accompany mineral composition variations indicating that the change in whole rock chemistry is not simply a function of varying mineral proportions. This coupling of mineral and bulk rock composition will be explored in a later section. The correspondence between major element chemistry, modal proportions and mineral composition is a characteristic of experimental investigations of peridotite residues produced in melting experiments (e.g. Mysen and Kushiro, 1977; Takahashi and Kushiro, 1983).

The Horoman peridotite is interpreted as a suite of residues produced from an initially homogeneous source by varying degrees of partial melting. With this interpretation samples with low MgO content and high total pyroxene, Al_2O_3, CaO, TiO_2 and Na_2O contents are considered to be least melted while samples with the opposite chemical relations are considered to be residues from the greatest degree of melting. Based on similar major element trends, similar interpretations have been made for other large alpine peridotite bodies (e.g. E. Mediterranean, Menzies and Allen, 1974; Ronda, S. Spain, Frey et al, 1985; Ivrea Zone, N. Italy, Sinigoi, 1980, 1983; Trinity peridotite, California, Quick, 1981). Dick (1977) formed a similar interpretation based on modal variations and detailed mineral chemistry. Abyssal peridotites are also believed to be residues of partial melting (Dick and Fisher, 1984; Dick et al, 1984).

The remarkable linearity of these major element trends is found at other ultramafic locations (Tafjord, Norway, Carswell, 1968; Ronda, Frey et al, 1985; Ivrea Zone, Sinigoi, 1980, 1983; Trinity, Quick, 1981; peridotite xenoliths worldwide, Maaloe and Aoki, 1977). This colinearity appears to be a prevailing chemical feature of the earth's upper mantle. Negative correlation is expected to a degree in major element variation diagrams merely for statistical reasons (Frey et al, 1985) but they would not be expected to be so linear nor would the colinearity extend to elements in trace amounts (TiO_2 and Na_2O Fig's. 8c and 8f, other trace elements presented later). Two principal explanations for these linear variation diagrams are commonly found in the literature. The first is that the trends are due to two component mixing, such as solid and interstitial melt. The second is that the observed trends are produced by residues of partial melting. These two interpretations are by no means mutually exclusive. Frey and others (1985) suggest three possible scenarios of partial melting and mixing as models for the linear correlation: (1) A uniform degree of partial melting throughout the entire peridotite followed by imperfect and variable extraction of the melt (Carswell, 1968) (2) Variable degrees of melting producing a compositionally uniform melt that may or may not be completely extracted and (3) Variable degrees of melting producing a compositionally heterogeneous melt that may or may not undergo complete

extraction. The third scenario would probably not produce linear variation diagrams. It is possible, however, that variations from linearity are small relative to errors associated with sampling and analysis (see Presnall, 1979; Fig. 3.3)

The distinction between (2) and (3) above seems to still be equivocal based on major element peridotite data and through experimental work. For scenario (2), phase equilibrium control would have to be such that an invariant melt was produced over a wide range of degree of melting. The composition of the solid residue would then vary along a linear extraction line in composition space. Yoder (1976), Mysen and Kushiro (1977) and Presnall (1979) all advocate invariant melting of peridotites based on laboratory experiments. Jacques and Green (1980), on the other hand, also based on laboratory experiments, concluded that varying degrees of melting can produce a wide range of melt compositions. There is little direct evidence for the presence of trapped melt at Horoman (Niida, 1984) or any of the previously mentioned locations as there is for layered intrusions (Irvine, 1982). It should be remembered however that these rocks are metamorphic so that any such textures may have been obliterated by subsolidus recrystallization. Another argument against the presence of trapped melt derives from theoretical calculations (e.g. McKenzie, 1985) which conclude that basaltic melts are very efficiently extracted and segregated in the mantle. Many researchers

however point to chemical, mineralogic and textural evidence in support of trapped melt. Plagioclase and clinopyroxene rich veinlets are frequently ascribed to trapped melt (Nicholas and Dupuy, 1984; Hamlyn and Bonatti, 1980; Dick, 1977; Dick and Bullen, 1984; Dick and Fisher, 1984; Jacobsen et al., 1984; Quick, 1981; Boudier and Nicholas, 1985).

Another point illustrated by Figure 8, along with the linearity, is the general correspondence of the trends for Ronda and Horoman. The match of both the trend and the total spread is surprising considering the differences in the sampling scales. The Ronda samples were semi-randomly collected from throughout the entire 300km^2 massif, while the Horoman samples were collected in a 300m thick stratigraphic section possibly representing the original mantle stratigraphy. The coincidence of the trends in both of the massifs *in toto* was shown by Obata and Nagahara (1986), but Figure 8 implies that the physical process controlling these trends takes place over a much smaller scale. The MgO content varies considerably over this section in this study (Fig. 12). It is no wonder than that Obata (1977), in his Ph.D. thesis on the petrology of Ronda, states, "No geographic correlation of the depletion of the peridotites is apparent,...". It is important, therefore, to be aware of this difference in scales when forming a hypothesis to explain the chemical data. What may be a reasonable hypothesis on the scale of kilometers may be intuitively improbable or even physically impossible on the scale of

Figure 12. MgO content versus stratigraphic height (in meters) for the Horoman peridotite.

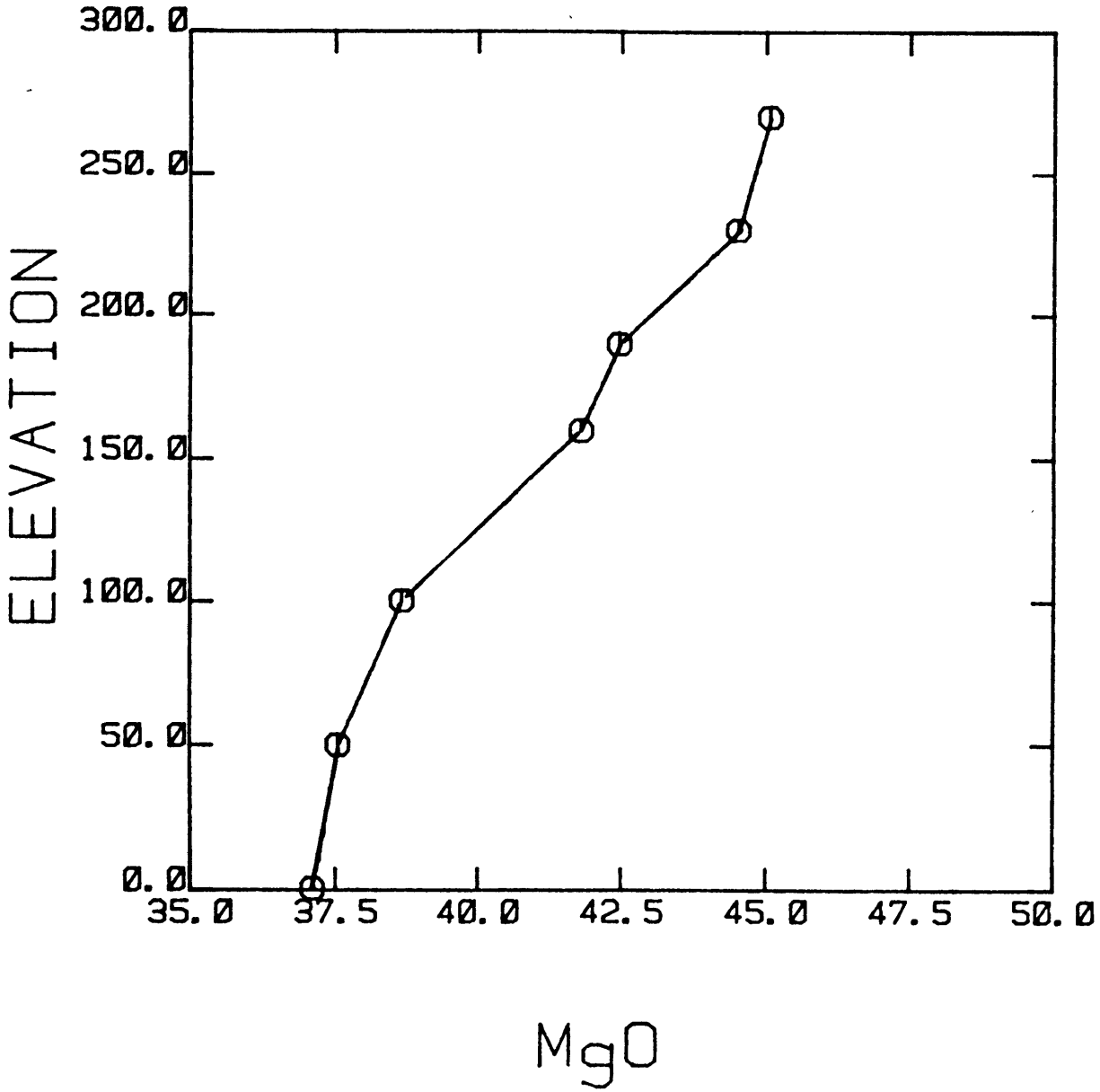
300.0
250.0
200.0
150.0
100.0
50.0
0.0
ELEVATION
35.0
37.5
40.0
42.5
45.0
47.5
50.0
MgO
HOROMAN

Figure 12

meters. In order to better understand and distinguish between the above melting/mixing models as well as placing these models in a physical framework, further analysis of the major elements is inadequate. Later, we shall use trace elements to help constrain the petrogenetic models. Initially though, the interpretation of the Horoman peridotites as residues derived by varying degrees of melting of a homogeneous source without trapped melt will be used as a working hypothesis.

With this assumption, Frey and others (1985) were able to determine the degree of melting (F) and to estimate the melt composition by utilizing the major element variations and the olivine compositions. This model will be used for the Horoman rocks. It is based on the work of Hanson and Langmuir (1978) relating MgO and FeO bulk rock data to K_D for olivine ($(Fe/Mg)_{ol}/(Fe/Mg)_{melt}$) and the mass balance formulations of Stockman (1982). Sample 62210 is used as the source composition. This sample is the most enriched in basaltic components and, as it turns out, has a composition very similar to most estimates of the fertile upper mantle composition. This question of the source composition will be explored in a later section. Although 62210 appears to be a fine choice as a source composition, its exact composition is immaterial since we are concentrating on processes which relate this sequence of rocks. In that sense, it does not matter whether the degrees of melting are true or relative.

Table 11: Degree of Melting in Percent for Horoman Peridotites Using Major Elements (see text) With Sample 62210 as the Source

	K_D = 0.30		K_D = 0.33		K_D = 0.35	
	F(equil.)	F(fract.)	F(equil.)	F(fract.)	F(equil.)	F(fract.)
62212	0.8	0.8	0.7	0.8	0.7	0.7
62213	4.9	5.0	5.1	5.1	5.2	5.2
62131	15.8	16.3	16.4	16.9	16.9	17.4
62130	16.5	16.7	17.1	17.3	17.4	17.7
62128	23.1	23.9	24.0	24.9	24.6	25.6
62127	23.7	24.5	24.5	25.5	25.1	26.2

The results of these calculations are shown in Table 11. The MgO and FeO^* variations are consistent with the calculated residues from 1 to 25% melting of 62210. This calculation however is dependent upon K_D for olivine and variations in K_D as a function of pressure and temperature are not entirely consistent among experiments done by various investigators (Grover et al., 1980; Ford et al., 1983; Takahashi and Kushiro, 1983). Table 11 show the results for three values of K_D which represent the spread for conditions in the spinel lherzolite stability field. The F values are not strongly dependent on K_D, but the calculated melt compositions are more so and results are shown for K_D values of 0.30 and 0.35. (Melt compositions for 62212 could not be calculated due to the close similarity of the MgO and FeO^* contents in the bulk rock between this sample and the source.) As noted by Frey and others (1985), this calculations has trouble with the oxidation state of Fe which at most causes F to be overestimated by 5% (i.e. F=0.100 would be calculated as F=0.105). The fractional and batch melting that is referred to in Table 11 refers to the assumed composition of the olivine (in equilibrium with the melt) used in the calculation. For batch melting, the olivine composition would be that in the residue at the end of melting. For fractional melting, however, the olivine composition in equilibrium with the melt changes throughout the melting process so that in this calculation a mean was used between the source olivine and the residue olivine.

There is not a significant variation in olivine composition for these rocks and it has only a slight affect on F. I believe that the fractional melting scheme is physically more realistic in this situation so melts were only calculated for this case.

The calculated melts (Table 12) are basaltic in composition with 48-51% SiO_2, 11-14% MgO, 7-9% FeO, 13-14% Al_2O_3, 12-13% CaO and ~1.6% Na_2O. (Melt composition for sample 62213 is not considered to be reasonable because within the errors of the calculation F is too small to use the mass balance equation and get significant results. It is not used in the compilation.) The calculated Horoman melts in comparison to similar calculations for Ronda have higher values of MgO, Al_2O_3, and CaO, but are slightly depleted in SiO_2 and FeO (Table 12). These Horoman melt compositions appear to be reasonably similar to parental MORB values (Table 12) but perhaps a bit enriched in MgO and CaO. Considering that the sample used for the source composition in the calculation is probably the residue from some small degree of melting, discussion of these discrepancies is minimized here. The melt compositions calculated here appear to be more picritic in composition than standard MORB and similar to some primary melts from the literature (Table 12).

Nickel- a highly compatible element

Olivine is the most abundant mineral in the Horoman samples and it is relatively refractory during melting. The

Table 12: Calculated Melts in Equilibrium With Horoman Peridotites Derived From Source Sample 62210 Compared to Calculated Melts For Ronda and Parental MORB Estimates

	62213		62131		62130		62128		62127	
SiO_2	52.3	52.1	49.0	48.7	51.1	50.7	48.5	48.2	49.7	49.3
TiO_2	0.5	0.5	0.6	0.5	0.5	0.5	0.6	0.5	0.6	0.5
Al_2O_3	13.2	12.9	14.3	13.6	14.0	13.4	14.0	13.2	14.5	13.6
Cr_2O_3	0.2	0.2	0.3	0.3	0.8	0.7	0.05	0.08	0.13	0.15
FeO^*	5.0	5.1	8.6	8.5	7.1	7.1	8.8	8.7	8.0	8.0
MnO	0.3	0.3	0.2	0.2	0.2	0.2	0.2	0.2	0.2	0.2
MgO	7.4	8.6	13.1	15.0	10.4	12.1	13.6	15.7	12.5	14.6
CaO	18.3	17.8	12.2	11.5	14.1	13.4	12.6	11.8	12.7	12.0
Na_2O	2.5	2.5	1.7	1.6	1.7	1.7	1.7	1.5	1.6	1.5
K_2O	0.09	0.08	0.03	0.03	0.03	0.03	0.03	-	-	-
P_2O_5	0.01	0.01	0.05	0.04	0.03	0.03	-	-	-	-
NiO	0.01	0.01	0.05	0.06	0.02	0.04	0.05	0.08	0.05	0.07
Assumed K_D	0.30	0.35	0.30	0.35	0.30	0.35	0.30	0.35	0.30	0.35
% Melting	5.0	5.2	16.3	17.4	16.7	17.7	23.9	25.6	24.5	26.2

	Calculated Melts From Ronda				MORB: Dungan & Rhodes (1978)	MORB: Elthon (1979) Green et al. (1979)	
	243		893				
SiO_2	50.4	50.0	51.3	50.3	50.0	47.8	48.3
TiO_2	0.93	0.86	0.59	0.52	0.65	0.59	0.60
Al_2O_3	12.0	11.3	11.9	10.6	14.5	12.1	13.7
FeO^*	9.5	9.4	9.3	9.1	8.3	9.0	7.9
MnO	0.40	0.38	0.19	0.19	-	0.12	0.12
MgO	14.2	16.4	14.9	18.6	11.7	17.8	16.7
CaO	12.4	11.6	10.8	9.7	13.0	11.2	10.9
Na_2O	0.09	0.11	1.04	0.92	1.71	1.31	1.65
Assumed K_D	0.30	0.35	0.30	0.35			
% Melting	4.2	4.6	26.4	31.7			

partition coefficient for nickel in olivine (and also in the bulk rock) is much greater than one (Hart and Davis, 1978). Therefore, during melting, one would expect little variation in Ni content. The range in Ni is from 1972ppm in 62210, to 2493ppm in 62127. Slight variation in Ni in ultramafic rocks has been used as an argument for the rocks being residues derived from partial melting and not olivine rich accumulates (Frey and Green, 1974; Frey and Prinz, 1978). This argument is derived from the governing equations for fractional crystallization and for fractional melting which are derived from surface equilibrium conditions:

$C_S/C_O = (1-X)^{(D-1)}$ (F.C.), $C_S/C_O = (1-X)^{[(1/D)-1]}$ (F.M.), where X is the degree of completion (melting or crystallizing), D is the partition coefficient (concentration in solid/concentration in liquid), C_S is the concentration in the solid and C_O is the concentration in the entire system. Using relevant D's (5-10) and X from 0.0-0.3, C_S/C_O can be shown to vary 4X for D=5 and 25X for D=10 for fractional crystallization compared to 1.33X and 1.38X respectively for fractional melting. (The variation would be about the same for equilibrium melting.) Certainly in reality D would change throughout the process so the above variation factors are only used to qualitatively differentiate between the two processes. Using sample 62210 as C_O, the maximum Ni variation is 1.26X which is consistent with the derivation of the peridotites as residues from less than 30% melting. A brief scan of the literature on layered intrusions shows

Ni_{max}/Ni_{min} to be ~15 in a 200m section of olivine-rich (~60%) "picrite" in the Inziswa complex in southern Africa (Lightfoot and Naldrett, 1984); 2 in a 45m section of harzburgites and dunites in the Great Dyke, Zimbabwe (Wilson, 1982); 2.5 across a 500m section of peridotite at Rhum (Dunham and Wadsworth, 1978); 3.7 across ~10m of olivine-rich cumulate in the Jimberlana intrusion in western Australia (Campbell, 1977); 30 in one 30m section of the peridotite in the Muskox intrusion in the Northwest Territories, Canada and about 3 in four other 130m sections of dunite at Muskox (Irvine, 1975); and finally 5.4 in the dunite and peridotite at Duke Island in southeastern Alaska (Irvine, 1974).

Nickel concentrations in the Horoman peridotites are positively correlated with MgO (Fig. 13). The correlation coefficient for the seven samples 0.997. Data from the Ronda peridotite is shown Figure 13 for comparison. The correspondence of the two trends is quite remarkable and suggests that similar processes took place in the 300m section of Horoman and the $300km^2$ samples at Ronda (Frey et al., 1985). The correlation between the Ni in olivine and the forsterite content is not as good (Fig. 14). This most likely is a simple function of the quality of the electron microprobe data for Ni. The counting was only for 20 seconds with a standard deviation of ~8% and the olivines are not completely homogeneous in Ni.

Figure 13. Anhydrous MgO variation diagram for Ni in peridotites from Horoman (circles) and Ronda (crosses) for comparison Correlation coefficient, r = 0.997 for Horoman, r = 0.978 for all. Only five Ronda samples significantly deviate from linearity but no explanation for this is known.

Figure 14. Forsterite content of olivine measured by electron microprobe versus Ni content in olivine also measured by electron microprobe. The correlation is much poorer than for the whole rock data but the general relation is the same. Variation from linearity is most likely due to the relatively poor quality of Ni analyses in olivine.

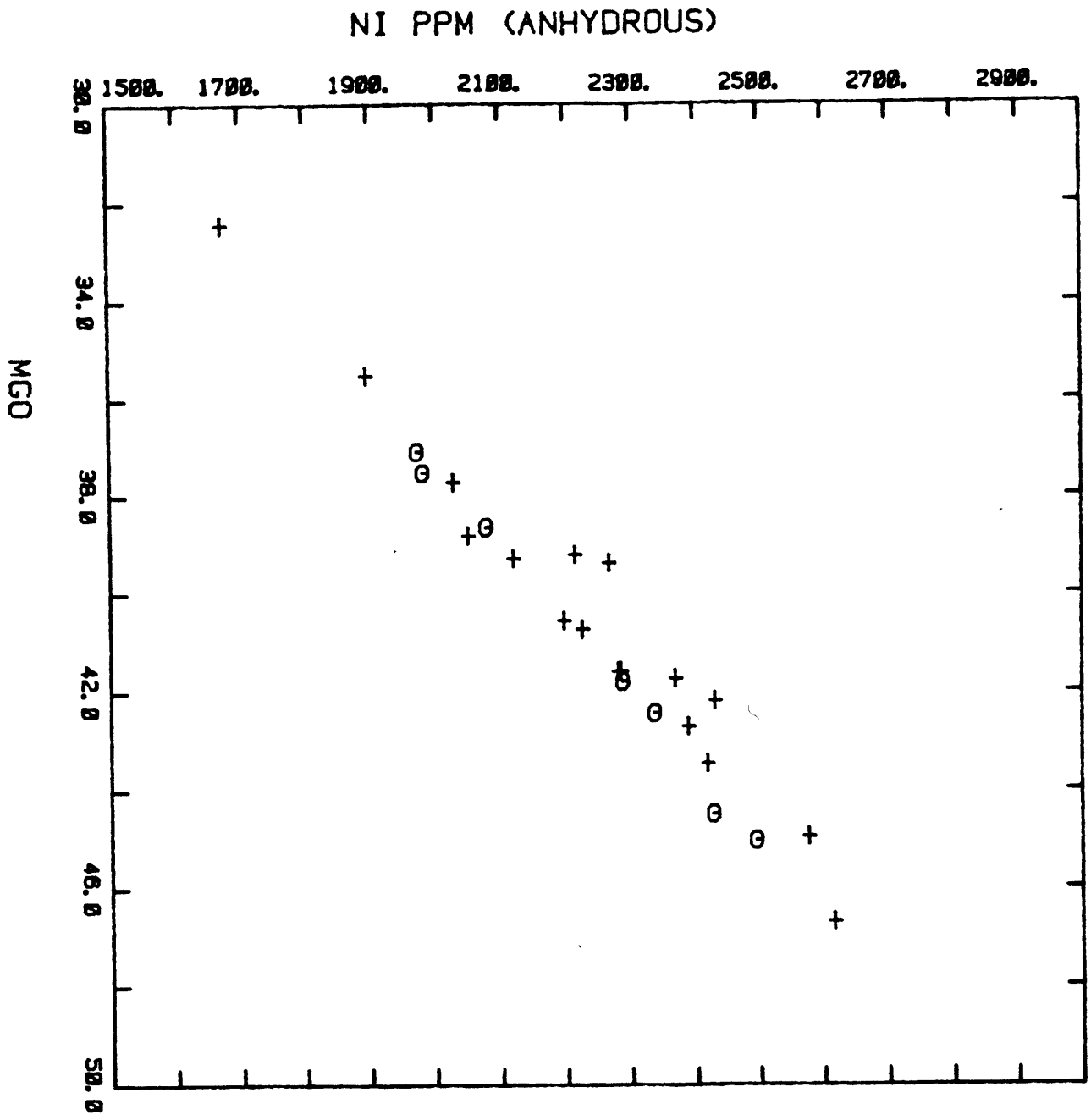
NI PPM (ANHYDROUS)
1500.
1700.
1900.
2100.
2300.
2500.
2700.
2900.
MGO
30.0
34.0
38.0
42.0
46.0
50.0

Figure 13

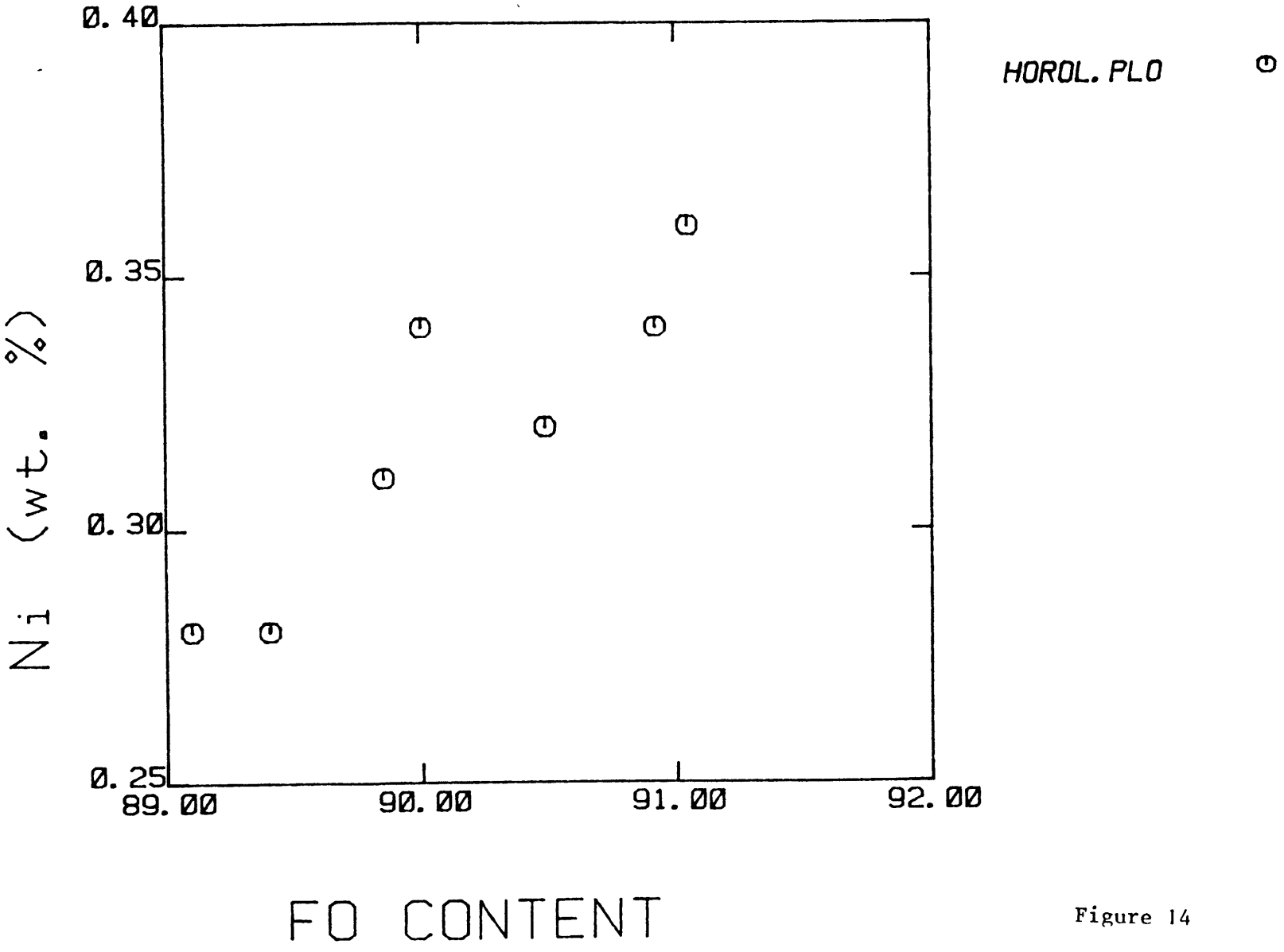

Figure 14

The variation in Ni abundance can be used to infer the degree of melting (F) required to produce the range in Ni content. The mass balance equation reduces to $C^{s}_{Ni}/C^{o}_{Ni} = 1/(1-F)$ for $D^{s/l}_{Ni} >> F$. It so happens that equations for non-modal equilibrium and fractional melting (Shaw, 1970) also reduce to this same form if D is large relative to F and the Ni-rich phase is relatively refractory. These assumptions are valid in the olivine-rich peridotites. Using this simple formulation, and 62210 as the initial Ni content, the estimates range from 62212 as the residue after 0.5% melting to 62127 as the residue after 21% melting (Table 13). As mentioned previously, it is doubtful that 62210 is actually unmelted source material. Estimates of "primitive mantle" Ni abundance are quite variable, ranging from ~1700 ppm (Ringwood, 1979) to ~2120ppm (Wanke, 1981). This problem becomes even more complex if a source Ni content is assumed that is greater than in 62210, but if we choose (somewhat arbitrarily) a source Ni content of 1807ppm (Palme and Nickel, 1985) then 62210 could be a residue from 8.4% melting and the other samples can be scaled up proportionally. This source Ni content is estimated from a more rigorously derived MgO content which, in Palme and Nickel (1985), is considerably lower than other estimates (see Table 15, primary upper mantle composition section). This degree of melting is therefore a maximum. Based on estimates of Ni content in the mantle, 62210 is a reasonable

Table 13: Degree of Melting in Percent Derived From Anhydrous Ni Data, Using 62210 as a Source, (see text for further explanation)

	62212	62213	62131	62130	62128	62127
A	0.5	5.1	13.7	15.5	18.7	20.9
B	0.5	5.7	16.5	17.8	22.5	24.6
C	0.5	5.7	17.0	18.3	23.5	25.9

A F derived from simplified mass balance equation using 62210 as the source.

B F derived from full mass balance equation using composition dependence formulation for D_{Ni} (Hart and Davis, 1978). Each sample's olivine data and approximation of MgO in melt from Table 12 was used for bulk D.

C Same as 2 except that sample 62210 olivine data rather than each sample's is used for bulk D. Since the melting process should alter the olivine chemistry gradually the true value of F is probably between estimates B and C.

approximation of "source" to make it safe to say that it was derived from only a very small degree of melting.

Using the mass balance equation:

$$F = D_{Ni}^{s/l} (C_o/C_s) (1 - C_s/C_o)/(1 - D_{Ni}^{s/l}),$$

a more rigorous estimation of F can be performed. $D_{Ni}^{ol/l}$ can be estimated from the empirically derived (from experimental data), composition dependent formulation of D from Hart and Davis (1978):

$$D=124.13(1/MgO) - 0.897$$

where MgO is the composition in the liquid in wt%. MgO content was taken from melt compositions derived from major element data presented previously. Bulk D can then be determined using modes (Table 1) and mineral/mineral partition coefficients given in Hart and Davis (1978). This calculation was performed for all of the samples using 62210 as a source composition (Table 13). This calculation is robust to partition coefficients as mentioned in the previous paragraph and thus is robust to MgO estimates for the partial melts (changes of bulk D by 2X only changes F by ~10%). F estimated in this way ranges from 0.5% for 62212 to 25.3% for 62127, in quite good agreement with the estimates derived from the major elements.

Potentially confusing the interpretation of the whole rock nickel data is the presence of trace amounts of Fe-Ni sulfide. The energy dispersive system of the electron microprobe (EDS) was used as a qualitative scan of the mineral composition in several samples. Based on this

result, the mineral is most likely pentlandite ($(Fe,Ni)_9S_8$). Pentlandite is the most prevalent sulfide analysed in mantle peridotites, in studies specifically relating to sulfides (Lorand, 1986; Garuti et al., 1984), although associated pyrrhotite and chalcopyrite are observed as well. If Fe and Ni are in equal molar proportions (as it appeared in the EDS spectrum) the pentlandite would contain 34 weight percent Ni, so that $D^{pent/ol}$ = 95-120. Furthermore, a high Ni content of the sulfide phase would be expected based on high values of $K_D{}^{sulf/oliv}{}_{(Ni-Fe)}$ determined by actual measurement (Thompson et al., 1984; Fleet et al., 1977) in equilibrium with olivine with significant Ni content (~0.3%), such as at Horoman. Ni partitioning between sulfide and silicate melts is poorly understood so the effect of the presence of pentlandite upon the previous melting calculations is unknown. As a rough approximation for the amount of pentlandite in the rocks, mass balance calculations were made using the Ni content in the olivine measured by electron microprobe, modes from Table 1, and olivine/mineral partition coefficients from Stosch (1981). Stosch reported a range of D's for nickel measured in spinel lherzolite xenoliths. For these calculations Stosch's minimum $D^{ol/min.}$ values were used, similar to those used by Hart and Davis (1978). Without any pentlandite, 75-91% of the nickel for the Horoman samples is accounted for, whereas assuming 0.1% modal pentlandite with 34 wt% Ni, 88-102% of the nickel is accounted for. Considering the errors in the

modal proportions, Ni content measured in olivine and partition coefficients used, Ni is quite well balanced with inclusion of a trace amount of pentlandite. A rough correlation is found between percent Ni accounted for and degree of depletion, i.e. more pentlandite would be required to perfectly mass balance the more enriched rocks (and less for the more depleted). This observation will be affected by studies that show that pentlandite becomes more Ni- rich in rocks more depleted by melting (Garuti et al., 1984) in agreement with theory (Rajamani and Naldrett, 1978). Mineralogic studies of sulfides in mantle peridotites show that pentlandite and associated sulfides in close association with spinel, such as at Horoman, are primitive mantle phases (Garuti et al., 1984; Lorand, 1986), in disagreement with Stockman (1982) who believes that the sulfides are subsolidus products resulting from the presence of trapped melts. Garuti and others (1984) believe that the sulfide assemblage is unique from materials produced by the crystallization of mantle derived melts, metasomatic or hydrothermal processes. The presence of even 0.1% pentlandite can considerably increase the bulk $D_{Ni}^{s/l}$, e.g. from 5.17 to 5.96 for 62127 giving rise to a slight decrease in estimated F from 25.3% to 24.6%.

Sulfur was not analysed for the Horoman rocks, but some speculations about sulfur can be made based on the limited observations of the presence of pentlandite and work done by others on mantle sulfides. The observation at Horoman that

the amount of sulfide decreases with melting is supported by similar, more quantitative, observations in other studies (Comin-Chiaramonti et al., 1986; Lorand, 1986; Garuti et al., 1984). In these studies, sulfur content was measured and was shown also to be less abundant in more depleted rocks, i.e. sulfur is acting incompatibly with melting. The melting point of pentlandite under mantle conditions is thought to be rather low (~1070-1150 ^{o}C) according to Lorand (1986) which may explain the sulfide and sulfur depletion with melting. Experiments on sulfur solubility in basaltic melts show that solubility increases with temperature quite dramatically and that temperature appears to be the most important parameter affecting solubility (Wendlandt, 1982; Haughton et al., 1974). This result would also concur with the sulfur depletion observation. Sulfides are found even in the quite depleted harzburgites at Horoman and other peridotite bodies (Lorand, 1986; Garuti et al., 1984) suggesting that basaltic melts in equilibrium with mantle rocks are probably saturated, or nearly so, in sulfur (Lorand, 1986).

Compatible Trace Elements: Cr and Co

At Horoman, cobalt abundance is positively correlated with MgO (Fig. 15) implying a bulk solid/liquid partition coefficient greater than one. If one makes the same simplification of the mass balance equation as done for Ni, assuming $D_{Co}^{s/l} >> F$, degree of melting can be estimated. F's determined using Co in this way are generally about 25

Figure 15. Anhydrous MgO variation diagram for Co in peridotites from Horoman (circles) and Ronda (crosses) for comparison showing positive corellation and general overlap of the two peridotite bodies.

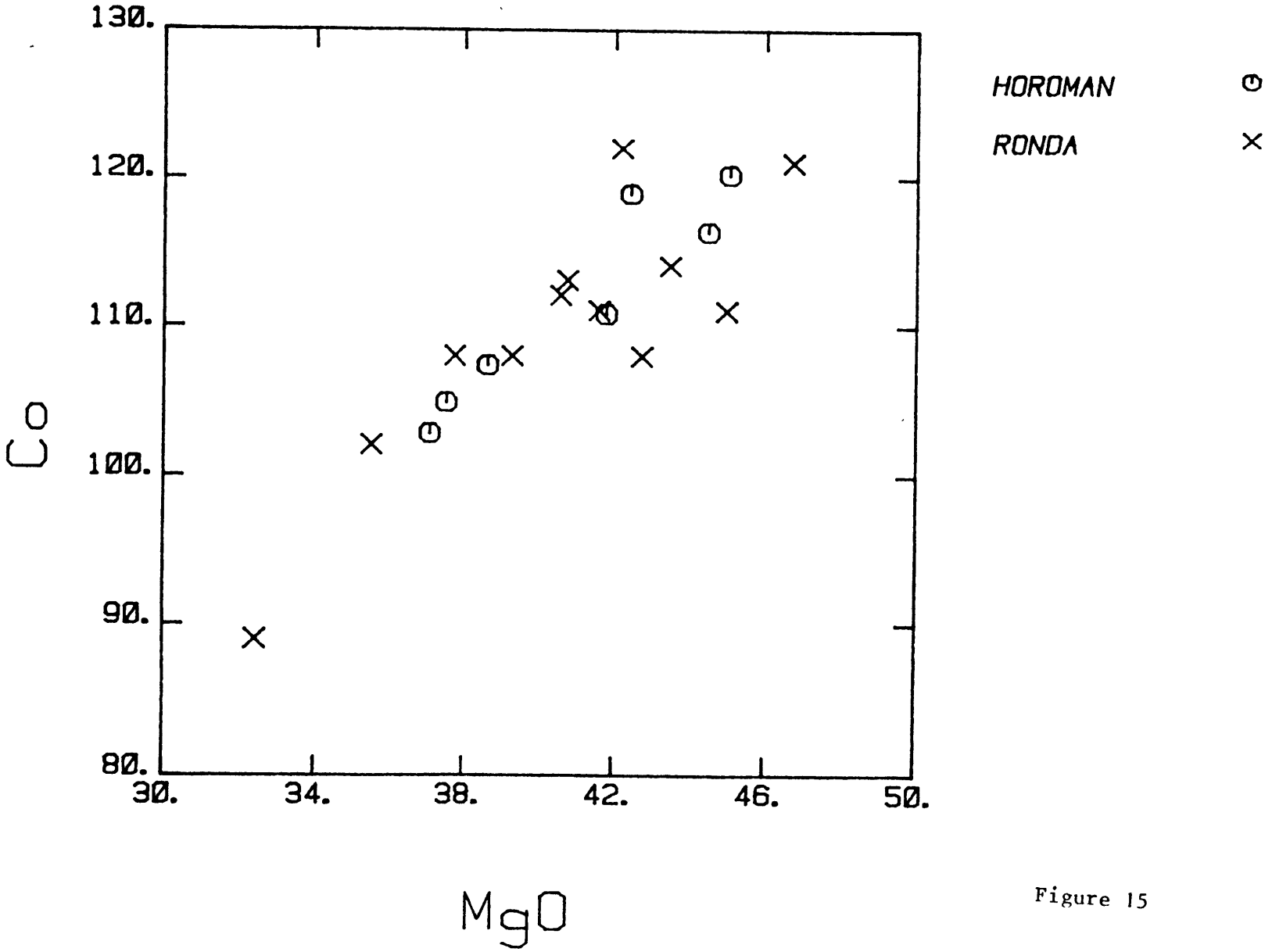

Figure 15

percent less than those determined with major elements, implying that the partition coefficient for Co is less than for Ni and that the simplification is not justified. This is consistent with experimentally derived partition coefficients that show D_{Ni} to be greater than D_{Co} for all ultramafic phases (Frey et al, 1978). Figure 15 shows the Horoman trend to be essentially identical to the Ronda peridotite trend.

Chromium, unlike Ni and Co, has a much more complex relationship with MgO for the Horoman samples (Fig. 16). Frey and others (1985), could not infer a bulk $D_{Cr}^{s/l}$ with the scatter of data from the Horoman peridotite (Fig. 16). They suggest the scatter may be due to heterogeneous distribution of spinel relative to the sample size. Chromium is generally thought to act as a compatible element as basalts have Cr in the ~500 ppm range. If one ignores the Horoman sample with very low bulk rock Cr (62130) a positive correlation does exist with MgO, and Cr appears to be acting compatibly. An analytic problem from INAA in bulk Cr seems likely for the anomalous sample but a mass balance calculation using the modes from Table 1 and mineral Cr_2O_3 compositions, indicates better than 90 percent accounting of Cr in all samples. (Furthermore, Cr was also analyzed for by XRF and 62130 had anomalously low abundance (~2090 ppm).) Considering mineral heterogeneities within samples and large errors in trace Cr in olivine, these calculations show that mineral compositions are consistent with the whole rock

Figure 16. Anhydrous MgO variation diagram for Cr in peridotites from Horoman (circles) and Ronda (crosses) for comparison showing more complex behavior than other compatible elements.

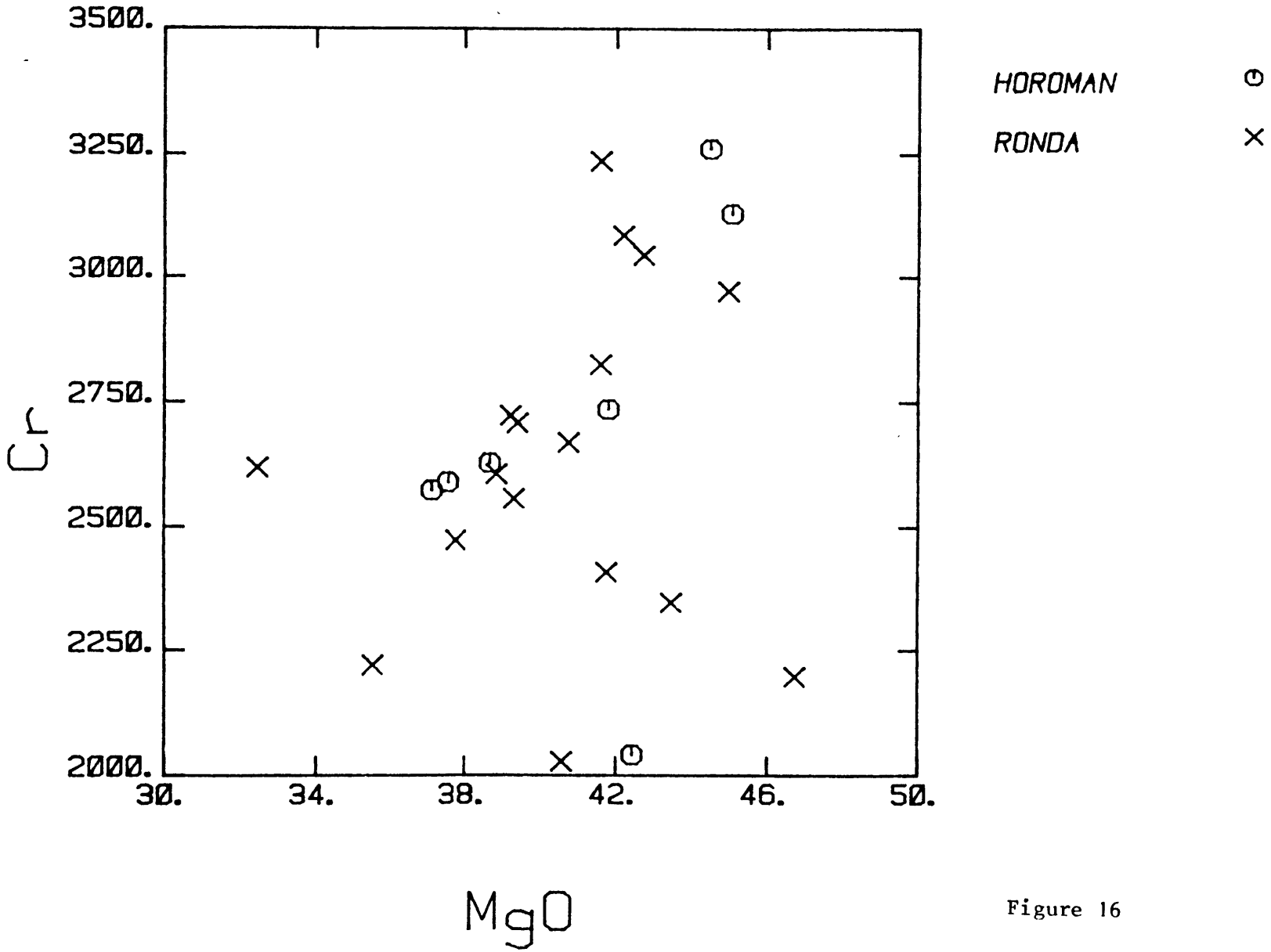
3500.
3250.
3000.
2750.
2500.
2250.
2000.
30.
34.
38.
42.
46.
50.
Cr
MgO
HOROMAN
RONDA

Figure 16

values. (This argument is slightly circular due to the fact that Cr is one of the eight elements used in the regression to obtain modes. Even with the weighting of the regression Cr is not a significant contributor to the multiple regression result and in looking at the residuals never appeared aberrant.) The Cr_2O_3 content in the minerals is not straight forward either (see the section on minerals for further discussion). Cr_2O_3 in orthopyroxene appears to be acting compatibly with partial melting (Fig. 17) and Cr_2O_3 in spinel also generally increases in the more depleted rocks with some exceptions (Fig. 18). The exact opposite relation was found in spinels and pyroxenes in a suite of lherzolite and harzburgite xenoliths from Austria (Kurat et al, 1980) indicating that Cr was acting incompatibly. But in clinopyroxene in the Horoman samples, Cr_2O_3 seems to rise and then fall again with degree of depletion perhaps representing a compatible element positive trend followed by subsolidus exchange reactions with spinel in the low-clinopyroxene harzburgites (Fig. 19). Perhaps a better way of representing how Cr is partitioned in the respective minerals in each sample is to utilize the mass balance calculation and plot the proportion of the total Cr budget that is in each phase (Fig. 20). In general the variation of the Cr budget in the minerals does not appear significant in the more enriched rocks. Total Cr in clinopyroxene tends to decrease with depletion while orthopyroxene and spinel act more antithetical and have more complex variation.

Figure 17. Mg# of orthopyroxene (Mg/Mg+Fe) versus Cr_2O_3 in orthopyroxene for Horoman peridotites (analyzed for this study at MIT, shown in circles, by Obata on the same samples for comparison, shown in X's). General positive corellation is shown by MIT data but Obata data shows essentially no corellation.

Figure 18. Cr_2O_3 in the bulk rock (roughly a monitor of depletion, Fig. 16) versus Cr_2O_3 in spinel for only MIT data showing general Cr increase in spinel in the more depleted rocks. The exceptions are sample 62130 with exceptionally low bulk Cr_2O_3 (see text) and sample 62128 with Cr in the spinel lower than expected.

Figure 19. Mg# of clinopyroxene (Mg/Mg+Fe) versus Cr_2O_3 in clinopyroxene for Horoman peridotites with data for this study (circles) and data from Obata on the same samples (X's) for comparison. The trend appears to show Cr acting compatibly with melting except for the most depleted samples perhaps representing sub-solidus reequilibration reactions with spinel in low clinopyroxene harzburgites.

Figure 20. Chromium budget with respect to stratigraphic height (in meters) for clinopyroxene, orthopyroxene and spinel (solid lines) and total bulk Cr (anhydrous) in ppm with stratigraphic height (broken line). See text for further explanation and discussion.

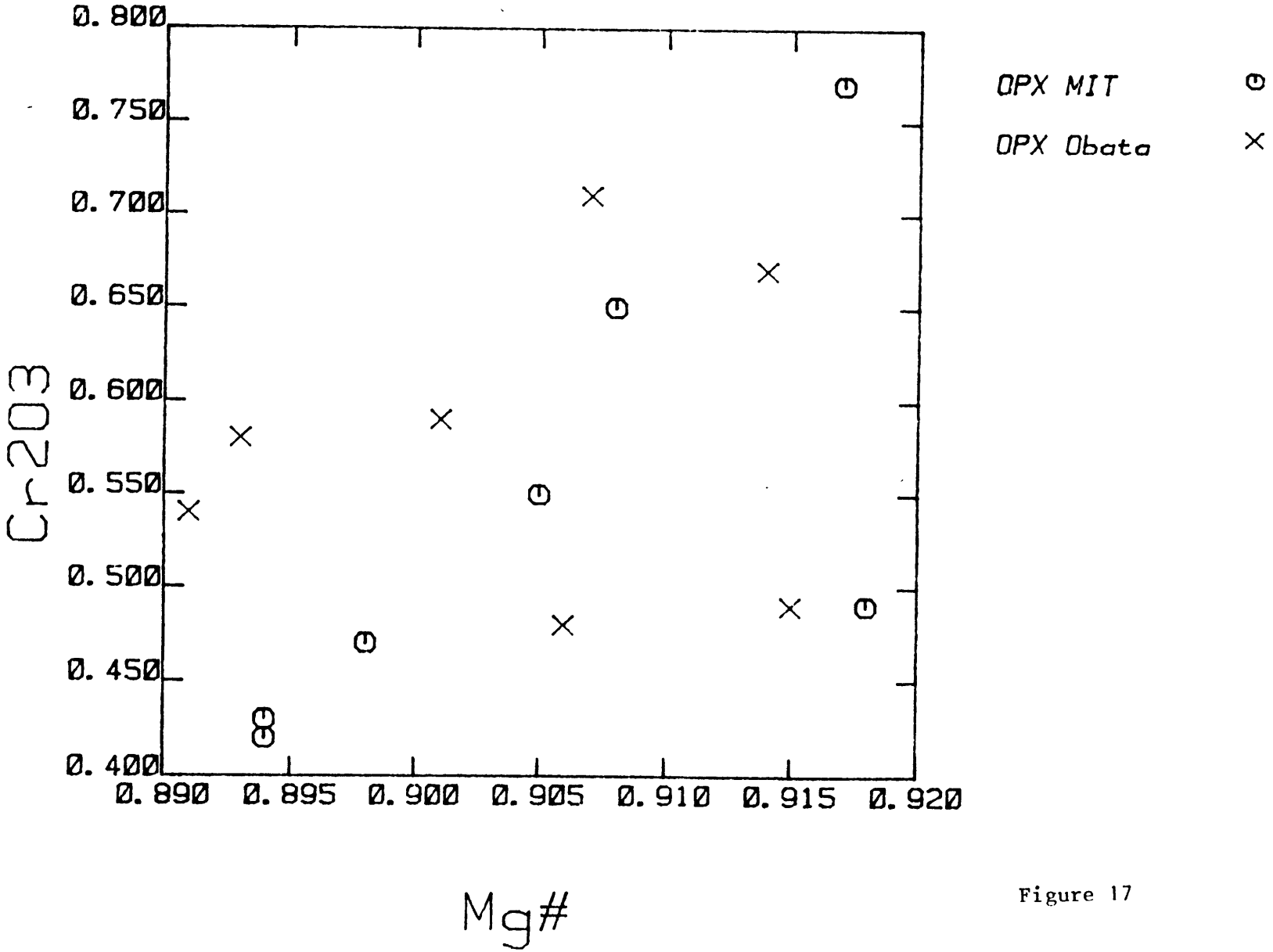
0.800
0.750
0.700
0.650
0.600
0.550
0.500
0.450
0.400
Cr2O3
0.890
0.895
0.900
0.905
0.910
0.915
0.920
Mg#
OPX MIT
OPX Obata

Figure 17

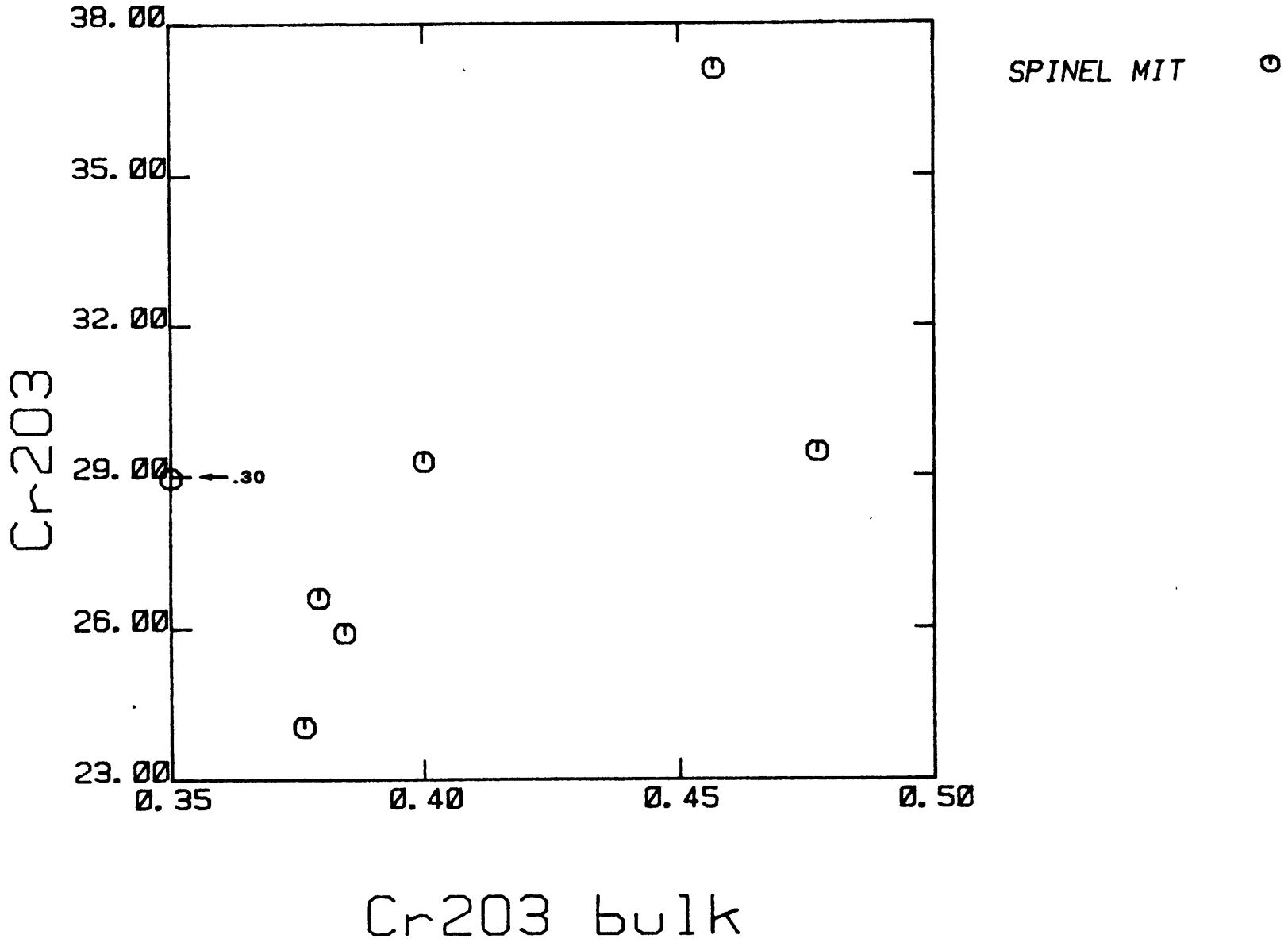
38.00
35.00
32.00
29.00
26.00
23.00
Cr203
.30
0.35
0.40
0.45
0.50
Cr203 bulk
SPINEL MIT

Figure 18

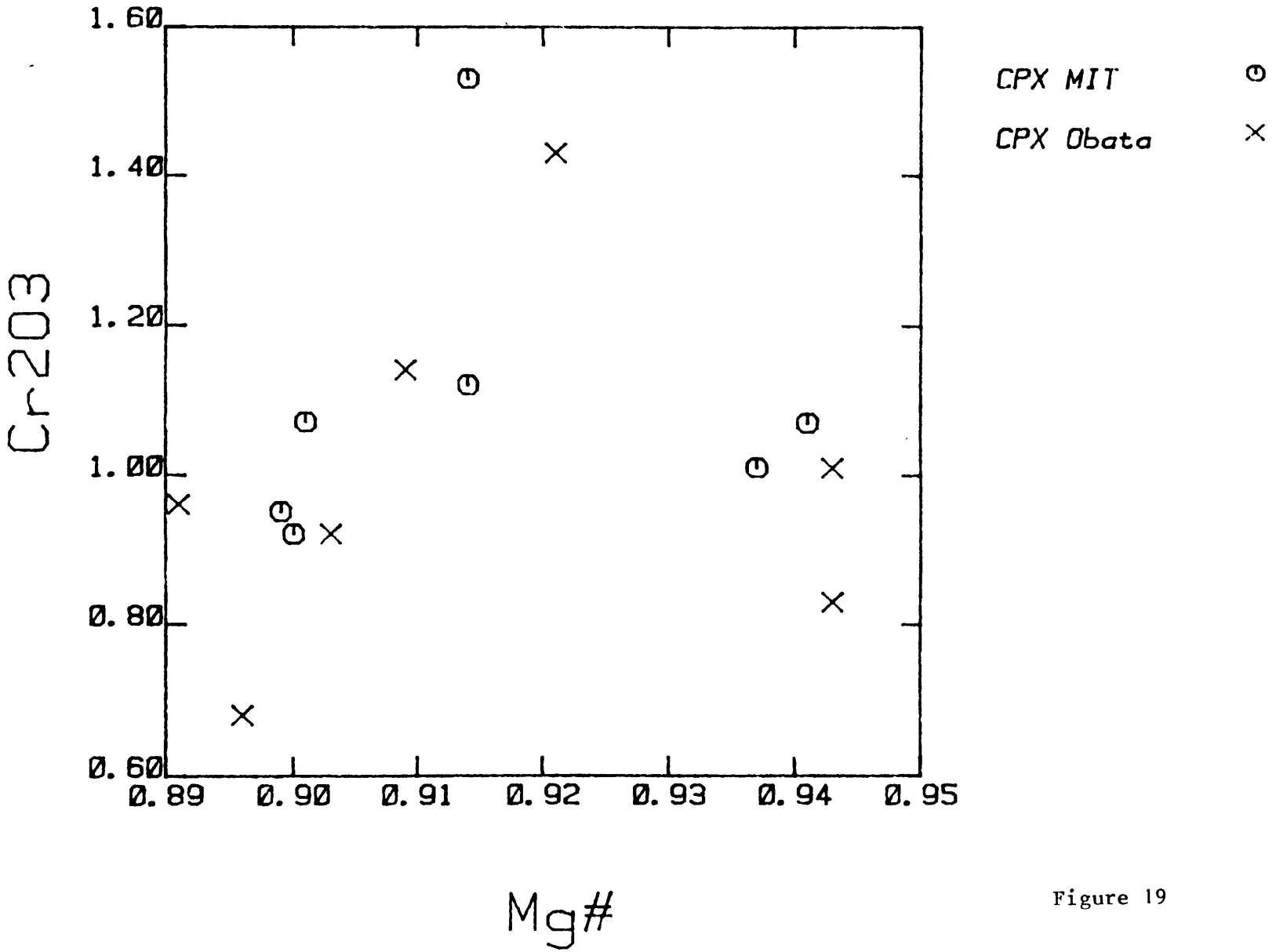
1.60
1.40
1.20
1.00
0.80
0.60
Cr2O3
0.89
0.90
0.91
0.92
0.93
0.94
0.95
Mg#
CPX MIT
CPX Obata

Figure 19

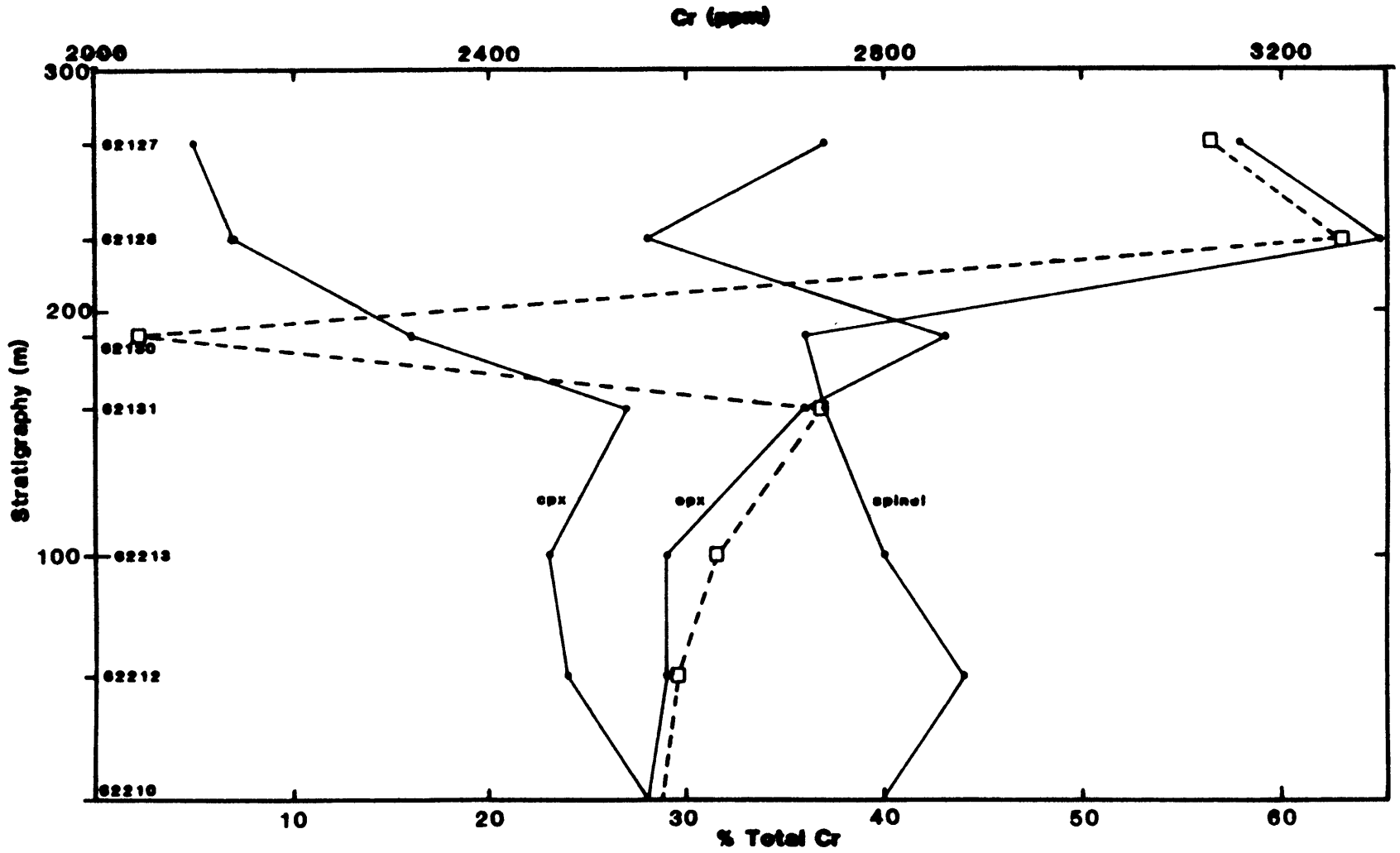
Cr (ppm)
2000
2400
2800
3200
300
200
100
62127
62128
62130
62131
62213
62212
62210
Stratigraphy (m)
cpx
cpx
spinel
10
20
30
40
50
60
% Total Cr

Figure 20

Total Cr is also plotted in Figure 20. In general the shape of the pattern is similar to Cr in orthopyroxene but the negative Cr spike in 62130 is not reflected in any anomalous partitioning.

It has been suggested that Cr and particular Cr content in spinel has a major bearing on exact position of the invariant point of spinel lherzolite melting and on the phase diagrams of ultramafic rocks (Sinigoi et al, 1980). These authors propose that the spinel phase volume expands at the expense of the olivine phase volume if the spinel contains Cr. The invariant point would then move slightly as the spinels became more Cr-rich with melting creating the possibility that spinel would become refractory and melting would occur based entirely on olivine, orthopyroxene and clinopyroxene phase relations. These type of melting relationships, if true, may produce some of the complications seen in the Cr variation diagrams.

Moderately Incompatible Trace Elements - Sc, V, Mn, Zn, Ga

Scandium and vanadium are usually considered to be compatible in clinopyroxene (e.g. $D^{s/l} > 1$) but generally have bulk partition coefficients less than one as they are incompatible in olivine. These two elements behave similarly in olivine, clinopyroxene and orthopyroxene with V having slightly smaller D's in these minerals, but V partitions into plagioclase, and particularly spinel, much more readily than Sc. Abundances of both of these elements in the Horoman peridotite are inversely correlated and

linear with MgO content (Fig's. 21 and 22) and essentially overlap the trend produced by the Ronda peridotites. This trend is consistent with equilibrium melting of a moderately compatible element. The gallium abundance is similarly negatively correlated with MgO content (Fig. 23) but shows more scatter and is conspicuously offset from the Ronda trend. The concentrations of Ga are quite low in these rocks so the possibility of analytical errors is rather large. Gallium is predicted to act incompatibly in all the peridotite phases (Goodman, 1972). Manganese abundance is also inversely correlated with MgO (Fig. 24) but should have a bulk partition coefficient very close to one (Sun, 1979). The zinc data shows a great deal of scatter with respect to MgO content (Fig. 25). Zinc is expected to act moderately incompatibly (Frey et al, 1985), although an argument in support of negative correlation in Figure 25 would be dubious based on the Horoman data. It is likely that Zn is complicated by inhomogeneous sampling of Cr-spinel similar to the complications seen in Cr but more pronounced. The presence of sulfides (see Ni section) may also complicate Zn partitioning.

The third transition element abundances in the Horoman peridotites have been normalized to "primitive" mantle estimates of Jagoutz et al (1979) and plotted versus atomic number (Fig. 26). The Ni/Co ratio and Yb/Sc ratios of the Jagoutz estimates are chondritic making normalization to these values compatible with interpretations based on REE

Figure 21. Anhydrous MgO variation diagram for Sc in peridotites from Horoman (circles) and Ronda (X's) for comparison.

Figure 22. Anhydrous MgO variation diagram for V in peridotites from Horoman (circles) and Ronda (X's) for comparison.

Figure 23. Anhydrous MgO variation diagram for Ga in peridotites from Horoman (circles) and Ronda (X's) for comparison. The conspicuous offset in the Horoman and Ronda trends is likely an analytic effect due to very low abundances of Ga in all these rocks.

Figure 24. Anhydrous MgO variation diagram for MnO in peridotites from Horoman in weight percent.

Figure 25. Anhydrous MgO variation diagram for Zn in peridotites from Horoman (circles) and Ronda (X's) for comparison. No correlation exists (see text).

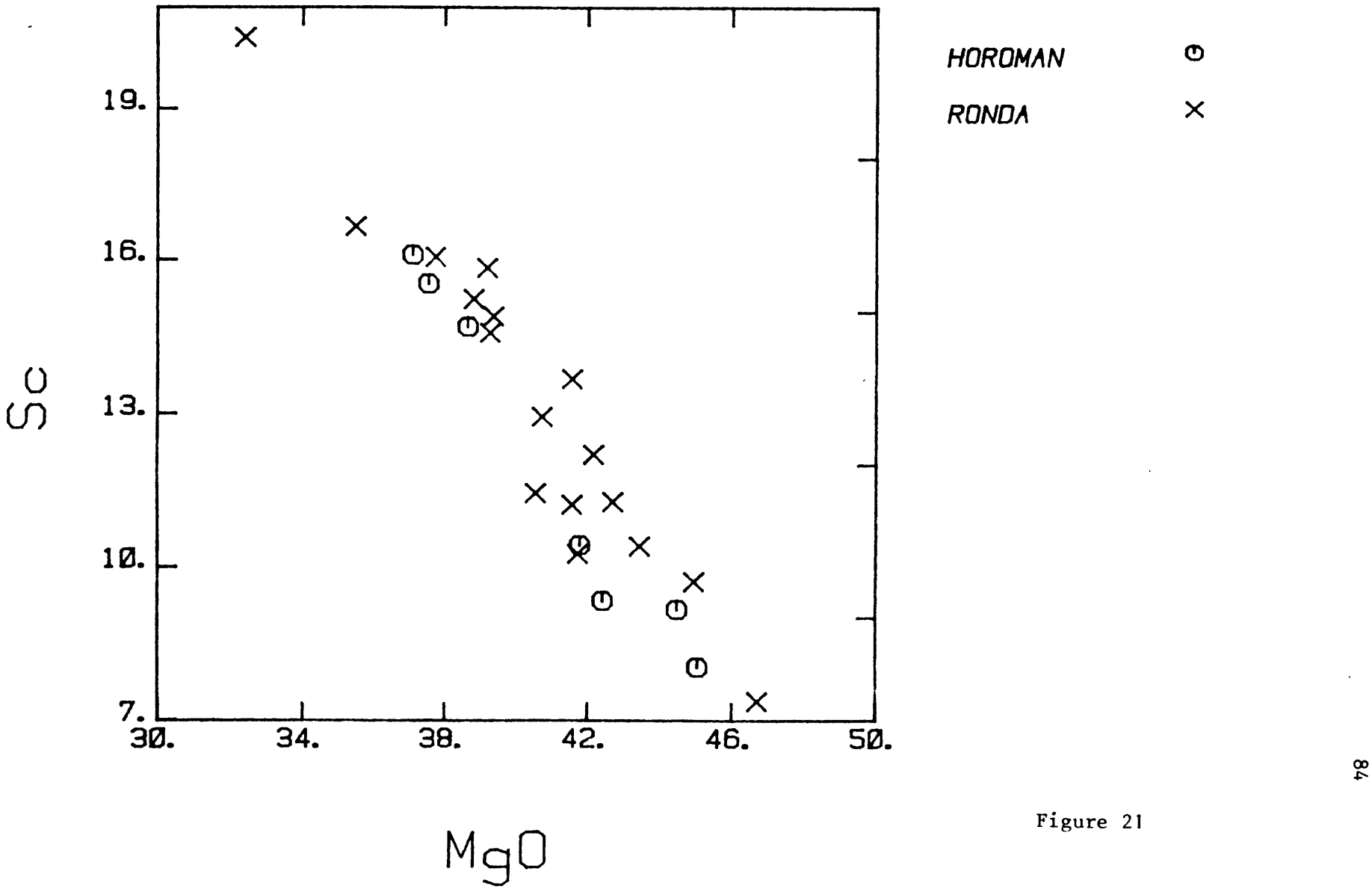

Figure 21

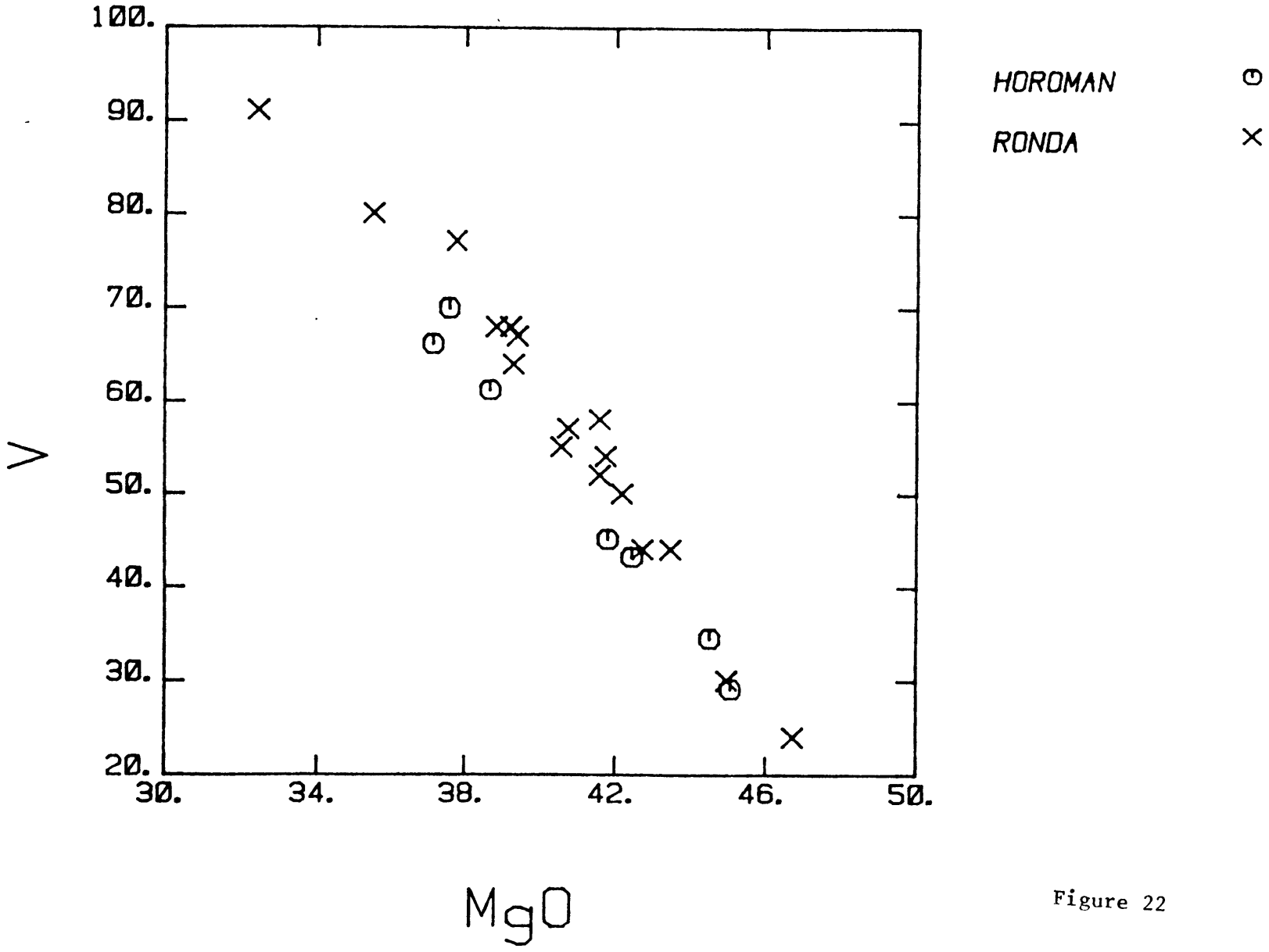

Figure 22

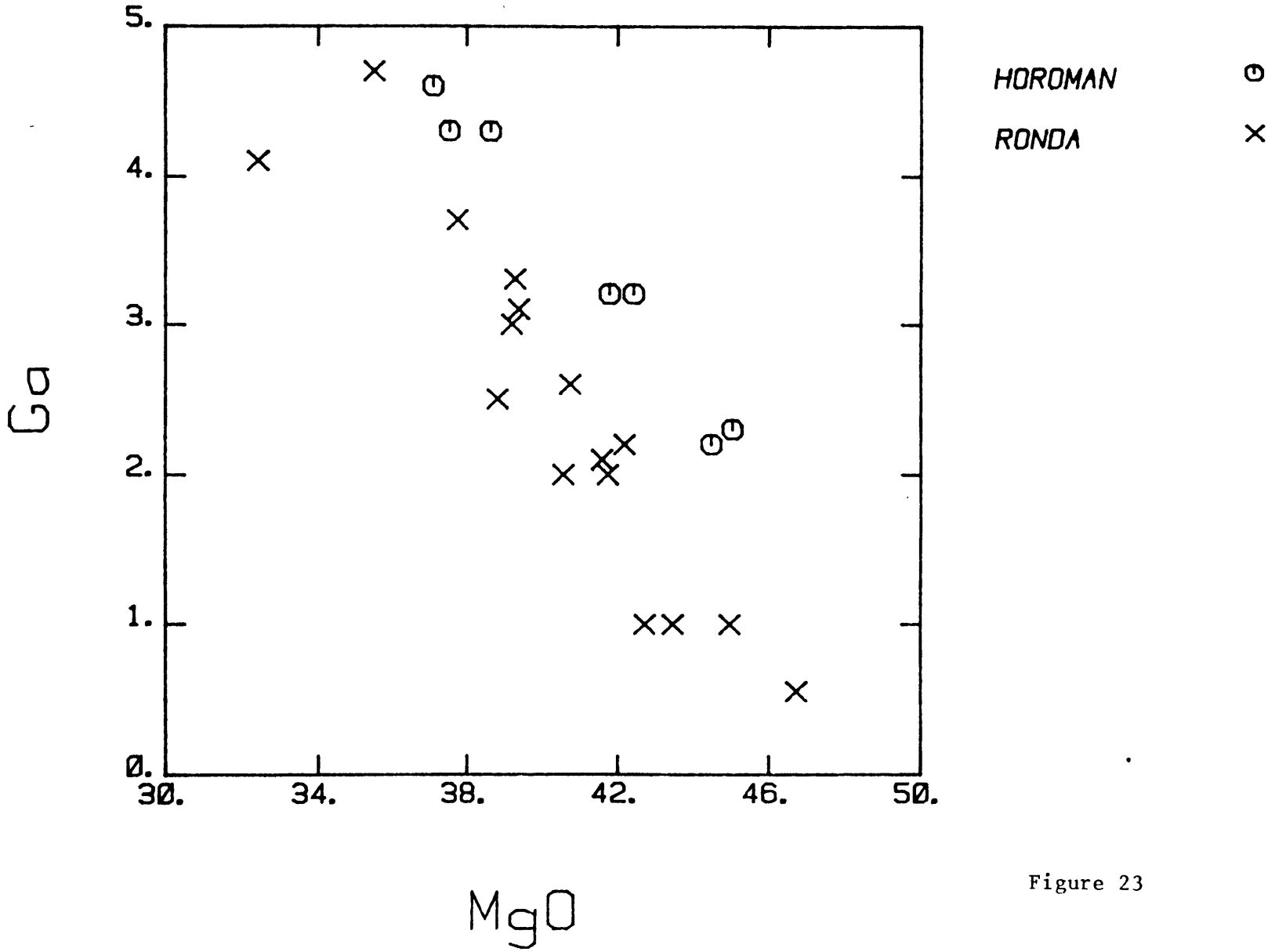

Figure 23

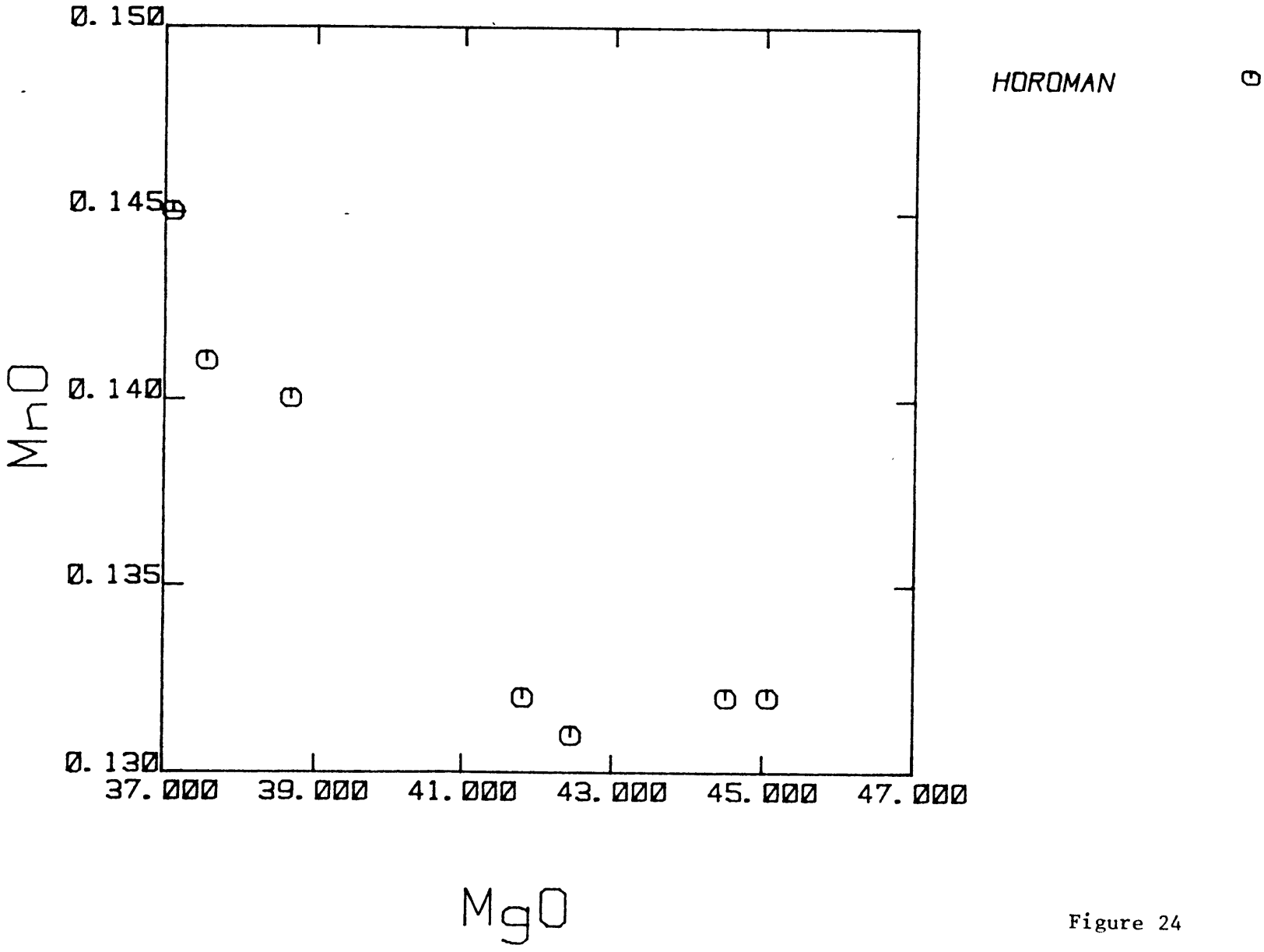
HOROMAN
MnO
0.150
0.145
0.140
0.135
0.130
37.000
39.000
41.000
43.000
45.000
47.000
MgO

Figure 24

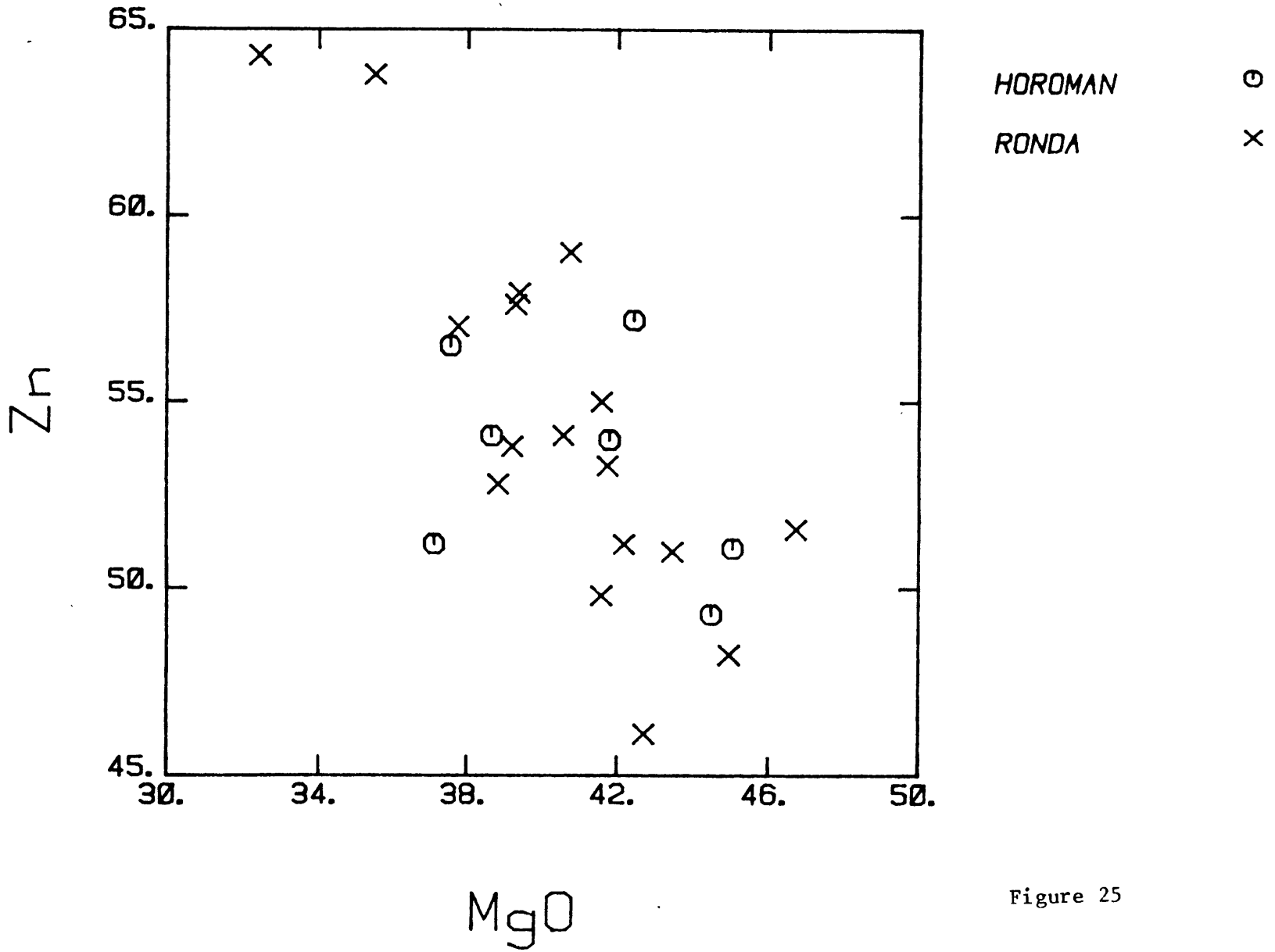

Figure 25

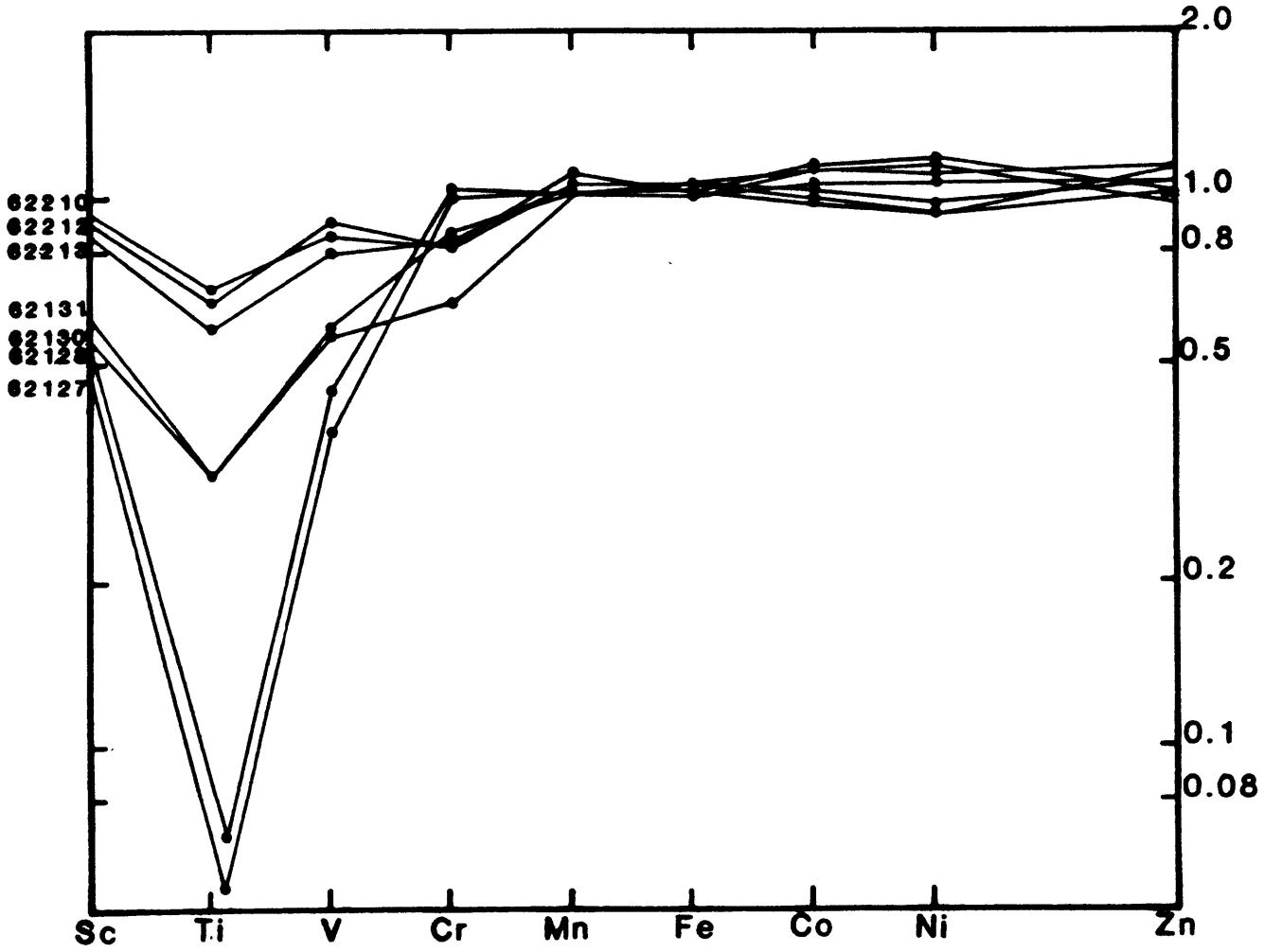

Figure 26. Diagram of third transition element abundances normalized to "primitive" mantle estimates of Jagoutz et al (1979) plotted versus atomic number.

diagrams. The patterns are essentially flat and near one, from Cr to Zn. The patterns are perturbed and show depletions at Sc, V and especially Ti. These depletions are more pronounced than transition element patterns or other peridotite bodies (Ottonello et al, 1984a; Ottonello et al, 1984b; Bonatti et al, 1986). the patterns are in general consistent with the REE data, as the most depleted rocks in REE are also most depleted in Sc, V and Ti and enriched in Ni and Co while the inverse is true for those samples most enriched in REE.

Highly Incompatible TE - La, Sm, Eu, Y, Yb, Zr, Sr

Highly incompatible trace elements are very sensitive to subtle changes in melting degree and to the melting process. The elements listed above have a wide range in bulk partition coefficients based on literature values but at Horoman all act very much the same. All these elements have near linear negative correlation with MgO content (Fig's. 27 to 33). These trends also overlap relatively closely with the Ronda data. These elements are also positively correlated with each other and with other melt sensitive major elements such as CaO and Al_2O_3. For most melting models one would not expect linear variation diagrams but it's difficult to draw anything but straight lines through this data, with the possible exception of La. Zr data for the two depleted harzburgite samples could not be obtained due to extremely low concentrations. These trends are compatible with interpretation of the Horoman

Figures 27-33. Anhydrous MgO variation diagrams for incompatible elements La, Sm, Eu, Y, Yb, Zr, and Sr in peridotites from Horoman (circles) and Ronda (X's) for comparison. All these elements show near linear negative correlation with MgO content with more scatter than more compatible elements and general overlap between the Horoman and Ronda trends.

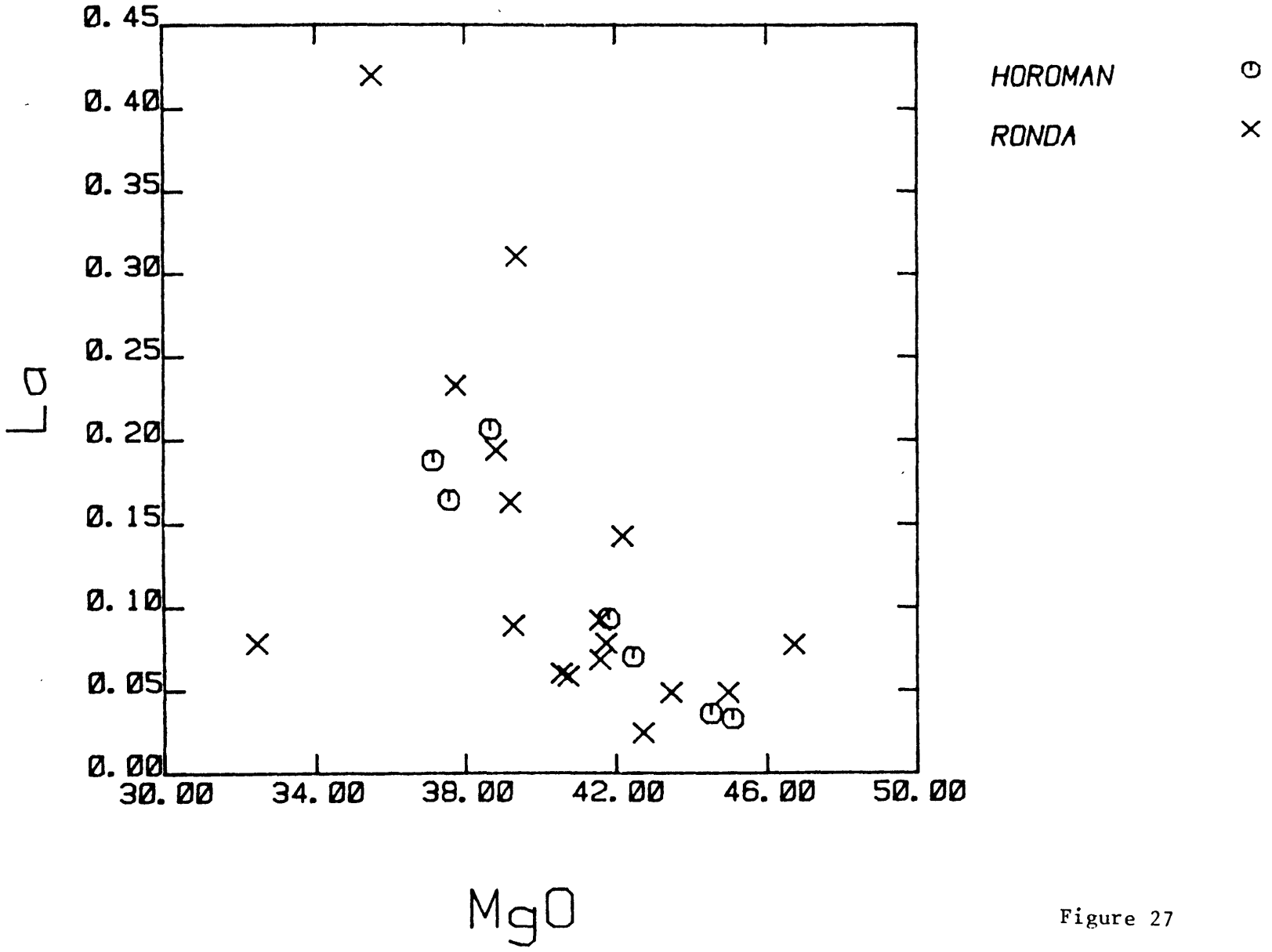
0.45
0.40
0.35
0.30
0.25
0.20
0.15
0.10
0.05
0.00
La
30.00
34.00
38.00
42.00
46.00
50.00
MgO
HOROMAN
RONDA

Figure 27

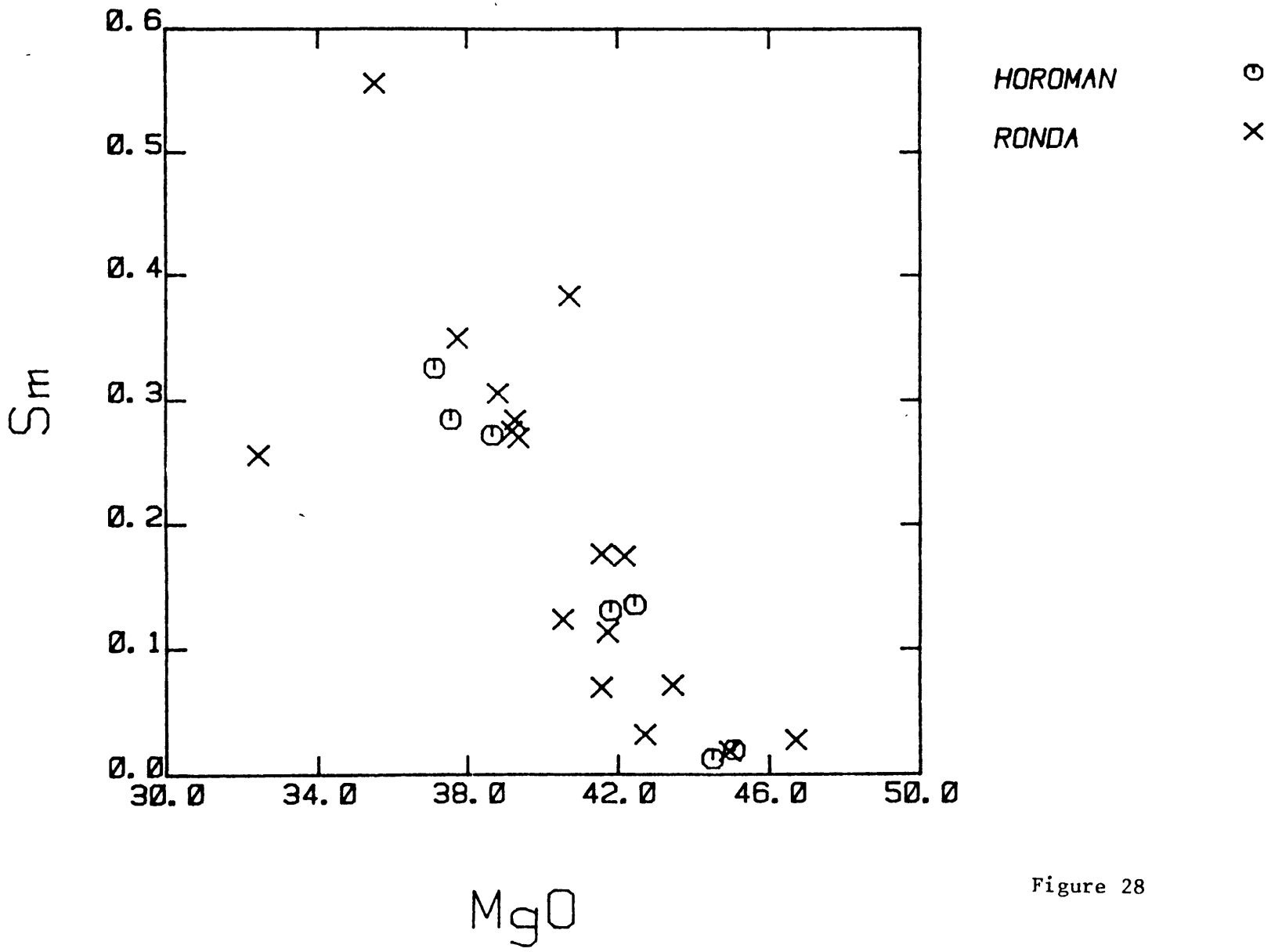

Figure 28

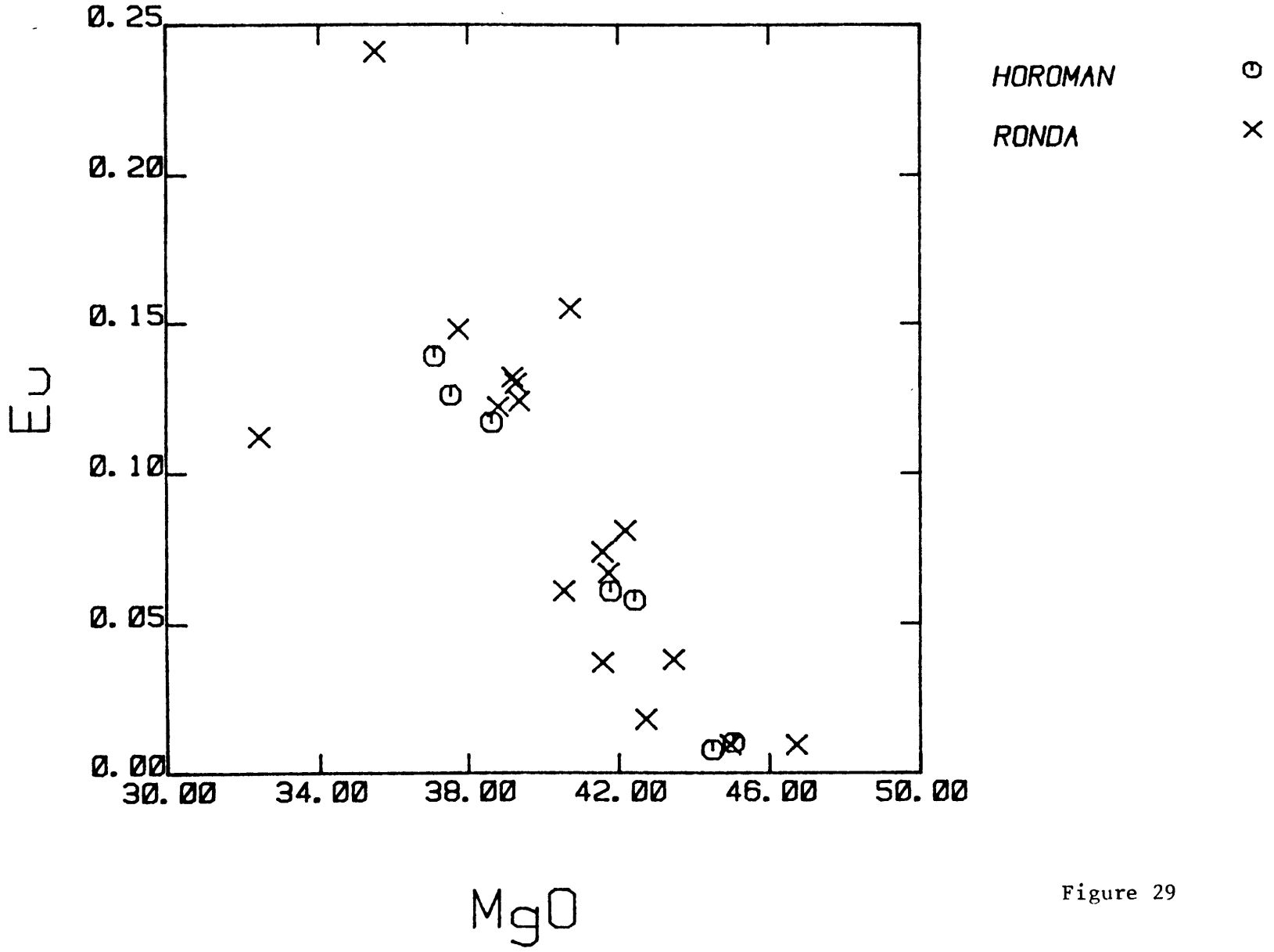
0.25
0.20
0.15
0.10
0.05
0.00
EU
30.00
34.00
38.00
42.00
46.00
50.00
MgO
HOROMAN
RONDA

Figure 29

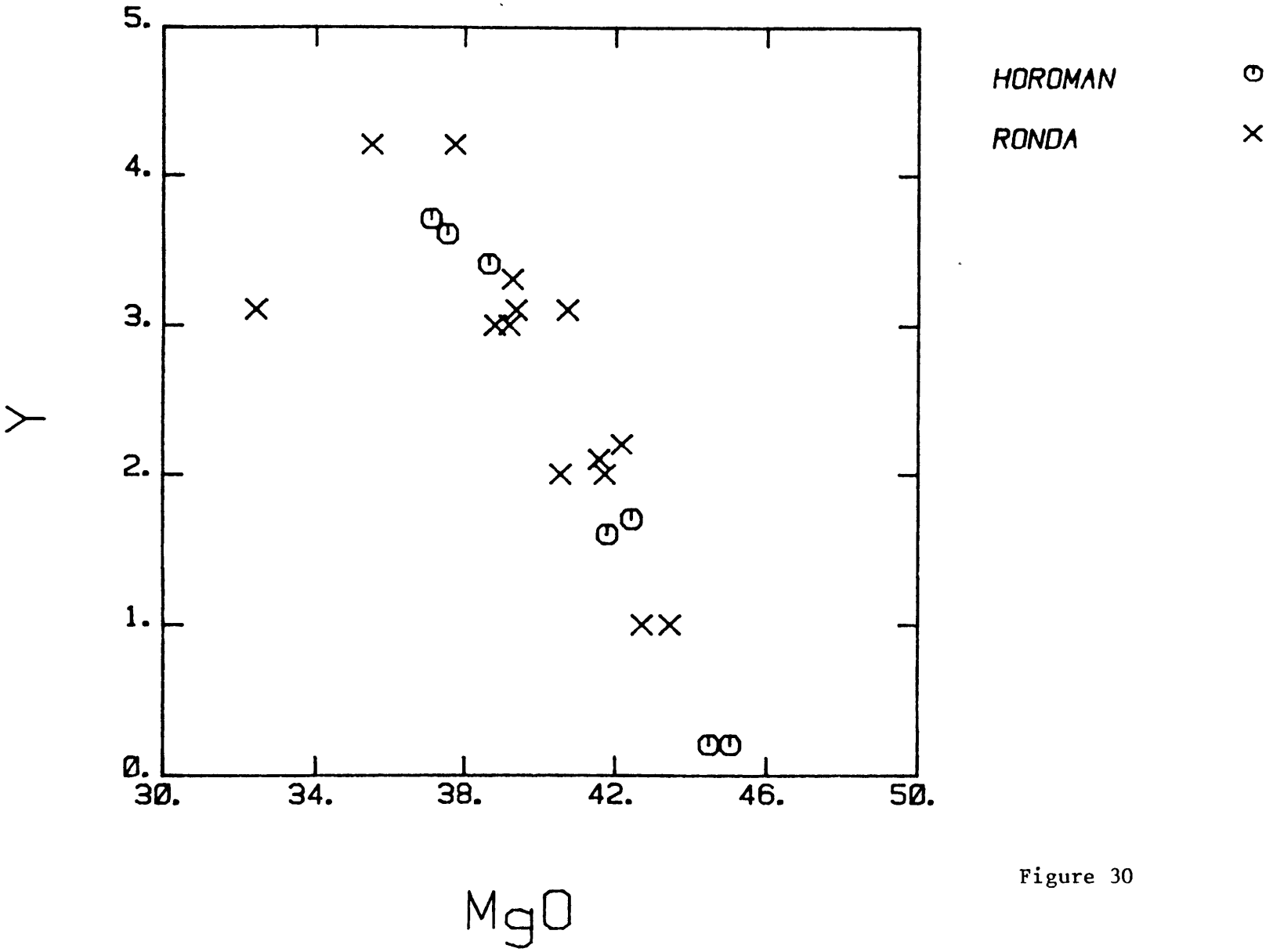

Figure 30

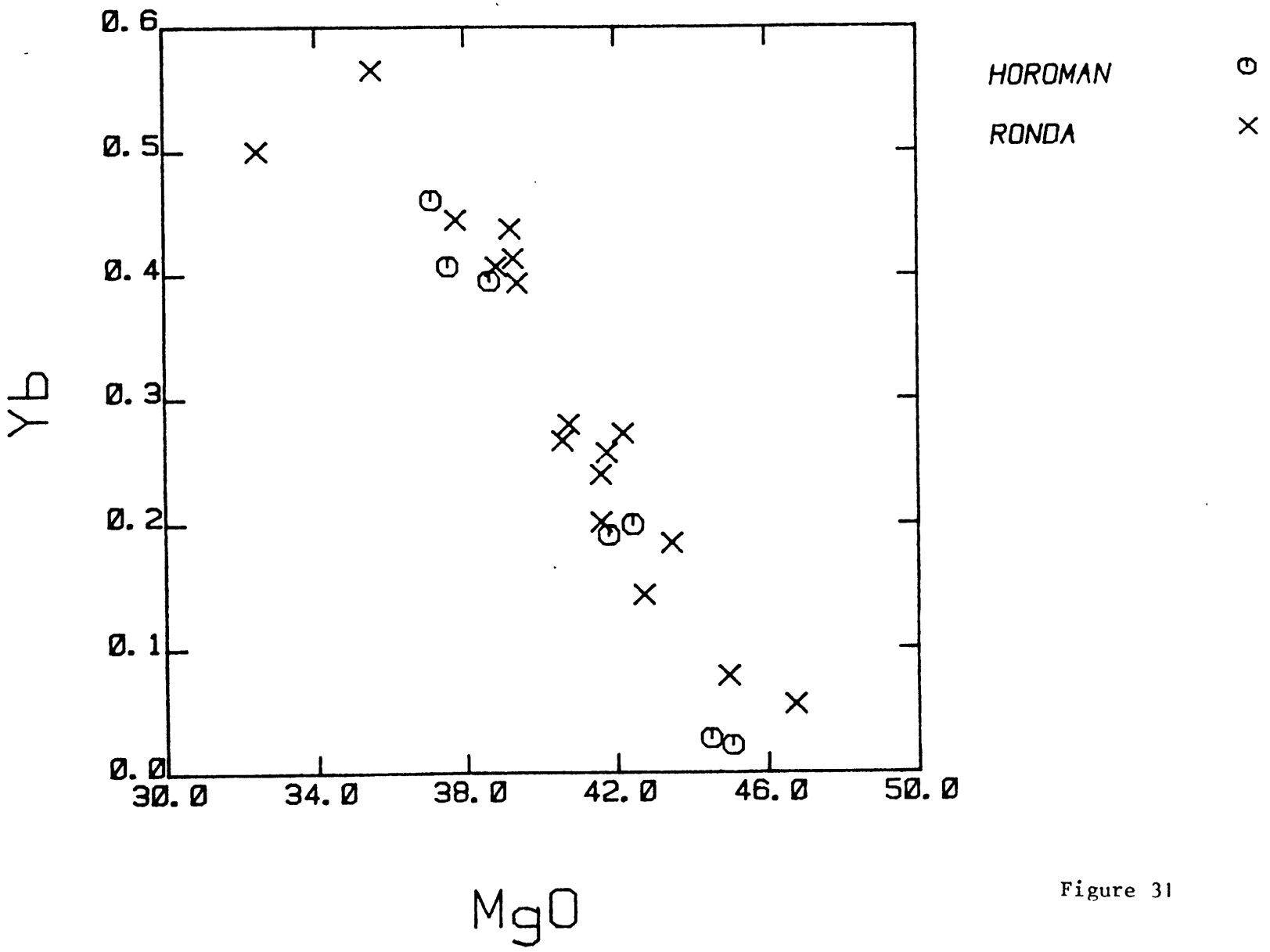

Figure 31

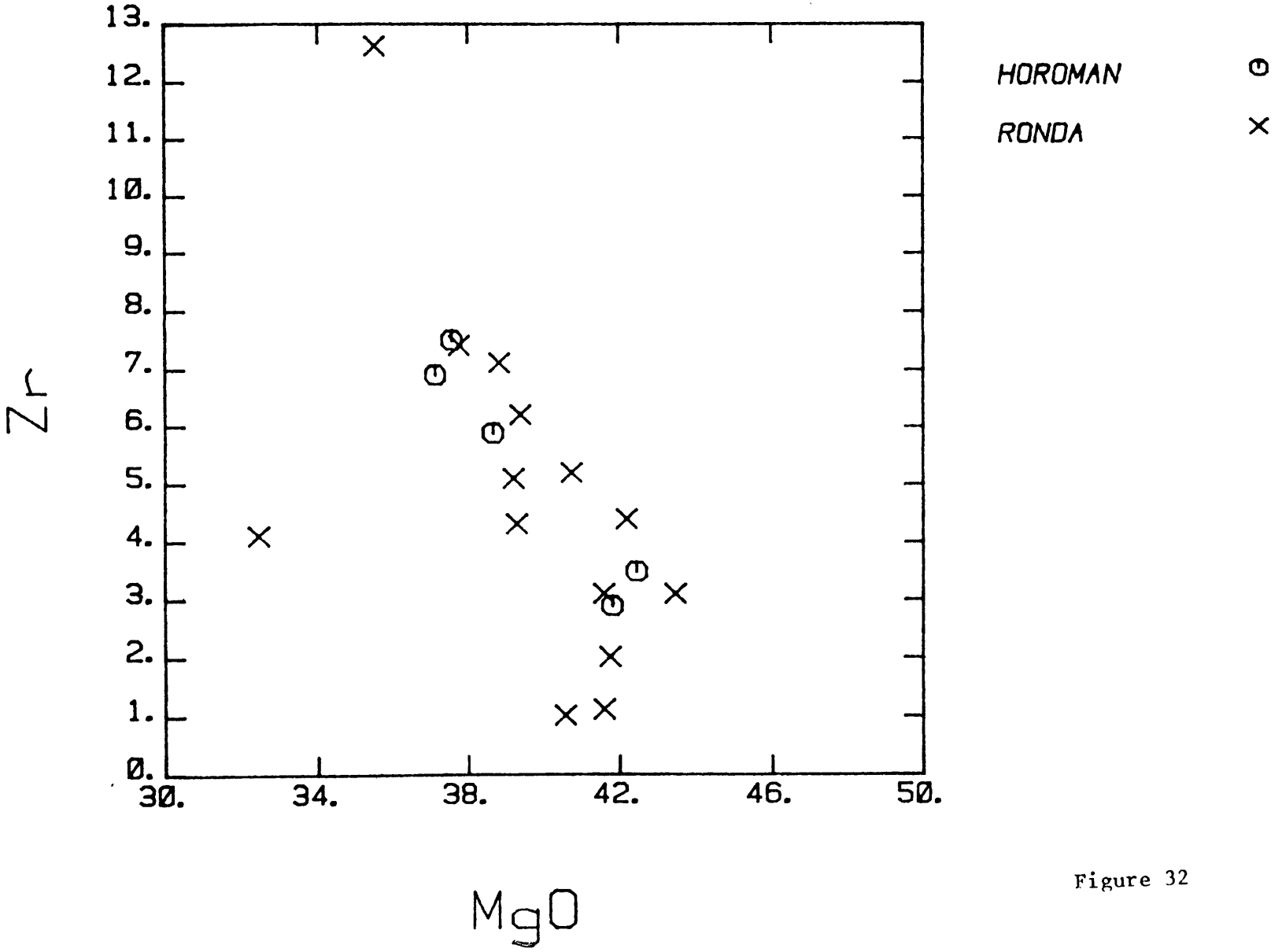

Figure 32

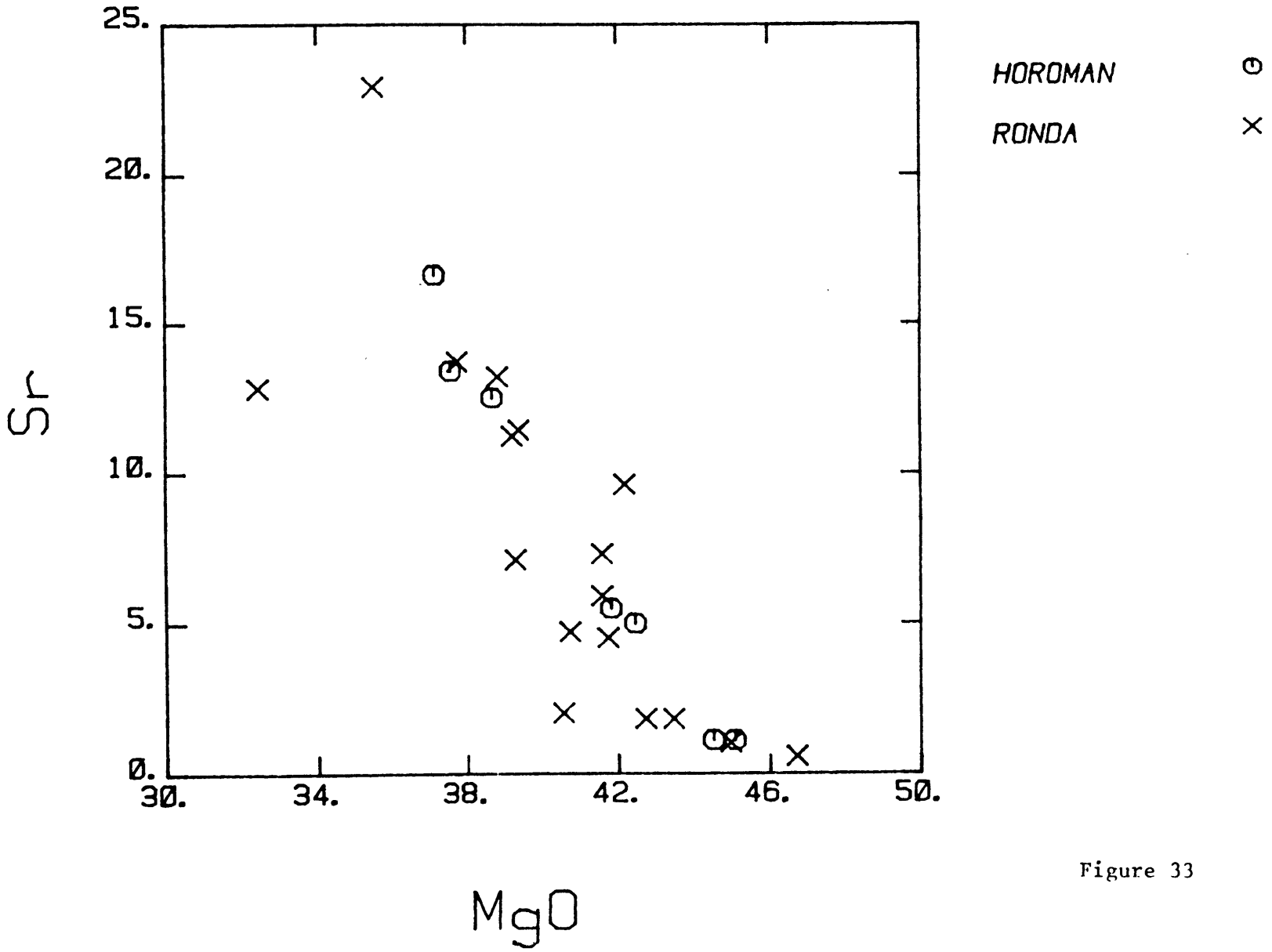

Figure 33

peridotites as residues from varying degrees of partial melting but certainly not as residues of simple equilibrium batch melting. This could not be said for the other elements discussed up to this point. Suen (1978), discussing the Ronda peridotites used a plot of Sr versus La as evidence for no melting in the plagioclase lherzolite field. A linear correlation with ~45 degree slope on a log-log plot between these two elements implied that La and Sr had approximately the same partition coefficient. If melting in the plagioclase facies occurred, Sr (compatible in plagioclase) should show a greater partition coefficient. In the Horoman peridotites this argument is equivocal. Figure 34 of Sr abundance versus both La and Eu shows a better correlation with Eu than La but with both elements more incompatible than Sr.

Rare Earth Elements

Based on rare earth elements, the Horoman peridotites break into three distinct groups (Fig. 35). These groups consist of three plagioclase lherzolites (62210, 62212 and 62213), two more depleted rocks labelled here transitional peridotites (62131 and 62130), and two very depleted harzburgites (62128 and 62127). Very little variation exists within groups. The plagioclase lherzolites show very little fractionation relative to chondrites and have patterns quite parallel except for a slight enrichment in LREE in sample 62213. The most enriched sample based on major elements (62210) is also the most enriched based on

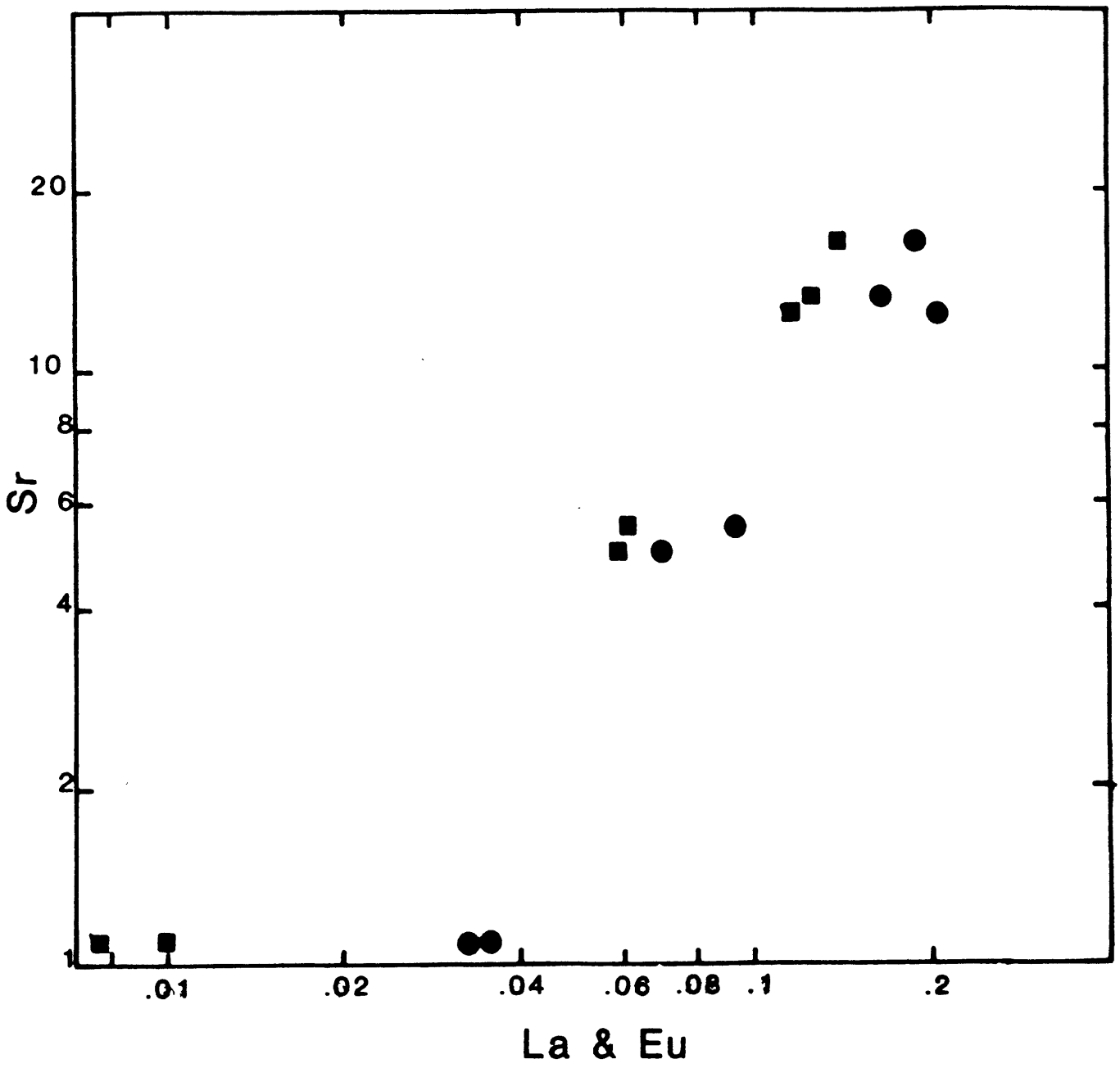

Figure 34. Anhydrous log-log variation diagram of La (circles) and Eu (squares) versus Sr. Corellation coefficient and Y-intercept of the La trend are 0.958 and -1.45 respectively, and 0.990 and -0.55 for Eu. This relation implies that La is the most incompatible of these three elements, then Eu, with Sr the most compatible.

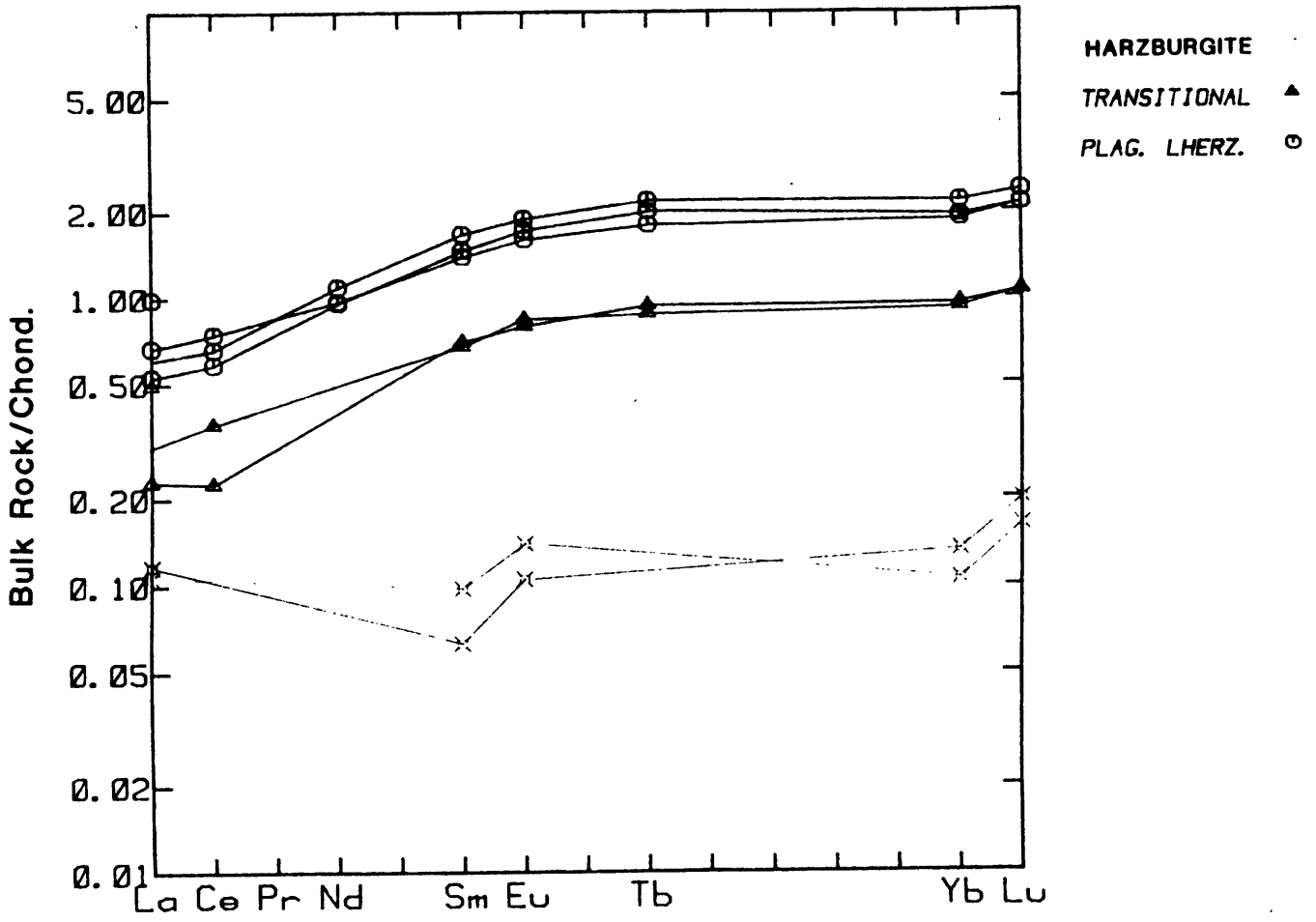

Figure 35. Chondrite-normalized plot (Boynton, 1984) of anhydrous REE abundances in Horoman peridotites. The three most enriched samples, plagioclase lherzolites, are indicated by circles; two intermediate samples, here called transitional peridotites, are indicated by triangles; the two most depleted samples, harzburgites, are indicated by square crosses.

the majority of the REE. The transitional peridotites have patterns that are practically indistinguishable in REE heavier than Sm with the more enriched sample by major elements slightly more enriched in LREE. The patterns of the transitional peridotites are generally parallel to the plagioclase lherzolites but more depleted. The harzburgites are very depleted with a near flat or slightly U-shaped pattern with $(La/Sm)_{CN} > 1$. (Re-analyses of Ronda harzburgite samples R771 and R893 also produced U-shaped patterns.) The harzburgite patterns also show what is likely to be a positive Eu anomaly based on the steep positive slope from Sm to Eu. Unfortunately, no data was obtained for any REE between Eu and Yb to be certain of the anomaly.

Figure 36 is a compilation of REE data from a variety of locations plotted on a chondrite normalized diagram. The data presented is predominantly from alpine peridotites although several ophiolitic and abyssal peridotites are included as well. Sample 62210 is shown in a field made up of the most enriched samples analyzed at eight other locations. (Locations and references for all the patterns in Figure 36 are included in the figure and caption.) The Baldissero sample (shown separately because it deviates to some degree from the field) appears to be unrealistically enriched. It is speculated that like several samples in the Ronda suite, this sample was collected in close proximity to a mafic layer and was affected by the process that produced

Figure 36. Chondrite-normalized plot (Boynton, 1984) of REE abundances of compilation of a number of data from primarily alpine peridotites. Horoman samples 62210 and 62127 are shown by thick lines in a field of most enriched and most depleted peridotites respectively, from a variety of locations from around the world. Four other samples are shown individually as they deviate from the two fields: Ba-4a and F-66, spinel lherzolites from Baldissero, W. Alps (Ottonello et al, 1984a); F-59b, a spinel lherzolite from Balmuccia, W. Alps (Ottonello et al, 1984a); and Li11a, a spinel lherzolite from Liguria (Ottonello et al, 1984b). The enriched field is defined by nine lherzolites: F-60 from Balmuccia, W. Alps (Ottonello et al, 1984a); 14R from Liguria (Ottonello et al, 1984b); R717 from Ronda (Frey et al, 1985); BB5 from Beni-Bouchera, Morocco (Loubet and Allegre, 1979); 70-367 from Lherz, W. Alps (Loubet and Allegre, 1982); 71-335 from Freychinede, W. Alps, (Loubet and Allegre, 1982); 775 from Lanzo, W. Alps (Loubet and Allegre, 1982); Z-92 from Zabargrad Island, Red Sea (Bonatti et al, 1986); and 62210 from Horoman. The depleted field consists of ten harzburgites: R771 and R893 from Ronda (Frey et al, 1985); K21-P1 from Samail (Pallister and Knight, 1981); 9 from Troodos (Menzies, 1976); A-7 from Puerto Rico (Frey, 1983); PCC-1 from Cazadero, California (Frey, 1983); Josephine, Oregon (Frey, 1983); V-209 from Vourinos (Noiret et al, 1981); and 62127 from Horoman.

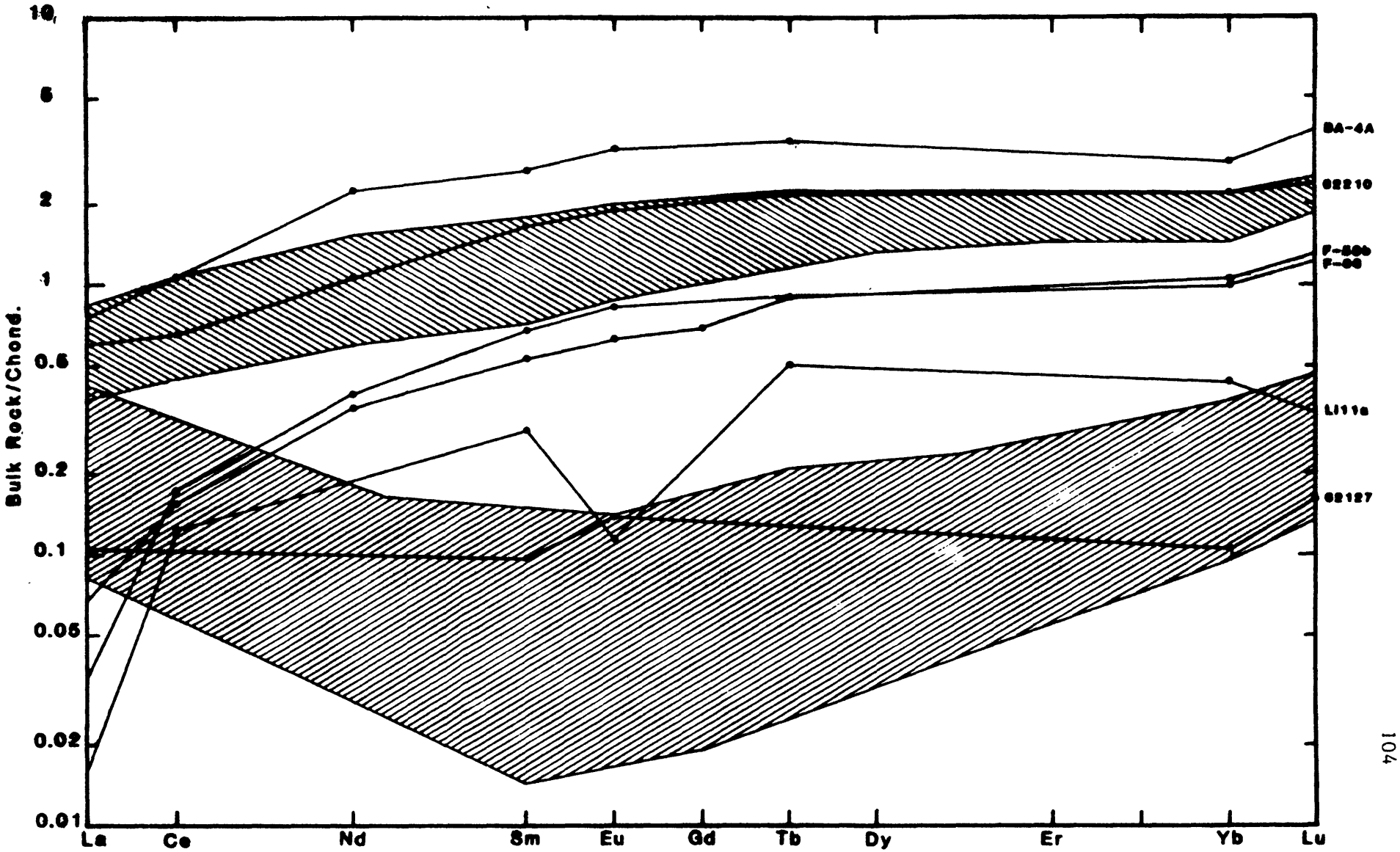
10
5
2
1
0.5
0.2
0.1
0.05
0.02
0.01
Bulk Rock/Chond.
La
Ce
Nd
Sm
Eu
Gd
Tb
Dy
Er
Yb
Lu
BA-4A
82210
F-806
F-86
LI11a
82127

Figure 36

the layer (Frey et al, 1985). The variation in this field is really very small especially considering how few analyses have been made. At several of the massif locations only a few analyses have been made, implying that it is likely that more enriched samples may exist at these locations. The range in the field can best be explained by varying small degrees of melting from a relatively homogeneous source with ~2.3X chondrites that may or may not be slightly LREE depleted. Considering the analytical problems, the parallel nature of individual patterns of these enriched peridotites, particularly in the HREE, is notable. This may allude to the fact that the first melting process is widespread and relatively uniform throughout the mantle, perhaps within the spinel lherzolite stability field. Modal information is not available for all the samples but all of the enriched peridotites are spinel lherzolites with or without plagioclase. Remembering what was said about the presence of plagioclase in terms of the possibility of trapped melt, the general character of these enriched patterns may tell us something about the nature of the trapped melt. One would expect a melt component to be LREE enriched but none of these generally enriched patterns give any indication of LREE enrichment.

Also in Figure 36 are REE patterns of depleted peridotites from many of the same regions. These patterns tend to be more complex than the enriched peridotites and more variable with LREE and HREE spanning more than one

order of magnitude. Sample 62127 is plotted in a field made up of nine other such patterns from ten localities. All of these are harzburgites and all show middle rare earth depletion or U-shaped patterns to some degree. Many harzburgites are characterized by this pattern (Frey, 1983) suggesting that, like enriched peridotites, a widespread chemical process has taken place in the mantle to produce them. Speculation about this process will not be made at this point but it does seem clear that the REE patterns of the Horoman peridotites are not unique. Another observation, based on the comparison of individual patterns in this field, concerns the Eu anomaly. The harzburgite data in general is of much poorer quality than for lherzolites due to the low concentrations. Quality data of the elements between Eu and Yb is particularly difficult to obtain making the recognition of Eu anomalies not straight forward. But the steepness and opposite direction of slope in the harzburgite samples between Sm and Eu (generally, among the REE, known the most precisely) is apparent. The Horoman sample, like a sample from Ronda and one from the Josephine peridotite appear to have a positive Eu anomaly while negative anomalies are suggested by several of the other patterns.

Figure 35 also includes REE patterns of three distinct, moderately depleted lherzolites from the Western Alps. These patterns are different from most intermediate lherzolites because of severe LREE depletion with only moderate HREE

depletion. This type of pattern is not common in the literature and probably represents a different petrogenetic process than that producing the more commonly seen pattern of moderately depleted lherzolites which is intermediate between the two fields, shown in Figure 36. The data show correspondence between the type of pattern and the type of peridotite (Fig. 36). This can be seen more easily when this same REE data is plotted versus CaO, a good indicator of degree of depletion by melting, i.e. amount of clinopyroxene. An excellent correlation can be seen between Yb content and CaO content (Fig. 37). The data give a reasonable linear relation with correlation coefficient of 0.957. The plot contains all the data from Figure 36 and so is heavily skewed towards the high and low CaO ends. If all the quality REE peridotite data from the literature were plotted, the 1-3 percent CaO portion of the diagram would be more densely filled. The HREE appear to be controlled by a simple depletion of clinopyroxene as would be expected from melting. In fact, the slope of the patterns between Yb and Lu is very consistent for practically all of the patterns in Figure 36. The relation between La and CaO (Fig. 38) is not nearly so simple. All the same samples plotted in Figure 37 show a great deal more scatter, implying that the LREE are not being partitioned completely into the Ca sites of clinopyroxene but that some other phase or phases must be involved in melting with significant LREE or that another

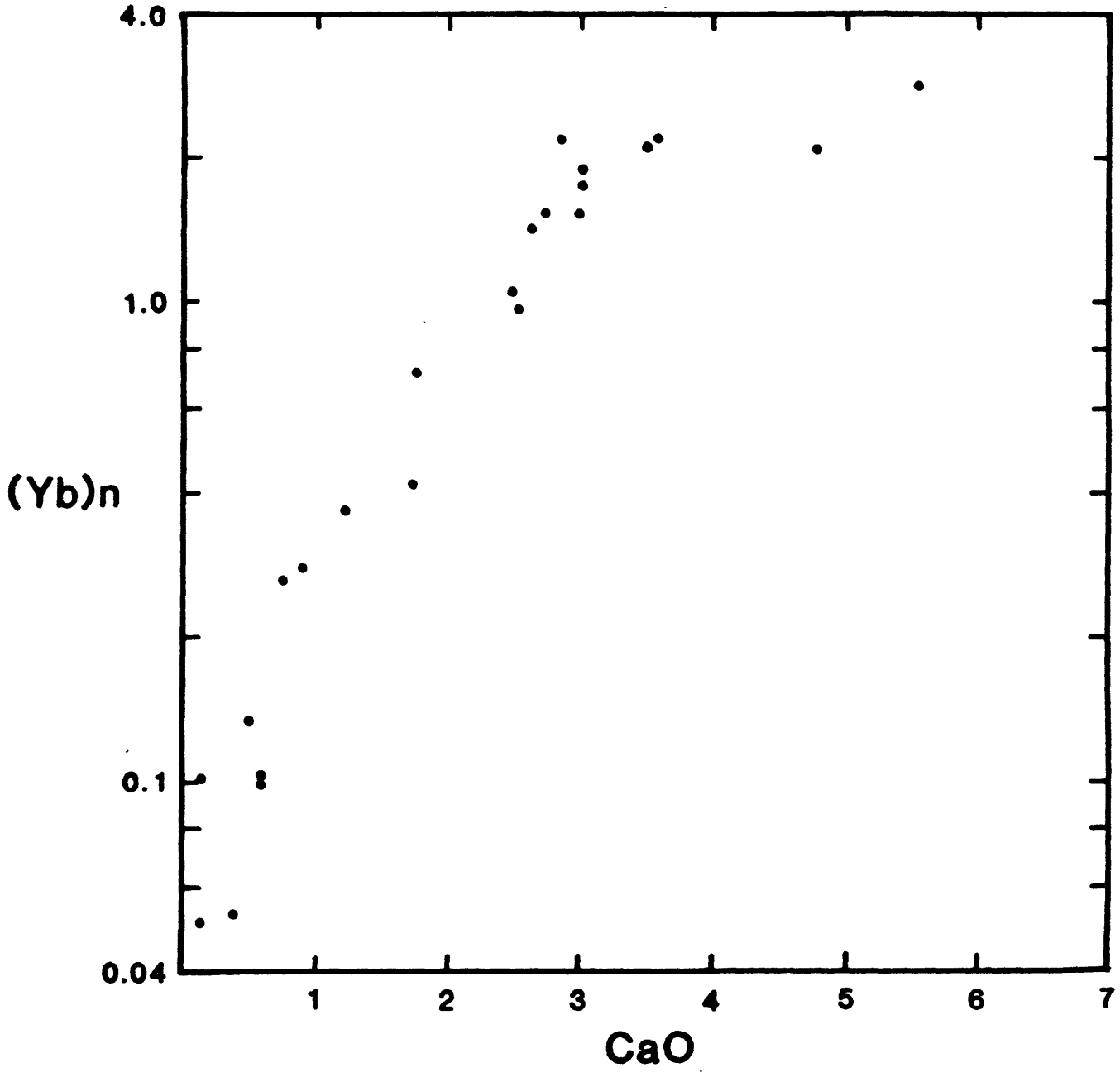

Figure 37. CaO versus chondrite-normalized Yb (Boynton, 1984) for the same peridotite samples in Fig. 36, with corellation coefficient of r = 0.957.

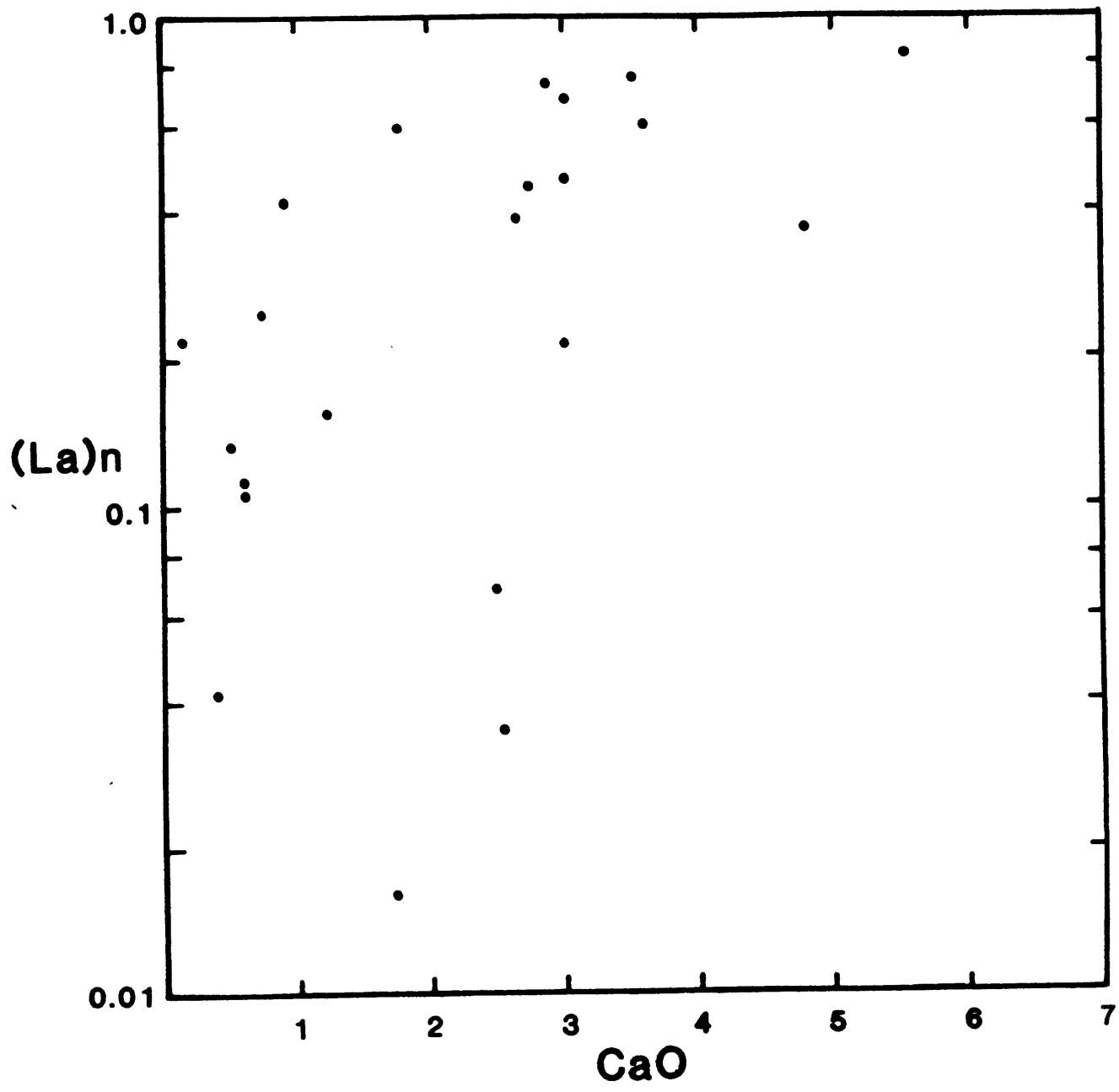

Figure 38. CaO versus chondrite-normalized La (Boynton, 1984) for same peridotite samples in Fig. 36.

process altogether is producing the scatter. Speculation about the cause of this will be left for a later section.

One way of presenting the shape of a REE pattern with respect to depletion is simply to plot ratios of chondrite normalized REE versus CaO. A plot of this same data with La/Yb versus CaO indicates an interesting and not completely expected result (Fig. 39). Frey (1983), with data from ultramafic xenoliths in basalt, found a negative correlation, i.e. LREE/HREE increased as CaO decreased. Based on mineral/melt REE distribution coefficients for the peridotite phases it is expected that this trend should be reversed. This same negative trend is seen in part of Figure 39. There are complications at the low end with samples that have intermediate CaO content and very low $(La/Yb)_{CN}$. Because of the U-shaped nature of the REE patterns of harzburgites in this plot the distinction between degrees of depletion of REE can be better seen with a plot of $(La/Sm)_{CN}$ versus CaO (Fig. 40). (The same information can be seen as in Figure 39 but the ratio is a bit more pronounced.) Again, I stress that the data plotted in Figures 39 and 40 are not all inclusive and in fact are primarily end members from specific locations. The few data that do not fall on a general negative trend from high CaO lherzolites to very low CaO harzburgites are moderately depleted lherzolites all of which come from peridotite massifs in the Western Alps (shown separately in Figure 36 for comparison). This trend represented by these few

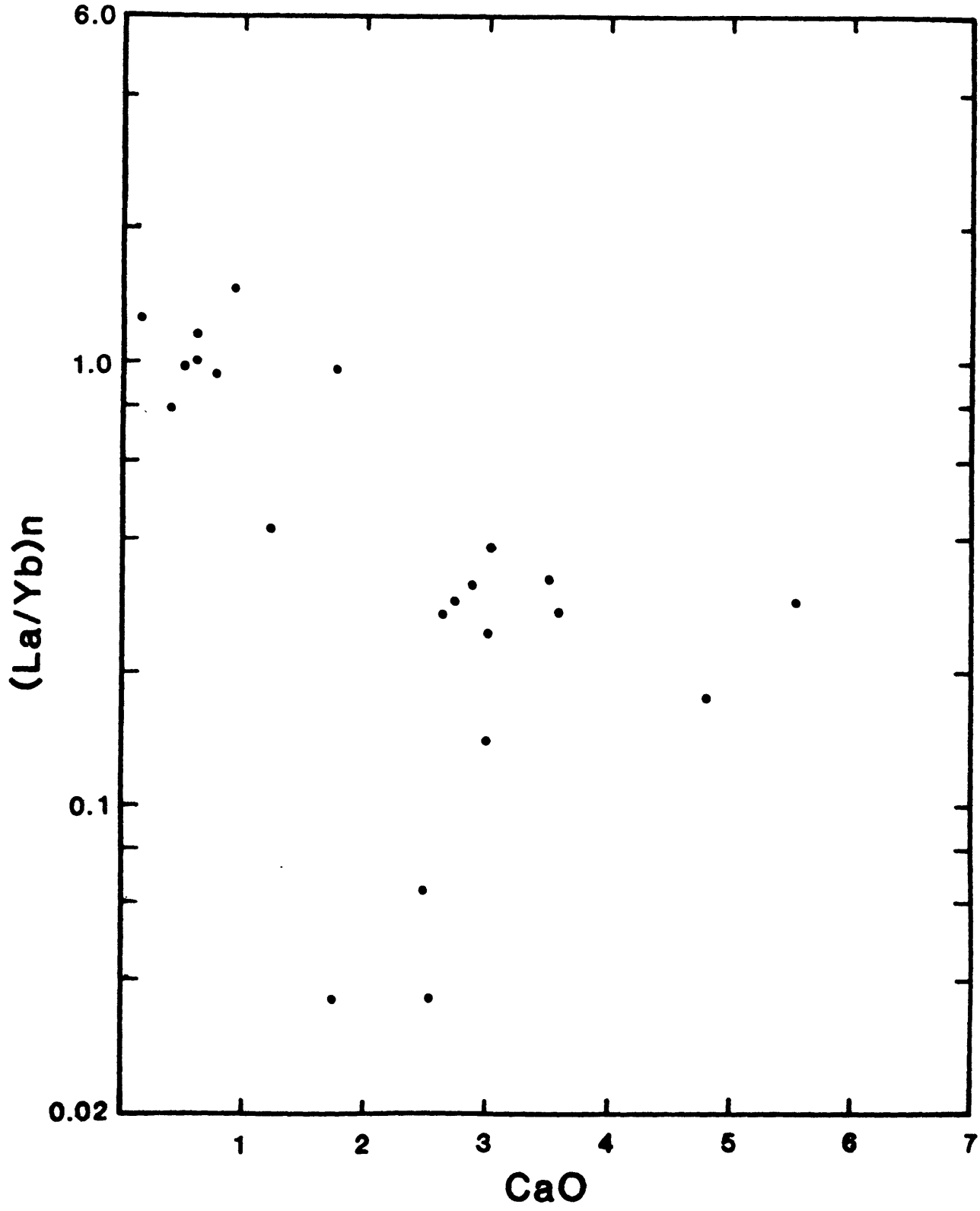

Figure 39. CaO versus chondrite-normalized La/Yb (Boynton, 1984) for same peridotite samples in Fig. 36.

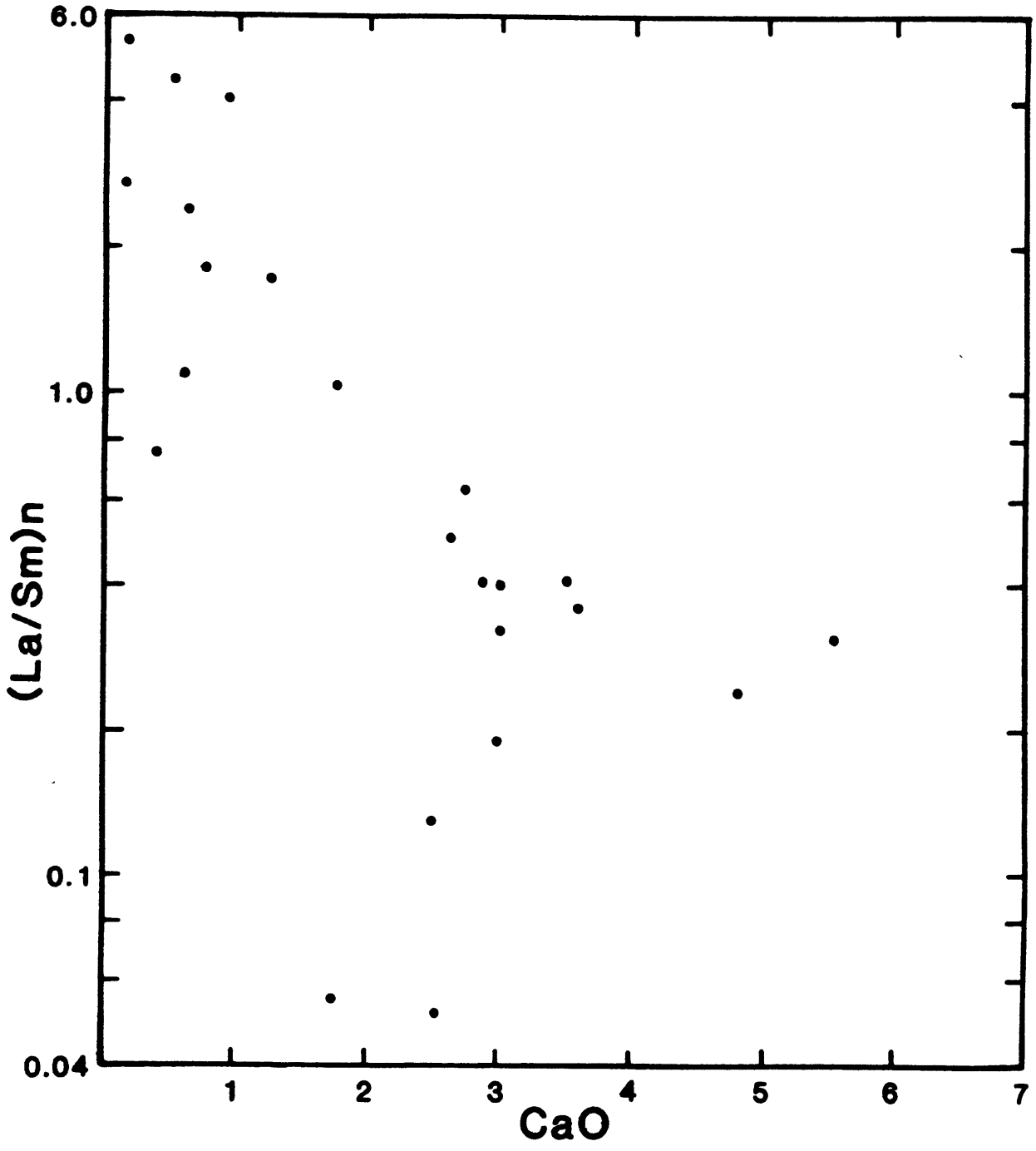

Figure 40. CaO versus chondrite-normalized La/Sm (Boynton, 1984) for same peridotite samples in Fig. 36.

samples from a localized region show the general trend one would expect from partial melting. Frey (1983) mentions several hypotheses to explain the negative correlation in xenoliths but the problem does not appear to have been adequately explained yet, particularly for alpine peridotites. The basalt xenolith data has a major difference in that the $(LREE/HREE)_{CN}$ ratios are generally all greater than one. No data from a single location yet exists that span across the entire range of the plot to show in detail the transition from slightly LREE depleted fertile lherzolite to the U-shaped harzburgites, nor the connection between the negative trend and the very LREE depleted lherzolites. It seems as if one or the other depletion variety exists but not both.

Mineral Chemistry

The major element mineral compositions, as measured by the electron microprobe, of olivine, orthopyroxene, clinopyroxene, Cr-spinel, and plagioclase (Tables 5-9) all vary with respect to degree of depletion of the bulk rock. The minerals, except for olivine, are not completely homogeneous. Care was taken through examination of many individual point analyses to choose representative mineral compositions. Means of these compositions were made to average out both intra- and inter-grain heterogeneity. The sub-solidus mineral history of alpine peridotites is quite complex (e.g. Dick, 1977; Obata, 1980; Conquere and Fabries, 1984). The Horoman minerals, particularly the pyroxenes,

reflect this complexity. The mineral data set in this work is used to enhance the bulk rock chemistry but is not detailed enough to be used to explain the sub-solidus history of the massif. In most of the mineral variation diagrams two data sets are presented; a set analyzed at MIT and a set analyzed by Obata for comparison.

Olivine

Olivine is modally the most dominant mineral by far in all the samples. It is the most homogeneous of all the minerals with variations within single grains and between different grains usually within microprobe counting statistics. There is a gradual increase in the forsterite content with degree of depletion from Fo_{89} in 62210 and 62212 to Fo_{91} in 62128 and 62127 (Table 5). Nickel behaves similarly but is more variable (Fig. 14). The forsterite content is yet another dissimilarity between layered intrusions and zoned complexes. Olivines from ultramafic rocks in these settings are generally much more variable and richer in fayalite component. Peridotites at Stillwater, Montana range from Fo_{80}-Fo_{94} (Jackson, 1961); at the Inziswa Complex, Transkei, southern Africa from Fo_{78}-Fo_{85} (Lightfoot and Naldrett, 1984); at the Great Dyke, Zimbabwe from Fo_{84}-Fo_{92} (Wilson, 1982); at Rhum, Scotland from Fo_{79}-Fo_{88} (Dunham and Wadsworth, 1978); at Duke Island, southeastern Alaska from Fo_{78}-Fo_{91} (Irvine, 1974); at the Jimberlana Intrusion, western Australia from Fo_{77}-Fo_{83} (Campbell, 1977); and at Union Bay complex, southeastern Alaska from

Fo_{78}-Fo_{83} (Ruckmick and Noble, 1959). Furthermore, the olivines at Horoman have very similar chemistry and variation to those of other alpine peridotites (Niida, 1984).

Orthopyroxene

Orthopyroxene is quite inhomogeneous in all the Horoman samples. Large porphyroclasts up to seven millimeters in size exist in all the samples with abundant very-fine Ca-rich clinopyroxene exsolution lamellae. Table 6 lists chemical analyses of the host orthopyroxene. Finer- grained recrystallized neoblasts are abundant and generally contain less Ca and Al. The porphyroclasts generally have complex zoning, as seen in Ronda orthopyroxenes (Obata, 1980). Analyses in Table 6 are means of several high quality analyses of core compositions. Rims are depleted in Al, Ca and Cr, and are similar to neoblast compositions. Mg# increases in the order expected with melting, with the least melted sample having the lowest Mg# and the sample having undergone the most melting has the greatest Mg#. Orthopyroxene Mg#'s are usually greater than olivine Mg#. The Mg# is also higher and less variable than in layered complexes which have orthopyroxene with more bronzitic composition.

Al_2O_3 has the same negative trend with Mg# as the whole rock trend, although poorly defined at low Mg#'s (Fig. 41). This trend is seen in abyssal peridotites (Dick and Fisher, 1984) and is best explained as a melting trend. The Cr_2O_3

Figure 41. Mg# (Mg/Mg+Fe) variation diagram for abundance of Al_2O_3 in orthopyroxene from Horoman peridotite samples analyzed for this study (circles) and analyses by Obata on the same samples for comparison (X's).

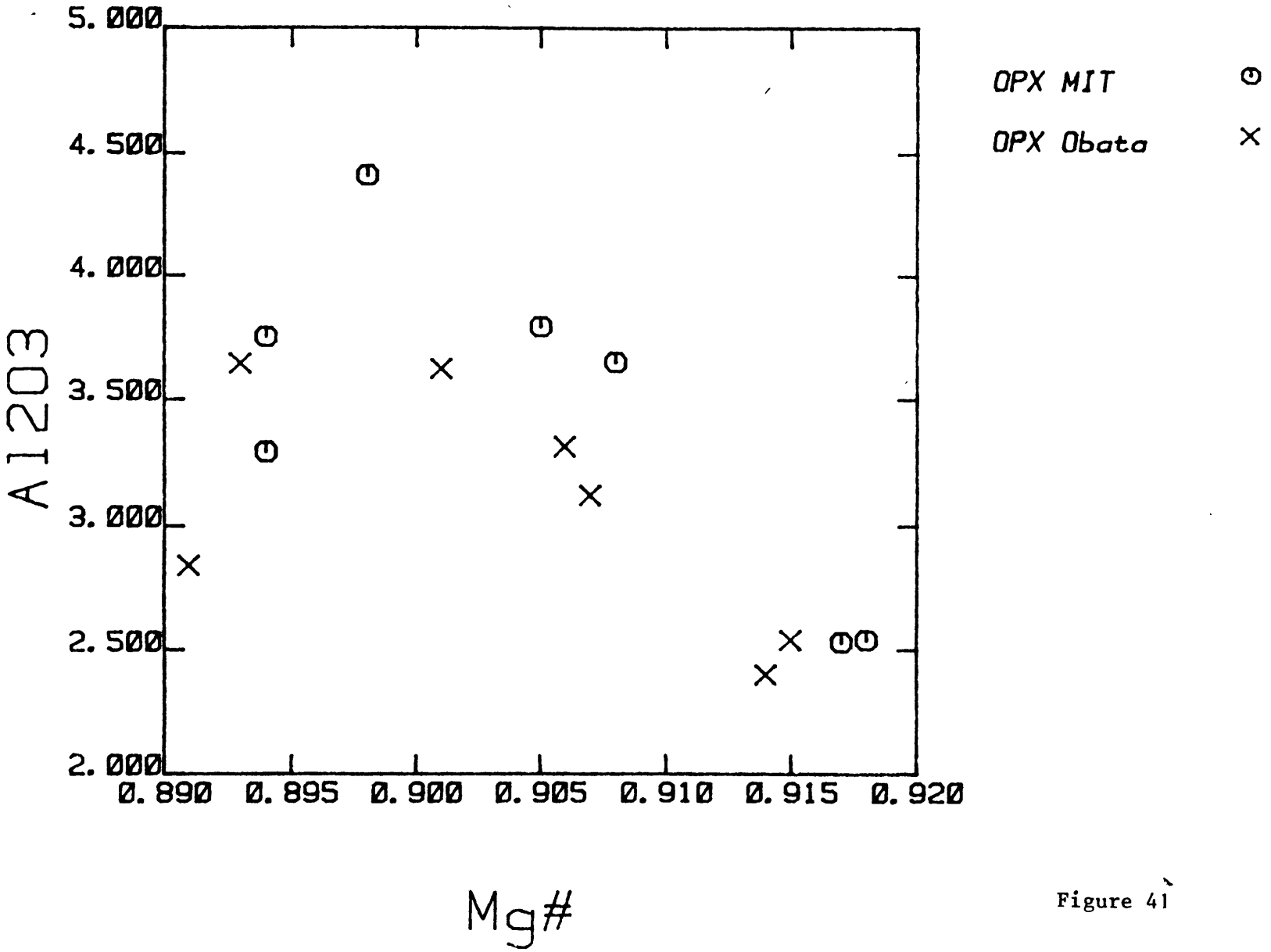
5.000
4.500
4.000
3.500
3.000
2.500
2.000
Al203
0.890
0.895
0.900
0.905
0.910
0.915
0.920
Mg#
OPX MIT
OPX Obata

Figure 41

variation diagram (Fig. 17) can also be explained as a melting trend. Cr is generally a refractory element so one would expect the Cr content to increase with melting, as does the bulk rock Cr (Fig. 16). SiO_2 shows a clear inverse relation with Mg# (Fig. 42) compared to the bulk rock trend (Fig. 8). TiO_2 with Mg# (Fig. 43), is also entirely consistent with a melting interpretation. The CaO variation diagram shows absolutely no trend with respect to Mg# (Fig. 44). One would expect a negative trend due to melting as is seen in the whole rock data (Fig. 8) and is seen in orthopyroxene from other peridotites (Dick, 1977). Sub-solidus reequilibration with clinopyroxene may be important as the CaO content in pyroxenes is temperature dependent. The two pyroxene solvus expands as temperature decreases, thus producing an expected positive trend in a plot such as Figure 44. It may be an analytic problem as it is difficult to avoid clinopyroxene exsolution lamellae in any single point analysis and the orthopyroxene is zoned with respect to CaO. From the data presented here it would seem that the Wo molecule in orthopyroxene is low and constant, probably reflecting conflicting effects of melting and reequilibration as well as analytical complexities. Dick (1977) points out that the Ca trend is difficult to explain by T dependent sub-solidus reequilibration.

Clinopyroxene

Clinopyroxene's in the Horoman peridotites are also variable in grain-size and chemical composition within a

Figures 42-44. Mg# (Mg/Mg+Fe) variation diagrams for abundances of SiO_2, TiO_2 and CaO in orthopyroxenes from Horoman peridotite samples analyzed for this study (circles) and analyses by Obata on the same samples for comparison (X's). See text for discussion.

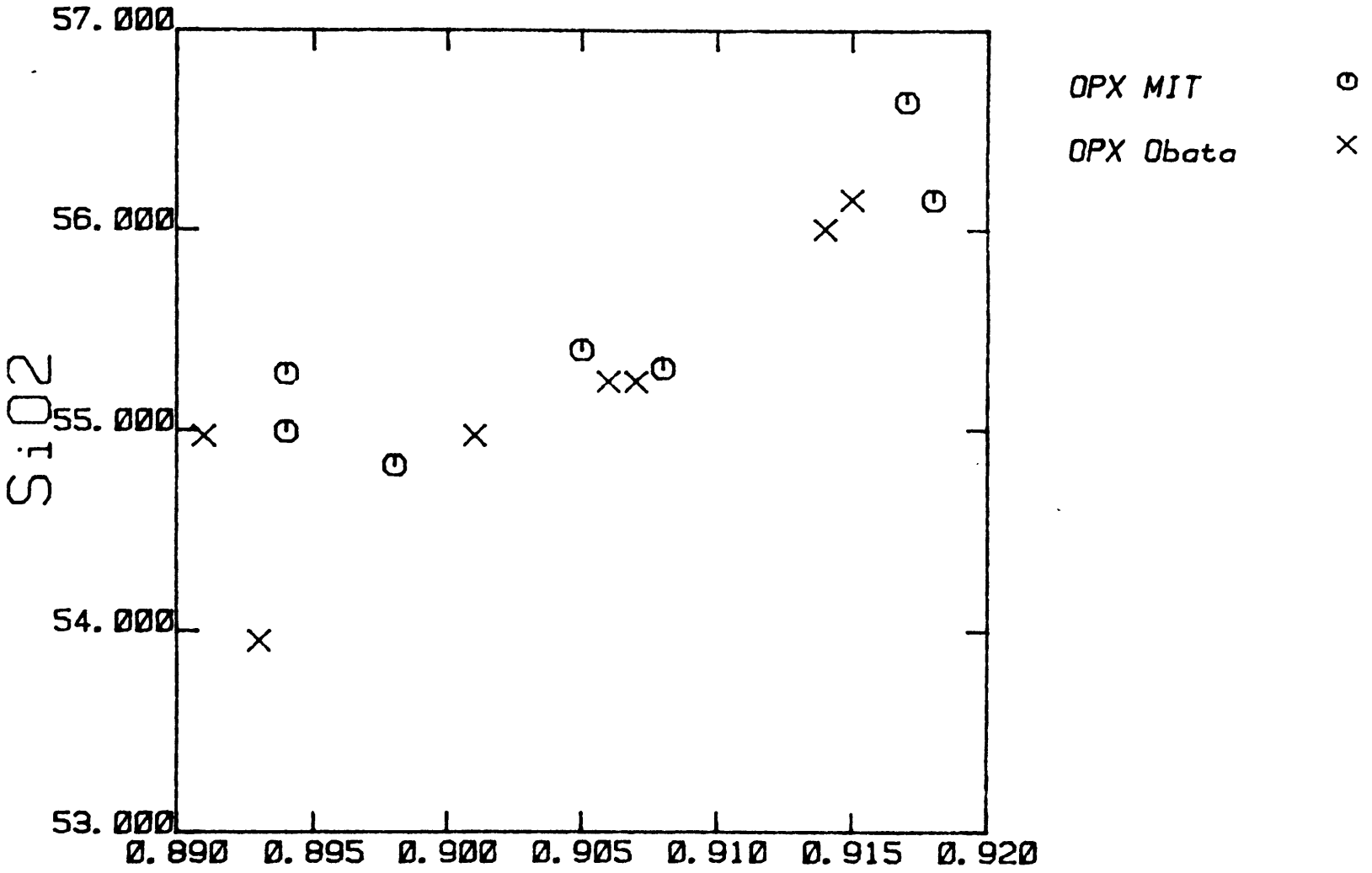
57.000
56.000
55.000
54.000
53.000
SiO2
0.890
0.895
0.900
0.905
0.910
0.915
0.920
Mg#
OPX MIT
OPX Obata

Figure 42

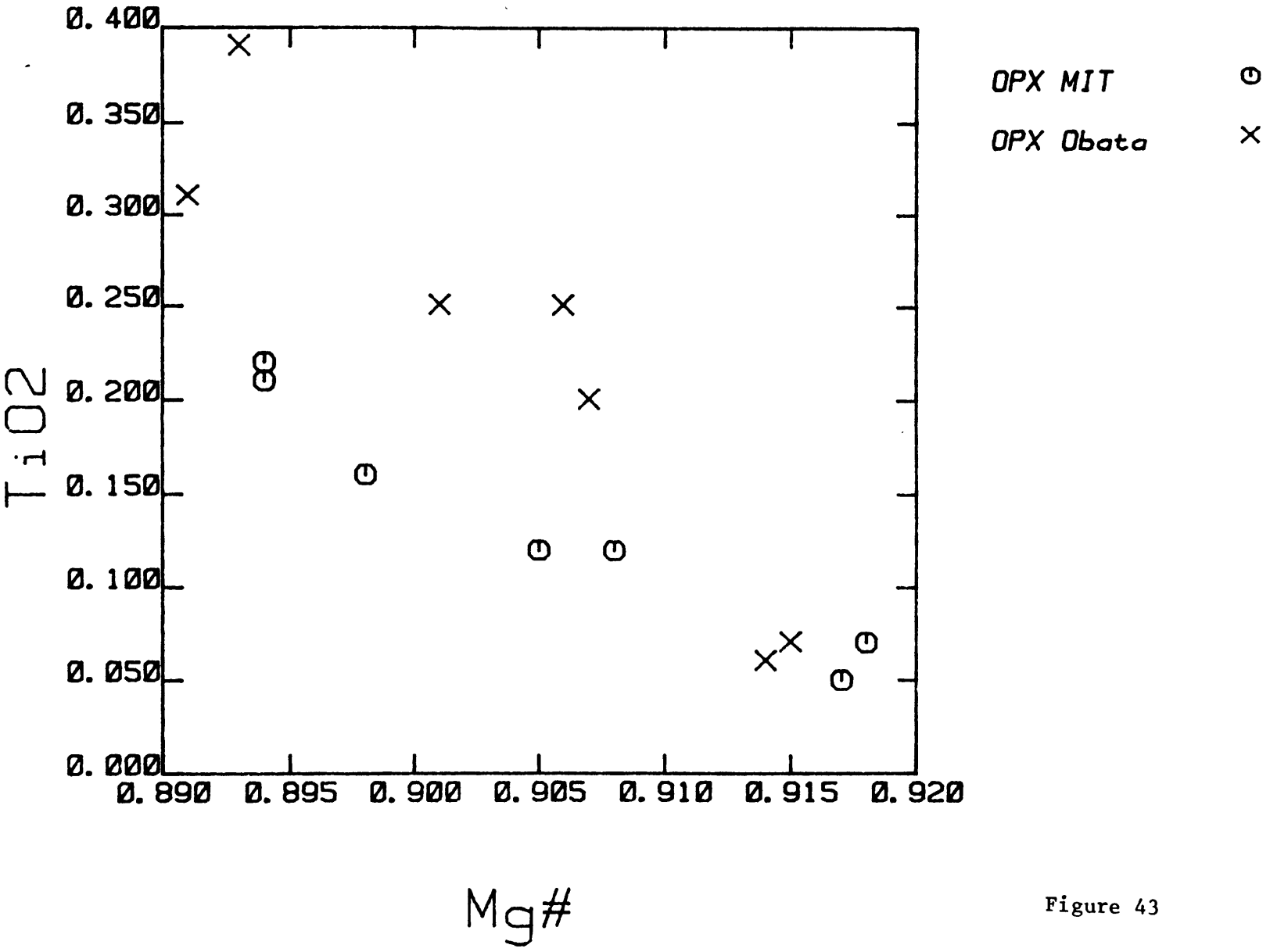
0.400
0.350
0.300
0.250
0.200
0.150
0.100
0.050
0.000
TiO2
0.890
0.895
0.900
0.905
0.910
0.915
0.920
Mg#
OPX MIT
OPX Obata

Figure 43

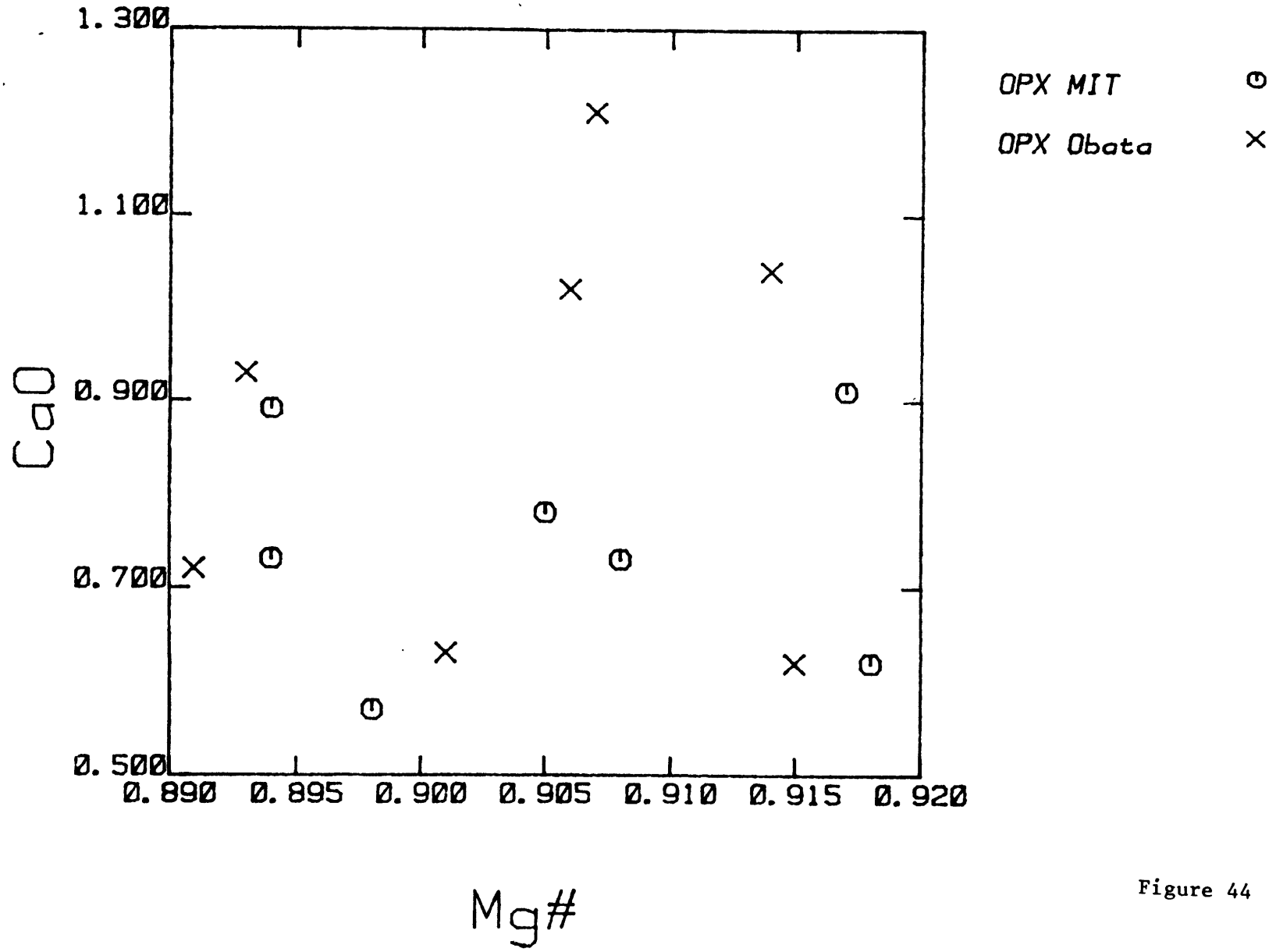
1.300
1.100
0.900
0.700
0.500
CaO
0.890
0.895
0.900
0.905
0.910
0.915
0.920
Mg#
OPX MIT
OPX Obata

Figure 44

sample. There is a considerable sub-solidus exsolution of orthopyroxene, and more rarely plagioclase and spinel. (See back scattered electron microprobe photographs, Plates 1-7 in clinopyroxene trace elements section.) Clinopyroxene is more magnesian than either olivine or orthopyroxene and like these minerals reflects the degree of depletion by melting. Once again, the compositions are much more Mg-rich and less variable than clinopyroxene from layered intrusions or zoned complexes. TiO_2, Al_2O_3 and Na_2O variation diagrams (Fig's. 45, 46, and 47) all show negative trends as one would expect from melting. These trends are similar to those seen in the bulk rock chemistry. Cr_2O_3 increases with Mg#, as an explanation of the rocks as a suite of residues from varying degrees of partial melting would predict, except for the most Mg-rich samples which are low in Cr_2O_3 (Fig. 24). The relatively low values in the Mg-rich samples probably reflects Cr partitioning into associated Cr-rich spinels, perhaps due to T effects (see CaO discussion below). SiO_2 exhibits a poorly defined increasing trend with Mg# (Fig. 48), like orthopyroxene, or perhaps two populations of clinopyroxene with near constant SiO_2. In a silicate melt the SiO_2 content would remain near constant. The increase in SiO_2 in pyroxenes is merely a closure constraint in response to depletion of Al, Ti and Na. CaO variation with Mg# (Fig. 49) has a similar pattern to SiO_2, either a poorly defined positive trend or possibly a second population of higher CaO at large degrees of melting. Expansion of a two

Figures 45-49. Mg# (Mg/Mg+Fe) variation diagrams for abundances of TiO_2, Al_2O_3, Na_2O, SiO_2 and CaO in clinopyroxenes from Horoman peridotite samples analyzed for this study (circles) and analyzes by Obata on the same samples for comparison (X's). See text for discussion.

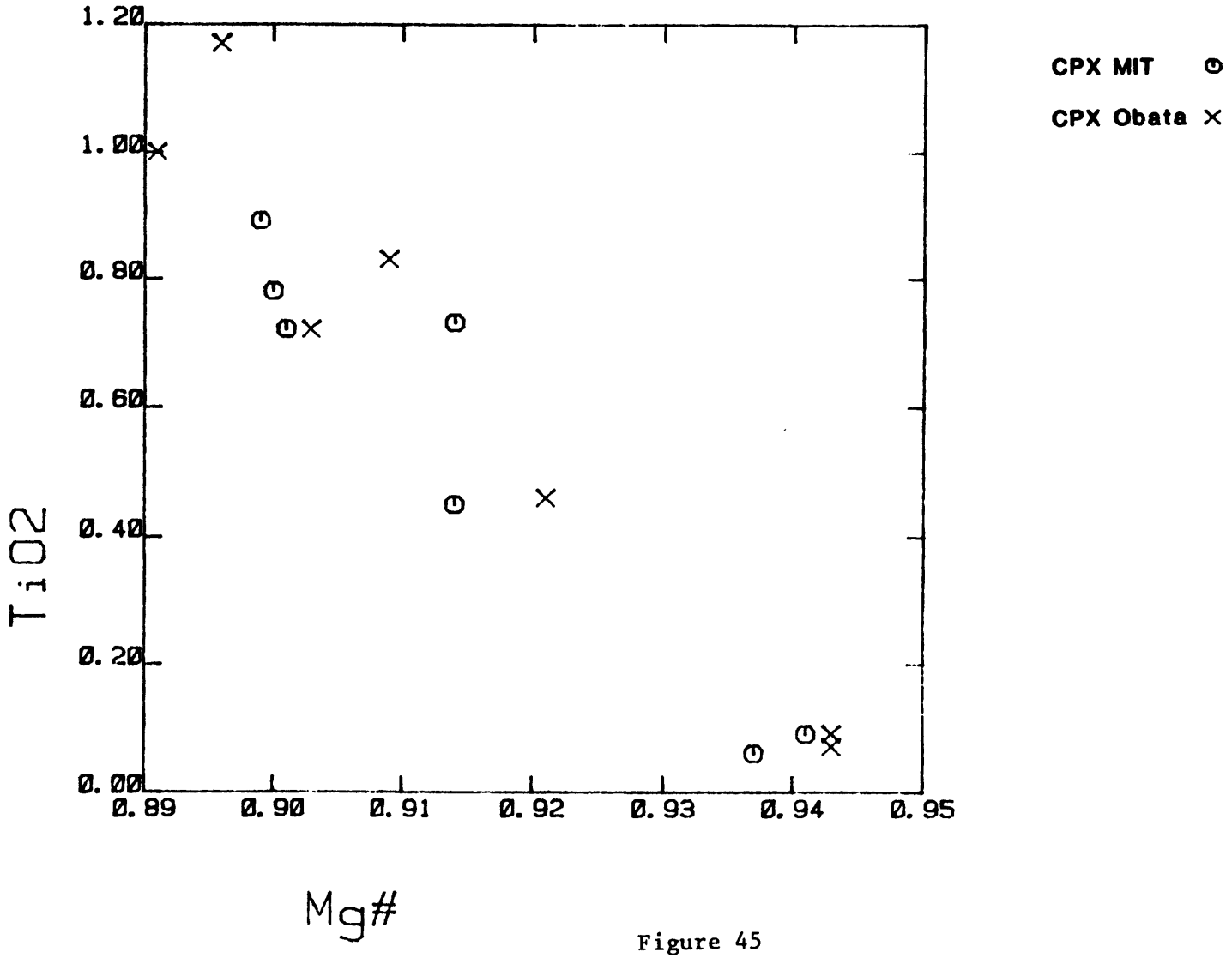
1.20
1.00
0.80
0.60
0.40
0.20
0.00
TiO2
0.89
0.90
0.91
0.92
0.93
0.94
0.95
Mg#
CPX MIT
CPX Obata

Figure 45

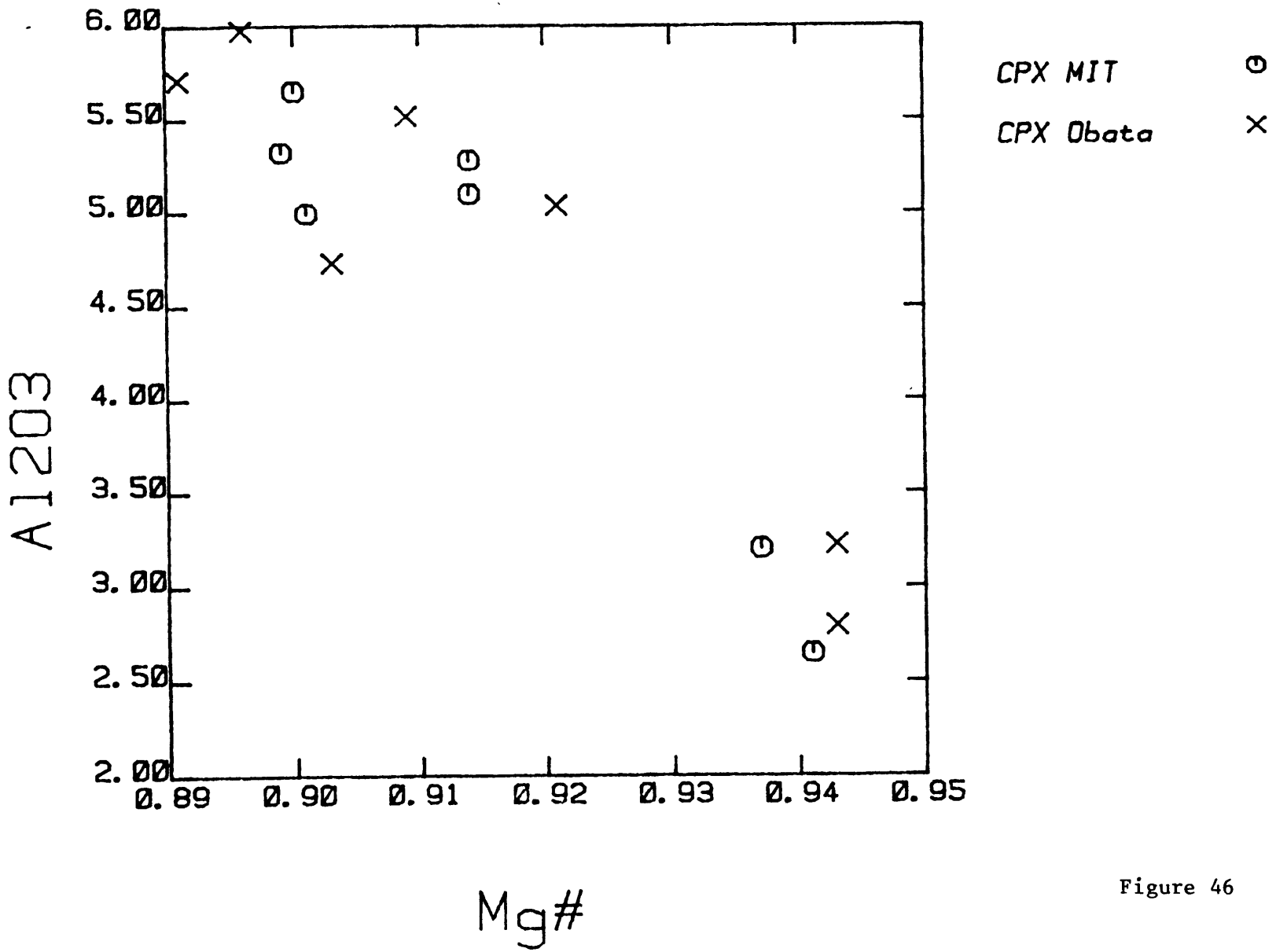
6.00
5.50
5.00
4.50
4.00
3.50
3.00
2.50
2.00
Al203
0.89
0.90
0.91
0.92
0.93
0.94
0.95
Mg#
CPX MIT
CPX Obata

Figure 46

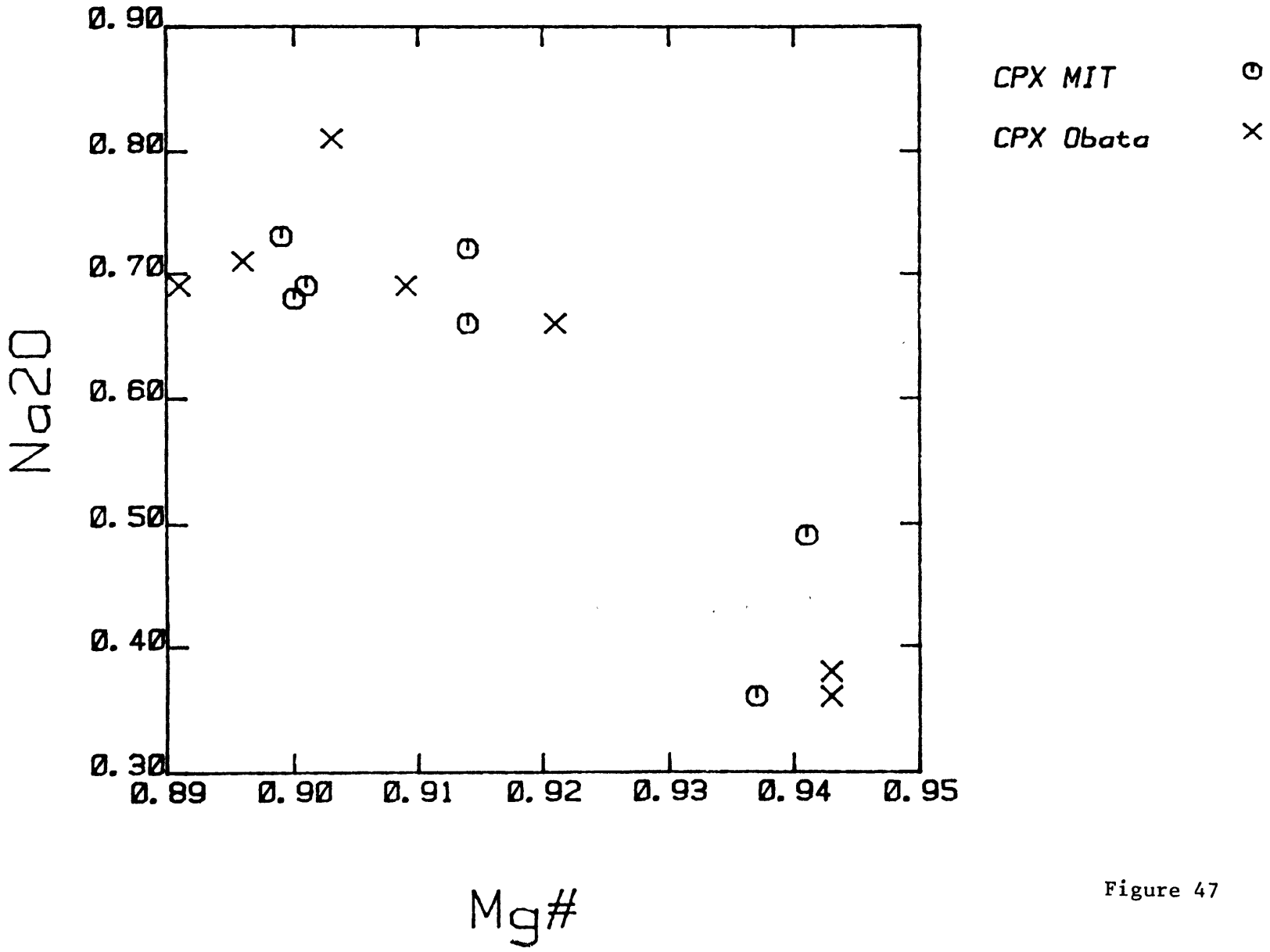
0.90
0.80
0.70
0.60
0.50
0.40
0.30
Na2O
0.89
0.90
0.91
0.92
0.93
0.94
0.95
Mg#
CPX MIT
CPX Obata

Figure 47

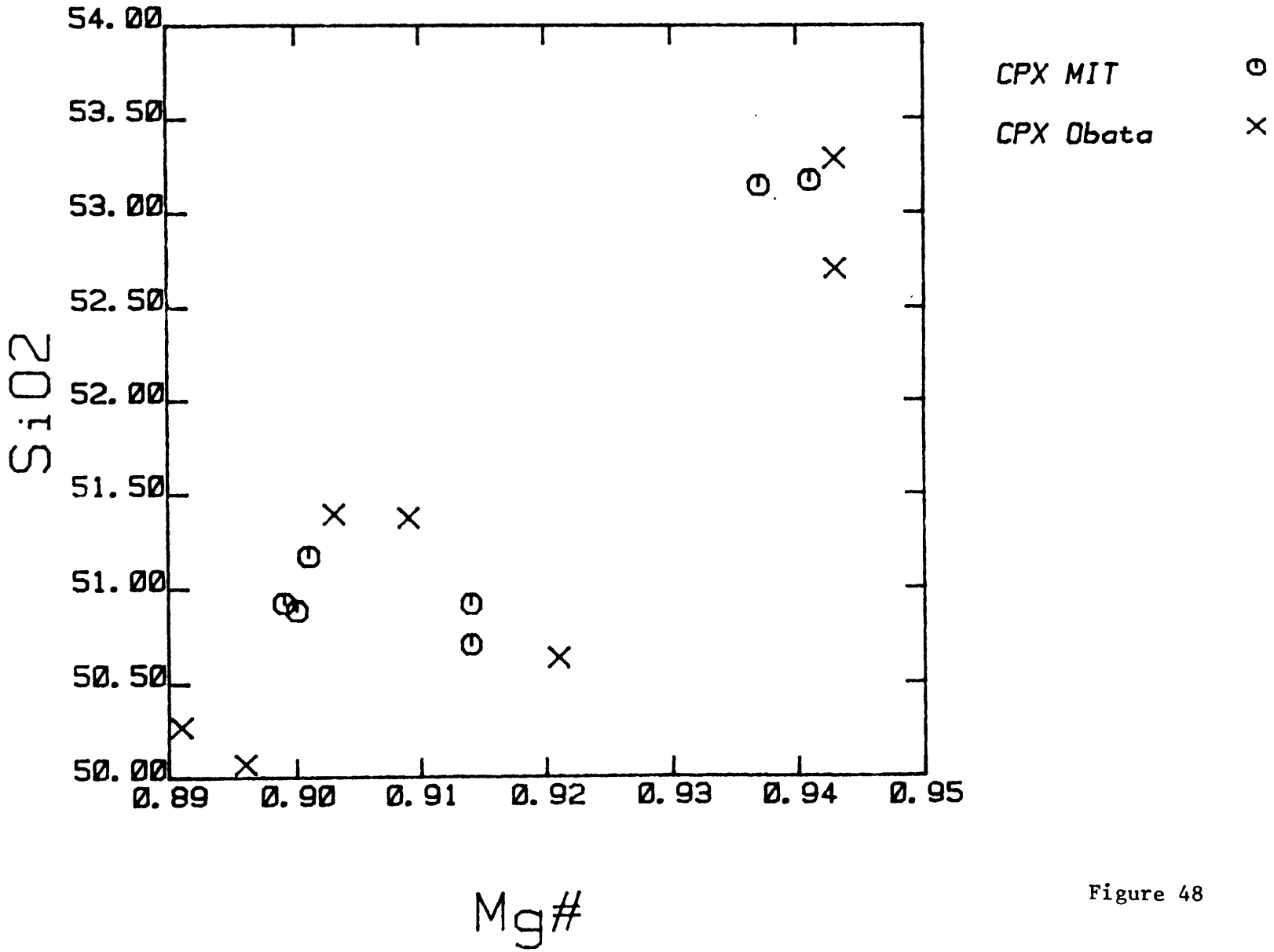
54.00
53.50
53.00
52.50
52.00
51.50
51.00
50.50
50.00
SiO2
0.89
0.90
0.91
0.92
0.93
0.94
0.95
Mg#
CPX MIT
CPX Obata

Figure 48

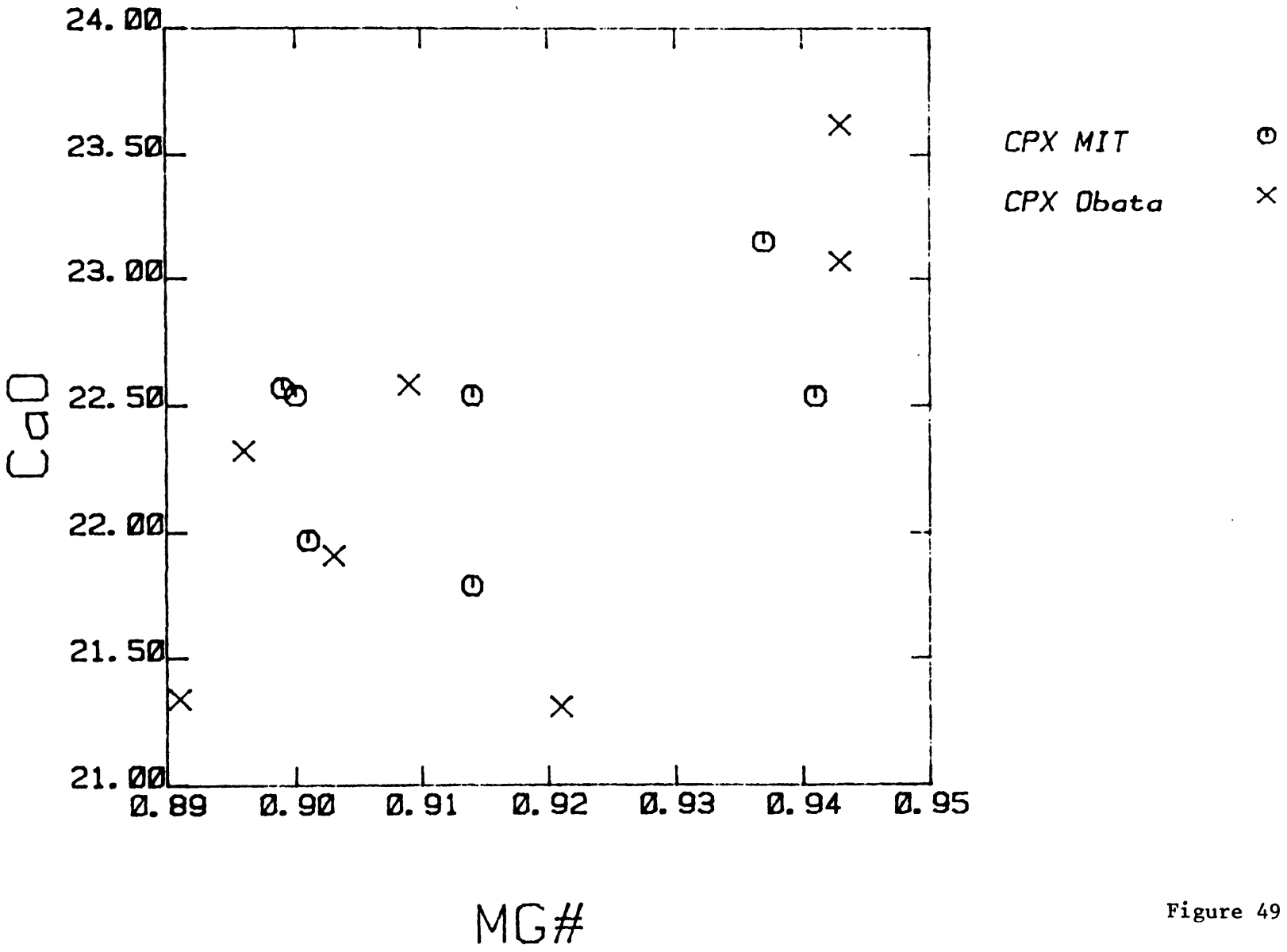
24.00
23.50
23.00
22.50
22.00
21.50
21.00
CaO
0.89
0.90
0.91
0.92
0.93
0.94
0.95
MG#
CPX MIT
CPX Obata

Figure 49

pyroxene solvus with decreasing temperature may have effect. Reequilibrated clinopyroxene should have a greater CaO content. Reequilibration effects may be largest in the Mg-rich pyroxenes where CaO is out of phase between pyroxenes, i.e. Ca-poor orthopyroxene with Ca-rich clinopyroxene. Again, one is faced with severe analytical problems in attempting to analyze host clinopyroxene without any exsolution orthopyroxene. Ca variation is expected within a grain simply due to the kinetics of sub-solidus reequilibration and exsolution.

The exsolution behavior of these clinopyroxene's are complex and quite interesting. Plates 2b and 4b, (see clinopyroxene trace elements section) back-scattered electron close up photographs of clinopyroxene's from samples 62212 and 62131 respectively, clearly exhibit two separate directions of exsolution lamellae. Robinson and others (1977) showed that exsolution lamellae are fossil indicators of the lattice parameters in monoclinic pyroxenes at high T and P. The orientation of lamellae exist as they do to minimize strain energy between host and lamellae and the strain energy is T dependent. Exsolution temperatures can be determined with knowledge of the lattice parameters and measurements of lamellae orientation. The dominant lamellae direction in all the Horoman clinopyroxene's is parallel to the (100) direction (Niida, 1984), similar to clinopyroxene at Ronda (Obata, 1980). These lamellae are often irregular or blebby in shape and are up to 40 μm

thick. Compositionally, these lamellae are very similar to orthopyroxene grains in the sample but were probably pigeonite originally. This set of lamellae exsolved at a high T (~1000 ^{o}C, T. Grove, personal communication). Lamellae grow in thickness as long as changes in lattice parameters from cooling and composition changes do not produce too large strain energies. Growth of lamellae will also occur longitudinally if lattice parameters are not drastically altered. Eventually growth may slow when lattice parameters produce too great a strain energy and a new set of lamellae form in the supersaturated regions far from the earlier lamellae. The new lamellae will have a new orientation reflecting the change in lattice parameters as a function of cooling and compositional change (Robinson et al, 1977). In the photos, particularly plate 2b, the second set of lamellae can be seen with a conspicuous "lamellae-free" zone immediately adjacent to the large first set of lamellae. This lamellae-free zone is caused by compositional heterogeneity in the clinopyroxene produced from the first set of lamellae. The second set of lamellae are probably also oriented parallel to the (100) direction but with respect to the pigeonite lattice at conditions of exsolution not the lattice of the original clinopyroxene. This set is likely to still be pigeonite in composition and definitely formed at a lower T (T. Grove, personal communication). None of these lamellae were analyzed in this study. Robinson and others (1977) then use the

relative angles of the multiple sets of lamellae to infer temperature information of exsolution. Unfortunately, the photographs shown here are randomly oriented and only an apparent angle can be seen. No quantitative information can be obtained but we can infer that two temperatures are recorded in the lamellae: a first set at about 1000 ^{o}C and a second lower-T set, perhaps ~700 ^{o}C. These complications in exsolution and sub-solidus reequilibration and recrystallization simply in chemical terms leads one to believe that geothermometry based on equilibration of clinopyroxene-orthopyroxene pairs may not give meaningful information. Exsolution commonly migrates across the grain boundary to form a new grain, also complicating matters. Another complicating process is recrystallization reactions involving other minerals. Estimates of T based on clinopyroxene-orthopyroxene equilibrium geothermometry range from 700 ^{o}C to 1100 ^{o}C using several methods (Wood and Banno, 1973; Wells, 1977; Bertrand and Mercier, 1985; and Mori and Green, 1977) and various mineral pairs. The temperature estimates are not consistent between methods or between samples. In short, geothermometry using limited mineral chemistry data appears to be an exercise in futility in the Horoman rocks with little useful information obtained. Even considering the T's obtained using these geothermometers are reasonably accurate, (unlikely, considering analytical problems and calibration errors of geothermometers) all that the T represents is that at which

those particular composition pyroxene pairs were in equilibrium. Little is learned about conditions in the rock as a whole that could not be estimated using general petrologic intuition. Conquere and Fabries (1984), in a careful microprobe study of samples from alpine peridotites in the french Pyrenees, were able to establish by inter-sample mineral variations and detailed geothermometry two distinct episodes of deformation and recrystallization. The first representing a high T (~1000 ^{o}C) episode in the upper mantle producing a stable state of equilibrium in most porphyroclast cores. The second is a lower T (~700 ^{o}C) partial recrystallization affecting the pyroxenes and spinels, probably occurring during tectonic emplacement. A similar scenario at Horoman may account for some of the mineral variation seen.

Trace Elements

No published trace element data currently exists for any mineral separates from an Alpine peridotite massif. This data does exist for peridotite xenoliths however (e.g. Frey and Prinz, 1978, San Carlos, Ariz.; Ottonello et al, 1980, Assab, Ethiopia; Kurat et al, 1980, Kapfenstein, Austria; Stosch and Seck, 1980, Dreiser Weiher, W. Ger.; Stosch and Lugmair, in press, Eiffel, W. Ger.) and has yielded information about partitioning of trace elements in peridotite phases and constrained the nature of mantle metasomatism to some degree. Table 10 consists of REE and

other trace element data from clinopyroxenes from six samples from the Horoman peridotite. These data allow some interesting general conclusions to be drawn about the nature of mineral partitioning and suggest that some complex processes occur during and accompanying melting.

Analytical Methods and Data Quality:

Rare Earth Elements - The analyses were made using the Cameca IMS 3f ion microprobe at MIT. Hand-picked clinopyroxene grains were mounted together in one standard probe mount along with a piece of clinopyroxene from a homogeneous megacryst from the Monastery mine in S. Africa as a working standard. One sample (62127) was ruined in sample preparation so only data for six samples is included. REE data was obtained for this sample but was deemed not acceptable except for qualitative comparison. Shimizu and Le Roex (1986) showed that with this technique trace element data can be considered as precise as within counting statistics of individual analyses. Relative errors of REE based on counting statistics ranged from 5-10% in all the samples except for 62128, which is in this same range for the LREE, but from Sm to Dy reaches near 20%. Sm, Eu and Er generally have the largest error of the REE. The data should be considered preliminary not because of accuracy but due to questions of statistical validity. REE abundances are based upon single spot analyses of single clinopyroxene grains. Generally, at least three spot analyses for REE of each grain was made. A procedural change was made between

data sets. The last set with the updated procedure is considered the best quality and is included in Table 10. The shapes of REE patterns are quite reasonable reproduced, particularly since it is not known *a priori* that clinopyroxenes are homogeneous with respect to REE. This is best seen by looking at multiple analyses of the Monastery standard compared to the accepted values obtained by isotope dilution for REE (Fig. 50). The relative position of the curves were constrained by pinning the Nd value to exactly that of the isotope dilution but it is apparent that the shapes match very well. No elements heavier that Er can be measured accurately due to interferences from pervasive molecular complexes. The five Monastery patterns in Figure 50 were all analyzed intermittently the same evening the sample data were collected. A known linear relationship exists between ion intensity and concentration called a working curve (Ray and Hart, 1982 and Shimizu and Le Roex, 1986). The working curve for this study consisted of nine Monastery clinopyroxene analyses and five clinopyroxene analyses from peridotite xenoliths from Hannouba, China. All of these fourteen analyses were made over a span of two days when the Horoman clinopyroxenes were analyzed as well to reduce the chance of instrument drift and ion beam focussing vagueries. Nd is the most intense REE peak, so Nd/Si ion probe measured ion intensity versus Nd concentration measured by isotope dilution was used as a working curve. Song Yan determined Nd concentration of the

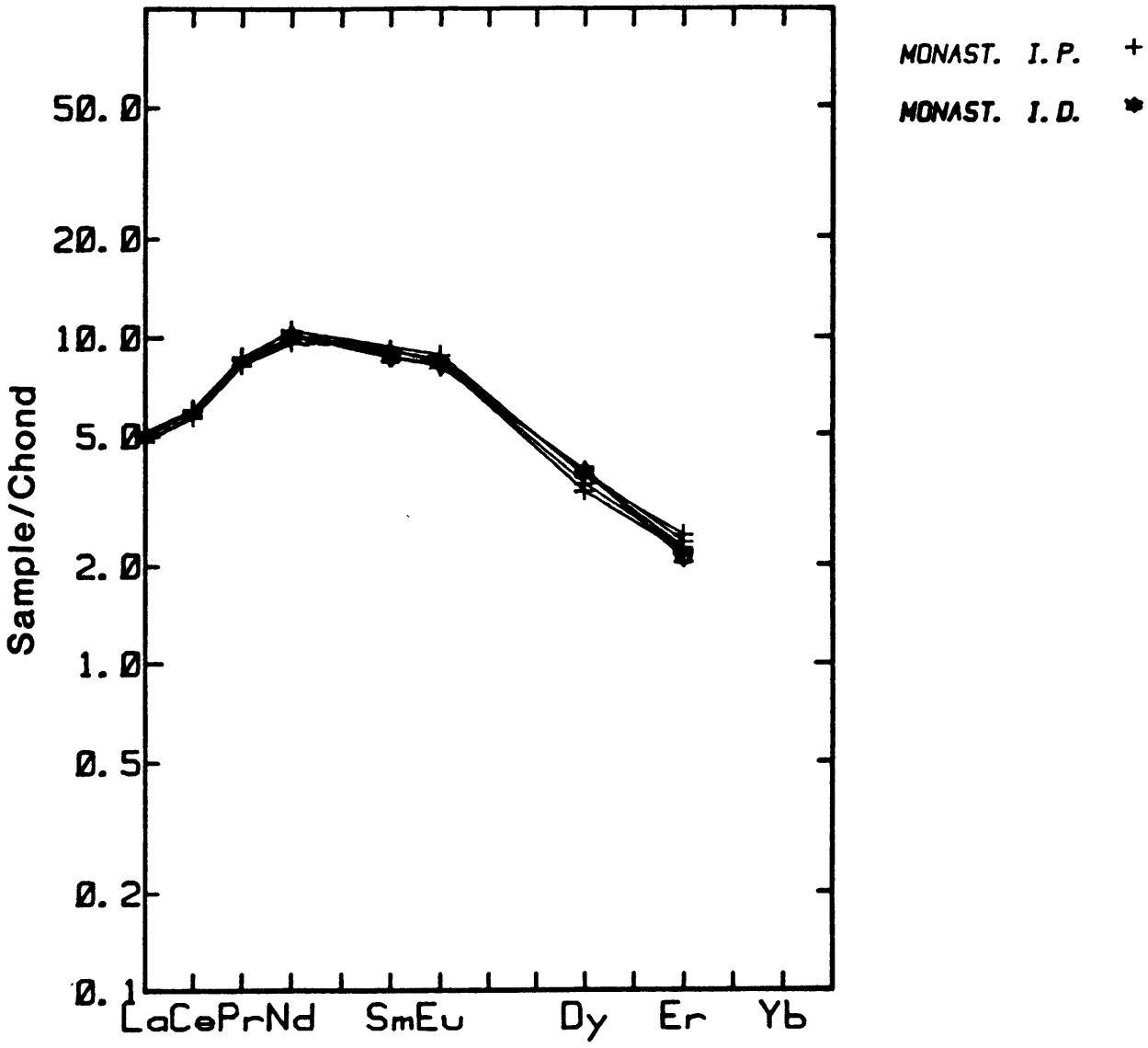

Figure 50. REE chondrite-normalized (Boynton, 1984) diagram of five separate ion microprobe analyses of Monastery clinopyroxene (used as a working standard) (crosses) shown with the same pyroxene analyzed by isotope dilution (star) for comparison. Nd is pinned at the ID value so that the shape of the patterns can be compared.

Chinese xenoliths by isotope dilution at MIT. The Nd/Si ratio measured for each clinopyroxene sample in this study was then fit to the regressed linear working curve to obtain Nd concentration and the other REE were normalized to Nd. Using this technique accuracy should be less than or about the same magnitude as precision if the working curve is good (Ray and Hart, 1982). The reproducibility of the Monastery patterns implies that the working curve for any of the REE should be as good as for Nd adding strength to the fact that all REE are relatively accurate. Also, Song Yan's clinopyroxene isotope dilution data for Nd was matched to within 10% with just a one point working curve using a mean Monastery value and constraining it with the origin. The regressed working curve is obviously vastly improved with the addition of these data suggesting again that the accuracy is relatively good.

The shapes of the REE patterns (Fig. 51) match quite well with those obtained previously using a much more poorly constrained working curve of Nd intensity versus Nd concentration of the Monastery standard only (Fig. 52). Many features of the REE patterns can be compared: The HREE depletion of 62131; the general depletion and near flat shape of 62128; LREE slope of samples 62128 and 62131; relatively flat MREE-HREE shapes of 62210 compared to slight HREE depletion of 62212 and 62213; high La for 62213 and 62128; and generally lower magnitude of REE than in Figure 51. All of these comparisons are qualitative features but

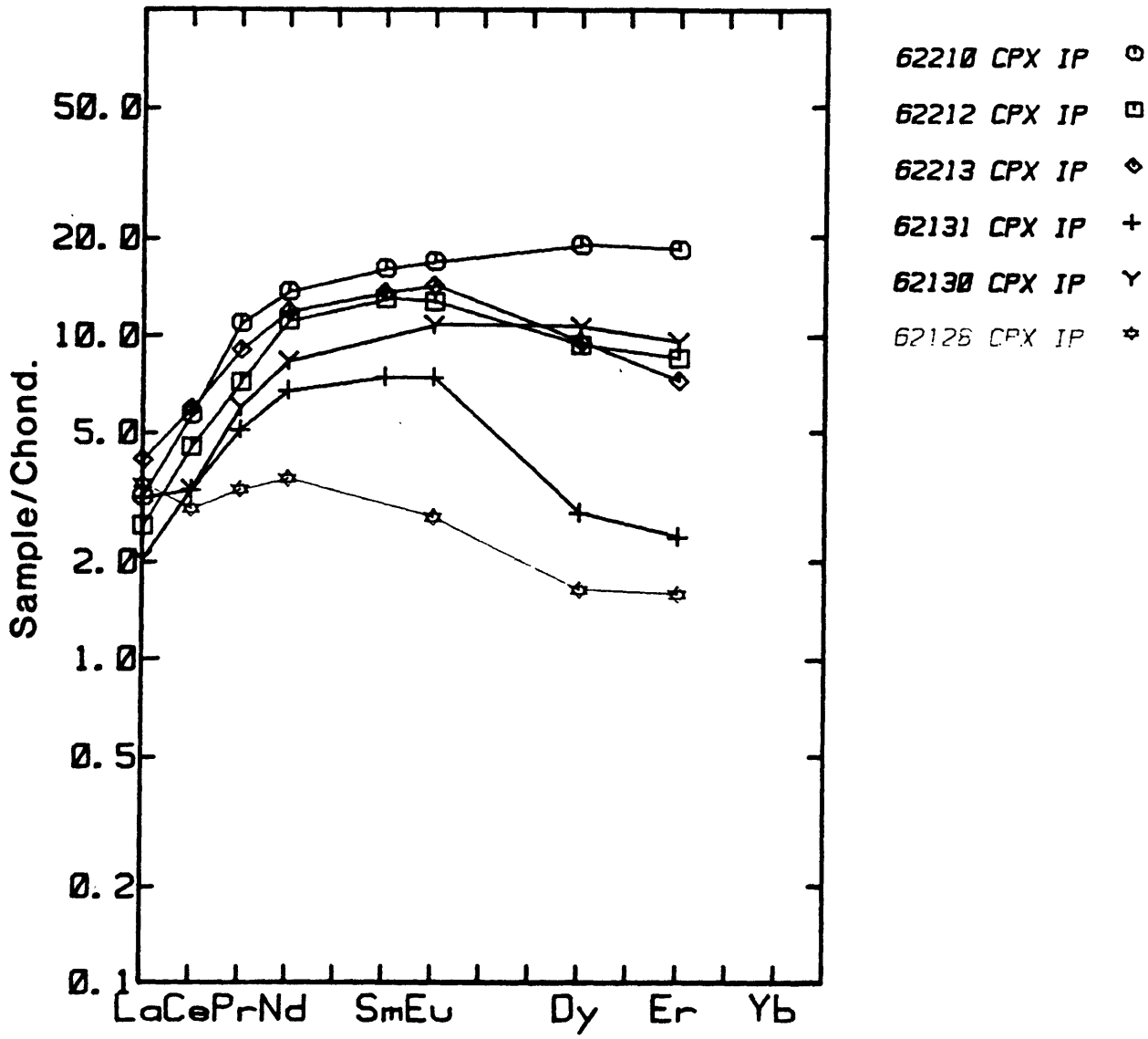

Figure 51. REE chondrite-normalized (Boynton, 1984) diagram for clinopyroxenes from 6 samples from Horoman using the Monastery standard.

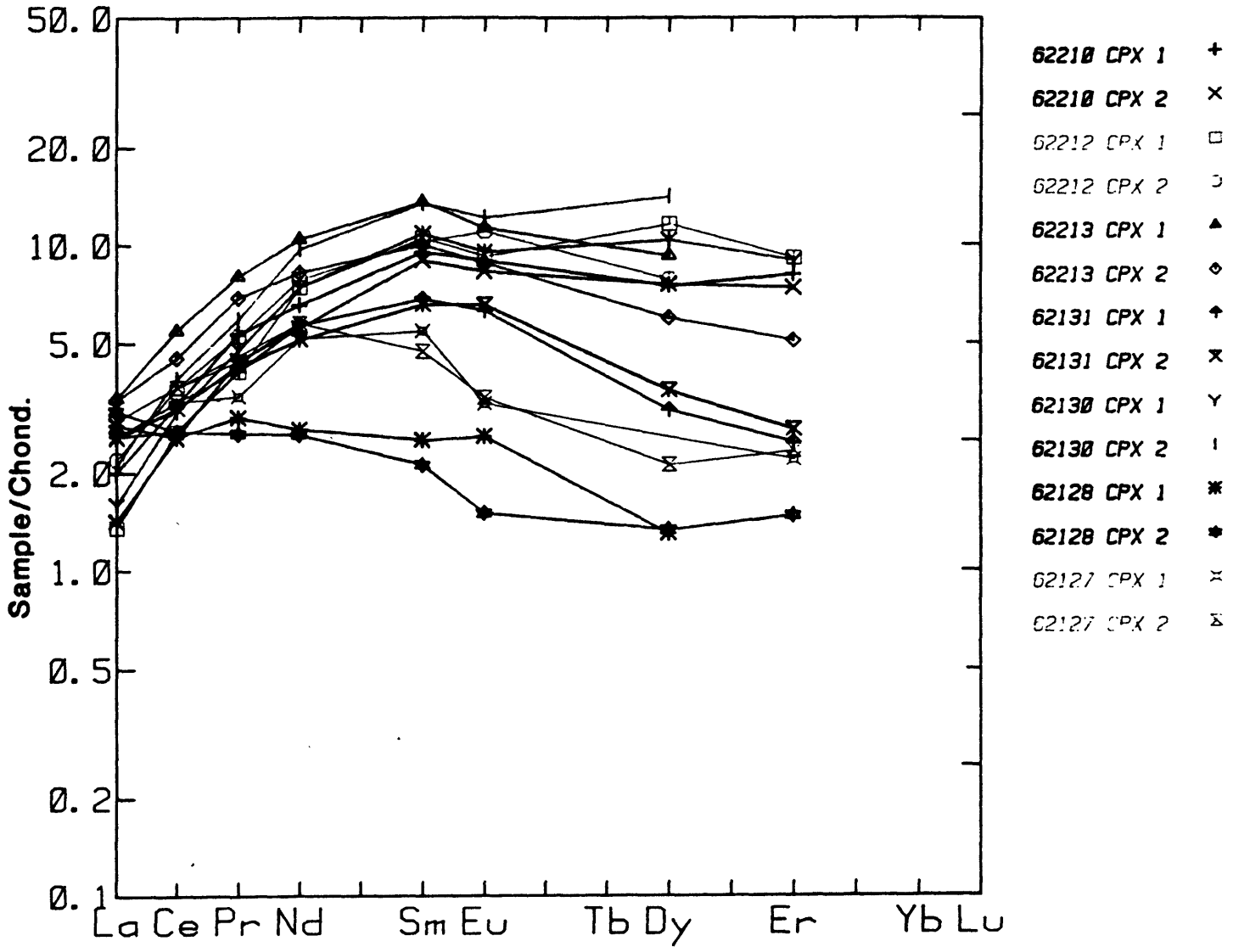

Figure 52. REE chondrite-normalized (Boynton, 1984) diagram for clinopyroxenes from 7 samples, with duplicate analyses using a poorer working curve and less resolved data collected previously to that in Fig. 51. These patterns are in general correspondence to those in Fig. 51. Sample 62127 should be considered only an estimate for reasons given in the text.

the patterns do appear to be relatively reproducible. Sample 62127 was placed on Figure 52 based on mass balance of Sm assuming it has similar partitioning to 62128. It was analyzed in a totally separate probe mount without a standard so that the REE pattern cannot be placed in a quantitative framework in the usual way. It appears to be approximately parallel to 62128 and is probably slightly more LREE depleted than 62128. One of the duplicates for each sample in Figure 52 was made close to the grain rim. No zoning in REE is obvious in any of these.

Other Trace Elements - The trace elements Sc, Ti, V, Cr, Sr and Zr were analyzed by the ion probe at a later session but on the same clinopyroxene grains. These elements are in much greater abundance than REE so the counting time can be much shorter to provide adequate statistics and the ion spot size is correspondingly smaller. Data are considered as precise as within counting statistics of individual analyses (Shimizu and Le Roex, 1986). Counting statistic errors for Sc, Ti, V and Cr are 2-4%, while Sr and Zr are 5-15%. Working curves for these elements are well established (Ray and Hart,1982), except for Zr which is poorer, so that concentration can be obtained from ion intensity. The accuracy is considered to be better than precision except for perhaps Zr. Table 10 includes data for these elements obtained by single spot analyses of single grains, just like for REE. The data for

62210 is an exception, as it is a mean of six quality spot analyses.

Exsolution and Associated Problems - The fact that the clinopyroxenes in these rocks are significantly exsolved with orthopyroxene lamellae creates a potential considerable problem. Analysis by ion probe essentially drills a small pit into the surface of a sample with the ion beam. It is important to be certain that the beam spot was in fact on clinopyroxene and not orthopyroxene exsolution lamellae. The samples are gold coated for the sake of conduction and the ion probe optics are poor enough so as to make this determination very difficult prior to analysis. One can use the chemistry of the sample as a guide but its difficult to monitor in real time with raw data. The best way is to look at the ion induced pit after analysis to confirm that in fact it was clinopyroxene that was analyzed. Plates 1-6 are a series of photographs taken of the samples using the back scattered electron imaging capabilities of the JEOL 733 electron microprobe. The photos take advantage of the ability to "mix" the scanning electron "topographic" capabilities with the compositional mode (average atomic number dependent, i.e. heavier phases are light colored and lower Z phases are dark). This mixing allows one to see both the exsolution and the ion probe pits. For each plate there is an (a) photograph of the entire grain and a (b) photo of a close-up of the pits. (Even more detailed observations of each pit were made during back scattered

Plates 1-6. A series of photographs of cpx grains from six Horoman samples taken with the JEOL 733 electron microprobe at MIT utilizing the back-scattered electron imaging capabilities. These samples were previously analyzed for REE and other trace elements using the ion microprobe. The photos show both "topographic" effects and compositional effects (materials with a greater average atomic number are lighter colored, lesser Z materials are darker). Thus one can see both exsolution and pits produced by ion microprobe analyses. These photos can be used to determine qualitatively whether the analyses are strictly of cpx, i.e. what is the degree opx contamination. Each plate has two parts, (a), a photograph of the entire grain and (b), a photo of a close-up view of the same grain showing the ion probe pits. Very bright white and light colored smears across the grains should be disregarded. The former is left over gold coat (used in ion microprobe analyses) not completely polished off the sample, and the latter is a preparation mistake of mounting epoxy smeared onto the grain by cleaning solvent. Opx lamellae are the darker colored lines and blebs within lighter colored cpx. The photos also include a 100 μm scale bar along the left side with the last four digits of the sample number.

Plate 1a) Photograph of a cpx grain from sample 62210, previously analyzed for REE and other trace elements by ion microprobe. Three REE pits and a traverse of thirteen trace element pits are apparent. Abundant exsolution lamellae of opx can be seen.

Plate 1b) Same grain as 1a but in a close-up view. Three ~40 μm REE pits (top left and bottom left-center are later better quality analyses with improved focussing than the pit in the center near the traverse which is from a previous analysis) can be seen. The top REE pit appears to be slightly more contaminated with opx than the bottom one. The traverse of thirteen trace element pits (~5 μm) can be clearly seen. Observation of these pits in terms of relative degree of opx lamellae is confirmed by chemical analyses (Fig 53, photo numbered from left to right) which shows that points 1, 4, 5, and 9 have the most opx (point 12 is in a crack). Lower-T, second generation exsolution lamellae can be seen in the bottom right hand corner of the photo in different orientation from the primary lamellae.

Plate 2a) Photograph of cpx grain from sample 62212, previously analyzed for REE and other trace elements by ion microprobe. Three REE pits and a single trace element pit can be recognized amid large exsolution lamellae of opx.

Plate 2b) Same grain as 2a but in close-up view. Two near identical REE pits can be seen at right with slight opx contamination. One more poorly focussed REE spot from a previous analysis can be seen in the upper middle. One trace element pit (~5 μm) can be seen between the two "2's" of the sample number at left that appears to be right on a microlamellae of opx. Chemically, the spot appears to be

contaminated only ~5%. A smaller second generation exsolution lamellae set is apparent at a different orientation. These two sets record two different temperatures (see text, in cpx major elements section). A second generation "lamellae-free" zone adjacent to the large first generation lamellae can be seen (see text for discussion).

Plate 3a) Photograph of cpx grain from sample 62213 previously analyzed for REE and other trace elements by ion microprobe. Three REE pits are visible in a line (left two are later, higher quality analyses) towards the lower center of the grain. One trace element pit can be seen near top-center and is free from opx (verified chemically).

Plate 3b) Same grain as 3a but in close-up view showing two REE pits. One towards the bottom left shows minor contamination from opx lamellae, while the other is quite pure.

Plate 4a) Photograph of cpx grain from sample 62131 previously analyzed for REE and other trace elements by ion microprobe. Splotchy exsolution style can be seen as can three REE pits in a line towards the top of the grain and one trace element pit on the left hand side of the line. The grain was analyzed for REE three separate times and shows that the quality of the focussing improved with time to a linear- shaped pit (right), to a triangular-shaped pit (center), and the best quality, near circular pit (left).

Plate 4b) Close-up view of the same grain as 4a. The best quality REE pit (center) shows some minor opx contamination as does the previously analyzed triangular-shaped pit. The trace element pit can be seen near the second "1" of the sample number at left and is uncontaminated. Second generation opx lamellae can be seen at a different orientation (as in 2a above).

Plate 5a) Photograph of cpx grain from sample 62130 previously analyzed for REE and other trace elements by ion microprobe. Two REE pits and one trace element spot can be seen towards the center of the grain amid opx exsolution lamellae.

Plate 5b) Close-up view of the same grain as 5a. In the REE pits minor opx contamination can be seen. The trace element spot (lower right) does have slight opx contamination which is verified chemically.

Plate 6a) Photograph of cpx grain form sample 62128 (mis-labelled in photo) previously analyzed by ion microprobe for REE and other trace elements. Two poorly focussed REE pits can be seen at right (linear shape) as well as two better quality REE pits and one trace element pit directly in the center of the photo.

Plate 6b) Under exposed close-up view of the same grain as in 6a. The best quality REE analysis is quite clean (top right) as is trace element pit (top left).

Plate 1

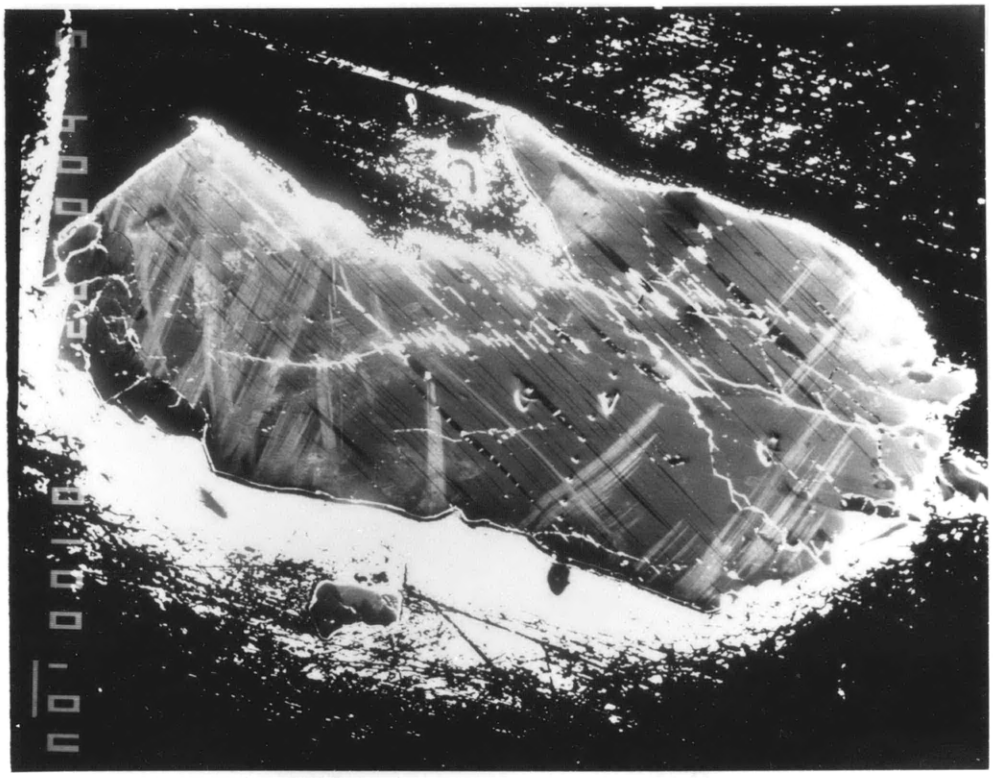

(a)

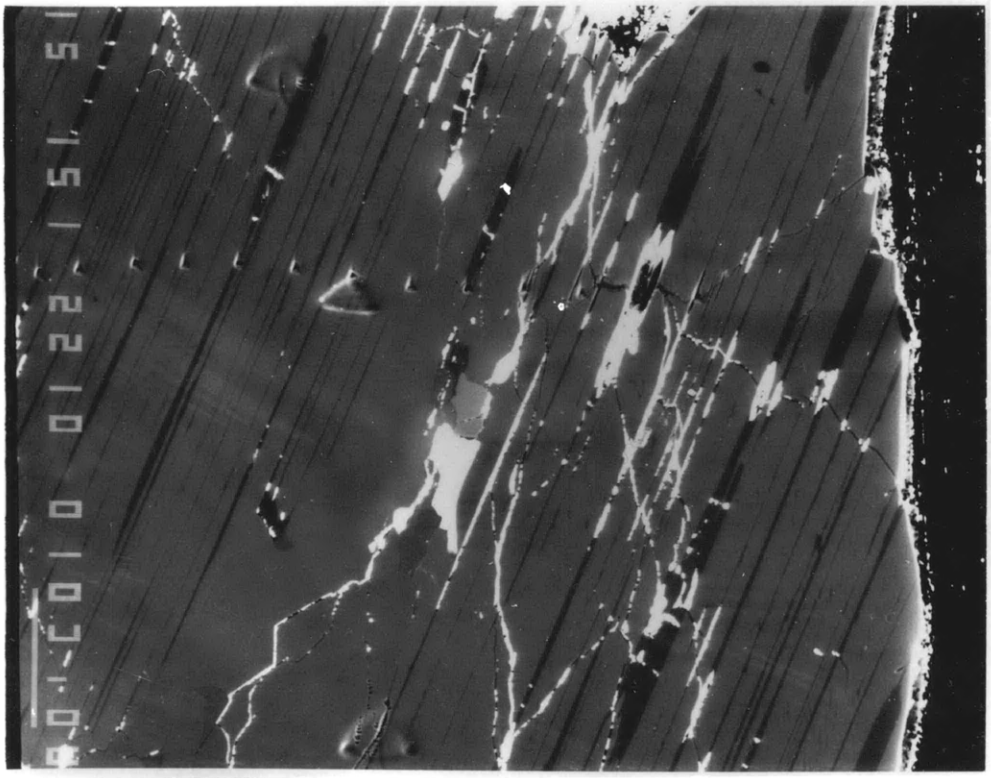

(b)

Plate 2

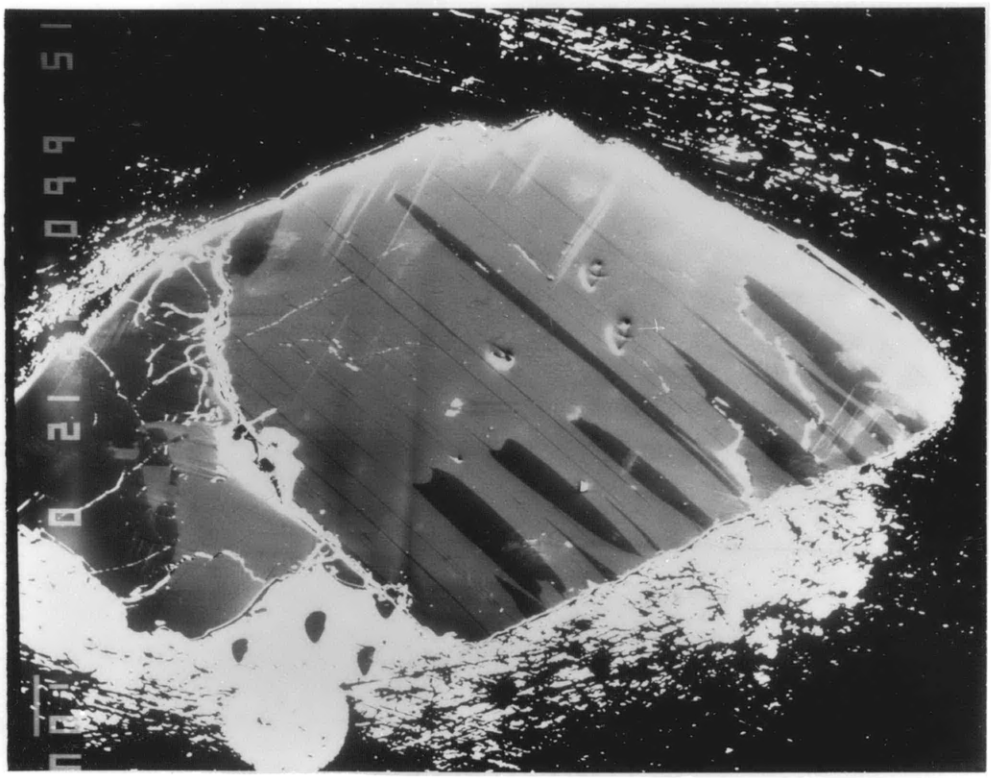

(a)

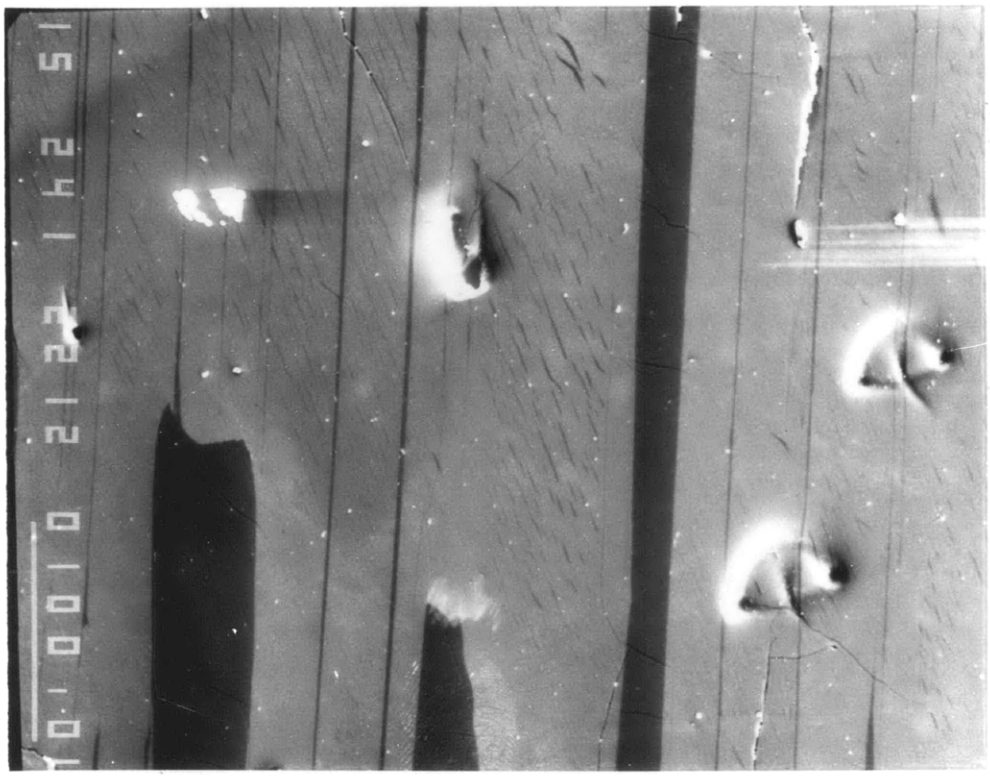

(b)

Plate 3

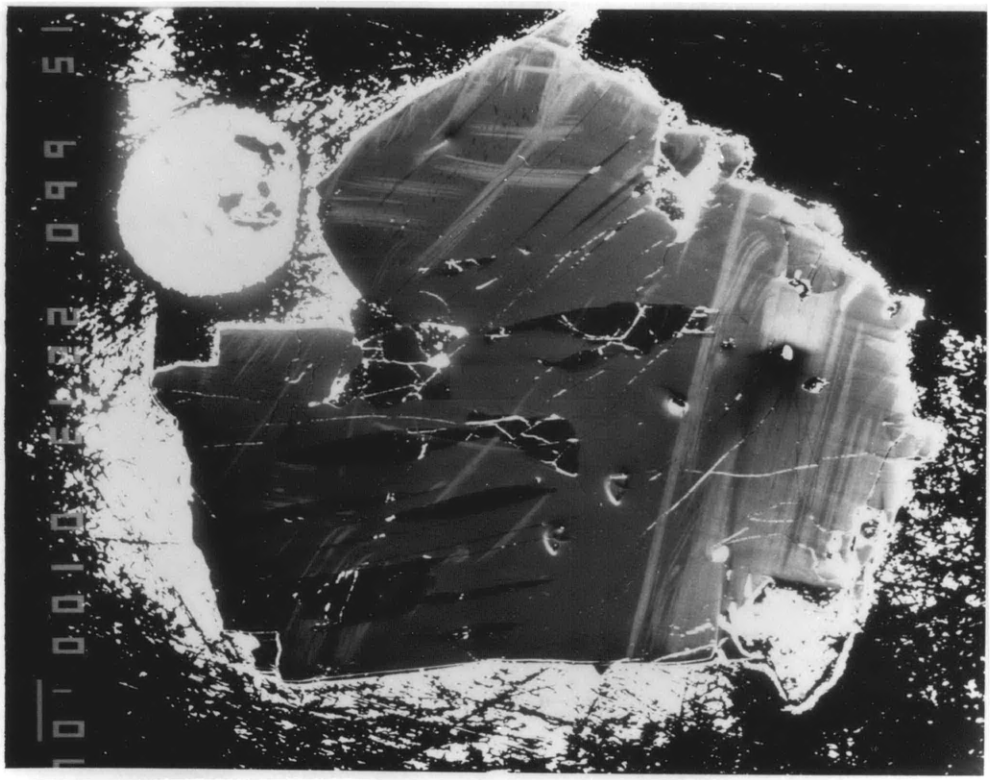

(a)

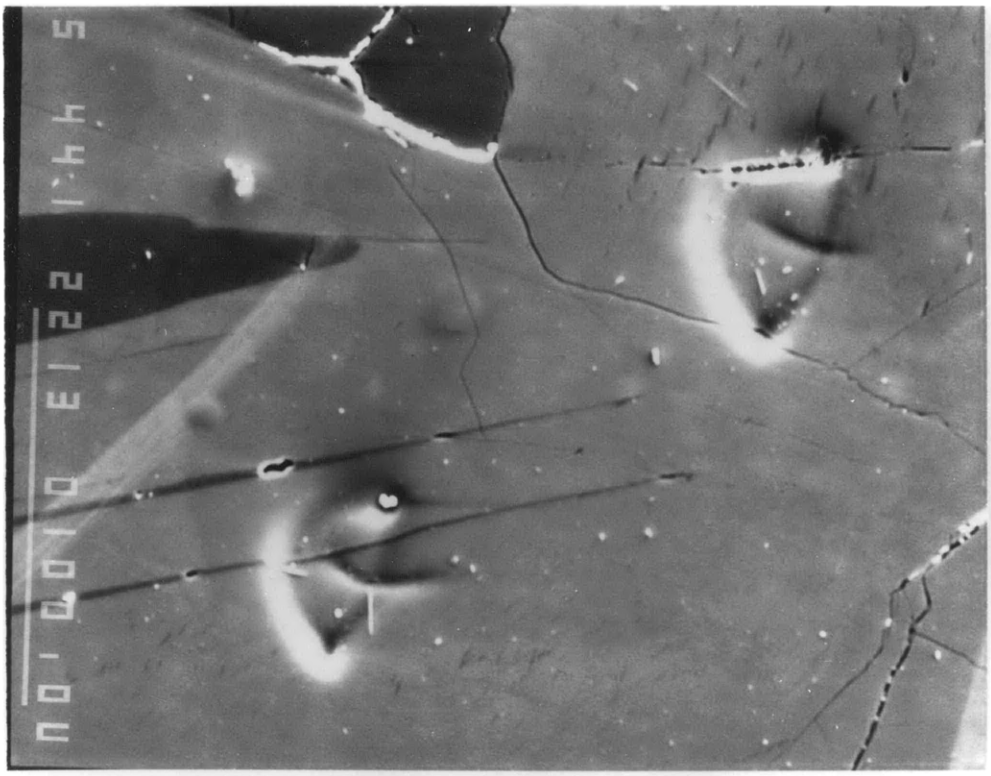

(b)

Plate 4

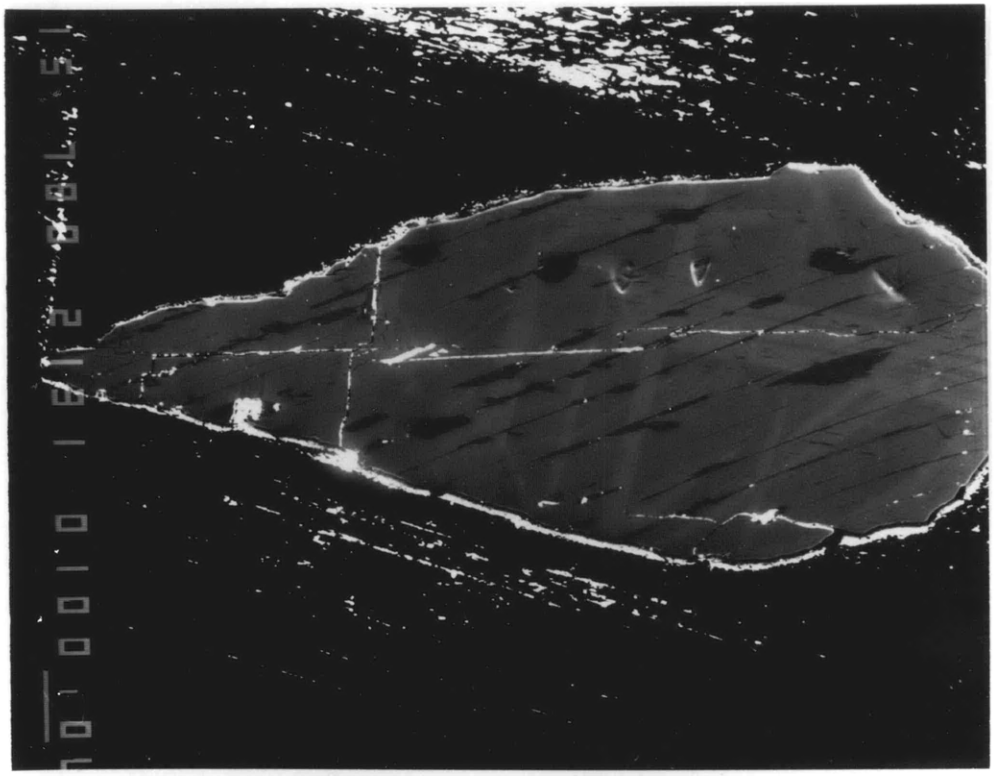

(a)

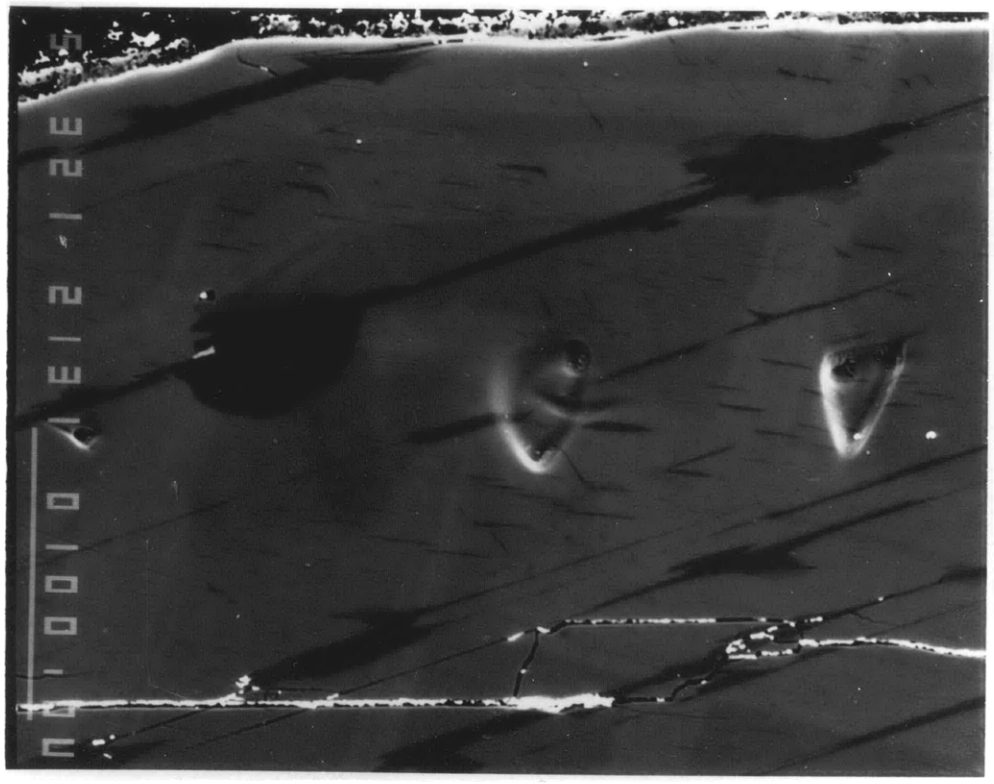

(b)

Plate 5

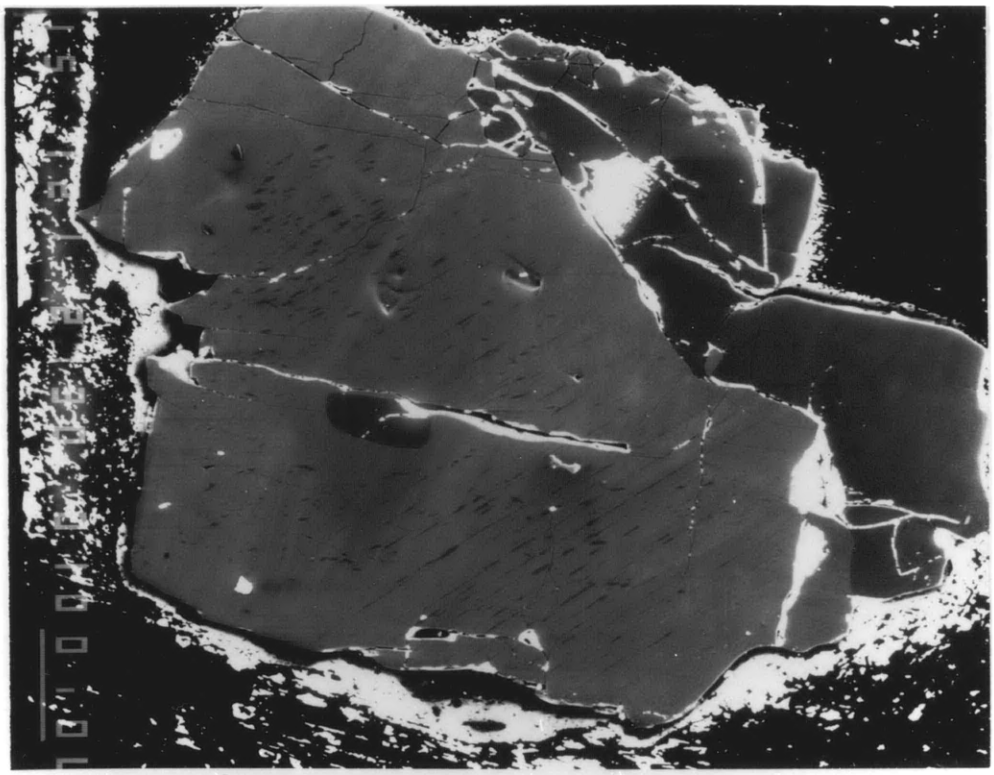

(a)

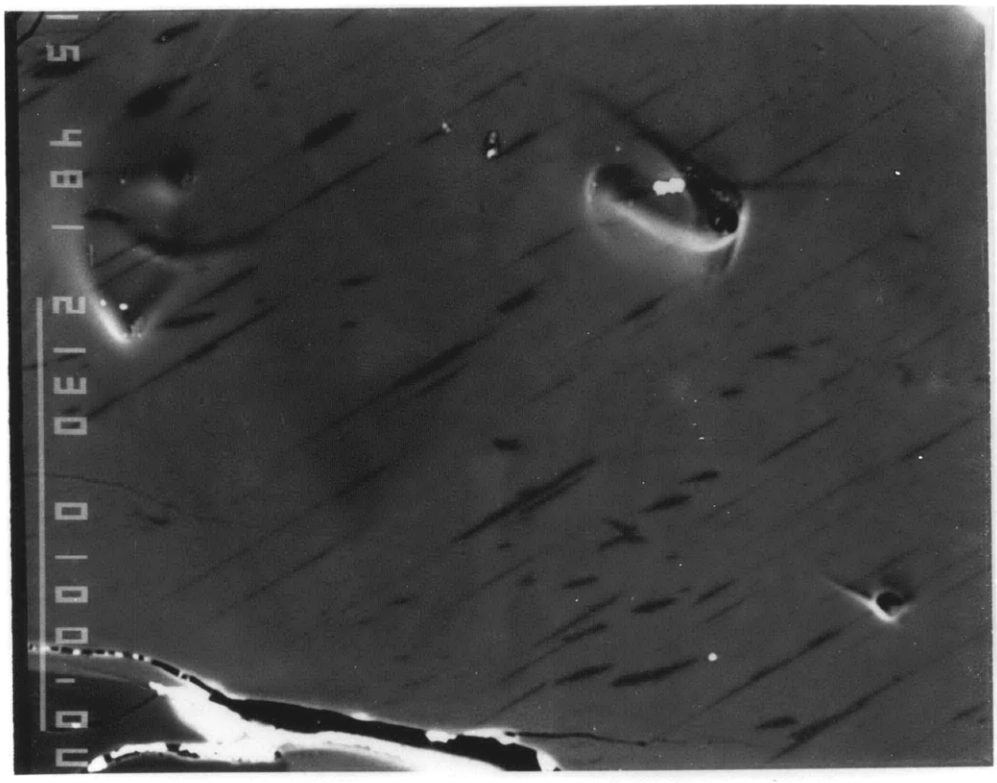

(b)

Plate 6

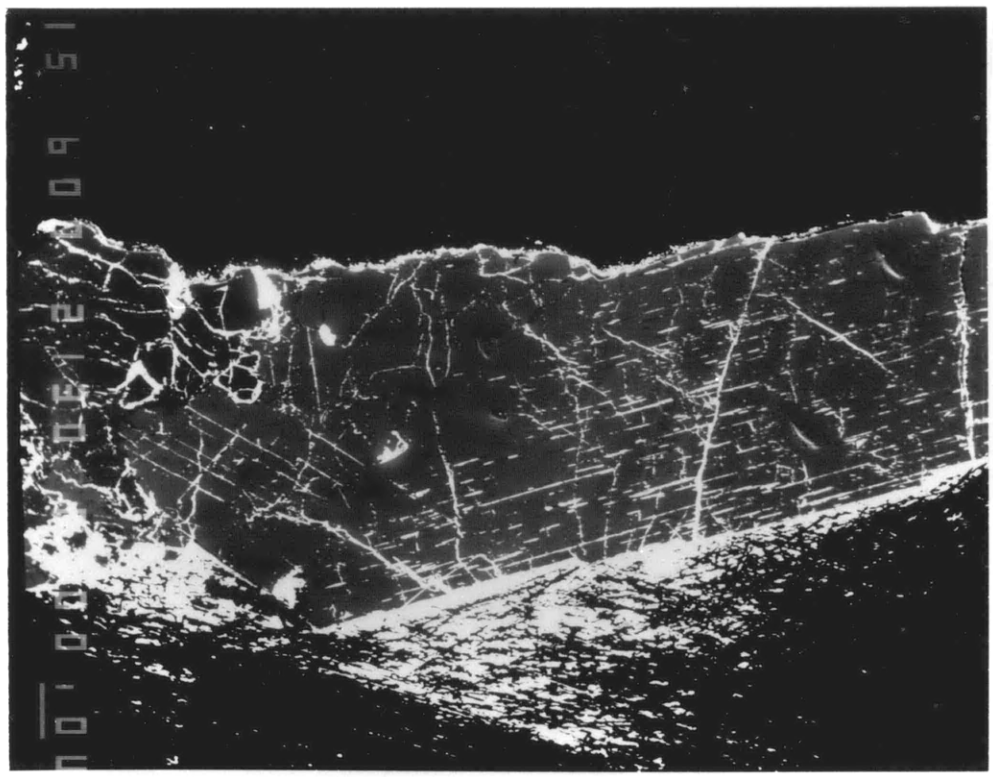

(a)

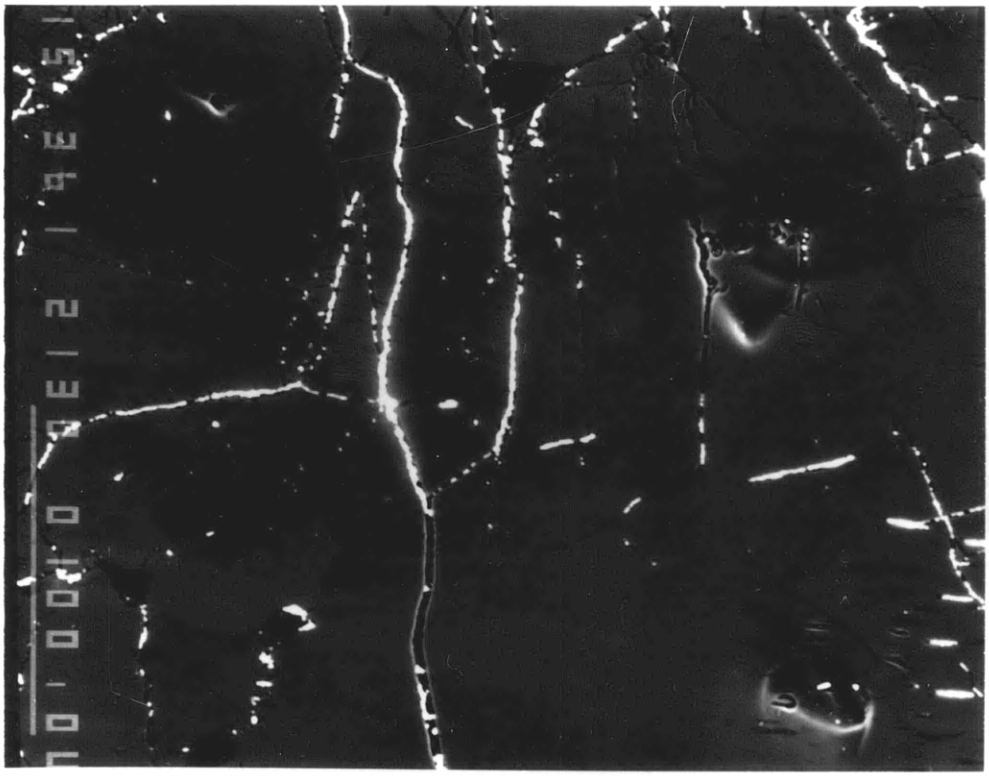

(b)

electron observation to confirm the quality of the analysis, but photographs were not made.) The very bright white in these photos is left over gold coat not completely polished off. The light colored smears across the grain is a sample preparation mistake, epoxy smeared onto the grain by cleaning solvent. The orthopyroxene lamellae are obvious dark colored lines and blebs. The photographs also feature a 100μm scale bar along the side of the photo. In Plate 1b three ~30μm REE pits and a traverse of thirteen ~5μm trace element pits can be seen. REE analyses made at a later date have different pit shapes owing to improved focussing of the ion beam by the operator. In this way later generation, better quality analyses can be identified (Table 10). None of the REE pits appear to have greater than about five percent orthopyroxene in the form of microlamellae which would simply act as a dilutant. Plates 1-6 legitimize the REE data with respect to orthopyroxene pollution. One unknown factor is the relative sputtering rates of the two phases but there is no evidence to suggest that they are different.

The same visual check can be made for the smaller trace element pits. None of these pits appear to be on orthopyroxene lamellae with the exception of some of the traverse points of sample 62210 (Plate 1b) and possibly the spot for 62212 (Plate 2b). Fortunately for these pits we can confirm this chemically with the Ca/Si ratio measured along with the trace elements. Shimizu (1986), studying

simple silicate glasses with the ion probe, observed a very good positive correlation between Ca/Si ion intensity and Ca/Al atomic ratios that were consistent with testing of natural silicate minerals. Using this relationship average clinopyroxene Ca/Si compositions (Table 7) were converted to intensity ratios and compared to the ion probe spot analyses. This is not a quantitative test, for the actual major element composition of the clinopyroxene grains studied with the ion probe are unknown. However, for three samples (62213, 62131 and 62128) the measured ion probe Ca/Si intensity is greater than that calculated indicating little if any orthopyroxene contamination. Sample 62130 suggests minimal orthopyroxene mixing (~1-2%). 62212 which exhibits possible orthopyroxene contamination in the photograph, (Plate 2b) chemically indicates ~5% orthopyroxene. Both the visual and chemical evidence again legitimizes the ion probe trace element data with respect to orthopyroxene mixing (or dilution). Quantitative analyses of exsolved pyroxenes should not be done with the ion probe without this kind of confirmation.

A unique addition to this problem is provided by the traverse of 13 spot analyses for trace elements for the sample 62210 clinopyroxene. Using the same mixing argument used above, based on Ca/Si intensity ratios, the analyses range from mostly orthopyroxene in point 9 (~40% clinopyroxene) to almost entirely clinopyroxene in a number of points. The chemical profiles of both major element

intensity ratios and trace element abundances fit with a model of simple mixing of clinopyroxene and orthopyroxene (Fig. 53). The best indicators of mixing are the Ca/Si ratio and the exact opposite behavior of the Mg/Si ratio. All the other profiles, with the exception of Fe/Si, essentially follow the Ca profile. This is expected as most trace elements should substitute in the Ca site of clinopyroxene. There are some subtle differences but generally, if you remove the most "orthopyroxene-like" points (4,5 and 9; point 12 is on a crack and is not plotted), the trace element distribution in the clinopyroxene is relatively homogeneous. There does appear to be a slight surplus of trace elements in clinopyroxene in the vicinity of orthopyroxene lamellae (e.g. Zr, Sc and Ti in positions 8 and 10; V, Cr, and Sr in position 3) as would be expected. Relative position of these peaks for different elements suggests a way of looking at relative mobility of the elements in the solid state. This data suggests the possibility of a yet unstudied phenomenon of trace element partitioning in exsolution lamellae.

Data and Discussion - Several first order observations can be made about the REE patterns of the clinopyroxenes (Fig. 51). First, the patterns generally have the same shape as the whole rock patterns (Fig. 35). Second, there is much more variability in the HREE (greater than 10X) than in the LREE (less than 3X). Clinopyroxenes in ultramafic xenoliths sometimes have similar REE patterns

Figure 53. Chemical profile based on 13 spot analyses across ~500u clinopyroxene from sample 62210 for major elements (Fe, Na, Mg (broken line), Ca and Al plotted as relative intensities to Si) and trace elements (Zr, Sc (broken line), Sr, Cr, Ti and V as actual abundances in ppm) showing variation due to exsolution of orthopyroxene (see text).

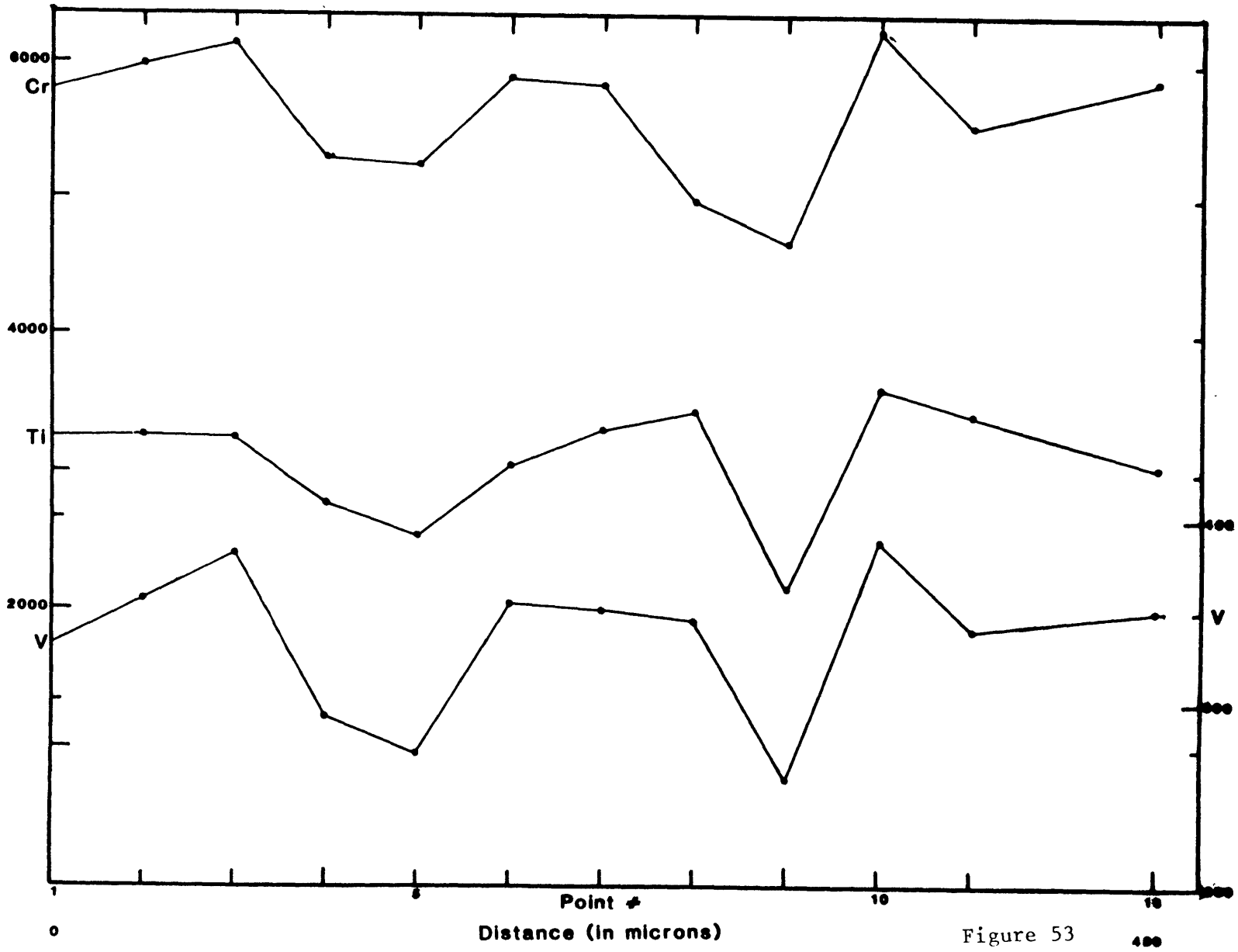
6000
Cr
4000
Ti
2000
V
1
5
10
15
Point #
0
Distance (in microns)
400
V

Figure 53

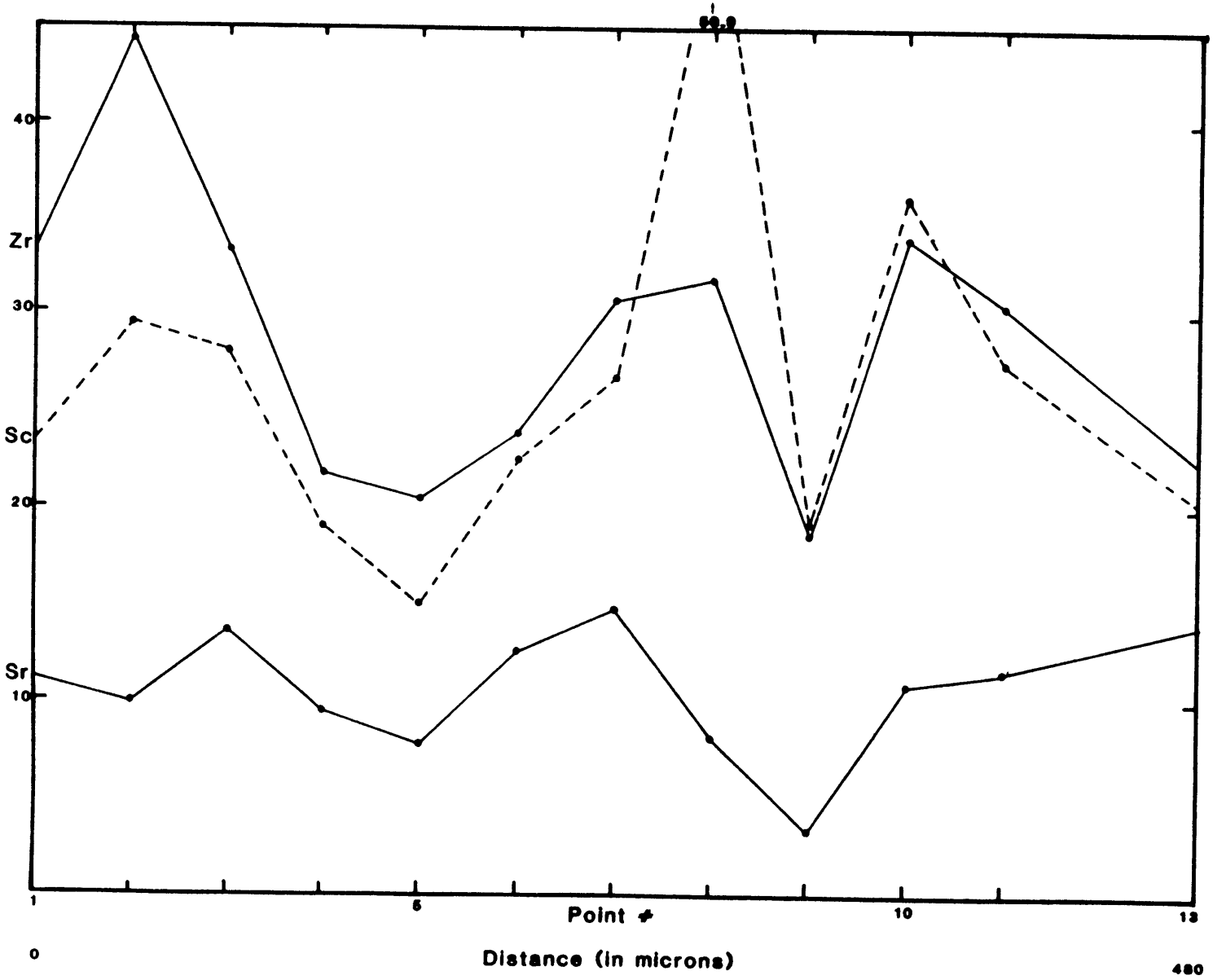

Figure 53, cont...

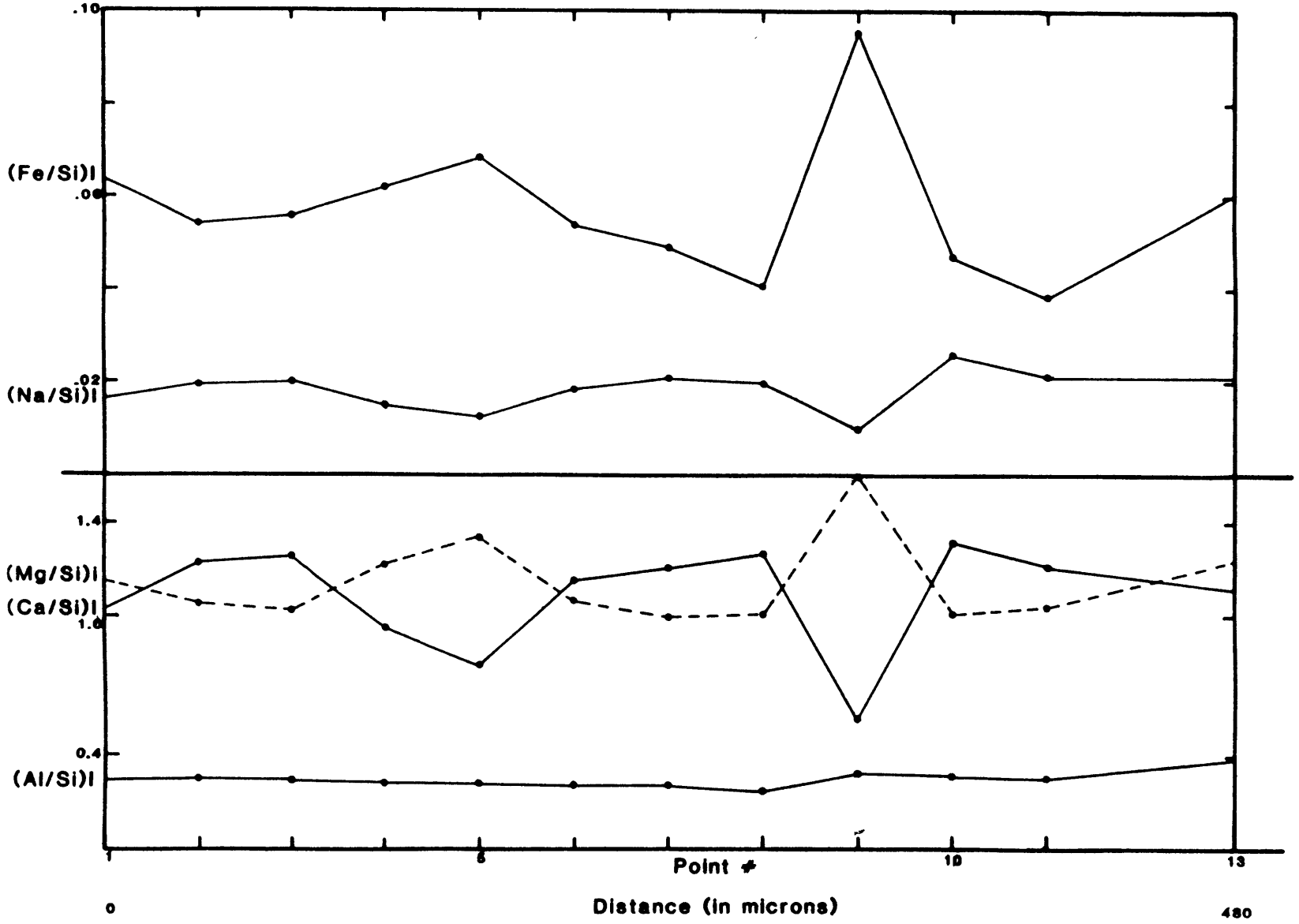

Figure 53, cont...

to the Horoman clinopyroxene REE patterns but they invariably have more variation in the LREE than in the HREE (e.g. Stosch and Seck, 1980; Stosch and Lugmair, 1986; Kurat et al, 1980). The whole rock patterns also show more variability in the HREE than in the LREE. Third, there are clearly no negative Eu anomalies in any of the patterns as one would expect in plagioclase bearing lherzolites. (It should be mentioned that Sm is the poorest quality data of any of the REE. It is not even plotted for samples 62130 and 62128 because of poor quality. Incidently, these two Sm values would have plot very near the line but they did not meet the statistical criteria within the single analysis statistics. The fact remains that the clinopyroxenes have no Eu anomaly, irrespective of the quality of the Sm data). Some more specific observations and comparisons can also be made about the clinopyroxene REE patterns. (1) 62210, the least depleted sample by most criteria, has the most enriched pattern except for the LREE, just as it is in the whole rock pattern. (2) Sample 62213 has the greatest abundance of LREE as it does in the whole rock. (3) From the clinopyroxene patterns you could not pick out three distinct groups as you can from the whole rock patterns. (4) The pronounced HREE depletion in sample 62131 does not exist in the whole rock pattern and is similar to clinopyroxenite xenoliths patterns from Salt Lake Crater, Hawaii (Frey, 1980). (5) Samples 62212 and 62213 have nearly identical patterns between Sm and Er, as they do in

the whole rock, and are slightly HREE depleted. (6) Samples 62210 and 62130 have near parallel patterns. This pattern of LREE depletion and near unity for MREE/HREE ratio is fairly common in xenolith clinopyroxenes (Kurat et al, 1980; Stosch and Seck, 1980). (7) The pattern for sample 62128 is somewhat similar to the whole rock pattern but is more HREE depleted and shows no Eu anomaly. Similar patterns are seen in some xenolith clinopyroxenes (Stosch and Seck, 1980; Stosch and Lugmair, 1986) that are generally more enriched in all the REE than 62128 and also tend to be from harzburgite samples. It is clear from the previous discussion of major element clinopyroxene data that several complex processes, besides melting processes, determine clinopyroxene chemical variation. Any model used to explain the chemical variation in the Horoman peridotites should ultimately fit the above REE observations as well.

It is useful to combine mineral separate data with information about how much of the mineral is contained in the rock to adequately compare rock chemistry. In Figure 54 the proportion of each REE in the whole rock accounted for by clinopyroxene is shown. The result is not entirely expected. The Horoman samples show general parallelism between rocks, with marked depletion in the LREE and the HREE. The same information for a number of lherzolite xenoliths is plotted for comparison. The clinopyroxene proportion of the total REE budget appears to be the greatest at Nd for the majority of the Horoman samples,

Figure 54. REE diagram plotted with respect to proportion of each REE accounted for by clinopyroxene, *i.e.* (cpx conc.) x (cpx mode) / (whole rock conc.), for six Horoman samples (heavy solid lines), and from the xenolith literature for comparison: five clinopyroxenes from Dreiser Weiher, W. Germany, IB-2, IB-6, IB-8 and IB-24 (Stosch and Seck, 1980) D-42 (Stosch and Lugmair, 1986) (broken lines and open circles); one clinopyroxene from Kapfenstein, Austria, KA-168 (Kurat et al, 1980) (open squares); and one clinopyroxene from Assab, Ethiopia, 3G-15 (Ottonello et al, 1980) (open triangles). Modal clinopyroxene is shown following each sample in parentheses. See text for further explanation.

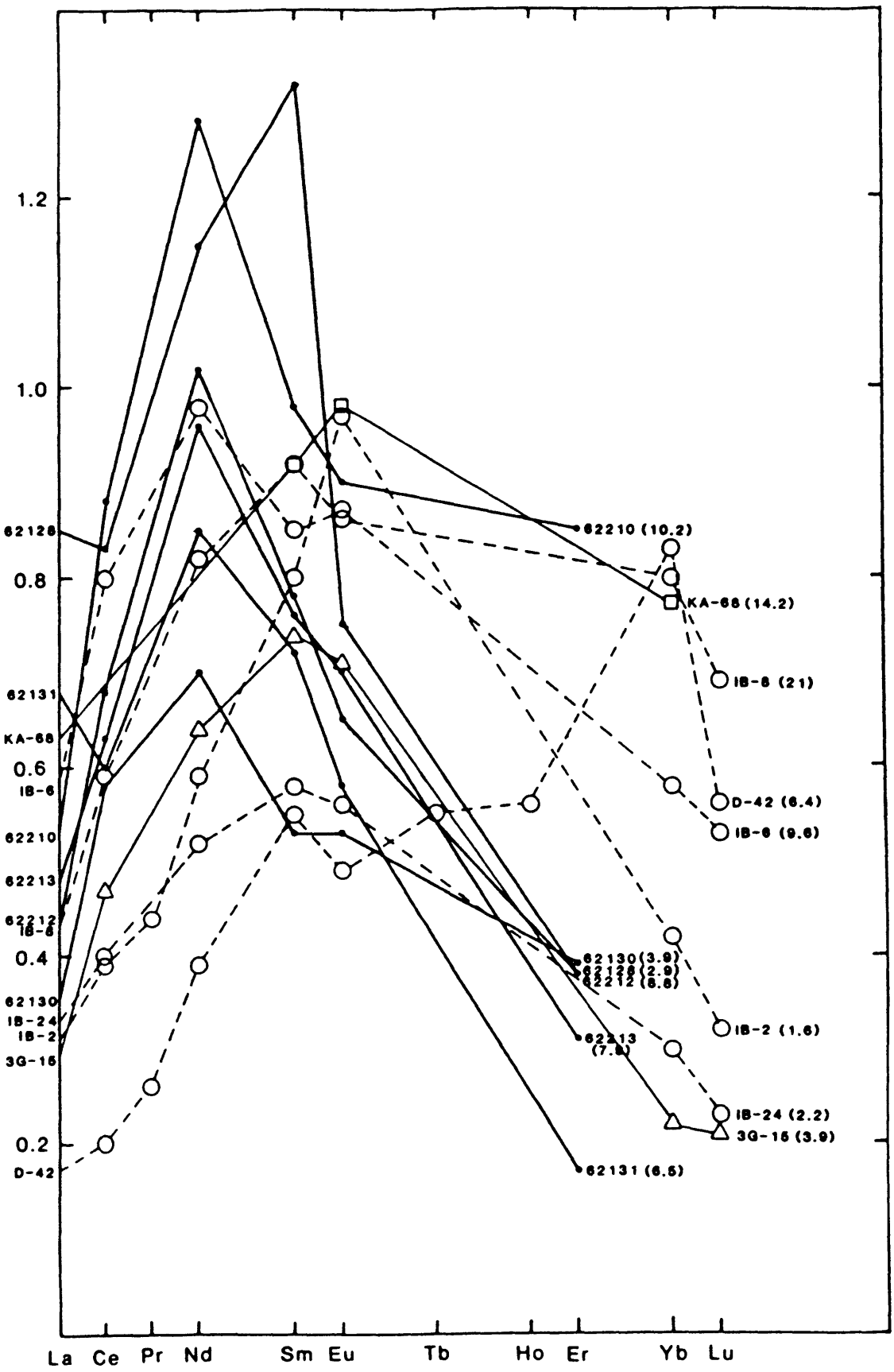
1.2
1.0
0.8
0.6
0.4
0.2
62128
62131
KA-68
IB-6
62210
62213
62212
IB-6
62130
IB-24
IB-2
3G-15
D-42
62210 (10.2)
KA-68 (14.2)
IB-6 (21)
D-42 (6.4)
IB-6 (9.6)
62130(3.9)
62128 (2.9)
62212 (6.6)
IB-2 (1.6)
62213
(7.6)
IB-24 (2.2)
3G-15 (3.9)
62131 (6.5)
La Ce Pr Nd Sm Eu Tb Ho Er Yb Lu

Figure 54

while Sm is best accounted for by clinopyroxene in the xenoliths. Total modal clinopyroxene is shown in the figure for each sample and in general, particularly for the xenoliths, a larger proportion of clinopyroxene HREE occurs in the samples containing more clinopyroxene. This is intuitive considering that we know orthopyroxene and olivine favor the HREE over the LREE. In other words olivine and orthopyroxene will account for a larger proportion of HREE in the rocks that contain more olivine and orthopyroxene. Relation between total REE proportion in clinopyroxene and amount of clinopyroxene is not straight forward in the Horoman samples. In the MREE, with the exception of the harzburgite (62128), the samples are arranged in descending order of clinopyroxene REE proportion and modal clinopyroxene. But this pattern does not exist in the LREE or the HREE.

The next logical extension of this type of treatment is to use the clinopyroxene data with mineral/mineral partition coefficients from the literature to estimate concentrations in the other phases and thus reconstruct a whole rock concentration using the modes. This mass balanced estimate based on clinopyroxene concentrations can then be compared to the real whole rock value. Figures 55 and 56 show the ratio of the estimate to the actual analyzed whole rock abundances for the REE using two different sets of partition coefficients. Ideally if the clinopyroxene REE concentrations are representative of all the clinopyroxene

Figure 55. REE diagram showing ratio of total rare earth abundance predicted for six Horoman samples based on measured clinopyroxene concentrations using partition coefficients from Prinzhofer and Allegre (1985) and modes (Table 1), to actual measured bulk rock rare earth abundance. Ideally, lines for all samples should be straight at ratios of one if the cpx REE concentrations are representative of all the cpx in the sample, are analytically correct, the calculated modes are correct, minerals are obeying standard equilibrium partitioning relationships from the literature, and finally the whole rock abundances are analytically correct.

Figure 56. Same as Fig. 55 except that partition coefficients of Frey et al (1978) Set 1, are used for all minerals in the mass balance calculation except for plagioclase where Prinzhofer and Allegre (1985) values were used. Er is not included because no partition coefficients are included for this element in Frey et al (1978).

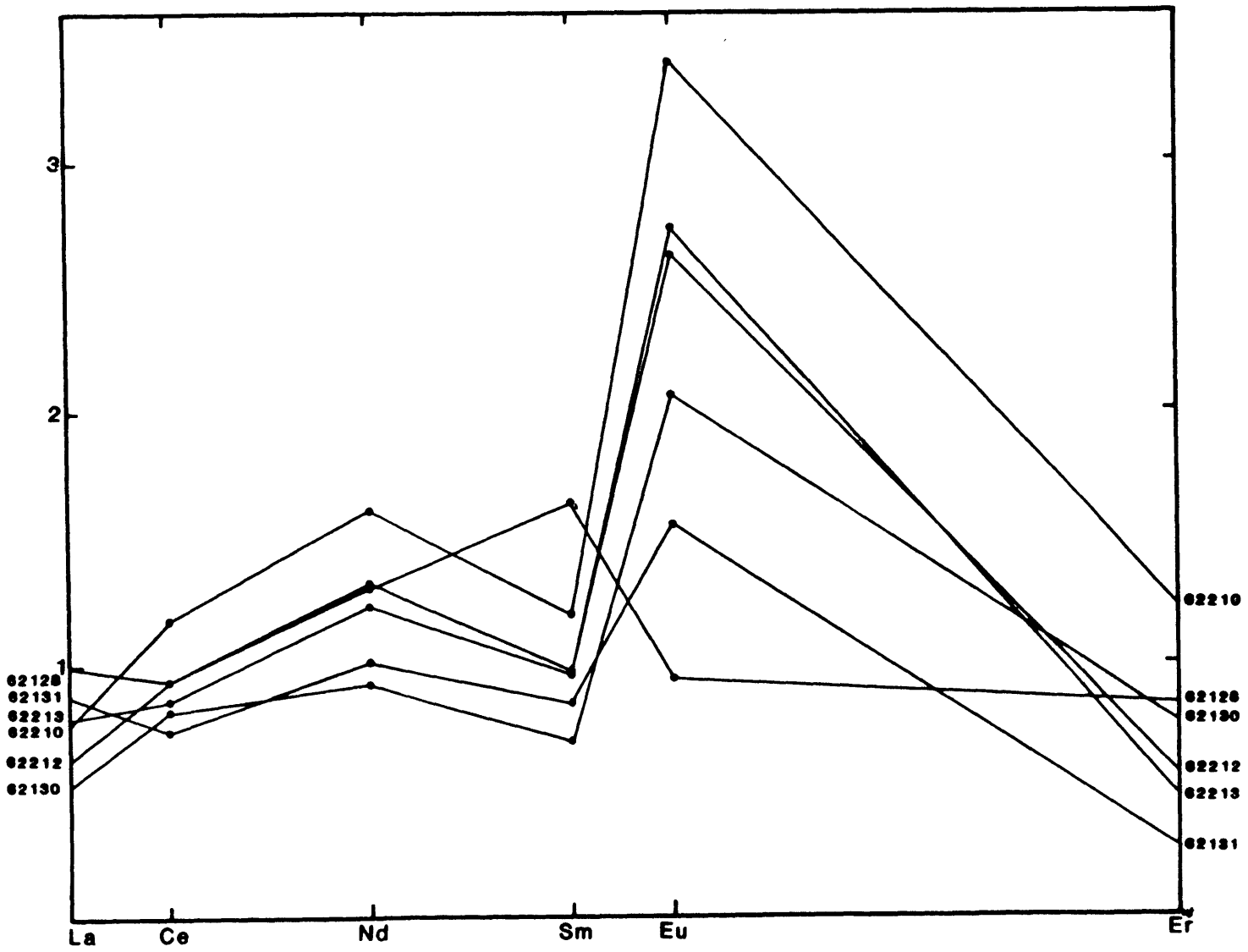
3
2
1
62128
62131
62213
62210
62212
62130
62210
62128
62130
62212
62213
62131
La
Ce
Nd
Sm
Eu
Er

Figure 55

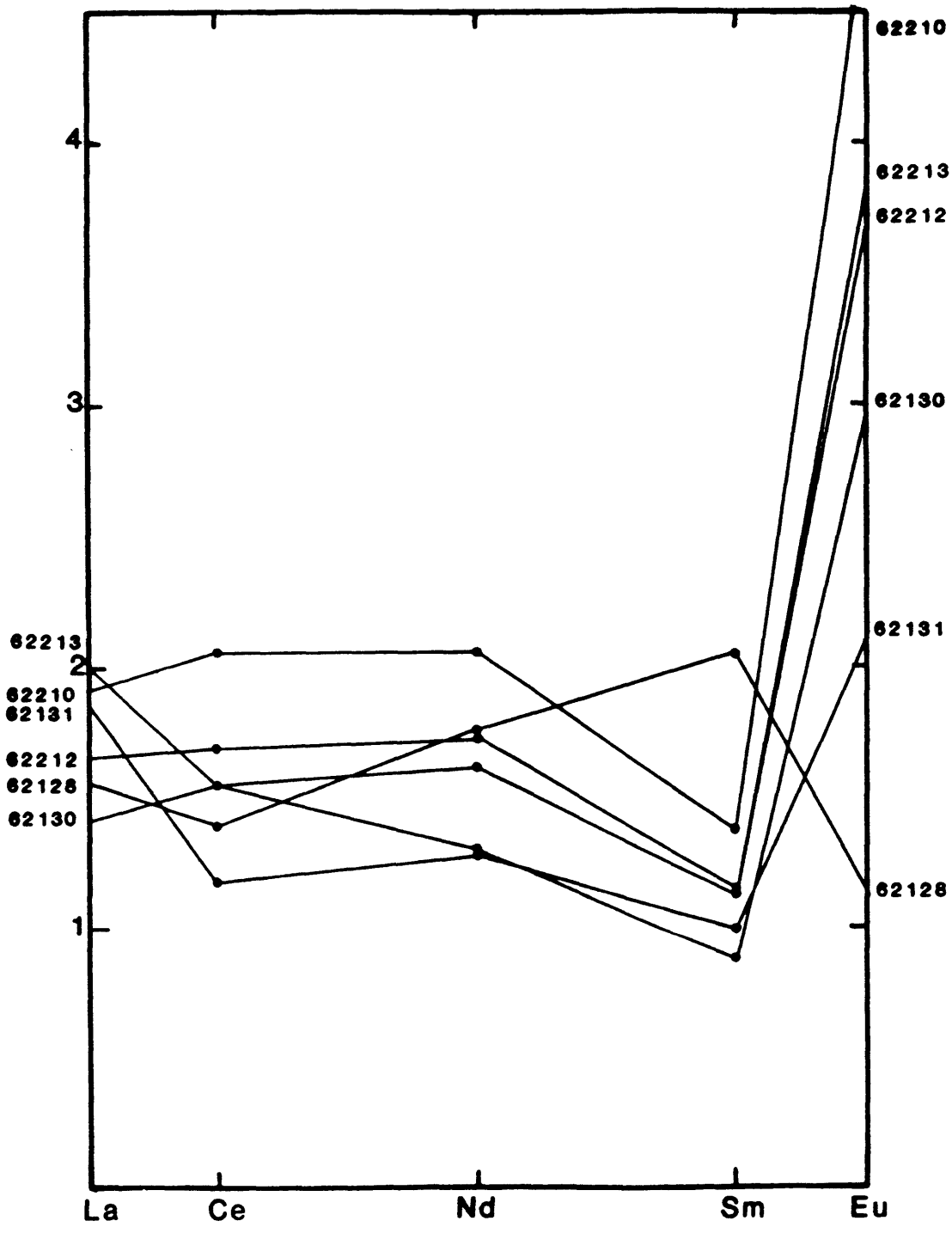
62210
62213
62212
62130
62131
62128
4
3
2
1
62213
62210
62131
62212
62128
62130
La
Ce
Nd
Sm
Eu

Figure 56

in the sample and if the minerals are in equilibrium with each other, obeying partitioning relationships, lines in the diagrams would be flat and approximately one. Clearly this is not the case. The figures represent a rather tenuous calculation due to possible errors in all the values used. The clinopyroxene REE abundance may not be representative of the sample as a whole and it includes an analytical error of ~5-10% as well; the modes calculated by linear regression, include some error; the partition coefficients used may not be appropriate and also contain some error; and finally the whole rock values of REE that are being normalized to have analytical errors associated with them. Despite the presence of these errors and possible combinations of them, the patterns from Figure's 55 and 56 should be relatively flat and cluster about unity.

The first obvious observation is that Eu is clearly being over estimated. The most likely cause of this is that the plag./cpx partitioning used in the calculations are inappropriate. There are two possible explanations for this. The first is that plagioclase and clinopyroxene are not in equilibrium so that Eu^{2+} has never partitioned from the clinopyroxene into the plagioclase, or perhaps only locally. If the plagioclase is actually produced by metamorphic sub-solidus reactions, as discussed later in the section discussing plagioclase, this may be likely. The other possibility is that there simply is no Eu^{2+} produced at the oxygen fugacity at which plagioclase and

clinopyroxene equilibrated so that plagioclase would not be expected to favor Eu over any of the other REE. If conditions are very oxidizing, i.e. high oxygen fugacity, the Eu^{2+} abundance will be quite low. Mantle conditions are generally much more reducing than surficial conditions. This is an argument against plagioclase at Horoman being a mantle phase. The Eu content in the harzburgite (62128) with no plagioclase is well matched by the estimated made from clinopyroxene abundance.

Figures 55 and 56, with different partition coefficients, share the same general features but also have some important differences. Using partition coefficients from Frey et al (1978) (Fig. 56), almost all the REE for all the samples are over estimated. (No D's are given for Er so it is not plotted.) With the partition coefficients of Prinzhofer and Allegre (1985) (Fig. 55), the LREE are under estimated, Nd is usually over estimated and Er again is under estimated. Between Nd and Eu the shapes are near identical for the two plots with only the magnitude enhanced in Figure 56. The shapes are different between the two figures in the LREE. This is potentially important for it is often stated, particularly in the ultramafic xenolith literature, that considerable LREE exist at grain boundaries and not in the phases themselves. Figure 55 would support this view while Figure 56 would not. The patterns in both diagrams are relatively parallel with the exception of 62128 and some crossing patterns between La and Ce and at Er.

These figures, especially Figure 55 still maintain the general features of the total clinopyroxene REE budget (Fig. 54). Ce, Nd, Sm and Eu are generally arranged in descending order with decreasing clinopyroxene or increasing degree of depletion (again, with the exception of the harzburgite). That is, if a rock contains greater abundance of REE, the clinopyroxene will contain proportionally more of the REE. This pattern is not understood and breaks down both with La and Er. This same information was plotted versus degree of melting for each REE element but no new understandable patterns emerged. The complexities in these figures really just reflect the complexity of the clinopyroxene REE patterns (Fig. 51), and suggest that partitioning between clinopyroxene and other mantle phases may be a much more intricate process than assumed for much work done with basalts. It is not clear whether these partitioning processes are taking place during the melting process itself or whether it is really re-partitioning we are seeing to various degrees and under various conditions.

A similar comparison of non-REE trace element contents estimated using measured clinopyroxene values and analyzed whole rock abundances was done (Fig. 57). This figure is different in that it is plotted versus degree of melting for each element but it contains the same information. (These elements are not all expected to act coherently so comparing patterns may be misleading, unlike REE.) Again, a great deal of scatter exists around unity for most of the

Figure 57. Similar plot to Fig's. 55 and 56 for other trace elements but plotted against F determined by major element calculation rather than against element, *i.e.* each element produces a line rather than each sample. Partition coefficients used: V, Clague and Frey (1982); Zr and Ti, Pearce and Norry (1979); Sr, Frey et al (1978) except for plagioclase from Drake and Weill (1975); and Sc, Sun et al (1979). Exceedingly high values for Sr are not plotted but shown separately and with the direction towards large F with broken line and arrow.

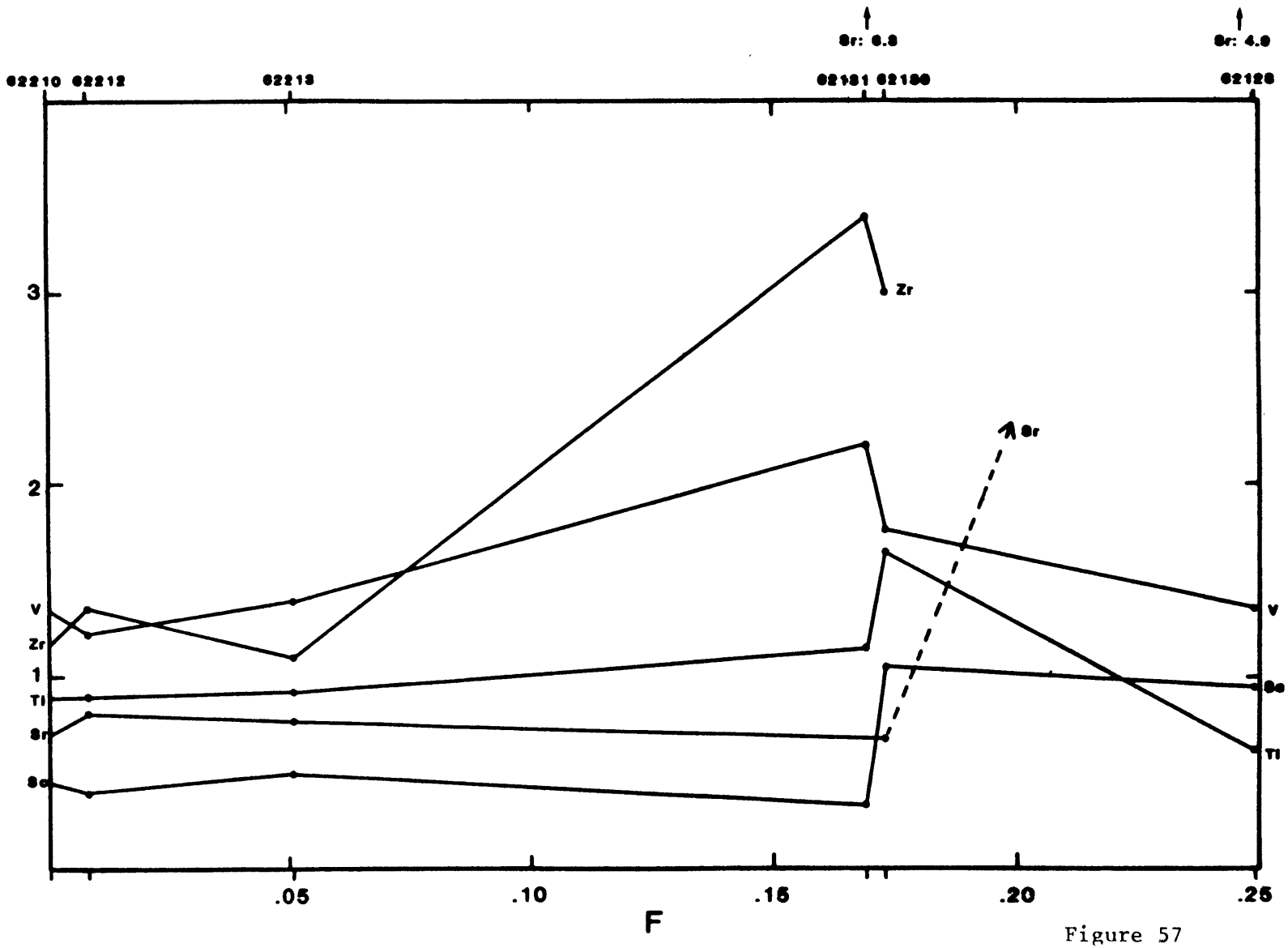
Sr: 6.8
Sr: 4.8
62210 62212
62213
62181 62186
62126
3
2
1
Zr
Sr
V
Zr
Ti
Sr
Sc
V
Sc
Ti
.05
.10
.15
.20
.25
F

Figure 57

elements. Ti is fairly well matched in the less depleted rocks while Sc is well matched in the two most depleted samples but is severely under estimated for the remainder of the samples. V and Zr appear to be over estimated, particularly at higher F values. Sr is underestimated by about a constant value except for two samples (62131 and 62128) where it reaches ridiculously high levels. Since Sr is thought to be compatible in plagioclase (Drake and Weill, 1975) the great disparity in Sr may be explained by varying degrees of re-partitioning of Sr between clinopyroxene and plagioclase. The two anomalous Sr values could be from clinopyroxene grains that were never in local equilibrium with plagioclase to allow Sr to re-partition into plagioclase. But 62128 has no plagioclase and 62131 only approximately four percent. These same two samples have the lowest Eu values in Figure 55 and 56 to contradict the local equilibrium hypothesis. The fact that the two elements that may partition strongly into plagioclase, Sr and Eu, act so strangely in the Horoman rocks suggests that they are being governed by local processes. The two elements appear to be behaving differently implying that the processes controlling their partitioning are not the same.

The apparent "step function" between samples 62131 and 62130, that steps both directions, is very curious. A similar step is seen in the REE data of these samples if plotted versus F. The observation from whole rock major element, REE and other TE data as well as mineral major

elements, that these two samples are quite similar is contradicted by trace elements in the clinopyroxenes. Perhaps it is a question of scale. Although the rocks as a whole may have undergone similar processes to similar degrees any two clinopyroxenes from these samples may not exhibit the effects of these processes to the same degree. The disparity of trace element contents in the clinopyroxenes of these two samples is exhibited in the remainder of the figures in this section.

In an attempt to better understand the relation of trace elements from clinopyroxene at Horoman a series of X-Y variation diagrams were made. The complications mentioned in the previous paragraphs are demonstrated in these figures as very few of the trace elements correlate in any understandable way. One goal was to see if any of the trace elements in clinopyroxene correspond to the general concept of varying degrees of depletion by partial melting. From the previous discussion of clinopyroxenes it is apparent that the melting processes are masked, or in some cases overwhelmed by other processes perhaps acting locally on a grain-to-grain scale. These masking processes may be related to sub-solidus recrystallization and re-equilibration.

One of the arguments used previously in discussion of the quality of ion probe data, was to compare it to another analytical technique, e.g. isotope dilution. For several trace elements we can compare ion probe data with electron

microprobe data. Admittedly, the comparison is not completely valid as the two values are not from the same clinopyroxene grain. The electron microprobe values are the mean of several analyses of several grains from a sample while the ion probe data is from a single spot on one grain. This comparison should allow us to test for wildly disparate values. The correlation is excellent with respect to Cr (Fig. 58), with a correlation coefficient of r=0.992 with like units. Only the very high value for sample 62131 with the ion probe is greater than ten percent different than the electron microprobe value and even this value seems within the realm of error for a single point. Four of the samples have agreement to within less than five percent. A similar plot for Ti shows poorer agreement (Fig. 59). The correlation coefficient of r=0.915 is quite poor. The strange thing is that the three samples that are considered the most depleted (62131, 62130 and 62128 exhibit near perfect agreement (r=0.9994, slope of 0.986) while the other three samples have approximately equal ion probe values that are all considerably too low in comparison to the electron microprobe data. This is not understood but there is no reason to suspect the ion probe data. The three apparently spurious points exhibit a good match between the clinopyroxene-based mass balance calculation and the analyzed whole rock values (Fig. 57). Also the 62210 Ti abundance is a mean from several ion probe spots with little dispersion (Fig. 53) discounting simply a "bad" analysis.

Figure 58. Cr_2O_3 in clinopyroxenes from Horoman samples measured by electron microprobe versus Cr (ppm) measured in clinopyroxene by ion microprobe showing excellent correspondence (r=0.992).

Figure 59. Clinopyroxene TiO_2 measured in Horoman samples by electron microprobe versus Ti (ppm) in clinopyroxene analyzed with ion microprobe. Correlation is quite poor (r=0.915) but is much better if not all samples are included (see text). Sample numbers are included.

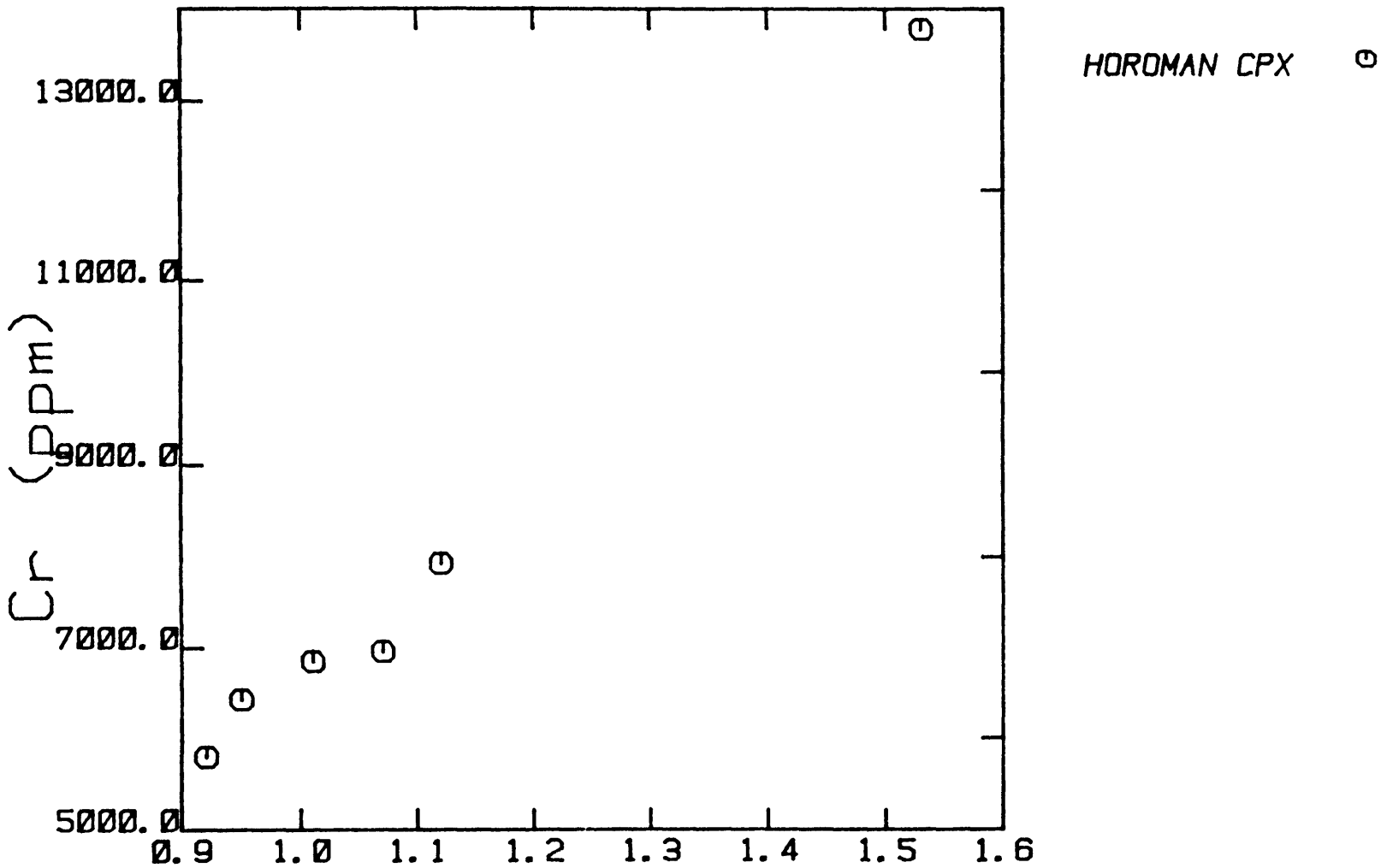
HOROMAN CPX
13000.0
11000.0
9000.0
7000.0
5000.0
Cr (ppm)
0.9
1.0
1.1
1.2
1.3
1.4
1.5
1.6
Cr203 (wt %)

Figure 58

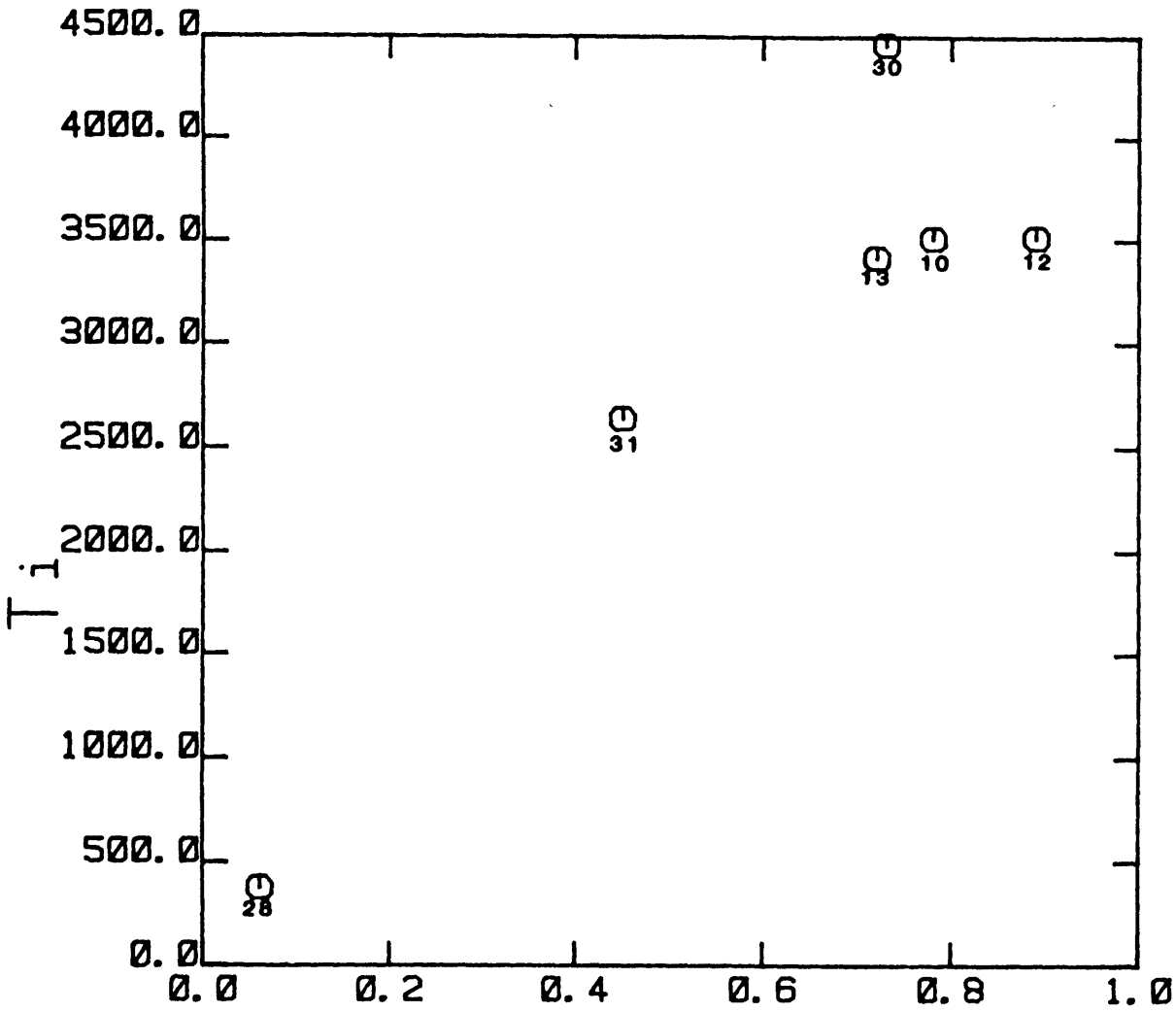
4500.0
4000.0
3500.0
3000.0
2500.0
2000.0
1500.0
1000.0
500.0
0.0
0.0
0.2
0.4
0.6
0.8
1.0
Ti
30
13
10
12
31
28
HOROMAN CPX
TiO2

Figure 59

The good agreement of Cr between analytical methods and the reasonably good agreement of Ti suggests that no constant error effects exist in the ion probe data that would affect the entire spot analysis.

The major elements do correlate with the clinopyroxene REE to a certain extent. In general, the more depleted a sample is in major elements the less LREE depleted it is. When chondrite normalized La/Eu is plotted against enstatite content a constant LREE depletion is seen at low En but tends to rise rapidly with depletion (Fig. 60). A plot of the slope of the entire REE pattern (La/Er) against Mg# (Fig. 61) shows a similar pattern but with even less correlation. One would expect that as a rock was melted the clinopyroxenes would preferentially lose LREE so that a standard indicator of depletion such as Mg# should have negative correlation with LREE/HREE, not positive as in these plots. This same counter-intuitive relation was also found in the whole rock data, equally poorly correlated. Whatever process is controlling degree of depletion of LREE in the whole rocks is apparently acting upon the clinopyroxenes in the same way (or more likely vice versa). The observation that LREE/HREE ratios in whole rocks results from the constituent clinopyroxenes has been seen in many ultramafic xenoliths suites (Nagasawa et al, 1969; Frey and Green, 1974; Stosch and Seck, 1980; Kurat et al, 1980) but apparently the first such observation from Alpine-type peridotites is this work. Similar metasomatic processes

Figure 60. Enstatite content in Horoman clinopyroxenes versus chondrite-normalized (Boynton, 1984) La/Eu ratio in clinopyroxene, with sample numbers indicated.

Figure 61. Mg# (Mg/Mg+Fe) in Horoman clinopyroxenes versus chondrite-normalized (Boynton, 1984) La/Er ratio in clinopyroxene, with sample numbers indicated.

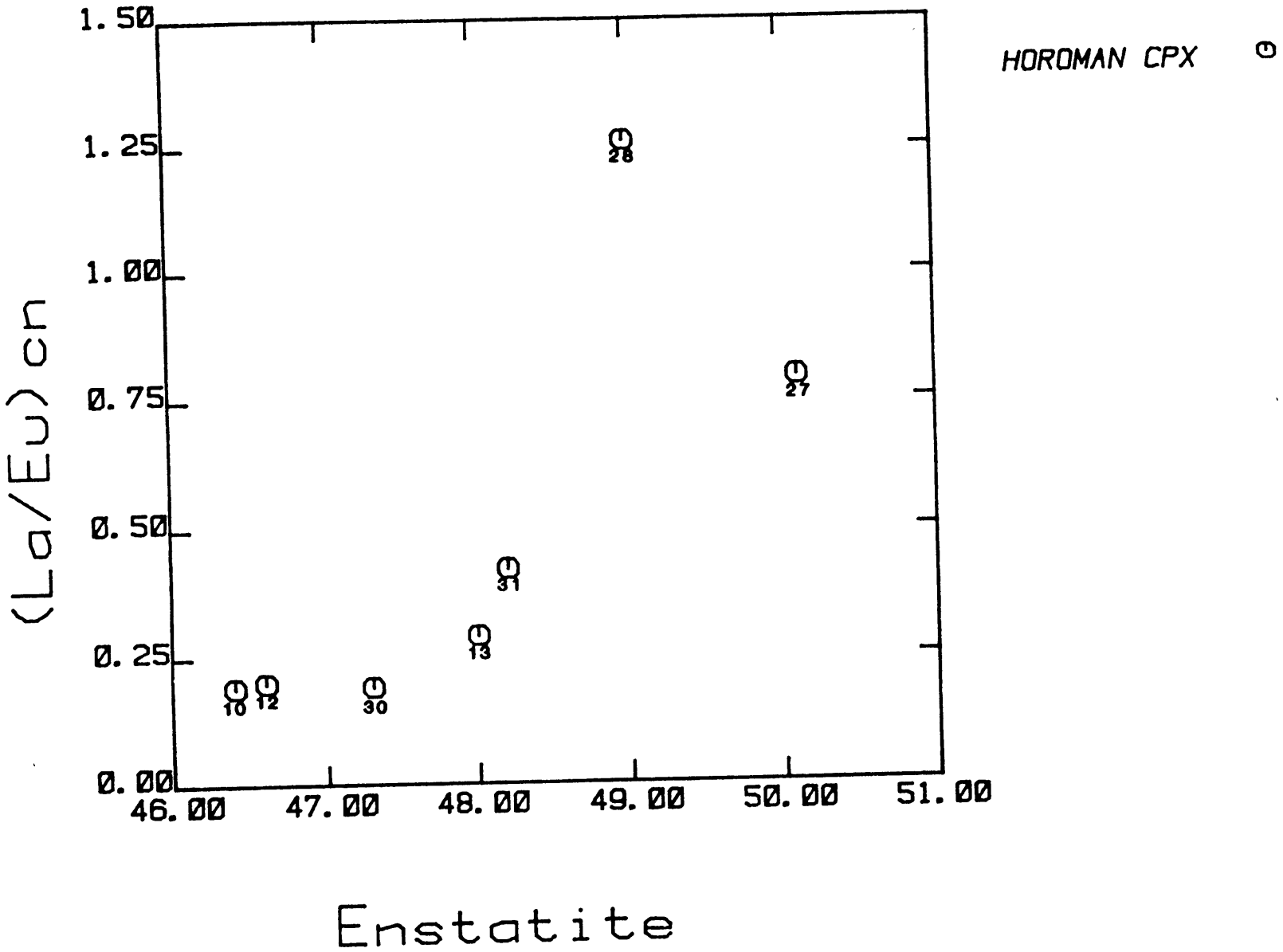
HOROMAN CPX
(La/Eu)cn
1.50
1.25
1.00
0.75
0.50
0.25
0.00
46.00
47.00
48.00
49.00
50.00
51.00
Enstatite
10
12
30
13
31
27
28

Figure 60

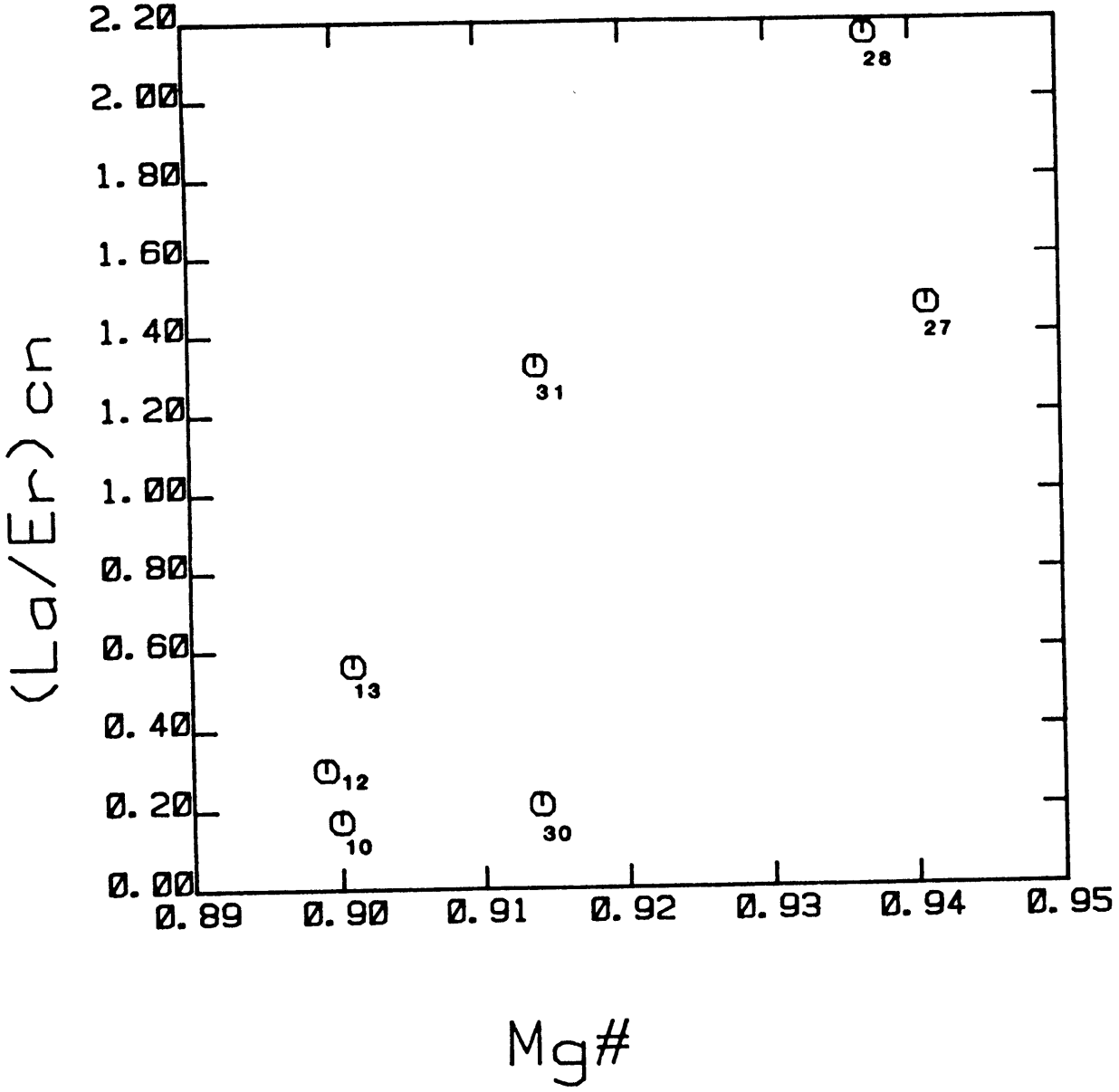
2.20
2.00
1.80
1.60
1.40
1.20
1.00
0.80
0.60
0.40
0.20
0.00
(La/Er)cn
0.89
0.90
0.91
0.92
0.93
0.94
0.95
Mg#
28
27
31
13
12
10
30
HORMAN CPX

Figure 61

often called upon to explain this observation in xenoliths may be acting upon the Horoman rocks. Ottonello (1980), using data from peridotite xenoliths from Assab, Ethiopia, proposed that the relative enrichment of LREE in the more depleted samples was caused by orthopyroxene and olivine partitioning of LREE. This hypothesis is discounted at Horoman by the observation that the whole rock trends tend to mimic the clinopyroxene patterns.

A plot of the slope of the right hand half of the REE pattern, Eu/Er versus Mg# (Fig. 62) indicates the surprising result of two general trends. The first shows a rapid HREE depletion with increasing residual character (samples 62210-->62212-->62213-->62131), while a more gradual HREE depletion with melting is also seen (samples 62210-->62130-->62128-->62127). No speculation about this feature is made but it does seem from observation of the clinopyroxene REE patterns (Fig. 51) that two type of patterns exist. There is some indication that the HREE are negatively correlated with depletion by melting as one would expect (Fig. 63) but the correlation is rather poor.

The REE don't tend to correlate at all well with the other trace elements. Eu and Sr, that we may expect to act similarly due to their potential strong partitioning into plagioclase show no correlation (Fig. 64). Ti and Er which have very similar partition coefficients in clinopyroxene (~0.3) would be expected to correlate positively (Fig. 65). They do but the correlation is weak. Ti correlates

Figure 62. Mg# (Mg/Mg+Fe) in clinopyroxenes from Horoman versus chondrite-normalized (Boynton, 1984) Eu/Er ratio in clinopyroxene, with sample numbers indicated.

Figure 63. Enstatite content in Horoman clinopyroxenes versus Er (ppm) with sample numbers indicated.

Figure 64. Sr versus Eu in clinopyroxenes from Horoman including sample numbers.

Figure 65. Er versus Ti in clinopyroxene from Horoman including sample numbers.

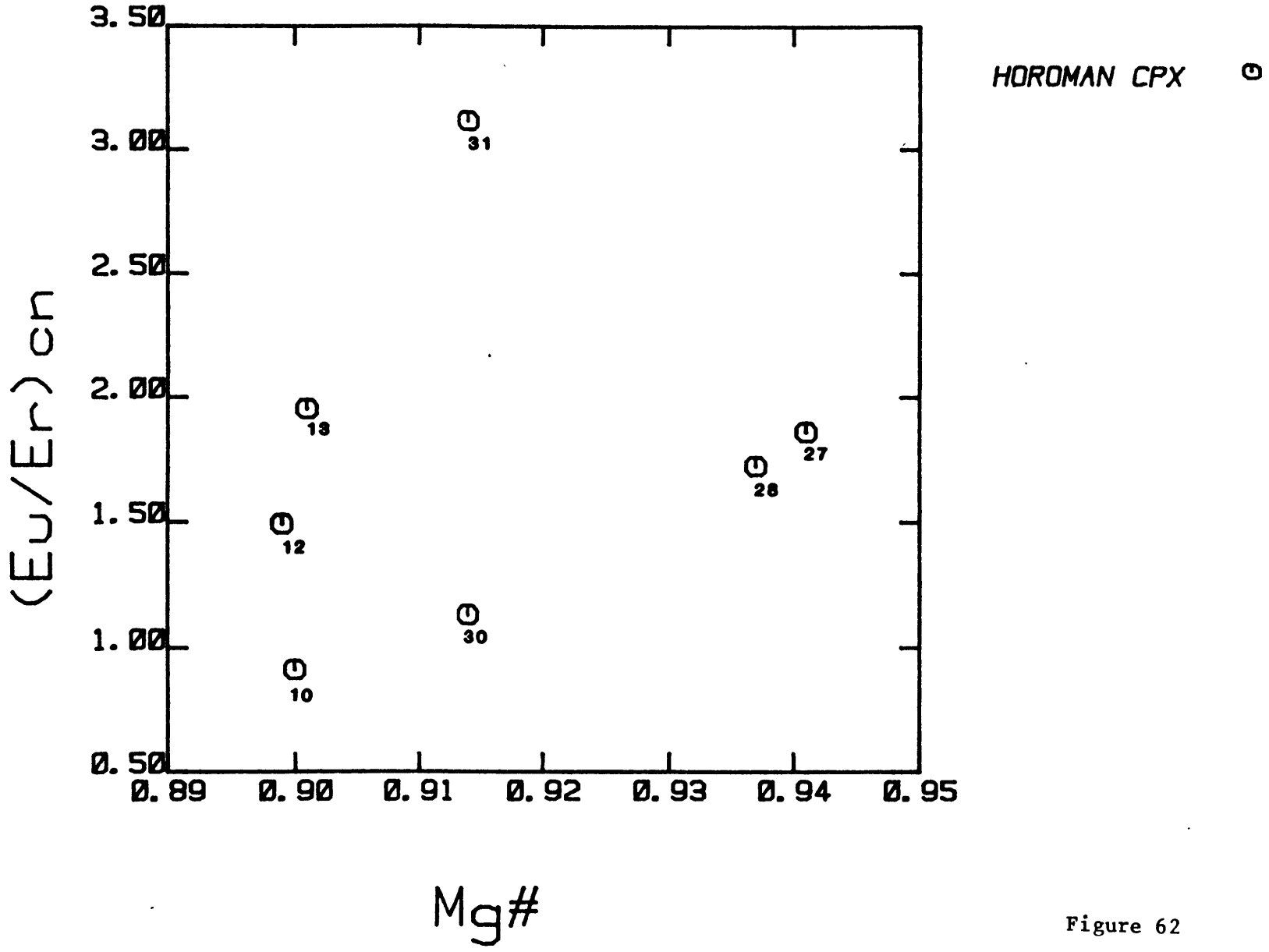
3.50
3.00
2.50
2.00
1.50
1.00
0.50
(Eu/Er)cn
0.89
0.90
0.91
0.92
0.93
0.94
0.95
Mg#
31
13
27
28
12
30
10
HOROMAN CPX

Figure 62

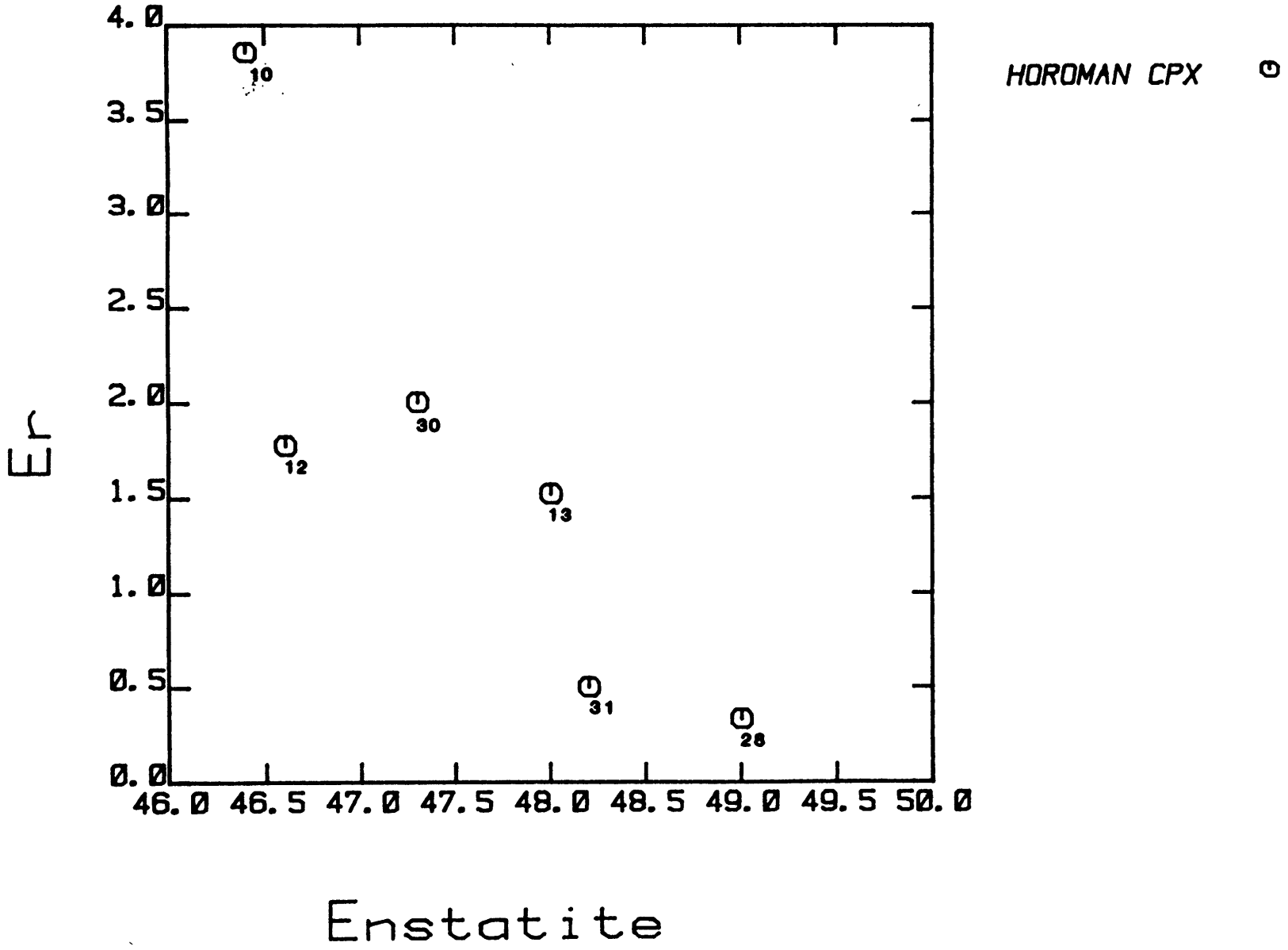
HOROMAN CPX
Er
Enstatite
4.0
3.5
3.0
2.5
2.0
1.5
1.0
0.5
0.0
46.0 46.5 47.0 47.5 48.0 48.5 49.0 49.5 50.0
10
12
30
13
31
28

Figure 63

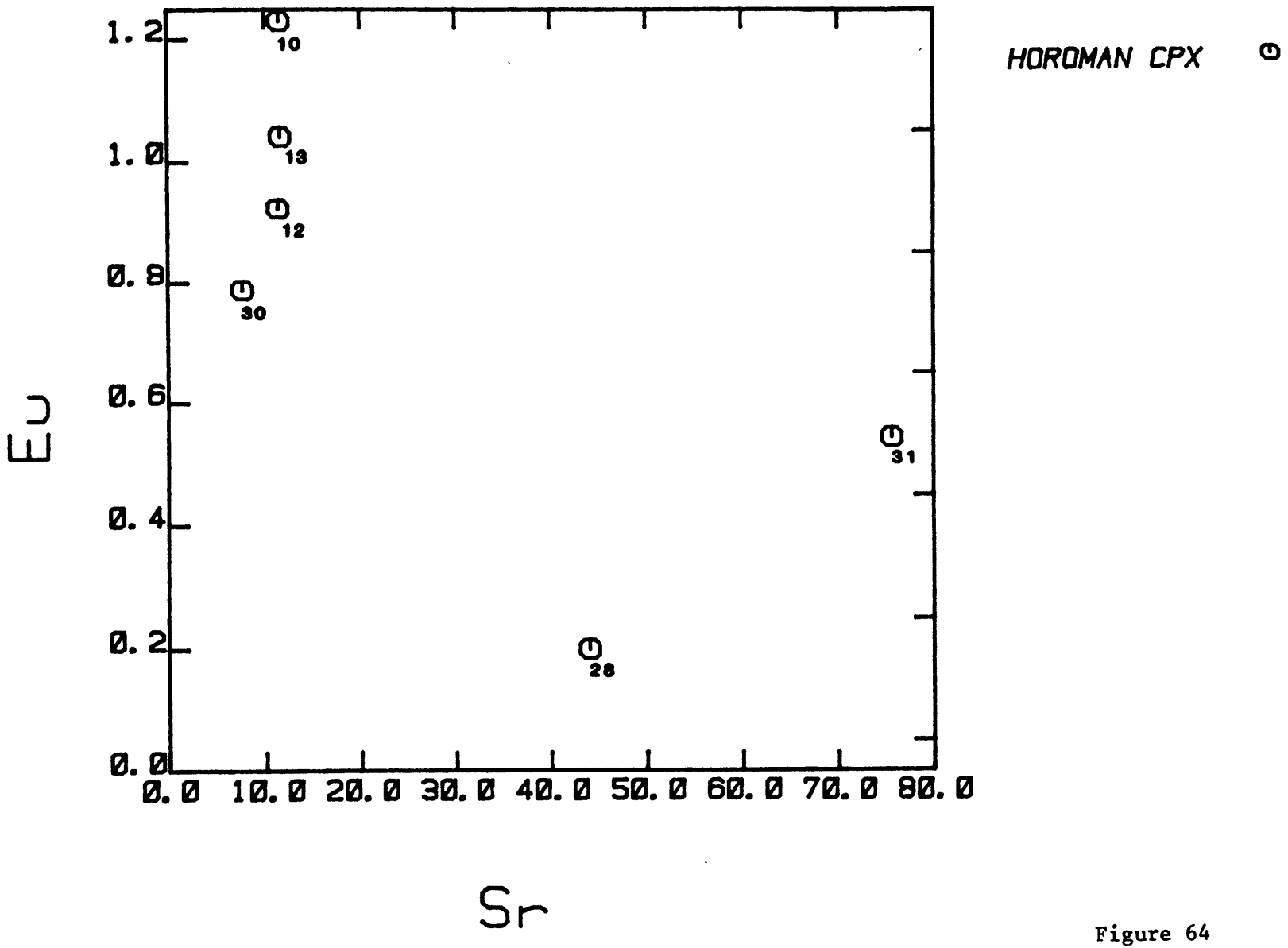
HOROMAN CPX
Eu
Sr
1.2
1.0
0.8
0.6
0.4
0.2
0.0
0.0 10.0 20.0 30.0 40.0 50.0 60.0 70.0 80.0
10
13
12
30
31
28

Figure 64

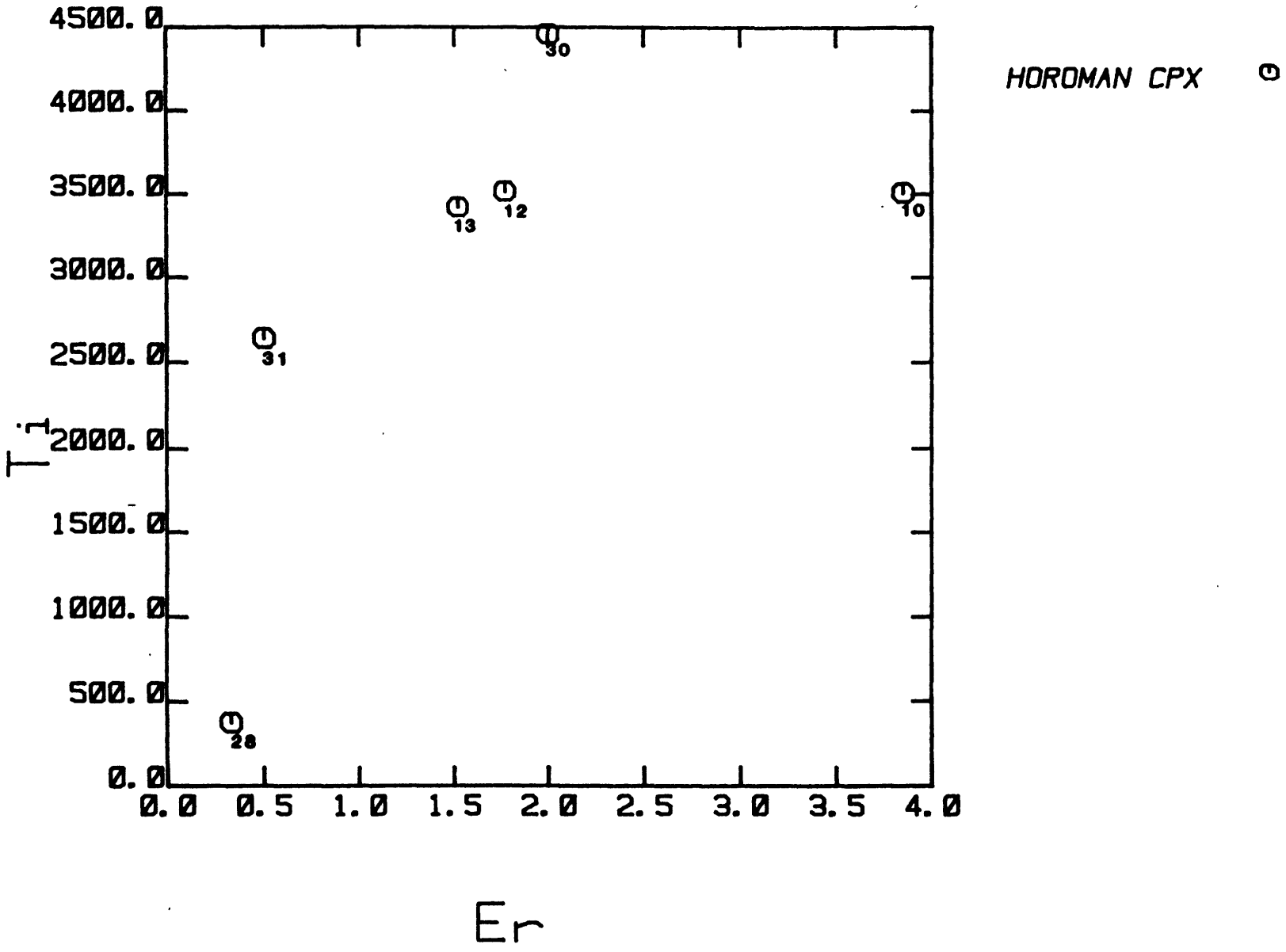
4500.0
4000.0
3500.0
3000.0
2500.0
2000.0
1500.0
1000.0
500.0
0.0
T
0.0
0.5
1.0
1.5
2.0
2.5
3.0
3.5
4.0
Er
30
12
13
10
31
28
HOROMAN CPX

Figure 65

negatively with La/Eu (Fig. 66). That is, samples that have more LREE depleted clinopyroxenes contain more Ti. This again is exactly the opposite effect one would expect based upon simple melting.

One last puzzling bit of information about the trace elements in the clinopyroxene is provided by inspection of Ti versus (Fig. 67). There is rough positive correlation and all of the samples except one (62128) have Ti/Zr ratios between 75 and 160. The whole rock Ti/Zr ratios fall in a more narrow range from 110 to 150. (Whole rock Zr data could not be obtained for 62128.) Shimizu and Allegre (1978) noted that clinopyroxenes from Group I garnet lherzolite xenoliths, whole rock Group I analyses and estimated "pristine" mantle all have Ti/Zr ratios of approximately 100, while Group II clinopyroxenes have values nearer to 10. They point out that residua from melting Group I nodules would produce greater Ti/Zr ratios. They concluded that the low values were produced from cumulates of a residual liquid after ilmenite crystallization took place. The Ti and Zr data from 62128, along with the Shimizu and Allegre data calls into question the entire residual from partial melting model of the harzburgites.

Spinel

Spinel in the Horoman peridotites makes up less than one percent modally. Table 8 shows the chemical composition of the spinels in the seven samples. Iron composition is reported as total iron in the ferrous state but ferric iron

Figure 66. Ti versus chondrite-normalized (Boynton, 1984) La/Eu ratio in clinopyroxene from Horoman including sample numbers.

Figure 67. Zr versus Ti in Horoman clinopyroxenes with sample numbers included. Lines of constant Ti/Zr are also shown.

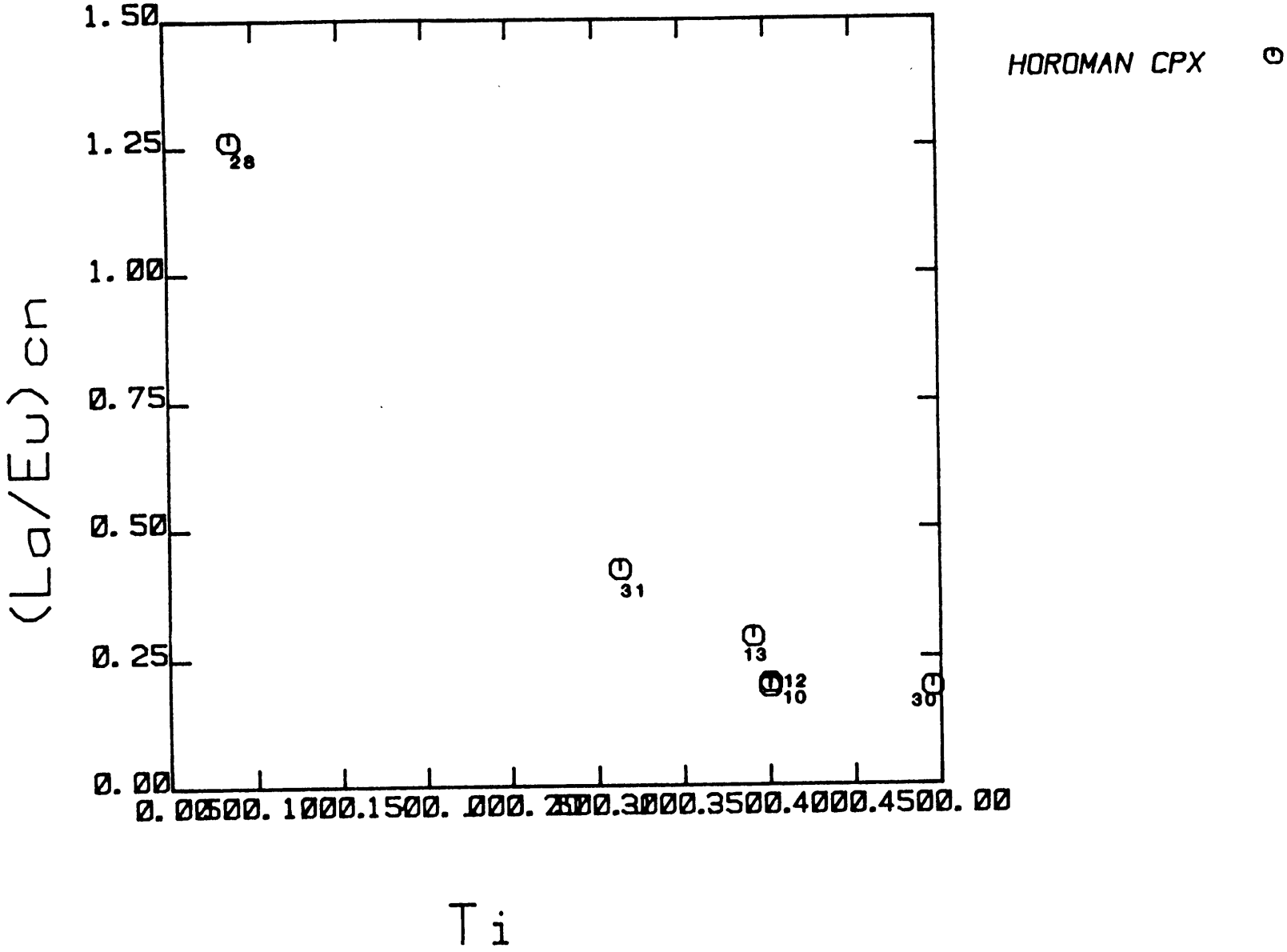
HOROMAN CPX
(La/Eu)cn
Ti
1.50
1.25
1.00
0.75
0.50
0.25
0.00
0.00 0.05 0.10 0.15 0.20 0.25 0.30 0.35 0.40 0.45 0.50
28
31
13
12
10
3

Figure 66

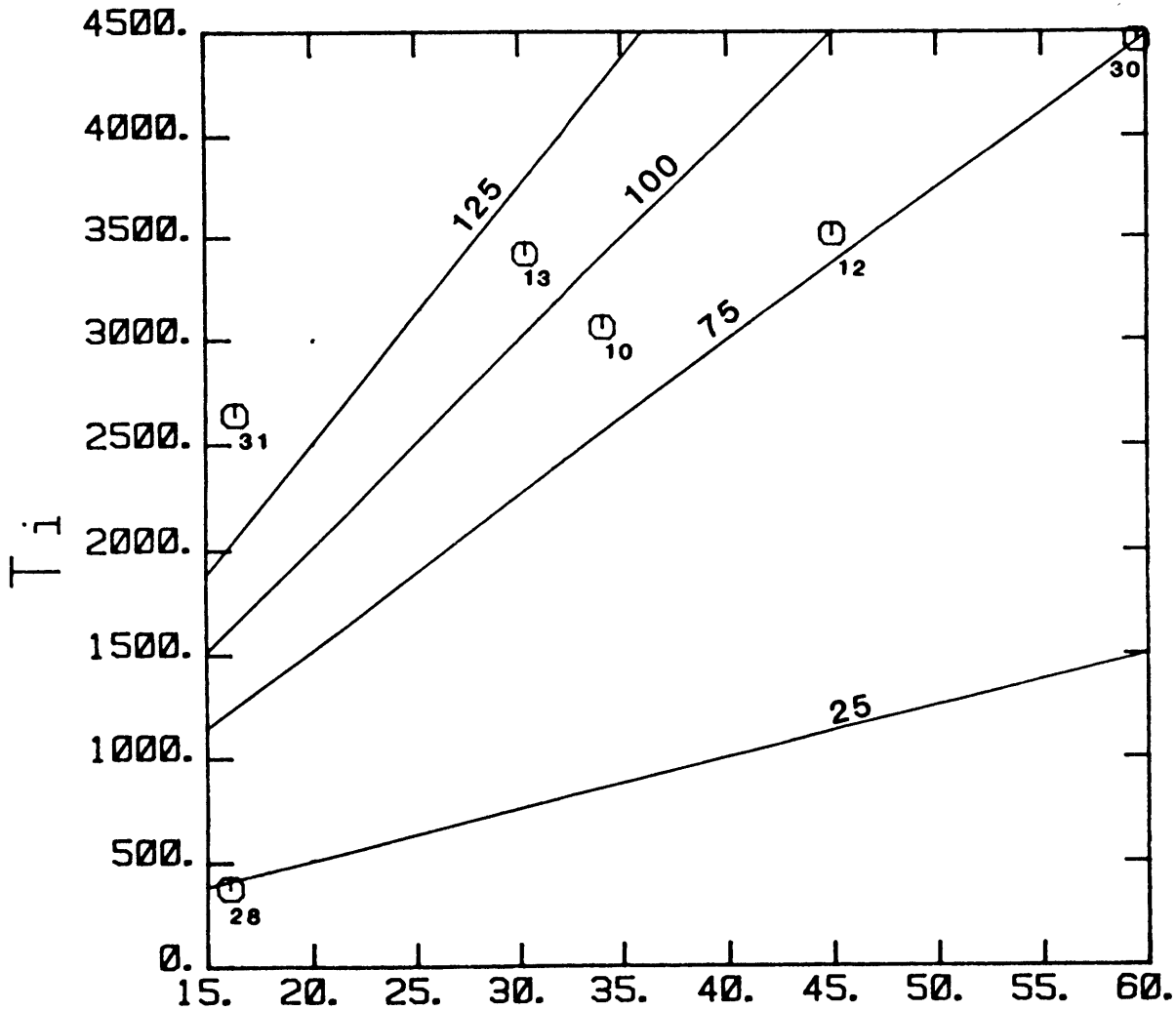

HOROMAN CPX

Figure 67

was calculated assuming perfect stoichiometry in the spinel. Spinel compositions are quite varied within samples and probably reflect sub-solidus complications. Dick (1977), Dick and Fisher (1984), Dick et al (1984), and particularly Dick and Bullen (1984), have championed the use of Cr-spinel as an important petrogenetic indicator in peridotites. A summary of the reasoning follows. 1) Cr-spinel, (Mg, Fe^{2+})(Cr, Al, Fe^{3+})$_2O_4$, is a ubiquitous accessory phase that has been found through experimental work to be sensitive to bulk composition mineralogy. 2) During crystallization or melting Al is highly incompatible while Mg and Cr are highly compatible in the spinel structure. 3) Partitioning of Mg and Fe_{2+} is temperature dependent. 4) The relative amount of Fe_{3+} versus Fe_{2+} is fO_2 dependent (Dick and Bullen, 1984).

Figure 68, of Cr# versus Mg# shows little if any significant correlation. According to the works mentioned previously, a distinct negative correlation is seen in alpine and abyssal peridotites with Cr# increasing with degree of melting and Mg# decreasing (in opposition to Mg# of silicates). Cr-spinel is most likely an indigenous mantle mineral in these rocks but it is also likely that it is produced by incongruent melting of pyroxene (Dickey et al, 1971; Dick, 1977) according to the scheme: cpx + opx + (ol + sp) --> Mg-richer ol + Cr-richer sp + liquid (Sinigoi et al, 1983). In the Horoman rocks Cr# generally does increase with melting, however, Mg# appears to increase

(Fig. 68). Furthermore, analyses of different sized grains within a sample show a large variation in Cr#-Mg# space with no apparent systematics. (Relative sizes of spinel grains are noted in Figure 68 when known.) Sample 62127 has the most distinct spinel size variation and the change in Cr# is counter-intuitive if one assumes the smaller grains to be later generation. A similar observation was noted in different spinel grain sizes within a sample by Conquere and Fabries (1984). They explained it as substitution of $MgCr_2O_4$ by $FeAl_2O_4$ during a second partial recrystallization event. Although this is rather a cursory electron microprobe study of spinels and some analytic problems did exist in producing good totals (Table 8), Figure 68 leads me to believe that chemical variation in spinel is not controlled merely by simple igneous processes but are complicated by the addition of poorly constrained metamorphic processes in the solid state. Another observation is that while Cr_2O_3 generally increases in spinel it behaves in a more complex manner in both clinopyroxene and orthopyroxene (Fig. 17-20, Tables 6 and 7). The Cr_2O_3 content in spinel behaves as one would expect if it acts compatibly in spinel (i.e. increases with greater degree of melting) (Table 8). But the Cr# variation is more complex due entirely to sporadic Al variation. Al should gradually decrease with increased melting as it behaves incompatibly in spinel; since it does not we must conclude that Al variation is being modified by sub-solidus

Figure 68. Mg# ($Mg/Mg+Fe^{2+}$) versus Cr# (Cr/Cr+Al) for spinel from Horoman with fields labelled for each sample. Spinel analyses from MIT chosen for use in linear regression for mode are indicated by circles, other MIT analyses are indicated by triangles, and analyses of Obata are indicated by X's. Sample 62212 was not analyzed by Obata and sample 62210 does not have a field but consists of two identical analyses within the field of 62213. Relative spinel size is also noted when it was known (see text for discussion).

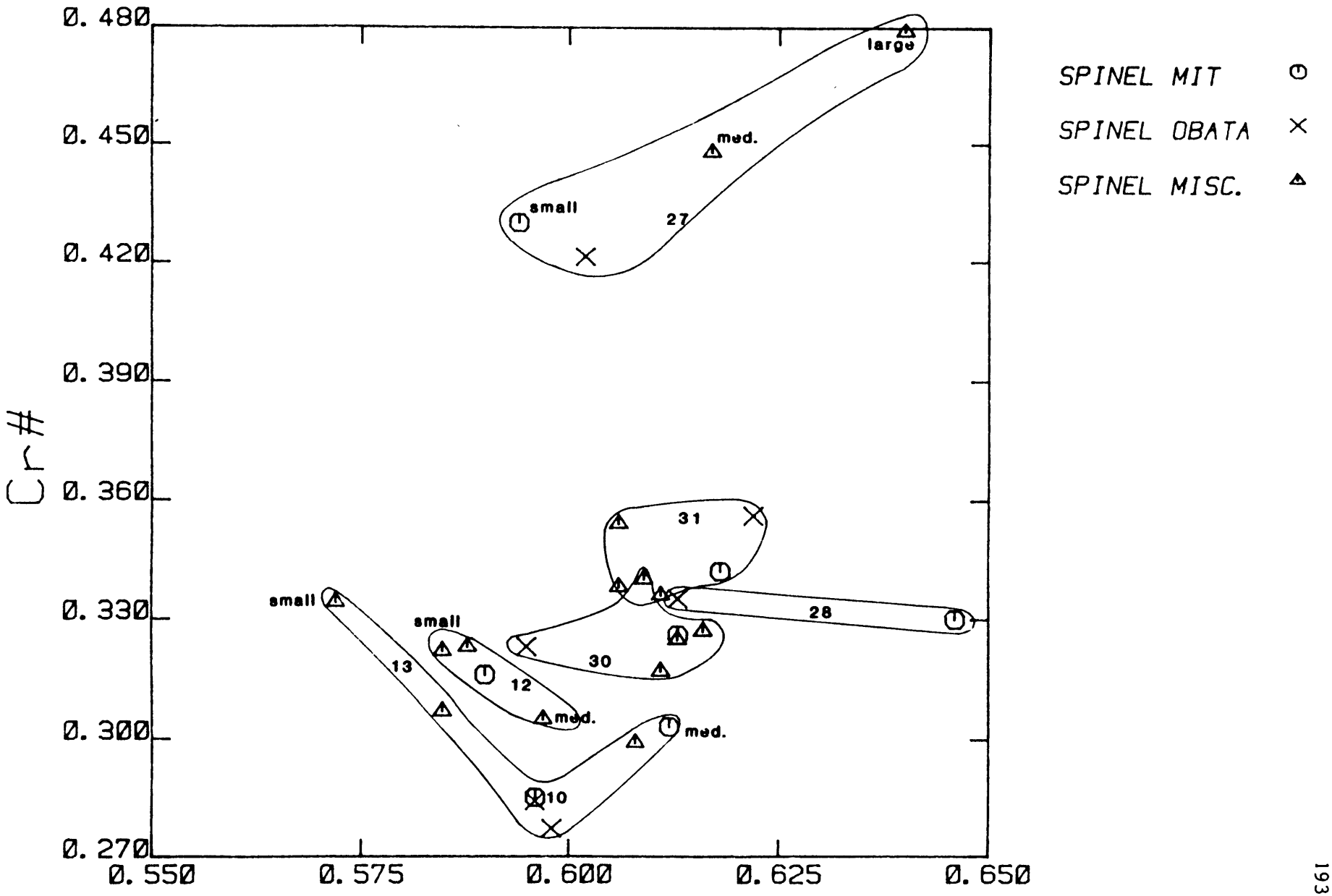
0. 480
0. 450
0. 420
0. 390
0. 360
0. 330
0. 300
0. 270
Cr#
0. 550
0. 575
0. 600
0. 625
0. 650
Mg#
large
med.
small
27
31
28
30
small
small
13
12
med.
med.
10
SPINEL MIT
SPINEL OBATA
SPINEL MISC.

Figure 68

reactions. This makes deciphering igneous processes through spinel chemistry very difficult.

Ferric iron tends to correlate negatively with Cr_2O_3 (Fig. 69) and positively with FeO (Fig. 70). Ferric iron is a trace element in the bulk peridotite that appears to be acting incompatibly in the spinels (Fig. 69, Table 8). Fe^{3+}, like Ti^{4+}, has no crystal field stabilization energy nor octahedral site preference energy, thus it is more amenable to tetrahedral and octahedral sites in the melt (Burns, 1973). Figure 70 is in contrast to the relation found by Dick and Fisher (1984) in abyssal peridotites.

A rather straight forward positive correlation is seen between the Cr_2O_3 content in the spinels and Cr_2O_3 in the bulk rock (Fig. 16), except for samples 62130 (with very low bulk Cr_2O_3) and 62128. The 62128 anomaly can be explained simply due to the sample having anomalously high modal spinel (Table 1), while 62130 is unexplained. Figure 16 is in marked contrast to the relation found by Kurat and others (1980) who found negative correlation indicating Cr may act incompatibly.

Plagioclase

Plagioclase is found in five of the seven samples. The compositions are listed in Table 9. The compositions range from about An_{60}-An_{70}. The plagioclase is always in small seams, very fine-grained and in close association with tiny spinel and less abundant olivine and clinopyroxene grains.

Figure 69. Cr_2O_3 versus Fe_2O_3 in spinels from Horoman with MIT analyses (circles) and analyses by Obata (X's) for comparison.

Figure 70. FeO versus Fe_2O_3 in spinels from Horoman with analyses made at MIT (circles) and by Obata (X's) for comparison.

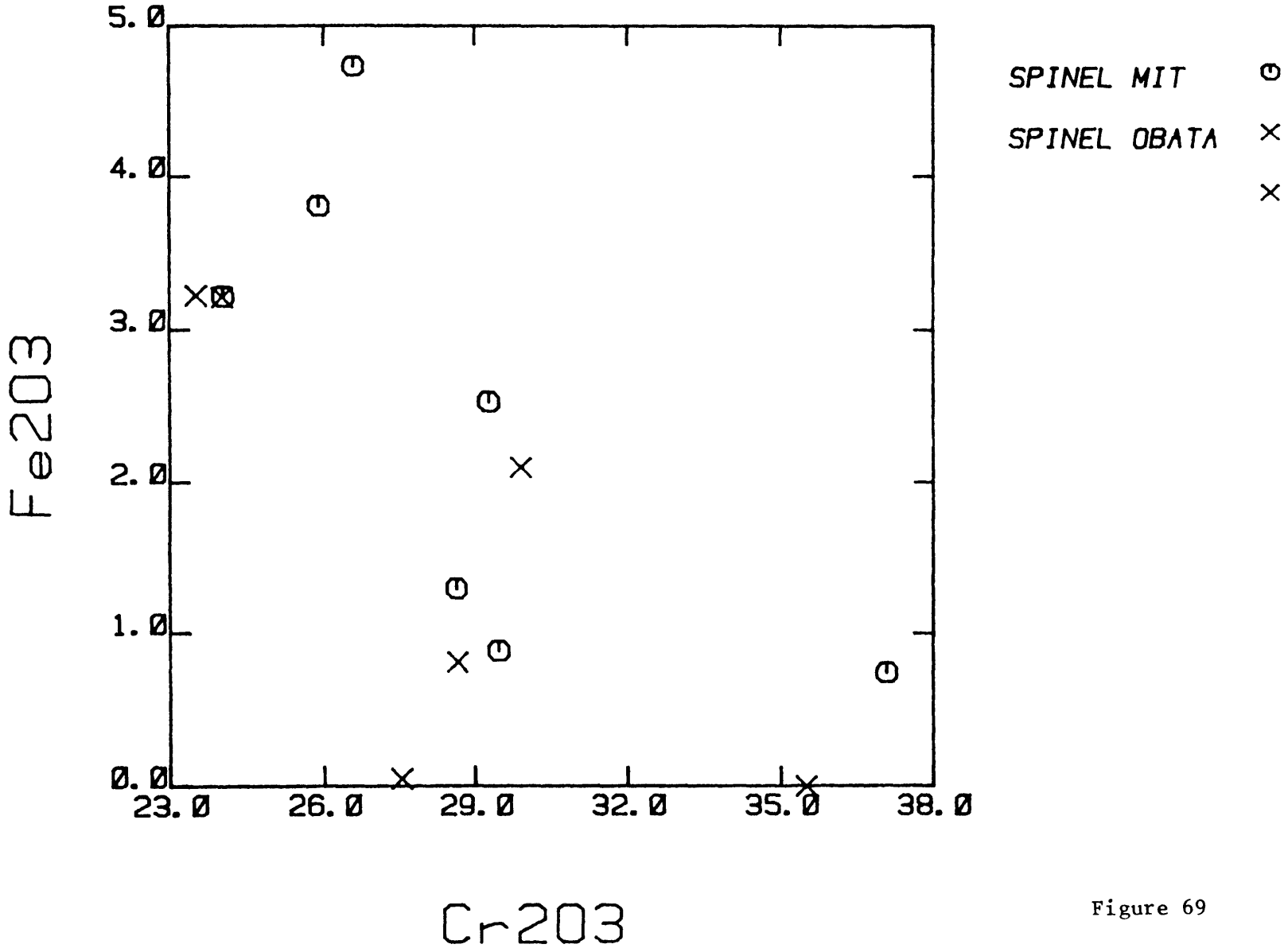
5.0
4.0
3.0
2.0
1.0
0.0
23.0
26.0
29.0
32.0
35.0
38.0
Fe203
Cr203
SPINEL MIT
SPINEL OBATA

Figure 69

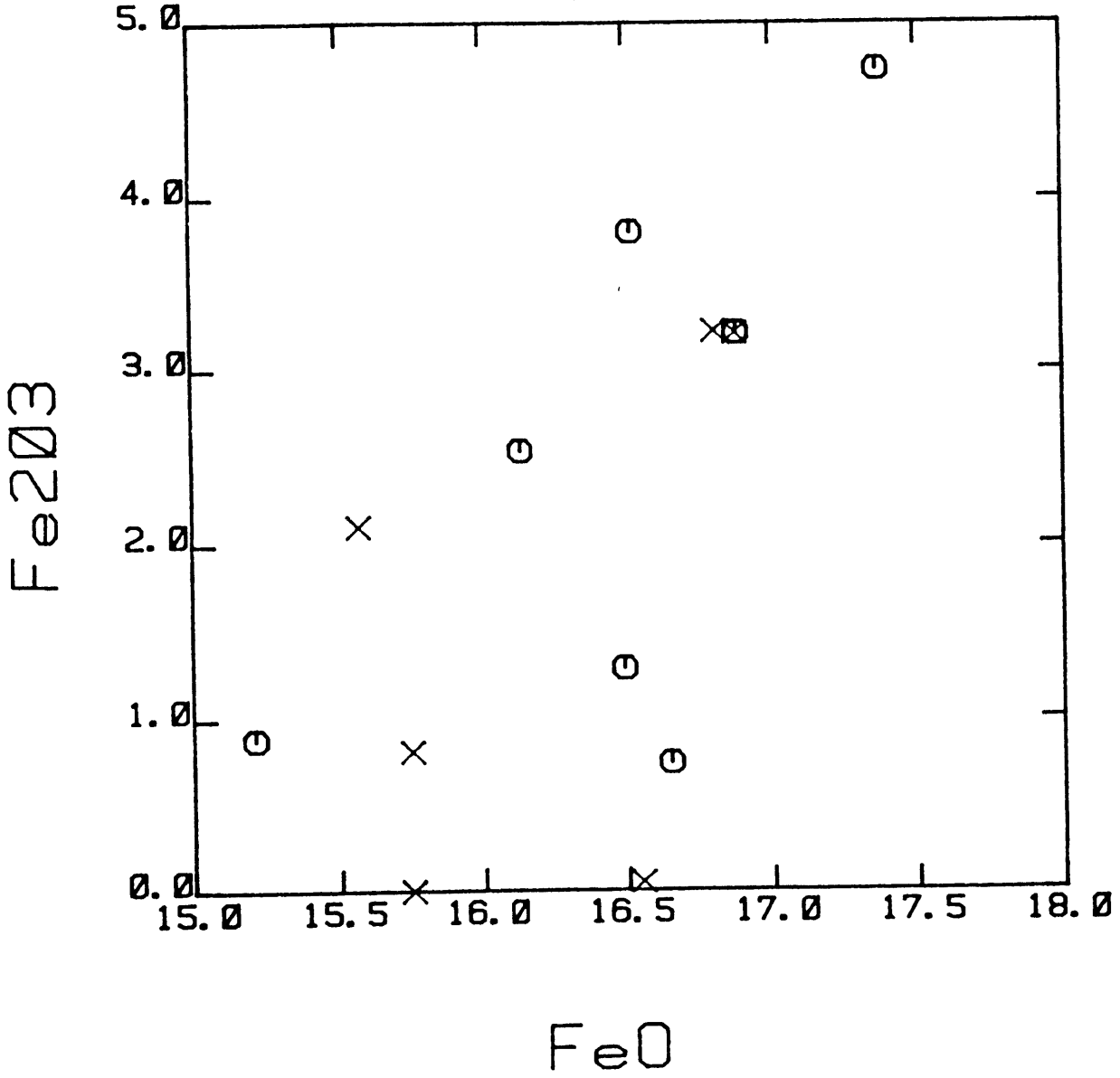
5.0
4.0
3.0
2.0
1.0
0.0
15.0
15.5
16.0
16.5
17.0
17.5
18.0
Fe203
FeO
SPINEL MIT
SPINEL OBATA

Figure 70

Plagioclase is a problematic mineral in peridotites as it has a variety of occurrences, textures and mineral associations that have led to alternative interpretations. They attempt to answer the question of whether the plagioclase in the rocks is an indigenous mantle mineral produced in the plagioclase peridotite stability field. Is it a metamorphic mineral produced by subsolidus reactions; or was it formed from melt trapped within the hot spinel peridotite? A survey of the literature reveals a wide variety of data on plagioclase bearing peridotites (Table 14). The association with spinel in fine-grained segregations is a common occurrence of plagioclase. It is clear that plagioclase and its association with spinel and olivine may be formed by the breakdown of pyroxenes by a reaction such as, Al-pyx --> An + ol (Green, 1964); or in reaction with spinel, pyx + Al-sp --> plag. + ol + Cr-sp (Obata, 1980). The more common explanation is that these plag.-rich mineral aggregations or seams are direct crystallizations of trapped melt (Nicolas and Dupuy, 1984; Quick, 1981; Boudier, 1978; Boudier and Nicolas, 1977; Menzies, 1976; Menzies and Allen, 1974; Jackson and Ohnenstetter, 1981; and Himmelberg and Loney, 1980), or by specified reactions involving the host peridotite and the trapped melt (Bonatti et al, 1986; Dick and Fisher, 1984; Dick and Bullen, 1984). This reaction would probably take the form of Al-sp + trapped melt --> plag. + Cr-sp (Bonatti et al, 1986; Dick and Bullen, 1984). Another common

Table 14: Compilation of Geologic Data from Plagioclase Peridotites.

Peridotite, Modal Plag., & An Content	Mineral Assoc./ Textures	Suggested Genesis/ Reactions
1. Horoman[1] 0-10% plag. 60-80% An	s&a: sp+plag (with ol & cpx)	Trapped melt/inter. of melt Al-opx -> opx+cpx+plag+sp Al-opx -> opx+plag+sp
2. Ronda[2,3,4] 0-8% plag. ---- An	1) s&a:sp+plag 2) coronas around sp (holly-leaf) 3) interstitial 4) in embayed sp	Not from melt Al-sp+pyx -> plag+ol+Cr-sp
3. Trinity[5] ~10% plag. 83-90% An	1) l&v w/ pyx+sp 2) interstitial 3) in embayed sp (holly-leaf)	Crystallized trapped melt
4. Lanzo[6,7,8] ~10% plag. 60-80 An	as at Trinity	Crystallized trapped melt
5. Erro-Tobia[9] trace plag. ----- An	1) seams 2) reaction rims betw. sp + pyx	No trapped melt, Partial substit. reequil. for sp assem. to opx+cpx+plag+ol
6.Othris[10,11,12] ~10% plag. 80-90% An	l&s gabbroic plag + cpx	Crystallized trapped melt
7.Troodos[11,12] trace plag. ----- An	minor pods of gabbroic assem.	Cystallized trapped melt
8.Uenzaru[13] ----- plag. 54-80% An	1) fine-grained aggreg.: plag+ cpx+ol+sp 2) exsolved in cpx	Breakdown of cpx into: low Al-cpx+plag+ol, plag+ol+sp, or exsol.
9.Mt. Maggiore[14] ~10% plag. ---- An	similar to Lanzo & Trinity	Crystallized trapped melt
10.Lizard[15] 1-2% plag. ---- An	1) small segreg. 2) coronas of sp	Coronas:Mg-sp+cpx+opx -> An+ol+Cr-sp Other:Al-pyx -> An+ol sp+cpx+opx -> An+ol

Table 14, cont.

11.Canyon Mt[16] trace plag. ----- An	1) seams w/ cuspate sp 2) interstitial	Crystallized trapped melt
12.Red Mt.[17] ----- plag variable An	seams of plag+ cpx+sp	Reaction w/ trapped melt & transition of sp -> plag at different pressures
13.Zabargrad Island[18] 2-15% plag. 80-93% An	segreg. of plag +ol+sp	Reaction w/ melt: Melt+ Al-sp -> Cr-sp+plag. also, opx+cpx+Al-sp -> ol+plag+Cr-sp
14. Abyssal[19,20,21] tr-12% plag ---- An	segreg. of plag +sp+cpx	Reaction w/ melt: Melt+ Al-sp -> plag+Cr-sp also, opx+cpx+Al-sp -> ol+plag+Cr-sp

Abbreviations:
s&a - seams and aggregates
l&v - lenses and veins
l&s - lenses and segregation
tr - trace

References: (1) Niida, 1984; (2) Obata, 1977; (3) Obata, 1980; (4) Dickey, 1970; (5) Quick, 1981; (6) Boudier and Nicholas, 1977; (7) Boudier, 1978; (8) Ernst, 1978; (9) Ernst and Piccardo, 1979; (10) Menzies, 1973; (11) Menzies and Allen, 1974; (12) Menzies, 1976; (13) Komatsu, 1975; (14) Jackson and Ohnenstetter, 1981; (15) Green, 1964; (16) Himmelberg and Loney, 1980; (17) Sinton, 1977; (18) Bonatti, et al., 1986; (19) Hamlyn and Bonatti, 1980; (20) Dick and Bullen, 1984; (21) Dick and Fisher, 1984.

textural occurrence of plagioclase, not seen at Horoman, is as coronas around large, often "holly leaf" shaped, spinels or within embayments in spinel. This texture is best explained by partial substitution of mantle spinel by plagioclase at the pressure dependent transition of the spinel peridotite stability field to the plagioclase peridotite stability field via the reaction, Mg- and Al-sp + cpx + opx --> plag. + ol + Cr-sp (Green, 1964; Obata, 1980). If this reaction went to completion we may expect larger plagioclase grains than the very fine-grained aggregates found at Horoman. It seems likely that a complete continuum exists, dependent on factors such as cooling rate and melt composition, from complete crystallization of trapped melt to near complete solid state reequilibration/recrystallization reactions. I suggest that the Horoman peridotites do contain small amounts of trapped melt that has reacted with the surrounding peridotite to obscure the original igneous textures. These melt pockets would be in the vicinity of the fine-grained aggregates of plagioclase, spinel, and lesser clinopyroxene and olivine. The exact amount and chemistry of trapped melt is difficult to ascertain due to the reaction relations. The presence of trapped melt will be explored chemically in the following trace element sections.

Nicolas and coworkers (Nicolas, 1986; Boudier and Nicolas, in press; Nicolas and Dupuy, 1984) have developed a melt extraction model based on studies of peridotites in a

general framework of structure and geologic variation. The interpretation of plagioclase-rich seams and veinlets as well as larger gabbroic dikes, as peridotite melt features is essential to this theory. In this scheme, peridotite lithologic variation is ultimately caused by a mantle diapir's ascent rate and the depth at which the diapir cools below its solidus with intersection with the overlying lithosphere. Faster ascent implies greater degree of melting and contact with the lithosphere at shallow depth, with cooling taking place after almost complete extraction of melt, leaving behind a harzburgitic residue. Slower ascent rate produces less melt and extraction is not complete so the residuum is plagioclase lherzolite. Very slow ascent rate implies very little melting, limited melt extraction and cooling at depth in thick lithosphere leaving a fertile spinel lherzolite (Nicolas, 1986). This model may be relevant on the grand scale to which it is applied but may not be tenable at a single location such as Horoman where a wide range of lithologies exist apparently in complete continuity. Ophiolitic and oceanic lherzolites bearing plagioclase, such as those at New Caledonia, have been explained as being produced by impregnation of a melt into already depleted harzburgite and dunite from structural and geochemical evidence (Nicolas and Dupuy, 1984). It is unlikely that relatively fertile alpine plagioclase lherzolites such as those at Horoman, have been produced in this way.

Two notable comparisons that can be made from the plagioclase lherzolites listed in Table 14 are the amount and composition of plagioclase. When mentioned in the literature, few of the peridotites that have more than trace amounts of plagioclase have greater than about ten percent. This implies that whatever process produces the plagioclase, either subsolidus reactions or crystallization of trapped melt, has an upper physical limit. When analyzed, the chemistry of the plagioclase is always variable and falls into two distinct compositional groups. A group with An content from about 60 to 80 (Horoman, Lanzo, and Uenzaru) and a group with An content from about 80 to 90 (Trinity, Othris, and Zabargrad Island). Variation in An content makes it clear that if the plagioclase is produced by crystallization of trapped melt it did not simply crystallize everywhere from a pervasive homogeneous melt but was in a reaction relation with the peridotite host such as incongruent melting with orthopyroxene of fractional crystallization. At Red Mountain in New Zealand, harzburgite with trace amounts of plagioclase is overlain by a transitional peridotite of plagioclase bearing dunites and wehrlites where an incongruent relation seems likely with harzburgite and melt reacting to precipitate plagioclase and clinopyroxene at the expense of orthopyroxene (Sinton, 1977). This sounds distinctly like Nicolas and Dupuy's (1984) impregnation model but at pressures low enough that melt and orthopyroxene are not stable in contact and must be

in reaction. Anorthite content has been observed to be lower nearer to what are interpreted as melt extraction features (Nicolas, 1986) and also in plagioclase exsolved in clinopyroxene compared to separate recrystallized grains (Komatsu, 1975). The two compositional plagioclase groups could be produced by the same process but different melt compositions, perhaps with the higher An group having lost some of the more evolved Ab-rich melt component.

Primary Upper Mantle Composition

Most quantitative modelling of real geochemical data requires selecting a "primary" or "parental" source composition. A variety of processes may act upon this material affecting its chemistry and producing the compositions of the suite of rocks being modeled. A common ploy, following the assumption that all the samples collected from a single area are connected by understandable processes, is to choose the single most primitive composition from a group of samples as the primary composition and working from there. This method is generally necessary to facilitate geochemical modelling but it also has validity in that it keeps the model internally consistent. The danger of this method is that it is quite easy to lose sight of the specific nature of the conclusions being drawn. The conclusions from a successful model can only be that the particular suite of rocks are geochemically connected by certain processes, not that all similar rocks

must have this same causal connection. The breadth of the conclusions may be expanded if it can be proven that the original choice of source composition has some fundamental relevance to principal processes within the earth. This geo-philosophical digression serves the purpose of drawing attention to potential pit-falls of over generalizing from geochemical study. By placing specific modelling in to a more general perspective of the earth, the danger of these errors can be reduced.

In this section the relevance of these remarks will be shown by application to the case of the Horoman source composition. The composition of sample 62210, the most enriched in the study, has been chosen to use as a primary composition for the reasons outlined above. Because an attempt is made to say something about upper mantle processes in general, it is necessary to place the chemistry of sample 62210 in the context of what is known about the composition of the upper mantle. Fortunately, in recent years a great deal of work has been devoted to determining the "primitive" compositions of various regions of the earth. Table 15 is a compilation of some of the estimates of the composition of the primitive upper mantle, to compare with the Horoman sample. R717, the sample chosen to as undepleted source for Ronda (Frey et al, 1985), is also shown for comparison. Sample 62210 is remarkably similar to these estimates, and to the Ronda sample, for most major and compatible trace elements, as well as ratios between

Table 15. "Primitive" Upper Mantle Composition

	62210	R717*	(1)	(2)	(3)	(4)	(5)
SiO_2	44.95	44.97	45.14	46.0	45.1	45.1	46.2
TiO_2	0.15	0.17	0.22	-	0.2	0.22	0.23
Al_2O_3	4.14	3.91	3.97	4.06	3.3	4.14	4.75
FeO^*	8.04	8.28	7.82	-	8.0	7.82	7.70
MnO	0.14	0.13	0.13	-	0.15	0.13	0.13
MgO	37.10	37.97	38.30	37.8	38.1	38.0	35.5
CaO	3.59	3.51	3.50	3.27	3.1	3.54	4.36
Na_2O	0.41	0.31	0.33	-	0.4	0.36	0.40
Ni	1972	2028	2110	-	-	2122	1807
Co	103	108	105	-	-	104	95
Cr	2573	2471	3140	-	2737	3079	2943
Sc	16.1	16.1	17.0	-	-	17	19
Yb	0.46	0.44	0.42	0.42	-	0.44	0.62
Sc	16.6	13.7	19.6	28	-	-	-
Sm	0.325	0.349	0.38	0.38	-	-	-
Mg#	0.892	0.891	0.897	-	0.90	0.89	0.89
CaO/Al_2O_3	0.87	0.90	0.88	0.81	0.94	0.86	0.92
MgO/Al_2O_3	8.96	9.71	9.65	9.31	11.54	9.18	7.47
MgO/SiO_2	0.83	0.84	0.85	0.82	0.84	0.84	0.77
Al_2O_3/SiO_2	0.092	0.087	0.088	0.088	0.073	0.092	0.10
Yb/Sc	0.029	0.027	0.025	-	-	0.026	0.033
Ni/Co	19.1	18.8	20.1	-	-	20.4	19.0

References: * Frey, et al (1985); (1) Jagoutz, et al (1979); (2) Zindler and Hart (1986); (3) Ringwood (1979); (4) Wanke (1981); (5) Palme and Nickel (1985).

elements. Observation of incompatible elements in Table 15 (Sr, Sm and to some degree Ti) indicates that even relatively primary samples such as from Horoman and Ronda are depleted to some degree. The general correspondence between the mantle estimates and natural samples suggests that these samples may, with some qualification, be considered primitive. Conclusions drawn from geochemical modelling from these source rocks may then be placed more confidently into a framework of mantle processes in general. The similarity between what is considered source material from Horoman and Ronda suggests that specific comparisons of data and models between these two peridotite bodies may be made.

Discussion of Models

As mentioned previously, highly incompatible elements are very sensitive to melting process and to the degree of melting. We can use variation in abundances of these elements to help constrain the petrogenetic models discussed in the beginning of the paper. In general geochemical data shows a decoupling of these elements from major element abundances and more compatible trace elements reflecting their greater sensitivity to degree of melting. This decoupling is frequently seen in the form of non-linear variation diagrams between highly incompatible elements and the less melt sensitive elements compared to linear variation diagrams between most major elements. This decoupling would be expected in models 2 and 3 (see the

section on major elements). (In fact model 3 should produce non-linear major element correlations as well unless one specifies that the heterogeneous melt is near homogeneous, thus making the diagrams near linear within the scatter of the data.) Model one of a uniform degree of melting followed by varying degrees of extraction of a homogeneous melt should produce linear variation diagrams for all elements. In light of this the data presented up to now would favor model one. But the improbability of variable extraction of a homogeneous melt affecting the major elements, in particular Fe and Mg (even Fo content in olivine), to such a degree that the Mg-Fe calculation used to estimate F is completely unsuitable makes the model appear untenable. The large variation in mineral major element chemistry and particularly clinopyroxene trace element chemistry also do not fit the model very well. Models 2 and 3 require variation in degree of melting but also should produce the decoupling of the highly incompatible elements mentioned above. Frey et al., (1985) suggest that the trends in the variation diagrams for the highly incompatible elements in the Ronda peridotites are best explained by curved trajectories with rapid decreases in incompatible element content as MgO increases. I don't think the data supports this interpretation, particularly as the only signs of a curved fit to the data occurs at very low concentrations where the greatest analytical uncertainties exist as pointed out by Frey et al., (1986).

In the following section an attempt is made to explain the discrepancies of models 2 and 3 to the trace element data by using a model entailing the presence of trapped melt.

Trapped Melt Model

Models 2 and 3 predict that the highly incompatible elements should behave differently from major and compatible trace elements with varying degrees of melting. This difference should be manifested in variation diagrams with highly incompatible elements having non-linear correlation with major elements and major element and compatible trace element variation diagrams having linear or near linear trends. This type of decoupling is not seen in the Horoman data, which show near linear variation diagrams for all elements, but the decoupling of the highly incompatible elements manifests itself in a different way.

One can calculate what the bulk partition coefficient for each element should be for equilibrium partial melting with the degree of melting determined by major elements using the mass balance equation, $D^{s/l}=(C_R/C_oF)/[1+C_R/C_o(F-1)]$. Where $D^{s/l}$ is the bulk partition coefficient for the element of interest, C_R is the concentration of the element for a particular rock sample, C_o is the concentration of the element in the source, and F is the degree of melting determined by major elements for the rock of interest. The results of this calculation are given in Table 16. From this table it is clear that taking these results at face value, with the assumption that all the rocks are residues

Table 16: Partition Coefficients for Trace Elements in the Horoman Peridotites Derived by Mass Balance Calculation and From Literature Values

	References	62212	62213	62131	62130	62128	62127
% melting		0.8	5.1	16.9	17.3	24.9	25.5
La	Mass Balance:	0.054	*	0.143	0.094	0.056	0.052
	Literature: A[1]	0.0069	0.0060	0.0035	0.0031	0.0011	0.0009
	A[2]	0.014	0.012	0.0091	0.0071	0.0045	0.0037
	B	0.016	0.014	0.010	0.0071	0.0041	0.0029
Sr	Mass Balance:	0.032	0.059	0.077	0.069	0.017	0.018
	Literature: A[3]	0.159	0.138	0.076	0.072	0.020	0.019
Sm	Mass Balance:	0.053	0.204	0.101	0.109	0.0096	0.0156
	Literature: A[1]	0.018	0.016	0.013	0.0090	0.0061	0.0047
	A[2]	0.078	0.071	0.059	0.040	0.032	0.025
	B	0.027	0.024	0.018	0.0122	0.0083	0.0058
Zr	Mass Balance:	*	0.23	0.11	0.15	-	-
	Literature: C	0.023	0.022	0.020	0.018	0.017	0.016
Ti	Mass Balance:	0.12	0.22	0.13	0.14	0.027	0.022
	Literature: C	0.067	0.063	0.056	0.049	0.048	0.042
	D	0.07	0.07	0.034	0.041	0.026	0.023
Y	Mass Balance:	0.22	0.37	0.11	0.13	0.014	0.014
	Literature: A[4]	0.024	0.021	0.017	0.012	0.009	0.007
	C	0.100	0.093	0.082	0.070	0.067	0.057
Yb	Mass Balance:	0.058	0.24	0.107	0.117	0.016	0.013
	Literature: A[1]	0.030	0.027	0.023	0.018	0.015	0.013
	A[2]	0.138	0.126	0.111	0.086	0.077	0.063
	B	0.047	0.043	0.037	0.029	0.026	0.022
Ga	Mass Balance:	0.10	0.42	0.28	0.28	0.19	0.20
	Literature: E	0.24	0.22	0.17	0.16	0.14	0.12
V	Mass Balance:	*	0.38	0.27	0.25	0.21	0.16
	Literature: A[5]	≤0.41	≤0.38	≤0.31	≤0.26	≤0.27	≤0.22
	D	≤0.31	≤0.29	≤0.23	≤0.21	≤0.22	≤0.19
	F[5]	≤0.34	≤0.32	≤0.26	≤0.23	≤0.25	≤0.21

(cont'd.)

Table 16 (cont'd.)

	References	62212	62213	62131	62130	62128	62127
Sc	Mass Balance:	0.18	0.35	0.24	0.19	0.25	0.20
	Literature: A	0.68	0.64	0.60	0.53	0.53	0.47
	D	0.32	0.30	0.28	0.25	0.21	0.22
Mn	Mass Balance:	0.18	0.54	0.63	0.62	0.72	0.72
	Literature: D	0.81	0.83	0.86	0.86	0.90	0.90
Cr	Mass Balance:	5.57	1.72	1.54	0.40	6.55	3.30
	Literature: D[6]	~2.7	~2.7	~2.4	~2.1	~2.6	~2.2
Co	Mass Balance:	*	6.24	1.75	4.60	1.87	2.31
	Literature: D	2.1	2.2	2.3	2.4	2.5	2.6
Ni	Mass Balance:	2.31	*	5.34	9.86	4.03	5.54
	Literature: D	7.7	8.1	9.0	9.1	9.5	10.0
	G	7.49	9.94	5.96	7.79	5.99	6.61

Notes:
- [A] Frey et al. (1978), Tables A-1 and A-2.
- [B] Prinzhofer and Allegre (1985), Table 2.
- [C] Pearce and Norry (1979).
- [D] Sun et al. (1979), Table 4.
- [E] Goodman (1972), p. 172.
- [F] Clague and Frey (1982), Table 5.
- [G] Hart and Davis (1978) and melt compositions from Table 12 (this work).

- [1] Set 1 (with Prinzhofer and Allegre (1985) plagioclase).
- [2] Set 2 (with Prinzhofer and Allegre (1985) plagioclase).
- [3] Plagioclase (K_D = 1.4) from Drake and Weill (1975).
- [4] Plagioclase from Pearce and Norry (1979).
- [5] Spinel maximum from Sun et al., (1979).
- [6] Used K_D for spinel of ~100.

- * Partition coefficient incalculable
- - No data

from varying degrees of equilibrium batch melting, would lead one to the conclusion that none of the trace elements are truly acting highly incompatibly. Bulk partition coefficients can also be estimated from values of mineral partition coefficients from the literature using the modes from Table 1. The bulk D estimated this way is also in Table 16 for comparison. The decoupling of the "highly incompatible" elements comes when comparing these two methods of determining bulk D (Fig's. 71-73). These figures graphically show the match between these two estimates of D. Elements are arranged roughly in order of decreasing incompatibility from left to right. Lines are drawn connecting the mass balance estimates of D and between the literature values deemed best to use. Other literature partition coefficients are also shown for comparison. From the three figures, from a slightly depleted sample (62213), to moderately depleted (62131), to strongly depleted (62127), one can see a decrease in both estimates of D. This is expected because as mineralogy becomes more residual from melting, i.e. less clinopyroxene, more olivine, bulk D's must decrease. The important observation to be made from these figures is that for the compatible elements (Ni, Co and Cr) and the moderately incompatible elements (Mn, Sc, V and Ga) the match is quite good. That is, these elements are consistent with derivation of these rocks from equilibrium partial melting of varying degrees. The highly incompatible elements on the other hand show fairly severe

Figure 71. Two estimates of bulk partition coefficients for trace elements (in rough order of increasing compatibility to the right) in Horoman sample 62213 from Table 16. Calculated bulk partition coefficients from mass balance calculation (see text), small solid circles and solid line (not calculable when not shown). Bulk partition coefficients estimated from literature values utilizing modes from Table 1, large symbols with broken line connecting literature values considered best. Several literature values are shown for some elements for comparison.

Literature references: Frey et al (1978), (open circle) Table A-1, Set 1 for REE with plagioclase D's from Prinzhofer and Allegre (1985), Table A-2 for other trace elements with plagioclase D for Sr from Drake and Weill (1975) and spinel D for V from Sun et al (1979), (closed circle) Table A-1, Set 2 for REE with plagioclase D from Prinzhofer and Allegre (1985); Prinzhofer and Allegre (1985) for REE (open triangle); Pearce and Norry (1979) for Zr, Ti and Y (open square); Goodman (1972) for Ga (Star of David symbol); Sun et al (1979) for Ti, V, Sc, Mn, Cr, Co and Ni (solid triangle); Clague and Frey (1982) for V (closed square) with spinel D from Sun et al (1979); and Hart and Davis (1978) for Ni (open rectangle).

Figure 72. Same as Fig. 71 for sample 62131 (symbols as in caption for Fig. 71).

Figure 73. Same as Fig. 71 for sample 62127 (symbols as in caption for Fig. 71).

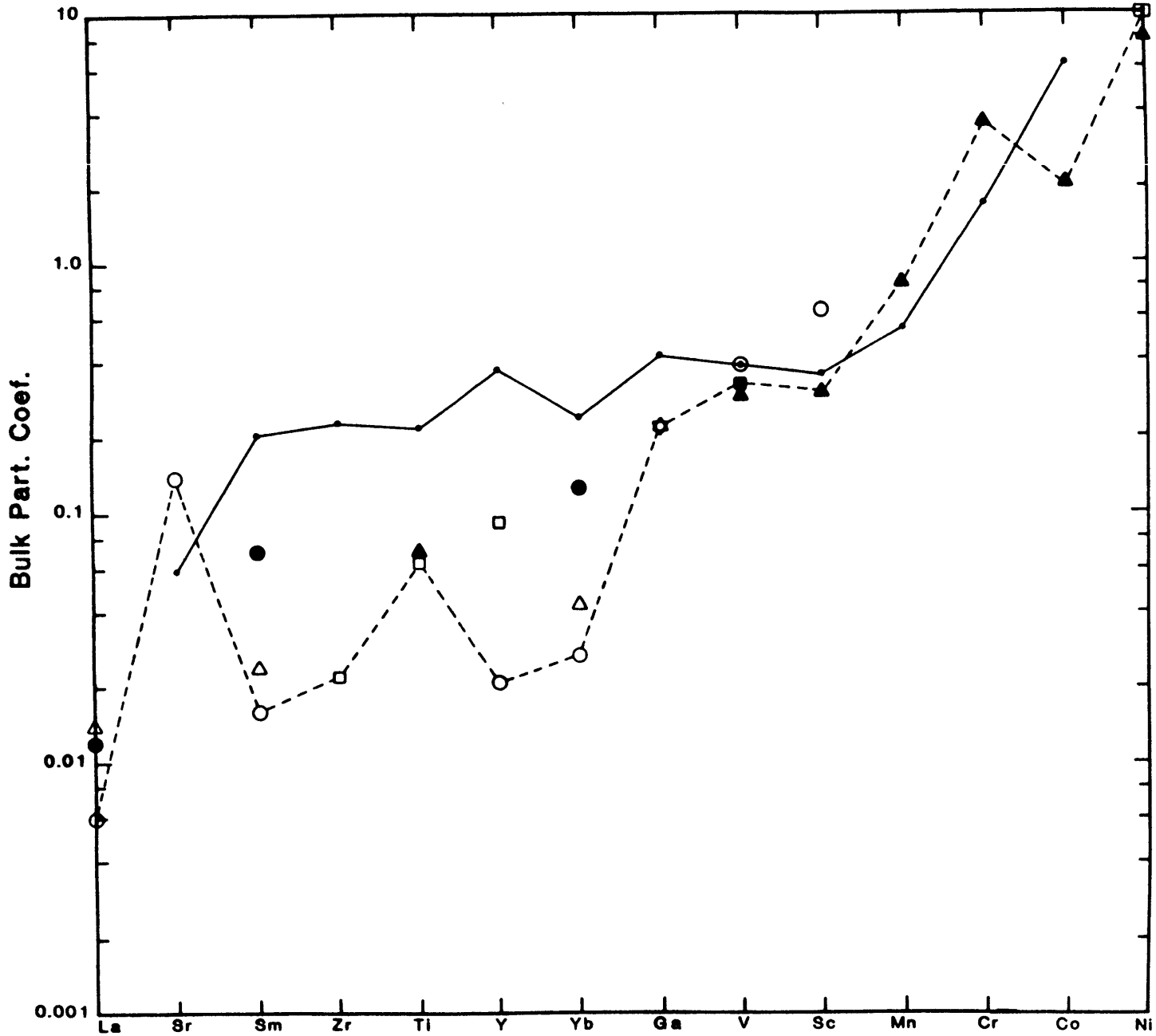
Bulk Part. Coef.
10
1.0
0.1
0.01
0.001
La
Sr
Sm
Zr
Ti
Y
Yb
Ga
V
Sc
Mn
Cr
Co
Ni

Figure 71

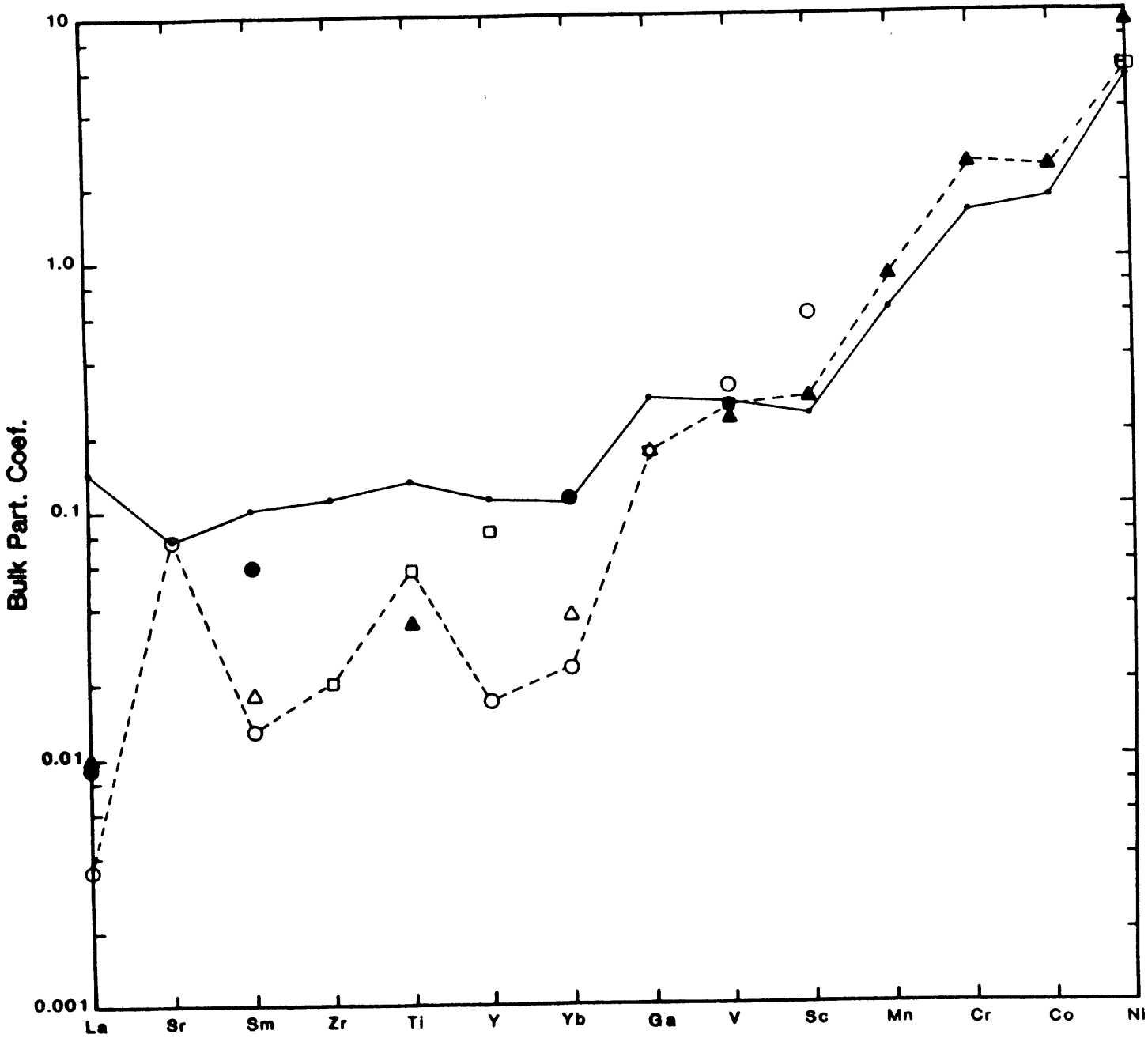
Bulk Part. Coef.
10
1.0
0.1
0.01
0.001
La
Sr
Sm
Zr
Ti
Y
Yb
Ga
V
Sc
Mn
Cr
Co
Ni

Figure 72

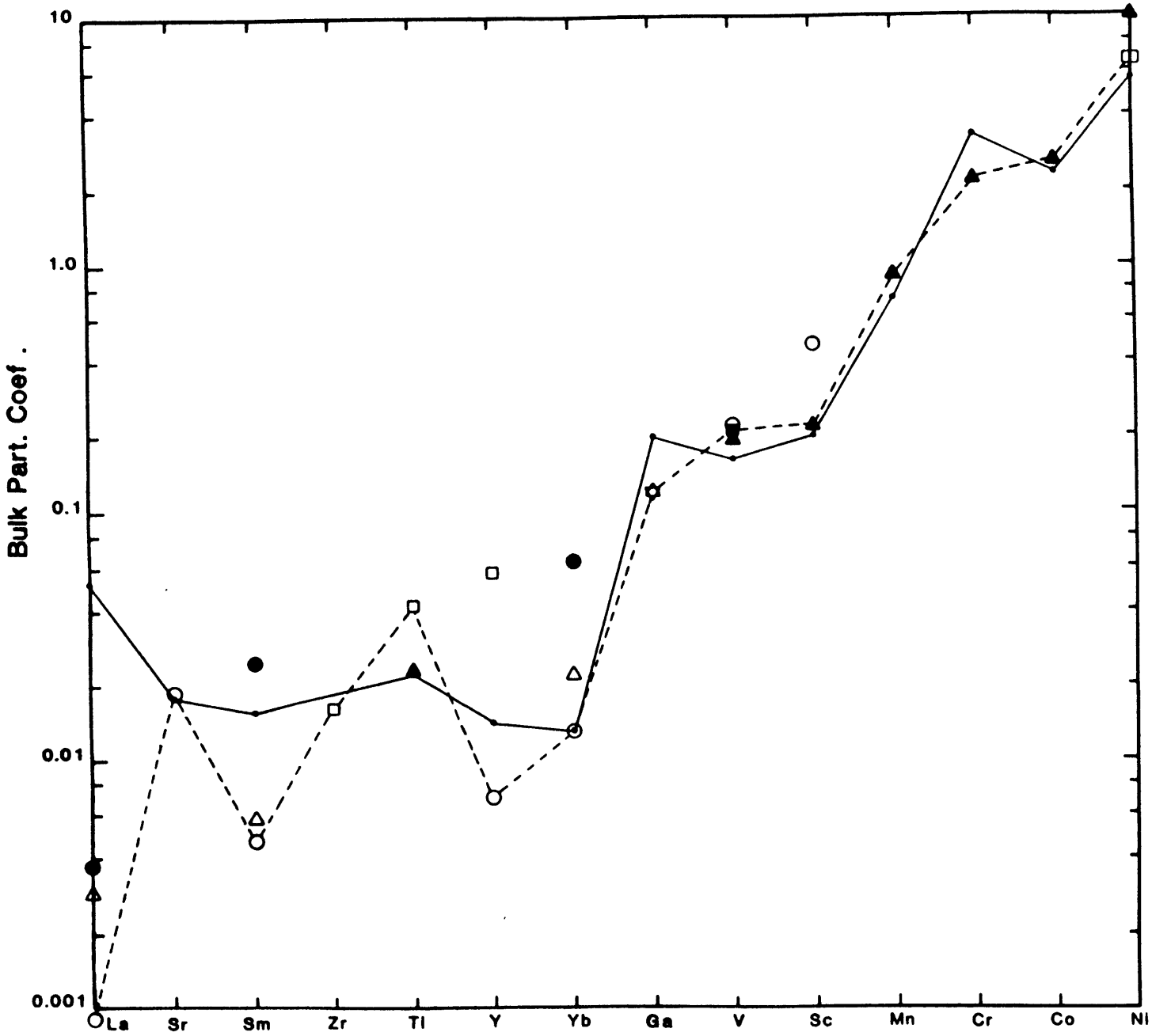
Bulk Part. Coef.
10
1.0
0.1
0.01
0.001
La
Sr
Sm
Zr
Tl
Y
Yb
Ga
V
Sc
Mn
Cr
Co
Ni

Figure 73

mismatch (up to a factor of 60X for La in 62127), with the exception of Sr. Sr is not really a highly incompatible element in these peridotites because of the large partition coefficient of Sr in plagioclase. The Sr values appear to be consistent with simple derivation by equilibrium partial melting in much the same way as Sc, except that Sc is controlled by clinopyroxene melting while Sr is controlled by plagioclase melting. The three figures show that, in general, the mismatch between the two estimates of D is greatest for the least depleted rocks and least for the most depleted (with the exception of La).

Another way of portraying this data that is perhaps conceptually more easily understood is to compare the abundances to theoretical trends for incompatible elements as a function of degree of melting. Table 17 lists a number of incompatible elements (including the major elements Na, Ca and Al for comparison) and the ratio of these elements in each sample normalized to their assumed source (62210) for their respective F value derived from major elements. This data with curves produced by the equilibrium melting equation ($C_R/C_O=D/F+D-DF$) at constant D for several values of D are plotted as a function of F (Fig. 74). It is apparent that none of the data fit these curves with the possible exception of the moderately incompatible elements.

To drive the point home that the incompatible elements are inconsistent with the derivation of these rocks by equilibrium melting, the mass balance equation can be

Table 17: Cr/Co for Trace Incompatible Elements and Some Major Elements For the Horoman Peridotites With 62210 as Co

	62212	62213	62131	62130	62128	62127
% melting	0.8	5.1	16.9	17.3	24.9	25.5
La	0.877	1.102	0.497	0.374	0.193	0.176
Sr	0.807	0.753	0.331	0.301	0.066	0.066
Sm	0.874	0.834	0.400	0.415	0.038	0.058
Eu	0.906	0.842	0.439	0.417	0.055	0.073
Zr	1.087	0.855	0.420	0.507	-	-
Ti	0.946	0.845	0.477	0.490	0.101	0.081
Y	0.973	0.919	0.432	0.459	0.054	0.054
Yb	0.855	0.859	0.415	0.433	0.060	0.048
Lu	0.896	0.896	0.442	0.436	0.083	0.068
Ga	0.935	0.935	0.696	0.696	0.478	0.500
V	1.056	0.924	0.681	0.653	0.521	0.437
Sc	0.965	0.912	0.647	0.580	0.569	0.500
Mn	0.965	0.958	0.910	0.904	0.910	0.910
Na	0.883	0.722	0.417	0.339	0.051	0.051
Ca	0.886	0.783	0.543	0.408	0.223	0.168
Al	0.942	0.884	0.529	0.516	0.258	0.184

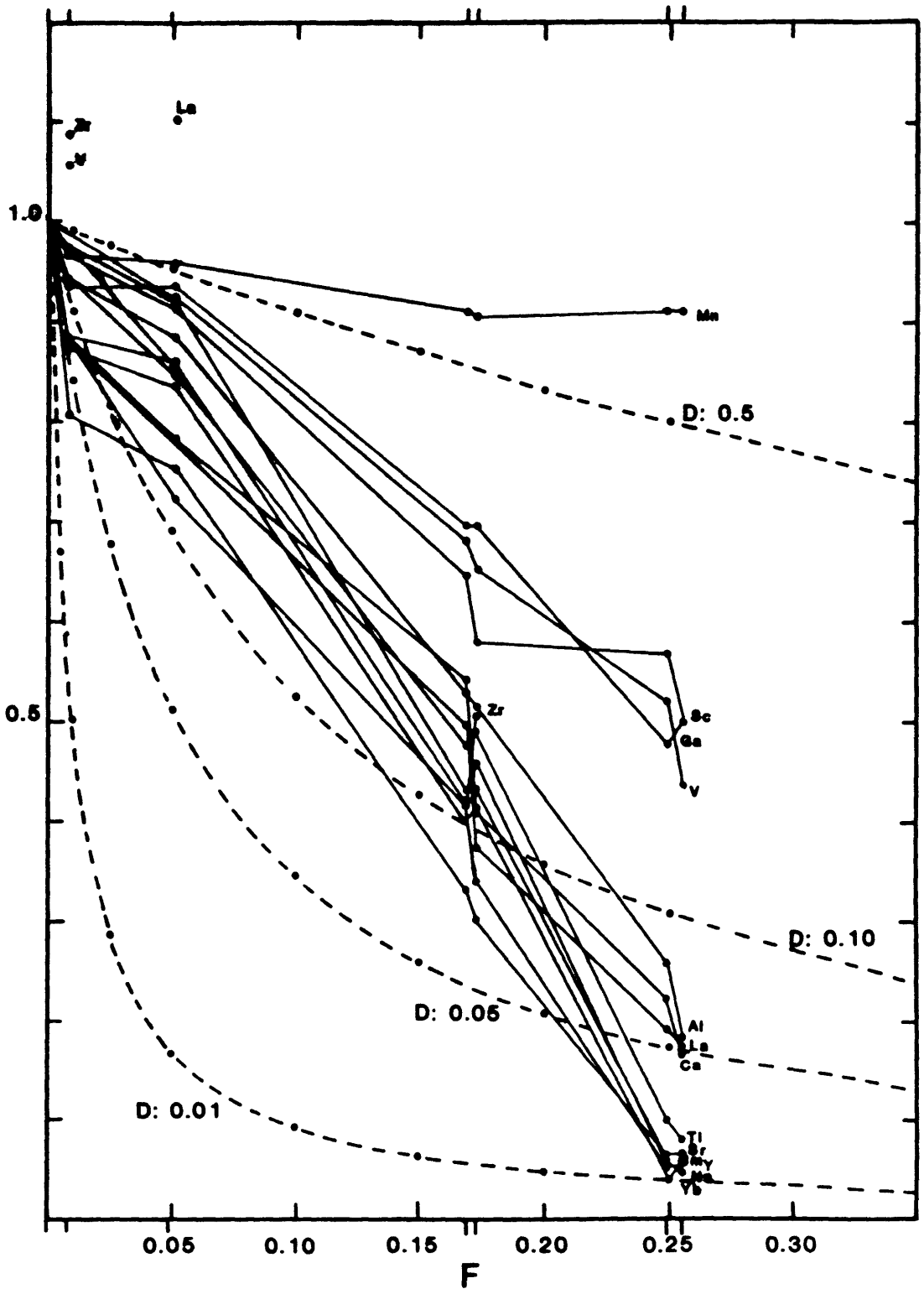

Figure 74. Degree of melting (F) versus ratio of concentrations in melted sample and assumed source, 62210 (C_R/C_O) from Table 17 for a variety of trace and major elements (solid lines). Equilibrium curves for constant D for several values of D are also shown (broken lines).

rearranged to solve for F, with literature values used for the bulk D's. This was done for La and Yb, using sample 62210 as a source. The La calculation predicts that all of the samples are produced by less than one percent melting, while Yb closely matches the F values of the Fe-Mg calculation for the harzburgites but predicts 2-3 percent melting for the transitional lherzolites and less than one percent for the two enriched samples.

A likely complexity, introduced in the plagioclase section, is the presence of trapped melt within the residual peridotites. This makes intuitive sense chemically, for a melt should be enriched in highly incompatible elements while only slightly enriched in moderately incompatible elements and certain major elements (e.g. Ca, Al and Na). A small amount of trapped melt could significantly affect the budget of highly incompatible elements while having little or no effect on the other elements. Furthermore, the degree of mismatch with various elements seems consistent with trapped melt, e.g. La, the most incompatible element in the rocks, appears to be affected the most. Finally, the observation that the most depleted rocks fit the equilibrium melting model the best is consistent with the petrologic observation that plagioclase and/or clinopyroxene content may represent trapped melt interaction.

Stockman (1982) developed a simple method of graphically and quantitatively evaluating the effect of trapped melt. It utilizes the following mass balance.

$$C_o = C_l F' + C_R'(1 - F) = C_l F + C_R(1-F)$$

where, C_l is the trace element concentration in the melt; F' is the weight fraction of rock melted; C_R' is the trace element concentration in the residue after complete extraction of melt; C_R is the concentration of the bulk residue including any trapped melt (F'-F); and F is the weight fraction of the rock which is segregated as melt. This mass balance is portrayed schematically in Fig. 75. C_l can be eliminated and the equation rearranged to obtain:

$$C_R/C_o = \frac{(F' - F) + (F - FF')C_R'/C_o}{F' - FF'}$$

Using this equation we can make a series of plots for each element showing the possible effects of various degrees of trapped melt upon what would be expected for batch equilibrium melting and compare these effects to the data (Fig's. 76-83). The equilibrium line in these figures (labelled C_R'/C_o) is that trend for which $C_R'=C_R$ and F=F', i.e. no trapped melt. The curvatures of the C_R'/C_o lines for each element are similar to the equilibrium curves in Fig. 74 except for one important difference. The C_R'/C_o curves in Fig's. 76-83 are produced by the equilibrium melting equation but with the more realistic condition of D varying with F. C_R/C_o for each element was calculated for the corresponding F value using the bulk partition coefficients for each element and for each sample from literature mineral partition coefficients (preferred values from Fig's. 71-73) and rock modes. Bulk D's were

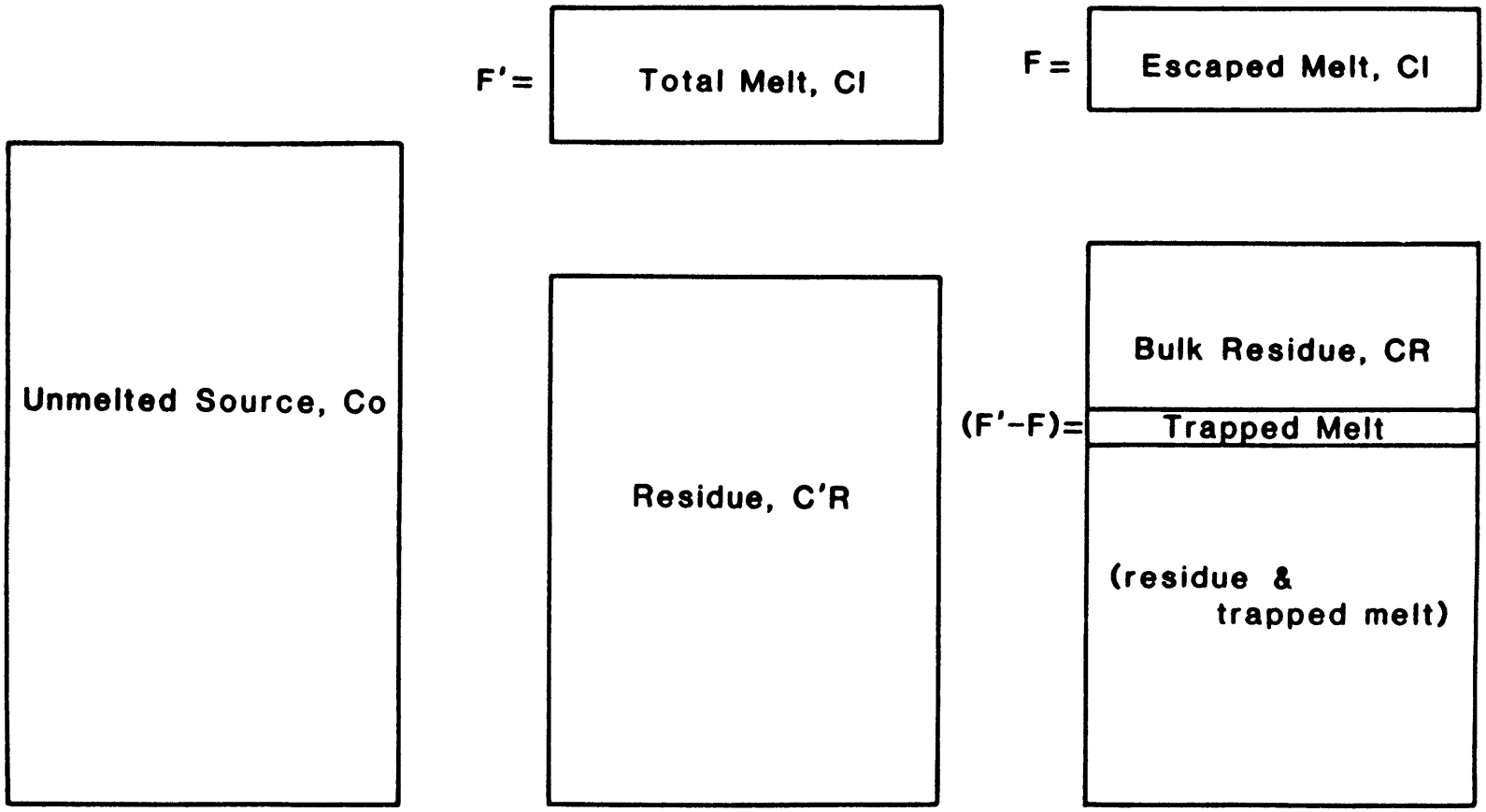

Figure 75. Schematic diagram portraying mass balance for trapped melt model used in Fig's. 76-83. See text for description of symbols and details of model.

Figure 76. F versus C_R/C_o diagram (as in Fig. 74) showing possible effect of trapped melt for Sc and V in the Horoman samples. Data for Sc and V are shown by thin solid lines with data points indicated. C_R'/C_o line (thick solid line) is the equilibrium line for which $C_R' = C_R$ and $F = F'$, *i.e.* no trapped melt, using the preferred bulk partition coefficients from Table 16 (as plotted in Fig's. 71-73). Only one C_R'/C_o line is used to model Sc and V because their bulk partition coefficients are quite similar. Iso-F' lines for various values of F' (broken lines) are shown. Estimates of amount of trapped melt possible to explain data can be determined graphically if data is above C_R'/C_o line, as trapped melt is (F'-F).

Figure 77. Same as Fig. 76 but for Sr. No F' curves are shown because trapped melt is not necessary to explain the data.

Figure 78. Same as Fig. 76 but for Ga. Data suggests possibility of trapped melt but this is not considered likely (see text).

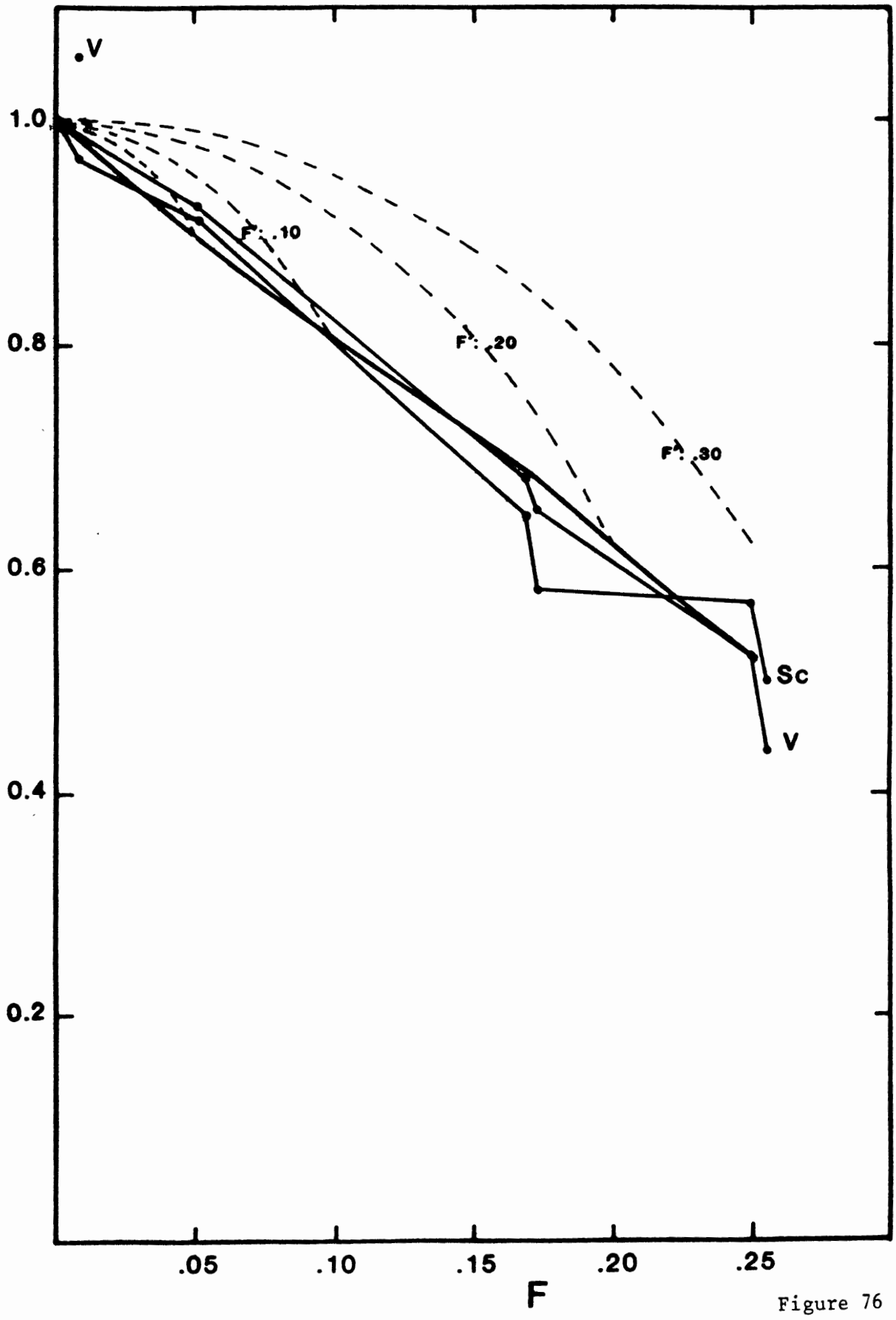

Figure 76

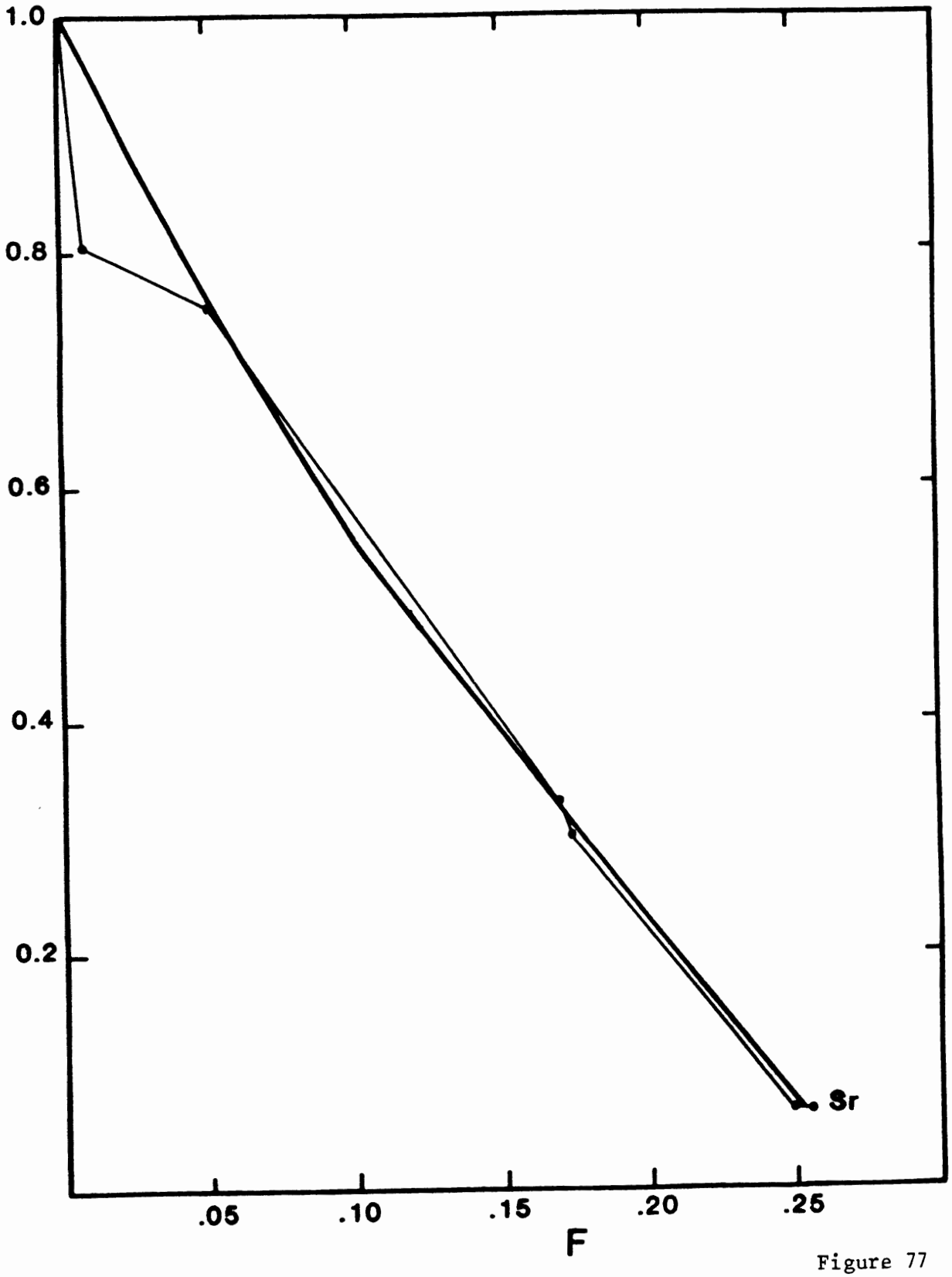

Figure 77

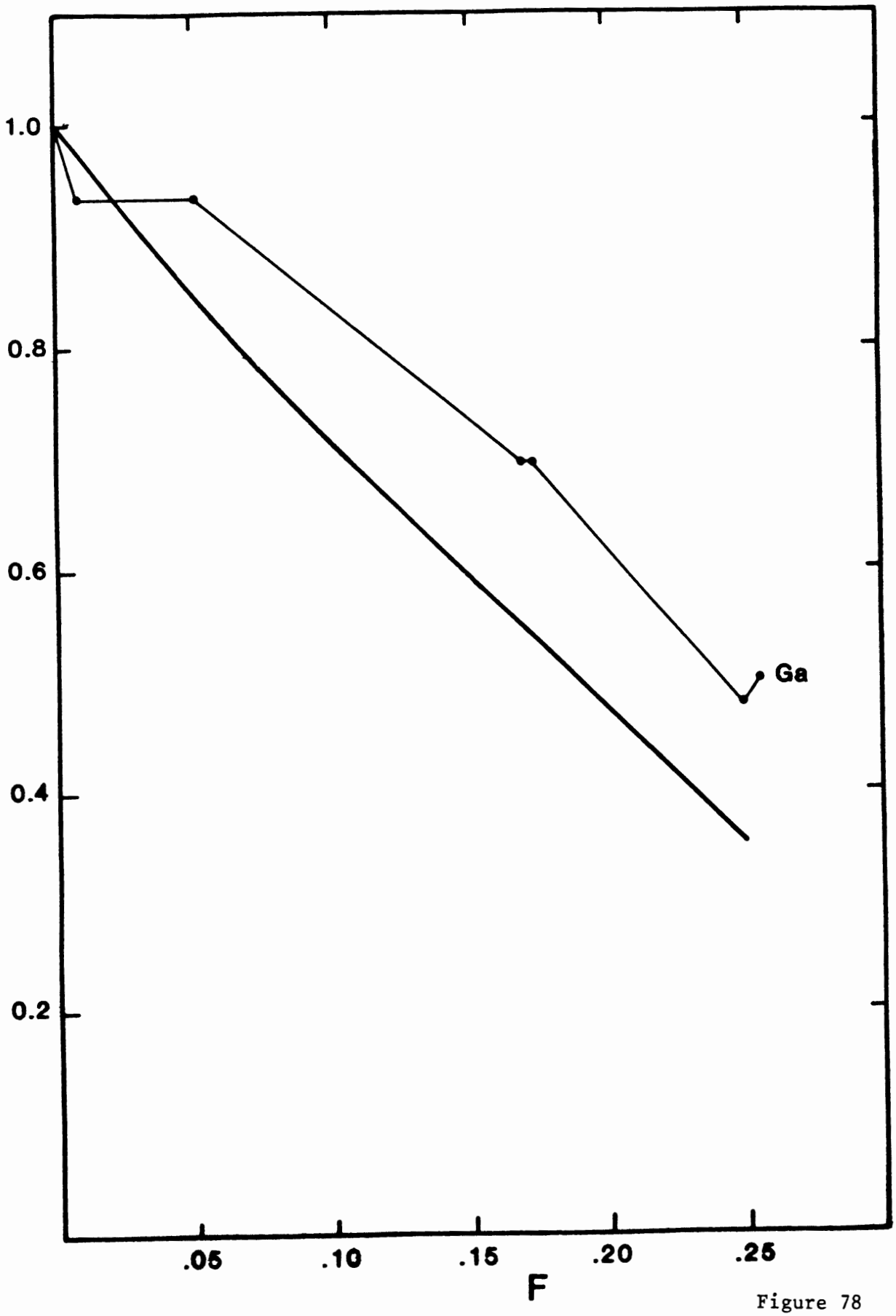

Figure 78

interpolated for intermediate F values to produce smooth C_R'/C_o curves. F is the variable determined by major element mass balance while F' is a hypothetical term that probably should not exceed 0.40 at which point a residue would be a dunite. A series of iso-F' curves can be drawn using the above equation and solving for C_R/C_o for each element.

Sc and V can be modeled using the same C_R'/C_o curve for their bulk D's are very similar. The trapped melt model for these two elements (Fig. 76) shows the variation can be relatively well explained without any trapped melt. In fact the data for some portion of the figure lies below the equilibrium line. The data could be explained by ~2% trapped melt for V in 62128, ~2% for V for 62213 and less for this sample by consideration of Sc data. The V content for 62212 is actually greater than the source composition so the degree of potential trapped melt can't be adequately evaluated. The Sr data essentially falls right on the equilibrium melting model indicating no trapped melt (Fig. 77). Gallium data is almost all above the equilibrium curve and is practically parallel to it (Fig. 78). With the general range of estimated Ga bulk partition coefficients and the fact that the data is almost coincident with V and Sc it is likely that the Ga D's used (Goodman, 1972) are too low. I don't believe that Ga variation really requires trapped melt. Ti should be behaving as a highly incompatible element but the data doesn't support this (Fig.

79). The data can be explained by ~1% trapped melt in 62212, ~7% for 62213, ~6% for 62131, and ~8% for 62130. The two depleted harzburgites are well explained by the equilibrium model. Yb acts similarly to Ti except for the 62213 data which requires ~15% trapped melt to explain it (Fig. 80). Once again the harzburgites can be explained by the equilibrium curve. The Zr data suggests similar degrees of trapped melt to Yb but can only be evaluated for three samples due to $C_R/C_o>1$ for 62212 and no Zr data for the harzburgites (Fig. 81). Sm and Y have similar partition coefficients so a single equilibrium model curve is used (Fig. 82). The two elements are not coincident at low degrees of melting. The trapped melt model requires ~1% for 62212 using Sm while Y requires ~7% to fit the data. Likewise, for sample 62213 Sm indicates about 10% while Y suggests closer to 20%. The values are closer for the rest of the samples and are generally consistent with Ti and Yb. The data also suggest a little bit of trapped melt in the two harzburgites. The La data was calculated for two equilibrium model curves based on two sets of D's, but only the set from Frey et al (1978) is plotted (Fig. 83). The La data requires the greatest quantity of trapped melt for the elements modeled, with ~1-3% (depending upon bulk D) for 62212, ~10% for 62131, 7-8% for 62130, ~3% for 62128 and ~2% for 62127. (La in 62213 is inexplicably greater than the source abundance.) Table 18 summarizes the approximate

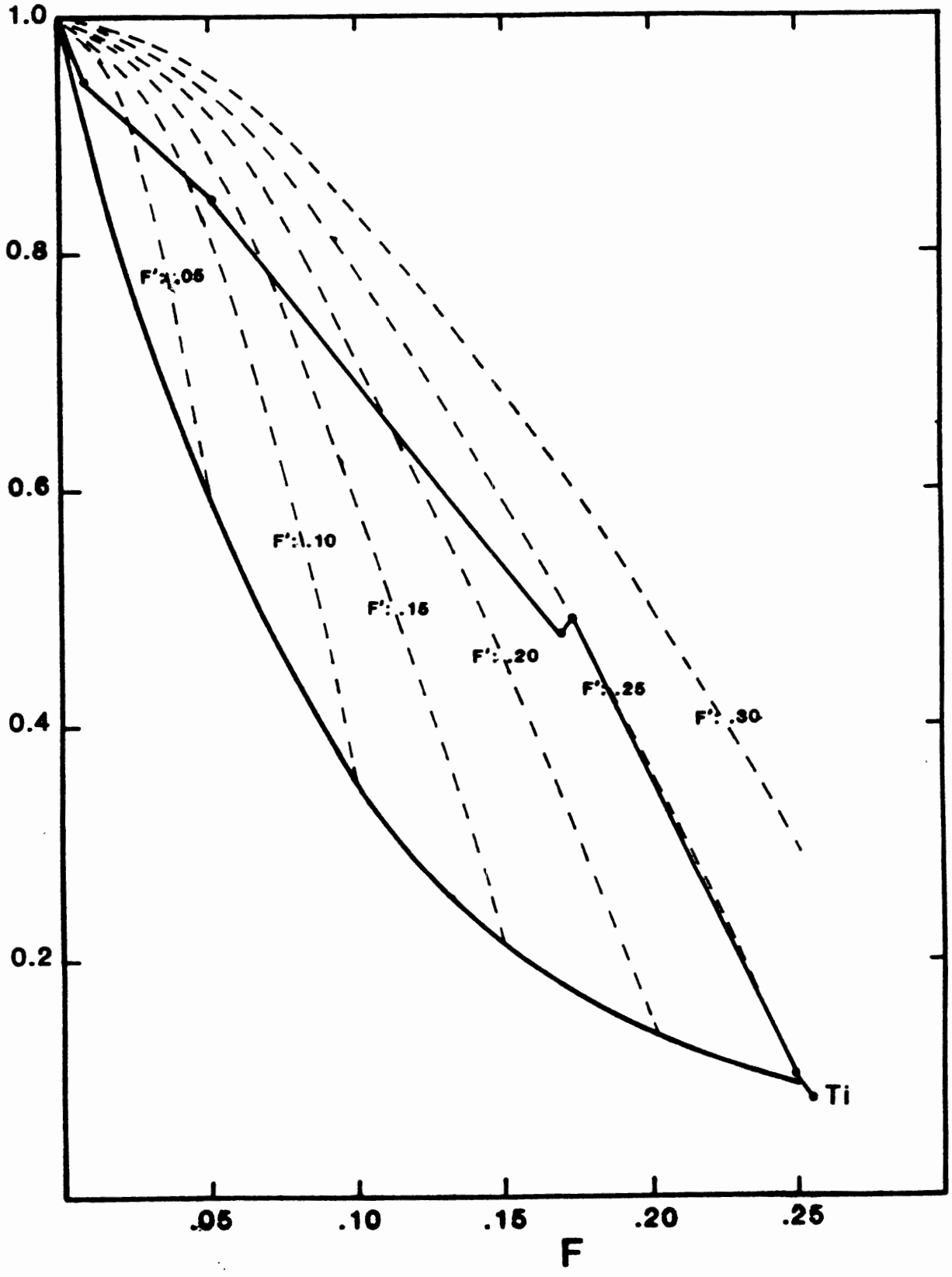

Figure 79. Same as Fig. 76 but for Ti.

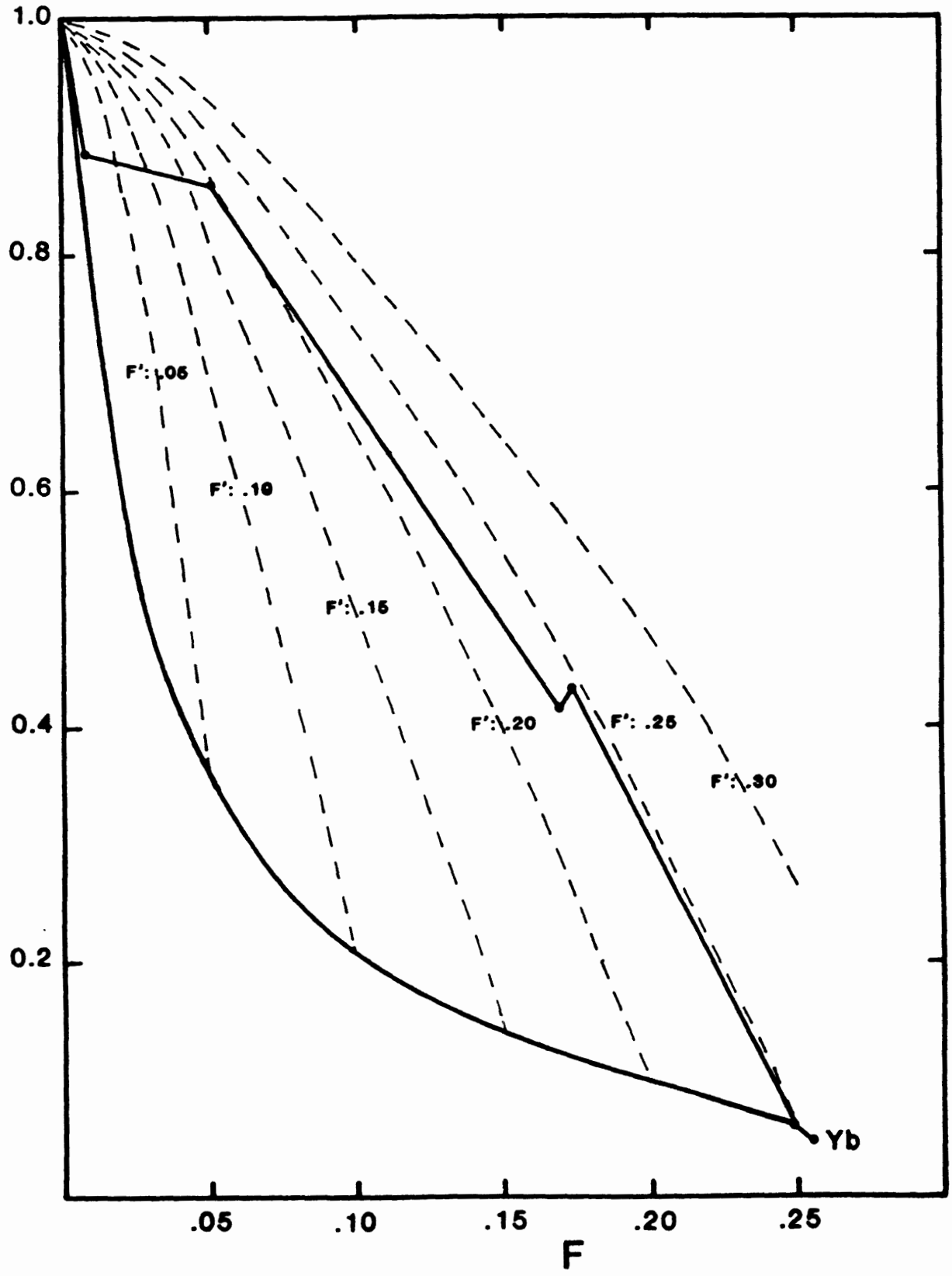

Figure 80. Same as Fig. 76 but for Yb.

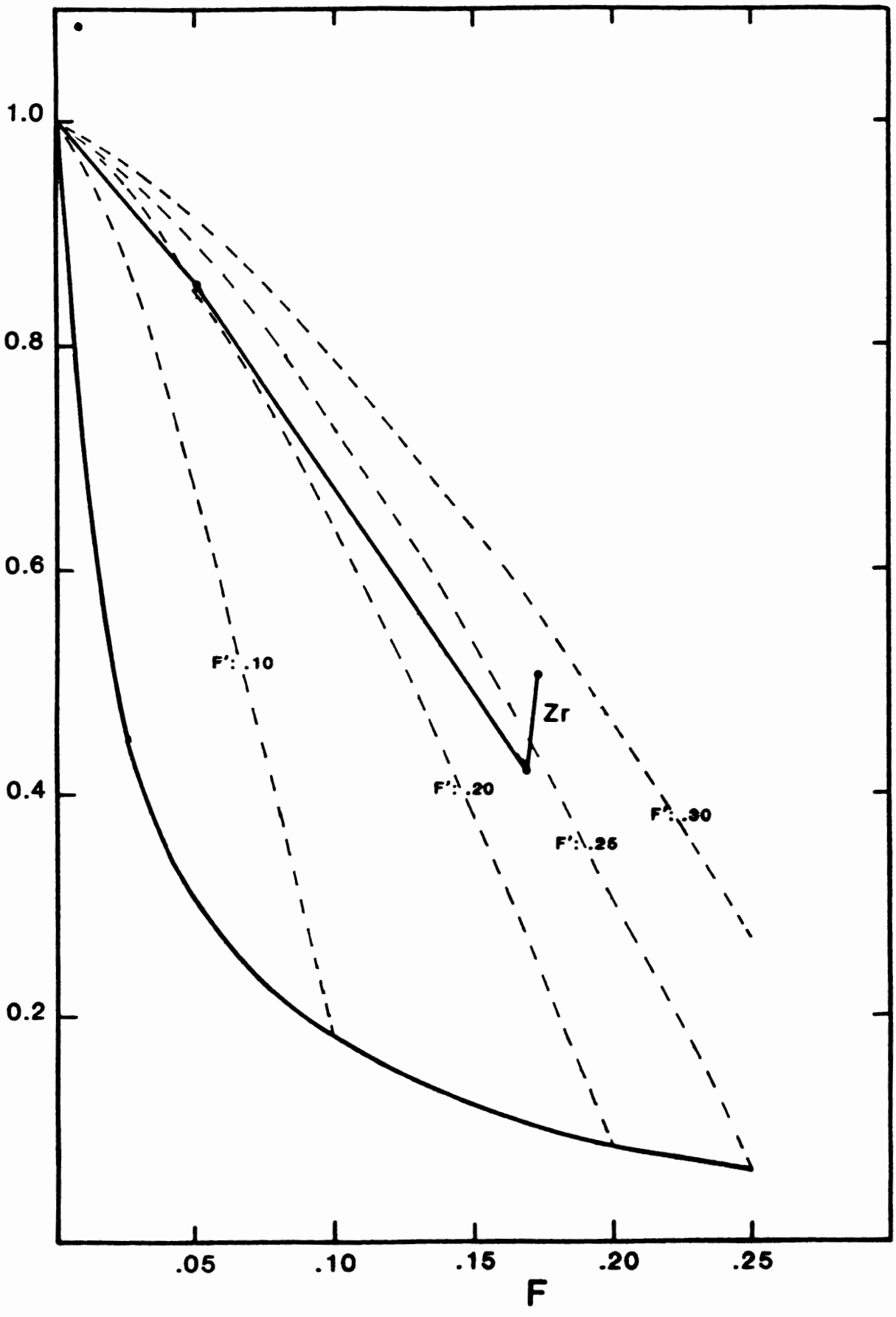

Figure 81. Same as Fig. 76 but for Zr.

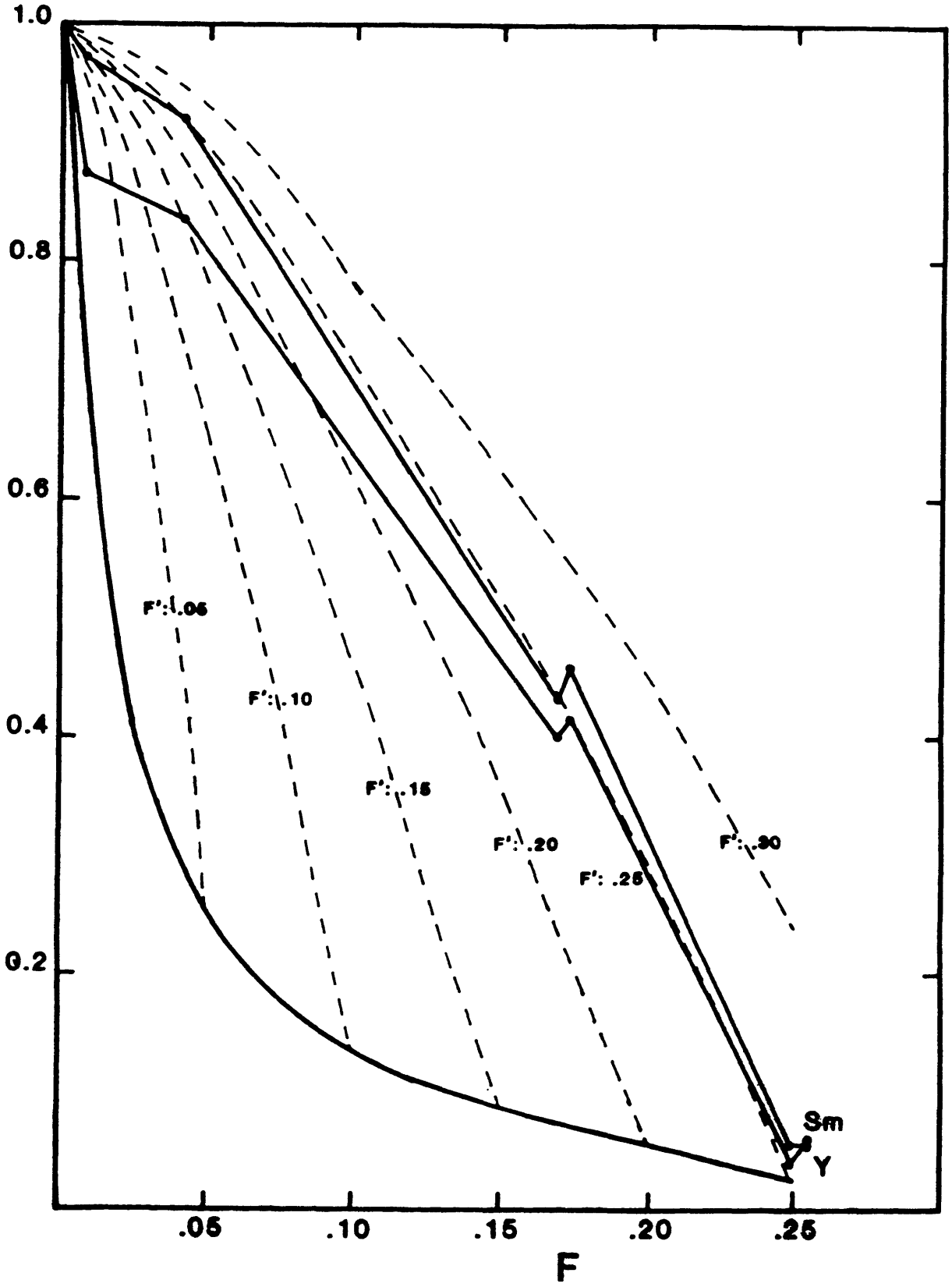

Figure 82. Same as Fig. 76 but for Sm and Y. These elements are shown together because their bulk partition coefficients are similar in these rocks so they are modelled by a single C_R'/C_O equilibrium line.

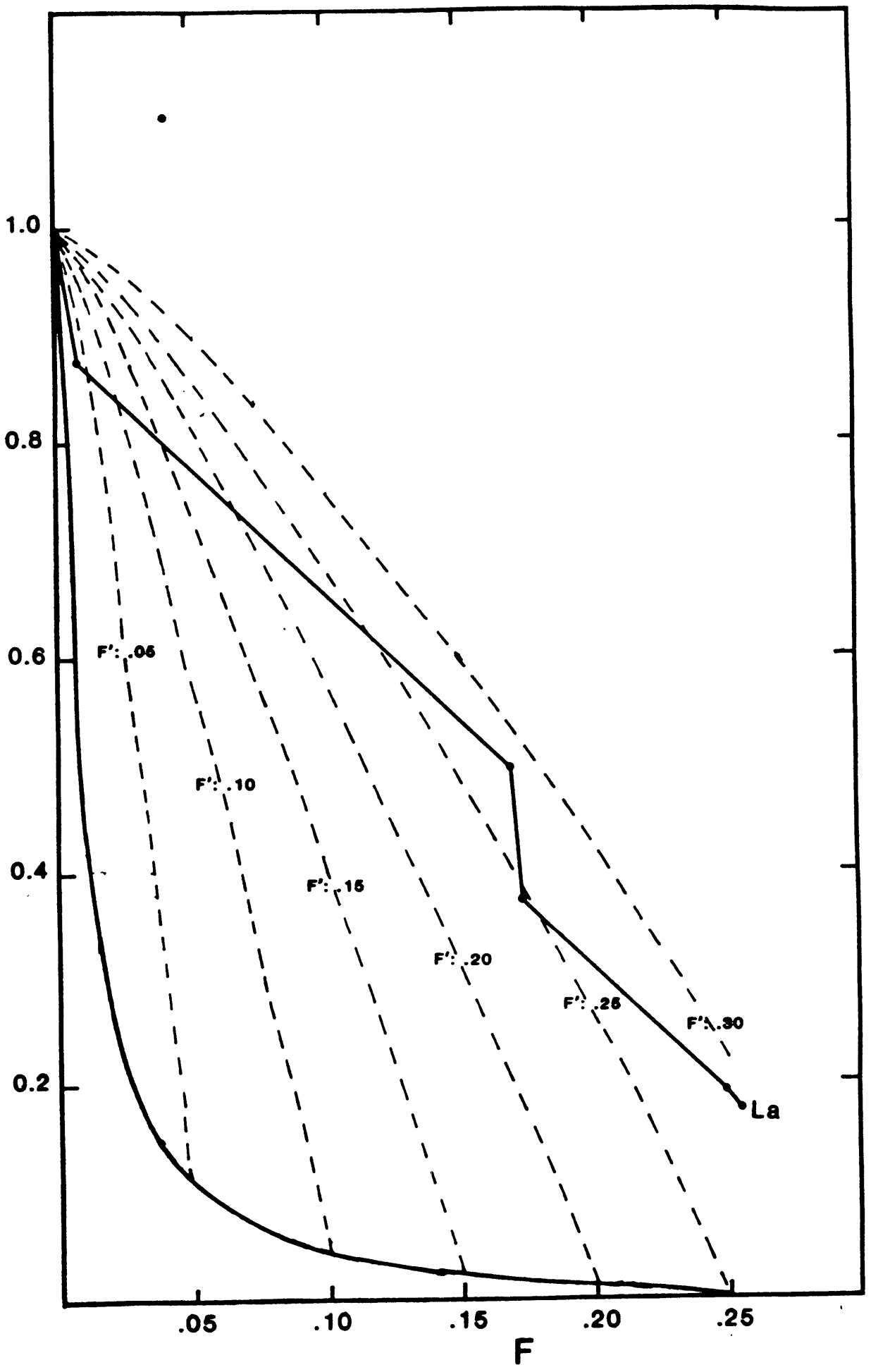

Figure 83. Same as Fig. 76 but for La.

Table 18: Compilation of Approximate Trapped Melt Required to Explain Trace Element Data Using Trapped Melt Model For the Horoman Peridotites in Percent

	K_D range used in model	62212	62213	62131	62130	62128	62127
% Melting		0.8	5.1	16.9	17.3	24.9	25.5
Sc	0.33-0.21	*	1	*	*	0	*
V	0.33-0.21	(1)	2	0	0	2	0
Sr	0.16-0.019	*	0	0	0	0	0
Ti	0.07-0.025	1	7	6	8	0	0
Yb	0.03-0.015	0.7	15	6	7	0	0
Sm	0.02-0.005	1	10	6	7	0	1
Y	0.02-0.005	7	20	7	9	1	1
La	0.007-0.001[1]	2.7	(12)	11	8	3	2
	0.016-0.003[2]	1.2	(10)	10	7	3	2
Zr	0.023-0.016	(6)	15	7	10	-	-

* CR/C_o value below equilibrium model so considered to be ~0.
( ) CR/C_o value greater than one so evaluated based on straight line interpolation between surrounding two CR/C_o values.
\- No data
[1] Partition coefficients from set 2, Table A-1, Frey et al. (1978)
[2] Partition coefficients from Prinzhofer and Allegre (1985).

degree of trapped melt required for the model for each element and for each sample.

This model is essentially a simple mixing model of residue and trapped melt. If all the samples were originally melted to the same degree (F′) and differences are ascribed to varying removal of melt (F) than all the data should fall on a single C_R/C_o versus F curve along a constant F′. A more complex occurrence would be if F′ can also vary for the different peridotite samples. In this case data can be accounted for with scatter anywhere between the C_R'/C_o curve and what would be considered the maximum degree of F′ (or more stringently, the maximum degree of trapped melt in terms of physical possibility). The scatter allowed by this second alternative will be greater for more incompatible elements but more narrowly constrained for less incompatible elements. The model can become even less constrained if one considers the possibility of melts produced by low F′ becoming trapped in residues from high F′ or by fractionation of the trapped melt.

This model is rather difficult to critically evaluate as it is rather poorly constrained due to the vary nature of the model as well as due to errors in data ratios, partition coefficients and F values. In some respects the results shown in Table 18 are consistent. Four elements (Sc, V, Ga, and Sr) indicate virtually no trapped melt for any samples, while the other more incompatible elements suggest 7-9% trapped melt for the two intermediate lherzolites, ~10-15%

for 62213 and a slight amount for 62212, 62128 and 62127. The particular composition of the melt that may be trapped is difficult to accurately calculate. In fact it is not necessarily the same composition for each sample. A mixing model such as this may work to explain the data but to be confident about it one would like to see better agreement of the degree of trapped melt estimated for various elements for a given sample.

The possibility of trapped melt, especially to the degree suggested here is rather controversial. Physical models based on simple assumptions of physical interaction between a solid matrix and a melt phase suggest that extraction of melt should be near complete (e.g. McKenzie, 1984; McKenzie, 1985a; Ribe, 1985). Geological observations suggest that trapped melt to the degree suggested here is possible (Boudier and Nicolas, 1985; Nicolas, 1986). Also, preliminary work at the grain-to-grain scale concerning melt connection at grain intersections suggest that it may be energetically favorable for the rock-melt system to retain ~2-5% melt under certain conditions (B. Watson, personal communication). Neither these experiments nor the physical models account for complications likely to occur in any alpine-type peridotite, such as possible rapid upwelling due to relatively near surface tectonic processes and shearing produced by upwelling or the actual emplacement by thrust faulting. These complications may allow the rock to retain more melt in segregations. The presence of trapped melt and

the degree to which it may occur seems equivocal at this time.

Forward Melting Modelling and Other REE Geochemical Models

A useful exercise in modelling geochemical data is to forward model using equilibrium melting of a source composition and various modes and melting phase proportions to try and reproduce the data. For this type of modelling the source REE composition is known (in this case, sample 62210), and the degree of melting is considered to be known, based on major element estimates. What is not known, are the phase proportions of the source rock in mantle conditions, the phase proportions that are going into the melt, and exact partition coefficients between mantle phases and melt. Also, one knows the REE composition of the rocks that one is trying to match, but again the equilibrium mantle phase proportions are unknown. Estimations of modal mineralogy can be made using experimental data at high pressure and high temperature of coexisting pyroxenes. What this amounts to is a mantle norm calculation with a relatively large margin of error. Experiments to determine melting proportions at mantle conditions have also been performed and this data can be used. Ideally, one would use a variety of model parameters, changing variables such as source mode and find the best of a great many models. Fortunately it's already been established that equilibrium melting can't explain the LREE data so the goal here is not so much to best model the REE data but to see the effects of

equilibrium melting to the whole REE pattern and possibly to explain the HREE. Figures 84 to 86 are the results of some limited equilibrium melting in the garnet lherzolite stability field (Fig. 84), in the spinel stability field (Fig. 85), and in the plagioclase stability field (Fig. 86). Each figure has (a) and (b) parts showing the results of two sets of partition coefficients. Recent work has shown spinel to be a negligible phase in mantle melting due to very low partition coefficients as well as being a minor phase modally (Stosch, 1982; Prinzhofer and Allegre, 1985). Phase proportions of the source and the phase proportions entering the melt are given in the figure captions. The garnet lherzolite figure shows how poor the LREE are predicted but the HREE are matched quite well. The spinel lherzolite diagram does a better job of matching the data for low degrees of melting. At first glance it appears that the REE patterns might match well for the transitional lherzolites (62131, 62130) because they are parallel but the degrees of melting are far off. Plagioclase lherzolite melting is not very realistic for any of the features seen in the Horoman REE patterns. All three of these models are even worse when one considers the mismatch of residual modes and not just the REE patterns. A modelling program utilizing continuous melting (Langmuir et al, 1977) was also tried but produced very similar results.

An interesting melting model was developed by Prinzhofer and Allegre (1985) (abbreviated P and A

Figure 84. Chondrite-normalized REE (Boynton, 1984) diagram showing results of forward modelling of equilibrium melting in the garnet lherzolite field, using Horoman sample 62210 as a source composition, with original modal proportions of 60% olivine, 10% clinopyroxene, 20% orthopyroxene and 10% garnet. The melt composition in the calculation is controlled by 0.63 gar + 0.41 cpx + 0.09 opx = 0.13 oliv. + Melt (Mysen, 1979). Lines are shown for degrees of melting approximating values calculated for the Horoman rocks. a) Calculation using partition coefficients of Frey et al (1978), Table A-1, Set 3. b) Calculation using partition coefficients from Prinzhofer and Allegre (1985).

Figure 85. Similar to Fig. 84 but for equilibrium melting in the spinel lherzolite stability field. Original source mode for calculation is 60% olivine, 20% clinopyroxene and 20% orthopyroxene. Melt composition is controlled by 0.54 cpx + 0.54 opx = 0.08 oliv. + Melt (Mysen, 1979). a) and b) as in Fig. 84.

Figure 86. Similar to Fig. 84 but for equilibrium melting in the plagioclase lherzolite stability field. Original source mode for calculation is 60% olivine, 10% clinopyroxene, 20% orthopyroxene and 10% plagioclase. Modal composition of the liquid is 41% cpx, 50% opx and 9% plag. (Prinzhofer and Allegre, 1985). a) and b) as in Fig. 84.

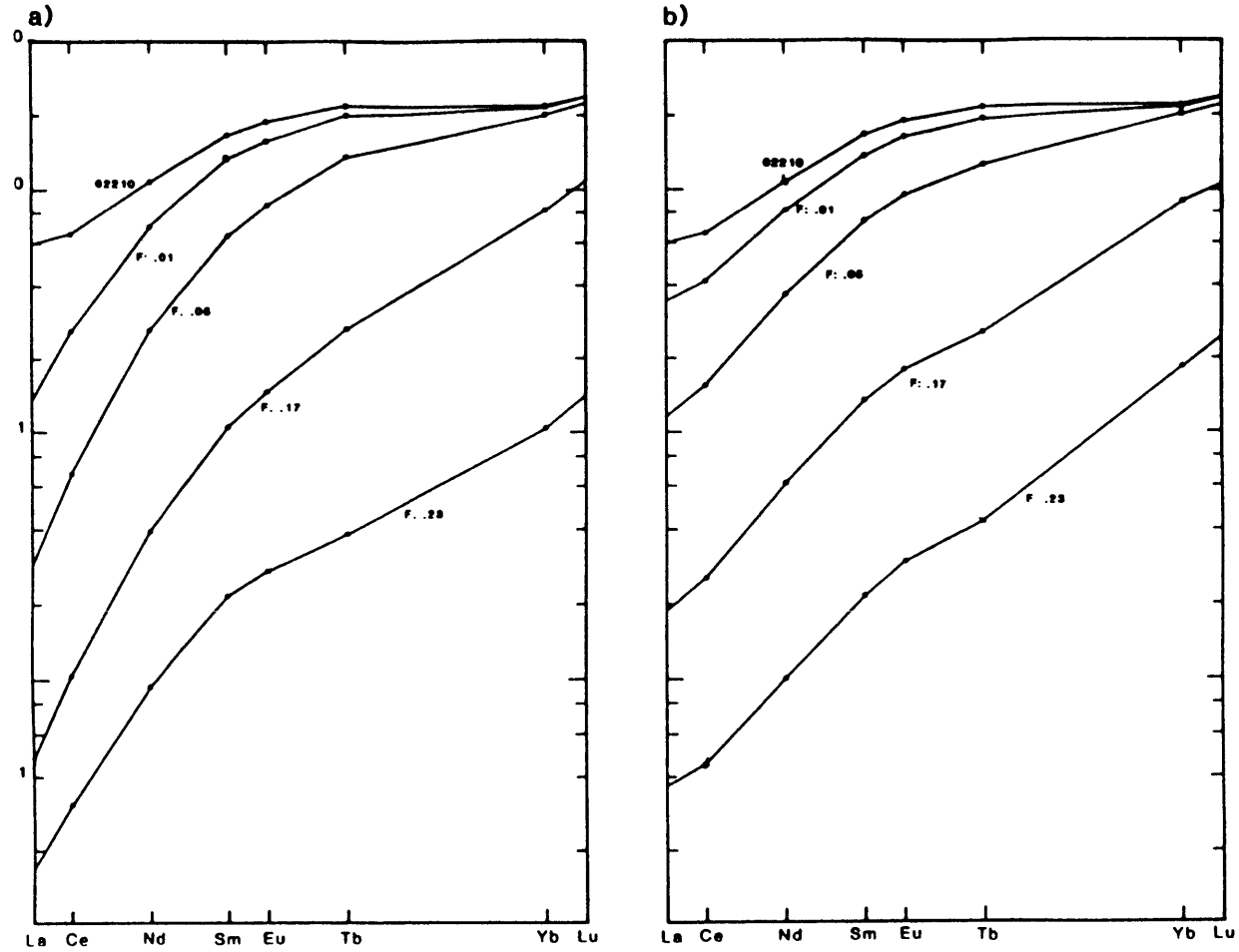

Figure 84

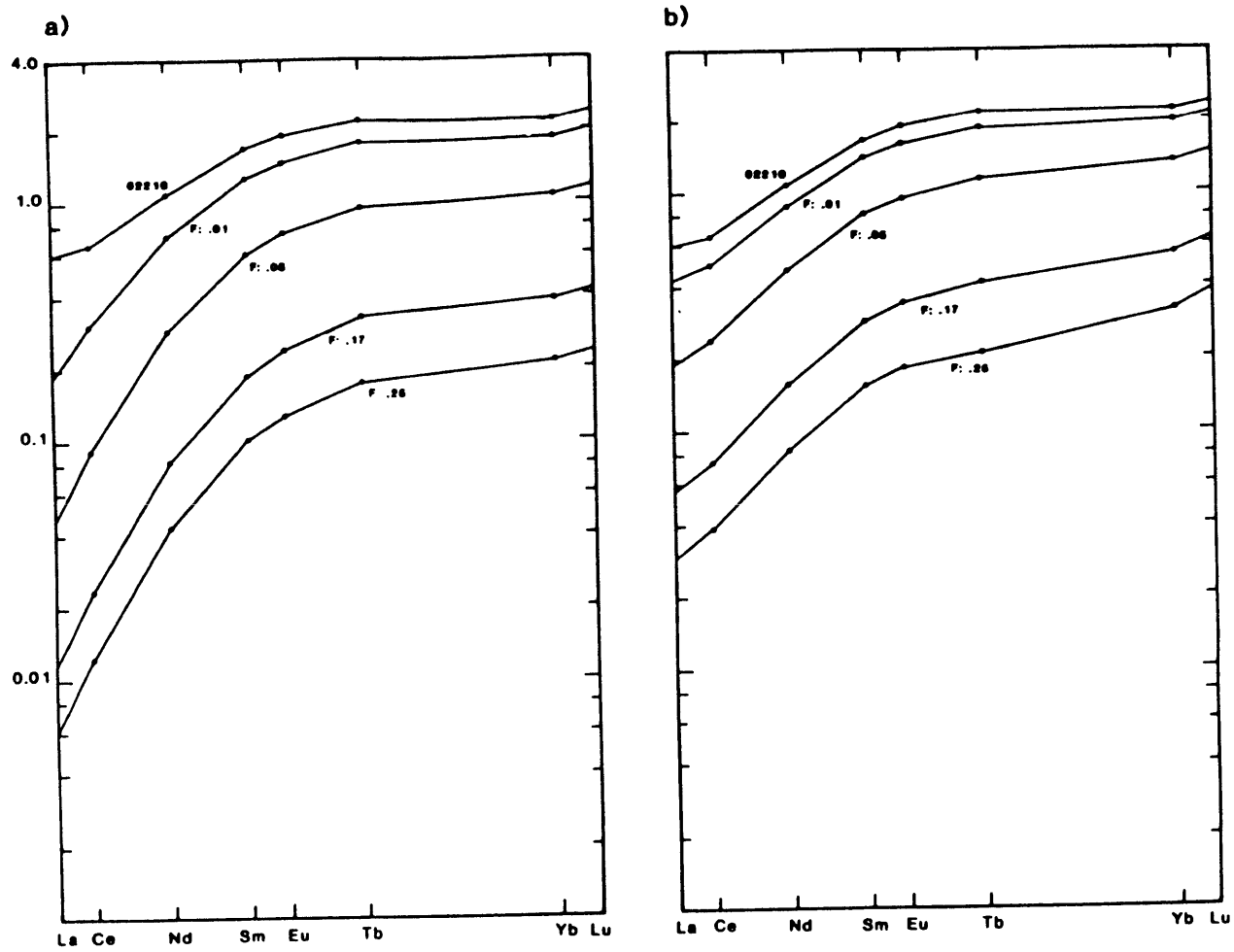

Figure 85

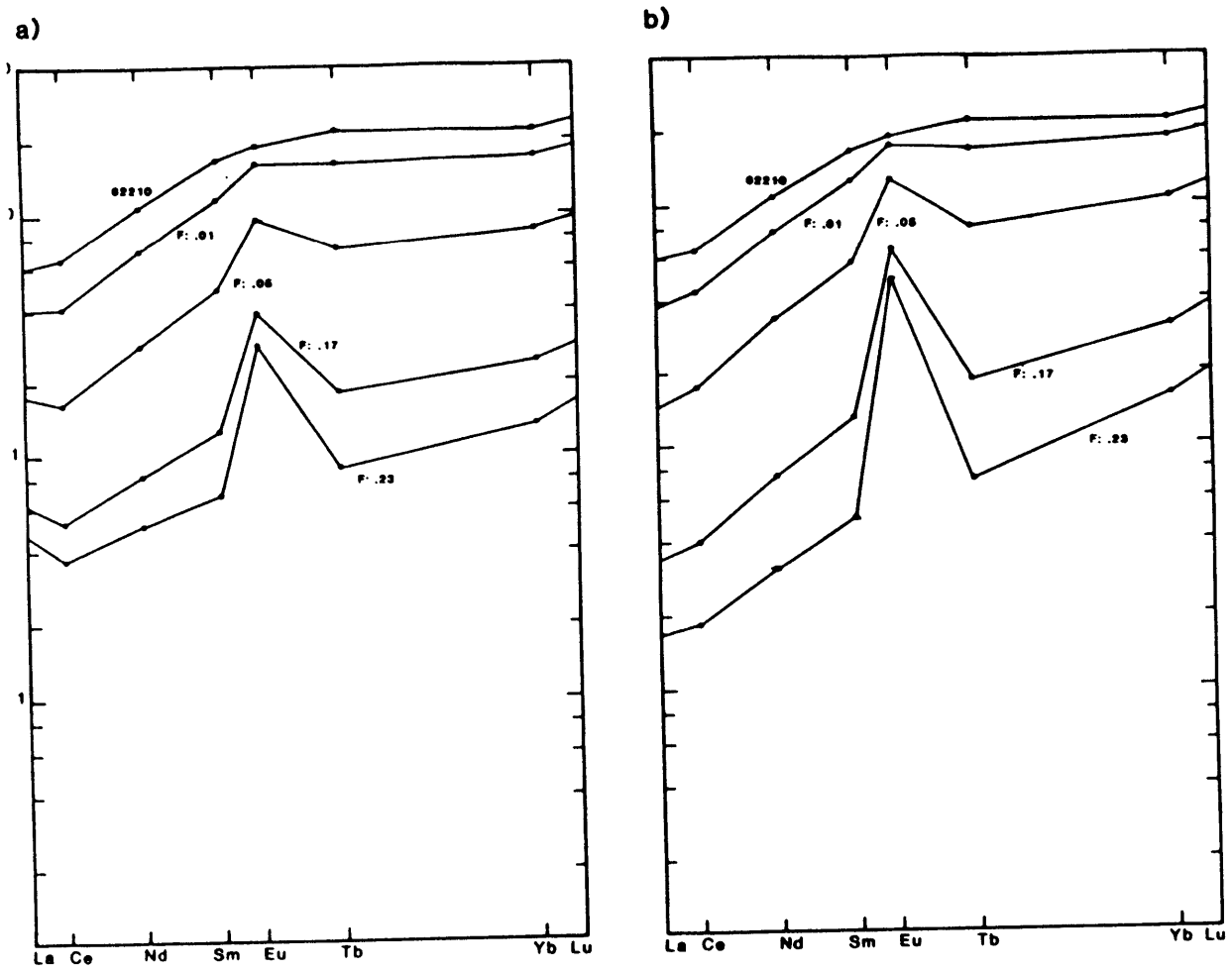

Figure 86

hereafter) to explain some U-shaped REE patterns in very depleted harzburgites and dunites that frequently have negative Eu anomalies from an ophiolite assemblage in New Caledonia. The model entails melting in disequilibrium as the mantle is rising through the three lherzolite facies. Thus, the LREE enrichment is produced by melting of garnet in the garnet lherzolite stability field and the negative Eu anomalies are produced by melting of plagioclase in the plagioclase facies without re-equilibration taking place between solid and melt. Facies changes from garnet to spinel to plagioclase are considered to occur very fast on a geological time scale and are modeled by simple reactions between end members of the mantle phases.

I experimented with the P and A model using 62210 as a source composition and an estimate of the mode in the garnet lherzolite facies where melting commences. This model has the usual problems of forward modelling alluded to previously. To evaluate the model properly a great number of iterations should be made varying the parameters necessary for the calculation. The number of parameters in the P and A model are multiplied by being able to vary F in any of the facies and by choice of reactions involved in changing mineralogy at facies boundaries. The rocks used by P and A were very depleted with no clinopyroxene, 0-8% orthopyroxene, and REE generally less than 0.01X chondrites for the LREE and less than 0.1X chondrites for the HREE. This is much more depleted than the Horoman rocks. P and A

also use a rather unorthodox set of olivine partition coefficients with a slight U-shape that allows them to match very depleted and U-shaped harzburgites and dunites. In my calculations using the P and A model I used their set of D's, varied F in all facies, used two set of values for melting proportions in the spinel facies, and used two reactions for the garnet to spinel transition. This last point is important for P and A use a reaction that is not only completely stoichiometrically incorrect but slightly irrelevant, as the reaction attempted only accounts for the grossular component, when in fact mantle garnets are known to be predominantly pyrope. This reaction (Eq. 14, P and A) was replaced by the following reaction based on analyses of Ronda garnets. 1 gt + 0.445 ol = 0.93 opx + 0.20 cpx + 0.297 sp (by weight). This reaction is based on a least squares regression of real garnet analyses and approximate pyroxene, olivine, and spinel analyses (accounting for solid solution) and as such does not balance perfectly. When used for the breakdown of garnet in the P and A model the final modes must be renormalized to one. Matching of samples 62128 and 62127 by this model was found to be impossible. Not only are these samples not nearly as depleted as the P and A samples but they have no negative Eu anomaly. U-shapes are actually very difficult to obtain with this model until essentially the residues from model melting are dunites, particularly with a LREE depleted source such as 62210. Plagioclase melting was tried using the P and A

model but abandoned due to lack of negative Eu anomalies in the Horoman rocks. The best model result out of many is shown in Figure 87. The REE patterns of samples 62131 and 62130 are fairly well matched within the errors of the calculation, by 5% melting in the garnet lherzolite stability field followed by 10% melting in the spinel lherzolite stability field (Near the 17% estimated from major elements). Source and resultant mode are given in the figure caption and may be similar to the sample modes at re-equilibrated surface conditions. The conclusion that the Horoman peridotites were produced by some partial melting in the garnet facies even though there is no garnet in the rocks is supported by petrographic observations by the Japanese (Obata and Nagahara, 1987) of a much greater sample set that suggests the Horoman massif was once in the garnet stability field but re-equilibrated into a plagioclase bearing assemblage. The P and A model may also better match sample 62212 at low degrees of melting than equilibrium batch melting. The P and A model clearly cannot explain sample 62213 with enriched LREE over the source and HREE not depleted as much as 5% garnet melting would predict, nor can it be used to explain the harzburgite samples.

The P and A model was proposed as an alternative to trapped melt or unspecified metasomatic processes and may work in certain instances, but at Horoman, even with more advanced melting mechanisms such as this, some sort of process secondary to melting seems to be required to explain

Figure 87. Best model result of fitting Horoman peridotite REE data using Sequential Disequilibrium Melting (Prinzhofer and Allegre, 1985). This specific model calculation involves melting a source composition of REE (62210, heavy solid line), with initial modal composition of 60% oliv., 20% opx, 10% cpx and 10% garnet, to varying degrees in the garnet lherzolite field (results, open triangles); followed by melting these resulting compositions to 5 or 10 percent melting in the spinel lherzolite field (open squares and open circles, respectively). Broken arrows connect source compositions to resulting composition for each step, with labels showing degree of melting and field where melting took place. Melt compositions consisted of 40% cpx + 10% opx + 65% garnet - 15% oliv. (Mysen, 1977) in the garnet lherzolite field and 54% cpx + 54% opx - 8% oliv. (Mysen, 1979) in the spinel lherzolite field. Reaction, used for transition from garnet lherzolite to spinel lherzolite, is the corrected version (see text). Partition coefficients used are from Prinzhofer and Allegre (1985). The residue produced by 5% melting in the garnet lherzolite field followed by 10% in the spinel field (middle open circles pattern) matches relatively well the REE patterns of Horoman samples 62130 and 62131. The calculated mode of this residue is 66% oliv., 26% opx, 5% cpx and 3% spinel or, in the plagioclase field, 71% oliv., 23% opx, 1.4% cpx and 4.6% plag.

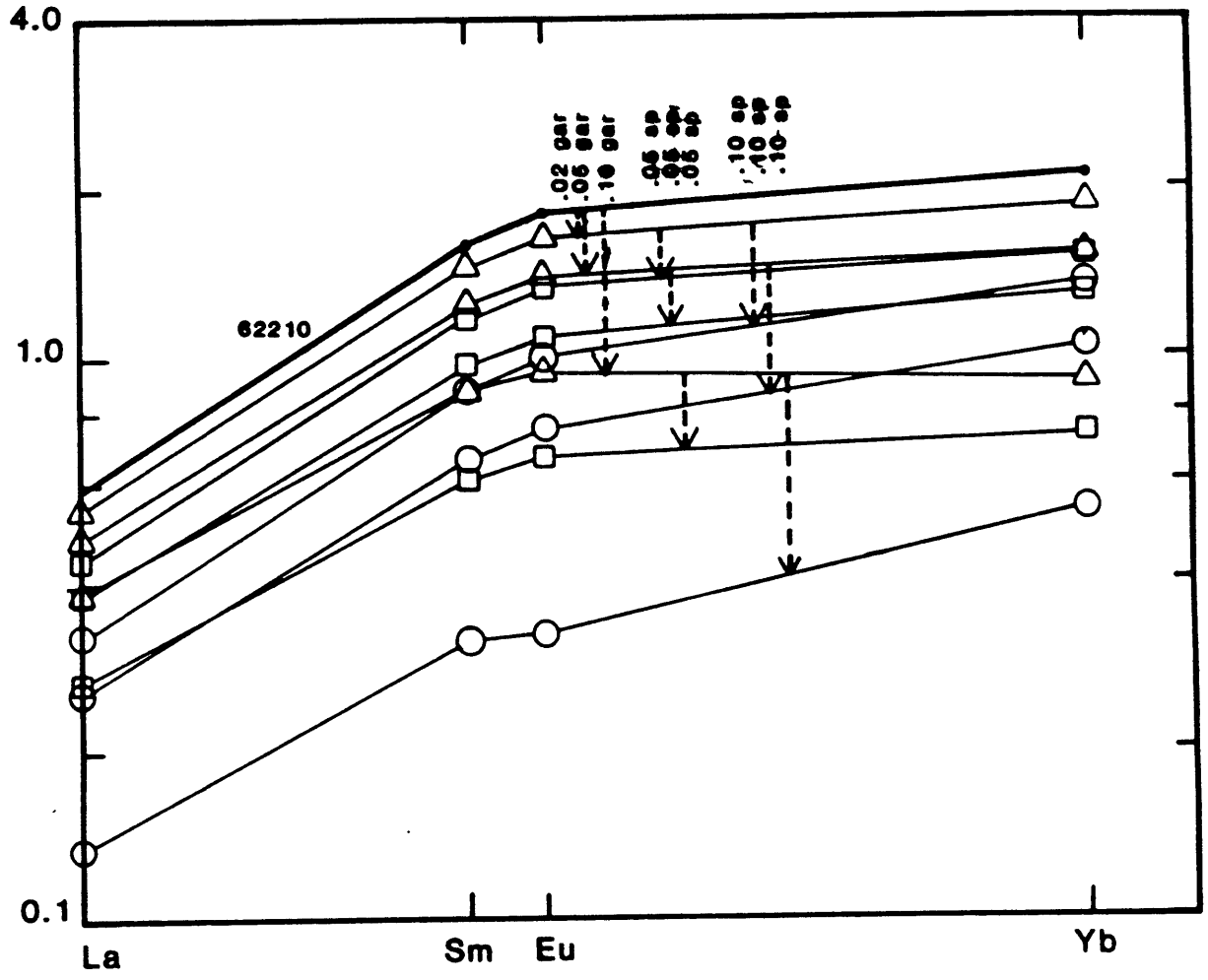

Figure 87

the data. The complex clinopyroxene REE data lends credence to this statement. Nevertheless, the P and A model seems more realistic, both physically and chemically than equilibrium batch melting. It has been known for some time that the most likely way for the mantle to melt to produce basalt is by decompressional melting during mantle upwelling. If melting is taking place during upwelling it is likely that melt would be produced at all depths and facies as suggested by the P and A model. The specifics of the upwelling rate and general tectonic history as well as the processes which segregate melt would determine the particular melting history of a peridotite body. This sort of argument is in line with models based on geologic observations of peridotites (see Nicolas, 1986; and the discussion in the plagioclase section). The P and A model is also based upon the premise that diffusion in the solid residual matrix is slow enough that it cannot continually re-equilibrate with the melt. This is similar to saying that the melting and extraction processes are rapid relative to re-equilibration as supported by physical models (e.g. McKenzie, 1984 and McKenzie, 1985b). Chemical support comes from work on ^{230}Th-^{238}U disequilibrium (McKenzie, 1985b) and the more reasonable forward modelling results using disequilibrium melting than with equilibrium melting. Some re-equilibration surely must occur and the important factor to consider for this is the relative rates of melting and extraction of melt. The relative rates of these processes

and the potential chemical effects produced by the melting process itself and possible related "metasomatic" mechanisms are important to the genesis of peridotites.

U-shaped REE patterns in peridotites can be theoretically produced by ion-exchange processes if a melt is not in equilibrium with the surrounding solid matrix (Navon and Stolper, 1987). This result comes from modelling melt, percolating upwards through the mantle, in terms of ion-exchange interactions, similar to those operating in a laboratory chromatographic column. The result is similar to mixing of enriched metasomatic fluid with a depleted peridotite matrix but with more realistic spatial and chemical considerations. A process such as that envisioned by Navon and Stolper (1987) may have produced some of the features of the Horoman peridotite. The ion-exchange process may be distinguishable from simple mixing in some cases (Navon and Stolper, 1987) but cannot be in the Horoman samples.

Physical Models

The physics involved in melting of mantle rocks, melt migration and its segregation has become much better understood in recent years (e.g. Turcotte and Ahern, 1978; Maaloe, 1981; Maaloe and Scheie, 1982; McKenzie, 1984; McKenzie, 1985a; Richter and McKenzie, 1984; Scott and Stevenson, 1984; Scott and Stevenson, 1986; Ribe, 1985). The greater extent of this work has developed from the principles of two-phase flow, which have been developed in

the study of fluid mechanics. Physical models of this type also owe a lot to material science which has long been concerned with the geometry and interconnectness of melt in a solid matrix. It is now known that the first melt in mantle rocks occurs at grain corners and edges, and that the melt is interconnected (Waff and Bulau, 1979). Segregation of melt, within this framework, involves very complex physical processes that can be described mathematically in idealized situations (McKenzie, 1984; Scott and Stevenson, 1984) but are still difficult to apply to geological problems.

From the geological perspective, two major results have come of this work. The first is that basaltic melt fractions greater than about two percent (and less, if the melt is volatile rich) are mobile and will separate from solid mantle material (McKenzie, 1987). This discovery is particularily important to geochemists studying highly incompatible elements, the behavior of which is dominated by the movements of low-degree melts. The second exciting result from the physical models is the possible existence of solitary waves of melt, propagating upwards, in higher porosity material (i.e. with a greater degree of melt) (Richter and McKenzie, 1984; Scott and Stevenson, 1984; Scott and Stevenson, 1986) and compaction fronts of solid matrix (McKenzie, 1987). McKenzie (1987) in a short review article questions, "whether the existence of solitary waves in two or three dimensions withe melting and compacting

regions have direct observational consequences". Obata and Nagahara (1987), however, believe, based on the layered structure and wavy major element charateristics of the massif, that the Horoman peridotite is in fact the product of these type of processes. In this scenario, the plagioclase lherzolite represents a region where melt has accumulated, while the depleted harzburgites represents a zone of compacted residual mantle. Processes of melting, melt segregation and matrix compaction within a dynamical framework of an ascending portion of upper mantle could then produce a layered structure with a wavy chemistry that is "frozen" in a body like the Horoman peridotite (Obata and Nagahara, 1987). Although this scheme is speculative, it does fit the gross physical and chemical observations.

The useful geochemical results of models based on the physical principles of melting and melt migration are still quite rudimentary (Ribe, 1985; Richter, 1986; Navon and Stolper, 1987) but it is this type of modelling which must be done to test the hypothesis of Obata and Nagahara (1987) for the Horoman peridotite. The data from this thesis, on the trace elements of the Horoman massif, suggests that complex and, at present, not well understood processes are involved in the formation of the Horoman peridotite. Whether these processes will be explained by the further results of melting and melt migration, and whether the

Horoman peridotite can be understood as the frozen result of processes originating only in the mantle, remains to be seen.

Conclusions

The Horoman peridotite, an alpine peridotite in southern Hokkaido, provides an excellent location to explore the genesis of basaltic melt. Because the upper mantle melting processes are inaccessible to in situ observation, we contribute to the understanding of these processes by study of rocks in which the relevant processes may be frozen.

The geology of the region suggests that the ultramafic massif was emplaced as a sheet (~3 km thick) in a province of complex tectonic interactions, during the latest Miocene to early Pliocene, along a deep-seated thrust zone which was probably produced by arc collision to the east. At Horoman well developed layering exists. This layering is seen in the field on several scales, and includes modal variation, as well as chemical variation, of the bulk rocks and the minerals for major and trace elements. Some of the layering sequences are repeated, producing chemical variations that have wavy and oscillatory patterns. This study examines in detail a portion of one of the largest of these waves across a section of layers believed to represent actual upper mantle stratigraphy of ~300 m in thickness. Although the rocks at Horoman have been metamorphosed and recrystallized

to some degree, the gross layering and compositional variation represents igneous features produced by the processes of partial melting and melt segregation. Furthermore, I have shown that the Horoman layered rocks are residual products and not cumulates. Layering, such as that seen at Horoman, is not an uncommon feature in alpine peridotites and may in fact be pervasive. It can easily be overlooked by investigators or, more likely obscured by structural and metamorphic processes.

The lower portion of Horoman consists of thick gradational layers of peridotite. This work is a detailed description of the geochemistry of a section of the lower portion (Fig. 7). The suite of rocks is made up of two harzburgites on the top of the section with 2 to 3 percent clinopyroxene; two transitional peridotites in the middle portion with 4 and 6.5 percent clinopyroxene and about 4 percent plagioclase; and three plagioclase bearing lherzolites at the bottom with 8 to 10 percent clinopyroxene and 8 to 10 percent plagioclase (complete modes, Table 1). All of the samples have less than one percent spinel but are believed to be originally from spinel-bearing depths in the mantle, not plagioclase bearing depths.

Whole rock major element analyses show an excellent correlation with MgO, and the trends and spread of the data coincide very well with a larger data set sampled from a much larger area from the Ronda peridotite in southern Spain. These trends are thought to be produced by various

degrees of partial melting with a homogeneous, or near homogeneous, melt composition. The degree of melting was determined using the Mg and Fe bulk rock abundance, Fo content in olivine, and some simple assumptions of K_D using one of the samples as a source composition. (This sample has a composition very similar to estimates of "primitive" upper mantle.) Using this method, the samples were determined to have been produced by one to 25 percent melting which was also supported by degree of melting calculations using Ni. Other compatible and moderately incompatible elements concur with this simple petrogenesis, also showing well correlated linear variation trends with MgO.

Mineral compositions also vary (generally in the same fashion as the bulk samples) in agreement with interpretation by various degrees of partial melting. The mineral chemistry is complicated, however, by the effects of sub-solidus reequilibration and recrystallization.

However, incompatible trace element variation, particularly Y, Ti, Zr and the LREE, cannot be explained by the simple hypothesis of varying degrees of partial melting for a number of reasons. Samples that are believed to have melted the largest degrees (by the calculations above) are still the most depleted in the incompatible elements, but not nearly to the extent that one would expect. Like the major and compatible elements, the incompatible elements have a linear correlation with MgO, although significant

curvature would be expected with partial melting. Furthermore, REE patterns show a "decoupling" from major and other less incompatible trace elements which simple melting models cannot produce. The REE patterns are quite similar to those from other alpine peridotites: slightly LREE depleted for the most enriched lherzolites; generally sub-parallel but more depleted for the less enriched transitional peridotites; and flat to U-shaped for the harzburgites. Standard equilibrium partial melting to the degrees suggested by major elements and compatible elements would produce REE patterns drastically more LREE depleted and would certainly not produce U-shapes as for the harzburgites. In fact the Horoman REE actually have greater variation in the HREE than in the LREE. The HREE variation can be explained by melting better than the LREE, but still show the effect, to a lesser degree, of whatever processes are affecting the LREE and other highly incompatible elements.

An ion probe study of REE and other trace elements was carried out for clinopyroxenes from the Horoman samples. The clinopyroxene REE patterns generally mimic the bulk rock patterns, including greater variability in the HREE than in the LREE, and the most enriched clinopyroxene patterns belong to the most enriched bulk samples. This work on clinopyroxene trace elements strongly suggests that whatever process that is affecting the highly incompatible elements is doing so through the clinopyroxenes, and not through

grain boundary material or trace element enriched phases as is often suggested in the literature. Since, to my knowledge, this is the first time that clinopyroxenes from an alpine peridotite have been analysed for these trace elements, it is difficult to generalize, but it seems likely that the processes suggested by the Horoman data are widespread in the upper mantle. This generalization is corroborated by similarities of the entire data set from Horoman to other alpine peridotites and in particular to the Ronda peridotite (Frey et al, 1985).

Chemical relations between clinopyroxene trace elements and between the trace elements and major elements in clinopyroxene are very complex as sub-solidus reequilibration reactions and repartitioning obscure the underlying igneous processes governing the variation as a whole. The complex relations seen in the detailed mineral chemistry observations also raise questions about the scales upon which various processes act. Although not entirely understood, these complexities may be important when considering the entire scenario, between when a melt is first produced in the mantle to when it is extracted as magma at the surface.

Standard forward modelling of equilibrium melting fails to produce the REE patterns of the Horoman samples. A melting model, coined "sequential integrated disequilibrium" (Prinzhofer and Allegre, 1985), also cannot explain the REE patterns although it does appear to reproduce the data

somewhat and may in fact describe some of the geochemical effects of the melting processes. An unspecified mantle metasomatic process, by infiltration of an enriched melt or other fluid, or the similar process of interaction between percolating low degree melts and the surrounding residue, cannot be ruled out, but are not quantitatively developed.

A mass balance model involving the presence of trapped melt within the peridotites was used to try and explain the incongruities between the major and compatible trace elements and the more highly incompatible trace elements. The model makes intuitive sense. The presence of a minor amount of melt could have a drastic effect on the elements that are enriched in the melt, i.e. the highly incompatible elements, while having a relatively smaller effect on the major and compatible elements. Furthermore, the samples that seem to require greater degrees of trapped melt contain greater modal amounts of plagioclase and clinopyroxene which are phases that may be produced by trapped melt or from the interaction of melt with the residue. This model reconciliates the apparent difference between the two sets of elements, but is by no means unique or well constrained. It suggests, however, that, with the most enriched sample as a source composition, the geochemistry of the samples can be explained by a slight amount of trapped melt in the harzburgites, six to ten percent in the transitional peridotites, ten to fifteen percent for one of the enriched

plagioclase lherzolites but only several percent for the least melted sample (Table 18).

A model requiring varying degrees of trapped melt in each sample that is only required by the incompatible elements and furthermore must repeat itself to some degree, (to produce the "waves" observed at Horoman) may appear to be a bit *ad hoc*. Yet actual physical processes producing variable degrees of trapped melt (which can be thought of as varying the rates of melt production, segregation and extraction) are not known and current theory suggests that melt extraction should be rapid relative to other rates in the mantle (e.g. McKenzie, 1984). Layered structure observed in many alpine peridotites may be produced by the very unusual turn of events which brought mantle material to the surface in the first place and is not necessarily a pervasive mantle feature. In other words, due to complex processes connected with rapid upwelling of mantle material and tectonic processes emplacing the massifs, affecting the afore mentioned rates, trapped melt may be an important feature manifested as frozen in layered structure in alpine peridotites. Other specific evidence (such as the textural observations of plagioclase in the Horoman and other alpine peridotites, the ubiquitous spinel occurrence and observations of its texture, the lack of any negative Eu anomaly in clinopyroxene, and other complex behavior in elements expected to partition between clinopyroxene and plagioclase, such as Sr) suggests that it is unlikely that

plagioclase is an indigenous primary upper mantle phase in these rocks, but that it may be related to the presence of trapped melt.

Study of the petrogenesis of ultramafic rocks believed to be produced largely by partial melting in the upper mantle, and associated complexities, should be fruitful in investigating the physics and chemical interactions in the processes in the mantle. Theoretical models of melting in the mantle are at present too simplistic to describe all of the physical processes acting in the mantle, but may in time be useful in studying real rocks. Models of melt generation using basaltic geochemistry, on the other hand, overlook certain smaller scale complexities of melting and segregation due to the "smoothing" nature of the basaltic data from a myriad of processes. Furthermore, at present, these two different approaches to understanding melting and melt segregation processes are poorly integrated. Perhaps quantitative descriptive studies such as in this thesis may help to bridge the gap.

REFERENCES

Albee, A.L. and L. Ray, 1970, Correction factors for electron probe microanalysis of silicates, oxides, carbonates, phosphates and sulfates, Anal. Chem., 42, 1408-1414.

Bence, A.E. and A.L. Albee, 1968, Empirical correction factors for the electron microanalysis of silicates and oxides, J. Geol., 76, 382-403.

Bertrand, P. and J.C. Mercier, 1985, The mutual solubility of coexisting orthopyroxene and clinopyroxene: toward an absolute geothermometer for the natural system?, Earth Planet. Sci. Lett., 76, 109-122.

Bonatti, E., G. Ottonello and P.R. Hamlyn, 1986, Peridotites from the Island of Zabargrad (St. John), Red Sea: petrology and geochemistry, J. Geophys. Res., 91, 599-631.

Boudier, F., 1978, Structure and petrology of the Lanzo peridotite massif (Piedmont Alps), Geol. Soc. Amer. Bull., 89, 1574-1591.

Boudier, F. and A. Nicolas, 1977, Structural controls on partial melting in the Lanzo peridotites, in Magma Genesis, Oregon Dept. Geol. Miner. Ind., 96, ed. H.J.B. Dick, 63-78.

Boudier, F. and A. Nicolas, 1985, Harzburgite and lherzolite subtypes in ophiolitic and oceanic environments, Earth Planet. Sci. Lett., 76, 84-92.

Boynton, W.V., 1984, Cosmochemistry of the rare earth elements: meteorite studies, in Rare Earth Element Geochemistry, ed. P Henderson, Elsevier, Amsterdam, 155-203.

Burns, R.G., 1973, The partitioning of trace transition elements in crystal structures: a provocative review with applications to mantle geochemistry, Geochim. Cosmochim. Acta, 37, 2395-2403.

Cadet, J.P., and J. Charvet, 1983 From subduction to paleosubductions in N. Japan, in Accretion Tectonics in the Circum-Pacific Regions, ed. M. Hashimoto and S. Uyeda, TERRAPUB, Tokyo, 135-148.

Campbell, I.H., 1977, A study of macro-rhythmic layering and cumulate processes in the Jimberlana Intrusion, Western Australia Part 1: the Upper layered series, J. Petrol., 18, 183-215.

Carswell, D.A., 1968, Picritic magma-residual dunite relationships in garnet peridotite at Kalskaret near Tafjord, South Norway, Contrib. Mineral. Petrol., 19, 97-124.

Clague, D.A. and F.A. Frey, 1982, Petrology and trace element geochemistry of the Honolulu Volcanic Series, Oahu: implications for the oceanic mantle beneath Hawaii, J. Petrol., 23, 447-504.

Coleman R.G. and T.E. Keith, 1971, A chemical study of serpentinization--Burro Mountain, California, J. Petrol., 2, 311-328.

Comin-Chiaramonti, P., G. Demarchi, V.A.V. Girardi, F. Princivalle and S. Sinigoi, 1986, Evidence of mantle metasomatism and heterogeneity from peridotite inclusions of northeastern Brazil and Paraguay, Earth Planet. Sci. Lett., 77, 203-217.

Conquere, F. and J. Fabries, 1984, Chemical disequilibrium and its thermal significance in spinel peridotite from the Lherz and Freychinede ultramafic bodies (Ariege, French Pyrenees), in Kimberlites II: The Mantle and Crust-Mantle Relationships, ed. J. Kornprobst, Elsevier, Amsterdam, 319-331.

Dick, H.J.B., 1977, Partial melting in the Josephine Peridotite I, the effect on mineral composition and its consequence for geobarometry and geothermometry, Amer. J. Sci., 277, 801-832.

Dick, H.J.B. and T. Bullen, Chromian spinel as a petrogenetic indicator in abyssal and alpine-type peridotites and spatially associated lavas, Contrib. Mineral. Petrol., 86, 54-76.

Dick, H.J.B. and R.L. Fisher, 1984, Mineralogic studies of the residues of mantle melting: abyssal and alpine-type peridotites, in Kimberlites II: The Mantle and Crust-Mantle Relationships, ed J. Kornprobst, Elsevier, Amsterdam, 295-308.

Dick, H.J.B., R.L. Fisher and W.B. Bryan, 1984, Mineralogic variability of the uppermost mantle along mid-ocean ridges, Earth Planet. Sci. Lett., 69, 88-106.

Dickey, J.S., 1970, Partial fusion products in alpine-type peridotites: Serrania de la Ronda and other examples, Mineral. Soc. Amer. Spec. Pap., 3, 33-49.

Dickey, J.S., H.S. Yoder and J.F. Schairer, 1971, Chromium in silicate-oxide systems, Carnegie Inst. Wash. Yearb., 70, 118-122.

Dickinson, W.R., 1978, Plate tectonic evolution of North Pacific rim, J. of the Physics of the Earth, 21, supplement S1-S9.

Drake, M.J. and D.F. Weill, 1975, Partitioning of Sr, Ba, Y, Eu^{2+}, Eu^{3+} and other rare earth elements between plagioclase feldspar and magmatic liquid: an experimental study, Geochim. Cosmochim. Acta, 39, 689-712.

Dunham, A.C. and W.J. Wadsworth, 1978, Cryptic variation in the Rhum layered intrusion, Mineralogic Mag., 42, 347-356.

Ernst, W.G., 1978, Petrochemical study of lherzolitic rocks from the Western Alps, J. Petrol., 19, 341-392.

Ernst, W.G. and G.B. Piccardo, 1979, Petrogenesis of some Ligurian peridotites--I. Mineral and bulk-rock chemistry, Geochim. Cosmochim. Acta, 43, 219-237.

Fleet, M.E., N.D. MacRae and C.T. Herzberg, 1977, Partition of nickel between olivine and sulfide: A test for immiscible sulfide liquids, Contrib. Mineral. Petrol., 65, 191-197.

Ford, C.E., D.G. Russell, J.A. Craven and M.R. Fisk, 1983, Olivine-liquid equilibria: Temperature, pressure and composition dependence of the crystal/liquid cation partition coefficients for Mg, Fe^{2+}, Ca and Mn, J. Petrol., 24, 256-265.

Frey, F.A., 1980, The origin of pyroxenites and garnet pyroxenites from Salt Lake Crater, Oahu, Hawaii: Trace element evidence, Amer. J. Sci., 280-A, 427-449.

Frey, F.A., 1983, Rare earth element abundances in upper mantle rocks, Rare Earth Element Geochemistry. Developments in Geochemistry, 2, ed P. Henderson, Elsevier, Amsterdam, 153-203.

Frey, F.A. and D.H. Green, 1974, The mineralogy, geochemistry and origin of lherzolite inclusions in Victorian basanites, Geochim. Cosmochim. Acta, 38, 1023-1059.

Frey, F.A. and M. Prinz, 1978, Ultramafic inclusions from San Carlos, Arizona: petrologic and geochemical data bearing on their petrogenesis, Earth Planet. Sci. Lett., 38, 129-176.

Frey, F.A., D.H, Green and S.D. Roy, 1978, Integrated models of basalt petrogenesis: A study of quartz tholeiites to olivine melilitites from South Eastern Australia utilizing geochemical and experimental petrological data, J. Petrol, 19, 463-513.

Frey, F.A., C.J. Suen, H.W. Stockman, 1985, The Ronda high temperature peridotite: geochemistry and petrogenesis, Geochim. Cosmochim. Acta, 49, 2469-2491.

Garuti, G., C. Corgoni and G.P. Sighinolfi, 1984, Sulfide mineralogy and chalcophile and siderophile element abundances in the Ivrea-Verbano mantle peridotite (Western Italian Alps), Earth Planet. Sci. Lett., 70, 69-87.

Goodman, R.J., 1972, The distribution of Ga and Rb in coexisting ground mass and phenocryst phases of some basic volcanic rocks, Geochim. Cosmochim. Acta, 36, 303-317.

Green, D.H., 1964, The petrogenesis of the high-temperature peridotite intrusion in the Lizard area, Cornwall, J. Petrol., 5, 134-188.

Grover, J.E., D.H. Lindsley, and A.E. Bence, 1980, Experimental phase relations of olivine vitrophyres from breccia 14321: the temperature- and pressure-dependence of Fe-Mg partitioning for olivine and liquid in a highlands melt-rock Proc. Lunar Planet. Sci. Conf. 11th, 179-196.

Hamlyn, P.R. and E. Bonatti, 1980, Petrology of mantle-derived ultramafics from the Owen Fracture Zone, Northwest Indian Ocean: Implications for the nature of the oceanic upper mantle, Earth Planet. Sci. Lett., 48, 65-79.

Hanson, G.N. and C.H. Langmuir, 1978, Modelling of major elements in mantle-melt systems using trace element approaches, Geochim. Cosmochim. Acta, 42, 725-741.

Hart, S.R. and K.E. Davis, 1978, Nickel partitioning between olivine and silicate melt, Earth Planet. Sci. Lett., 40, 203-219.

Hashimoto, S., 1975, The basic plutonic rocks of the Hidaka Metamorphic Belt, Hokkaido, Part I, J. Faculty Sci., Hokkaido Univ., 16, 367-420.

Haughton, D.R., P.L. Roeder and B.J. Skinner, 1974, Solubility of sulfur in mafic magmas, Econ. Geol., 69, 451-467.

Hickey, R. and F.A Frey, 1981, Rare-earth element geochemistry of Mariana fore-arc volcanics: Deep-Sea Drilling Project Site 458 and Hole 459b, in Initial Reports of the Deep-Sea Drilling Project, Vol. 60, eds. D.M. Hussong and S. Uyeda, et al, U.S. Government Printing Office, 735-741.

Himmelberg, G.R. and R.A. Loney, 1980, Petrology of ultramafic and gabbroic rocks of the Canyon Mountain Ophiolite, Oregon, Amer. J. Sci., 280-A, 232-268.

Irvine, T.N., 1974, Petrology of the Duke Island ultramafic complex, Southeastern Alaska, Geol. Soc. Amer. Mem., 138, 240 pp.

Irvine, T.N., 1975, Crystallization sequences in the Muskox intrusion and other layered intrusions--II. Origin of Chromite layers and similar deposits of other magmatic arcs, Geochim. Cosmochim. Acta, 39, 991-1020.

Irvine, T.N., 1982, Terminology for layered intrusions, J. Petrol., 23, 127-162.

Jackson, E.D., 1961, Primary textures and mineral associations in the ultramafic zones of the Stillwater Complex, Montana, U.S. Geol. Survey Prof. Paper, 358, 106 pp.

Jackson, M.D. and M. Ohnenstetter, 1981, Peridotitic and gabbroic structures in the Monte Maggiore massif, Alpine Corsica, J. of Geol., 81, 703-719.

Jacobsen, S.B., J.E. Quick and G.J. Wasserburg, 1984, A Nd and Sr isotopic study of the Trinity peridotite; implications for mantle evolution, Earth Planet. Sci. Lett., 68, 361-378.

Jagoutz, E., H. Palme, H. Baddenhausen, K. Blum, M. Cendales, G. Dreibus, B. Spettel, V. Lorenz and H. Wanke, 1979, The abundance of major, minor and trace elements in the earth's mantle as derived from primitive ultramafic nodules, Proc. Lunar Planet. Sci. Conf. 10th, Geochim. Cosmochim. Acta, Supplement II, 2, 2031-2050.

Jaques, E.L. and D.H. Green, 1980, Anhydrous melting of peridotite at 0-15 Kb pressure and the genesis of tholeiitic basalts, Contrib. Mineral. Petrol., 73, 287-310.

Kiminami, K. and Y. Kontani, 1983, Mesozoic arc-trench systems in Hokkaido, Japan, in Accretion Tectonics in the Circum-Pacific Regions, ed. M. Hashimoto and S. Uyeda, TERRAPUB, Tokyo, 107-122.

Kimura, G., S. Miyashita and N. Miyasaka, 1983 Collision tectonics in Hokkaido and Sakhalin, in Accretion Tectonics in the Circum-Pacific Regions, ed M. Hashimoto and S. Uyeda, TERRAPUB, Tokyo, 123-134.

Komatsu, M., 1975, Recrystallization of the high alumina pyroxene peridotite of the Uenzaru area in the Hidaka province, Hokkaido, Japan, J. Geol. Soc. Japan, 81, 11-28.

Komatsu, M., S. Miyashita, J. Maeda, Y. Osanai and T. Toyoshima, 1983, Disclosing of a deepest section of continental-type crust upthrust as the final event of collision of arcs in Hokkaido, North Japan, in Accretion Tectonics in the Circum-Pacific Regions, ed. M. Hashimoto and S. Uyeda, TERRAPUB, Tokyo, 149-165.

Komor, S.C.,D. Elthon and J.F. Casey, 1985, Serpentinization of cumulate ultramafic rocks from the North Arm Mountain massif of the Bay of Islands ophiolite, Geochim. Cosmochim. Acta, 49, 2331-2338.

Kurat, G., H. Palme, B. Spettel, H. Baddenhausen, H. Hofmeister, C. Palme and H. Wanke, 1980, Geochemistry of ultramafic xenoliths from Kapfenstein, Austria: evidence for a variety of upper mantle processes, Geochim. Cosmochim. Acta, 44, 45-60.

Langmuir, C.H., J.F. Bender, A.E. Bence, G.N. Hanson and S.R. Taylor, 1977, Petrogenesis of basalts from the FAMOUS-area: mid-Atlantic ridge, Earth Planet. Sci. Lett., 36, 133-156.

Lightfoot, P.C. and A.J. Naldrett, 1984, Chemical variation in the Inziswa Complex, Transkei, and the nature of the parent magma, Can. Mineral., 22, 111-123.

Lorand, J.P., 1986, Cu-Fe-Ni-S mineralogic assemblages in upper mantle peridotites from the Table Mountain and Blow-Me-Down Mountain ophiolite massifs (Bay of Island area, Newfoundland): Their relationships with fluids and silicate melts, Lithos, 20, 59-76.

Loubet, M. and C.J. Allegre, 1979, Trace element studies in the Alpine type peridotite of Beni-Bouchera (Morocco), Geochem. J., 13, 69-75.

Loubet, M. and C.J. Allegre, 1982, Trace elements in orogenic lherzolites reveal the complex history of the upper mantle, Nature, 298, 809-814.

Maaloe, S., 1981, Magma accumulation in the ascending mantle, J. Geol. Soc. London, 138, 223-236.

Maaloe, S. and K. Aoki, 1977, The major element composition of the upper mantle estimated from the composition of lherzolites, Contrib. Mineral. Petrol., 63, 161-173.

Maaloe, S. and A. Scheie, 1982, The permeability controlled accumulation of primary magma, Contrib. Mineral. Petrol., 81, 350-357.

McKenzie, D., 1984, The generation and compaction of partially molten rock, J. Petrol., 25, 713-765.

McKenzie, D., 1985a, The extraction of magma from the crust and mantle, Earth Planet. Sci. Lett., 74, 81-91.

McKenzie, D., 1985b, ^{230}Th-^{238}U disequilibrium and the melting processes beneath ridge axes, Earth Planet. Sci. Lett., 72, 149-157.

McKenzie, D., 1987, The compaction of igneous and sedimentary rocks, J. of the Geol. Soc. of London, 144, 299-307.

Menzies, M., 1973, Mineralogy and partial melt textures within an ultramafic body, Greece, Contrib. Mineral. Petrol., 42, 273-285.

Menzies, M., 1976, Rare earth geochemistry of fused ophiolitic and alpine lherzolites, I. Othris, Lanzo, and Troodos, Geochim. Cosmochim. Acta, 40, 645-656.

Menzies, M. and C. Allen, 1974, Plagioclase Lherzolite-residual mantle relationships within two eastern Mediterranean ophiolites, Contrib. Mineral. Petrol., 45, 197-213.

Miyashiro, A., 1977, Subduction zone ophiolites and island-arc ophiolites, in Energetics in Geological Processes, ed S.K. Saxena and Bha Hacharji, Springer-Verlag, New York, 188-213.

Mori, T. and D.H. Green, 1975, Pyroxenes in the system $Mg_2Si_2O_6$-$CaMgSi_2O_6$ at high pressure, Earth Planet. Sci. Lett., 26, 277-286.

Mysen, B.O., 1977, Partitioning of nickel between pargasite, garnet peridotite minerals and liquid at high pressure and temperature, Carnegie Inst. Washington Yearb., 76, p.557.

Mysen, B.O., 1979, Trace-element partitioning between garnet peridotite minerals and water-rich vapor: experimental data from 5 to 30 Kbar, Amer. Mineral., 64, 274-287.

Mysen, B.O. and I. Kushiro, 1977, Compositional variation of coexisting phases with degree of melting of peridotite in the upper mantle, Amer. Mineral., 62, 843-865.

Nagasawa, H., H. Wakita, H. Higuchi and N. Onuma, 1969, Rare earths in peridotite nodules: an explanation of the genetic relationship between basalt and peridotite nodules, Earth Planet. Sci. Lett., 5, 377-381.

Navon, O. amd E. Stolper, 1987, Geochemical consequences of melt percolation: The upper mantle as a chromatographic column, J. of Geol., in press.

Nicolas, A., 1986, A melt extraction model based on structural studies in mantle peridotites, J. Petrol., 27, 999-1022.

Nicolas, A. and C. Dupuy, 1984, Origin of ophiolitic and oceanic lherzolites, Tectonophysics, 110, 177-187.

Niida, K., 1974, Structure of the Horoman ultramafic massif of the Hidaka metamorphic belt in Hokkaido, Japan, J. Geol. Soc. Japan, 80, 31-44.

Niida, K., 1984, Petrology of the Horoman ultramafic rocks in the Hidaka metamorphic belt, Hokkaido, Japan, J. Fac. Sci., Hokkaido Univ., Ser. IV, 21, 197-250.

Noiret, G., R. Montigny and C.J. Allegre, 1981, Is the Vourinos Complex an island arc ophiolite? Earth Planet. Sci. Lett., 56, 375-386.

Obata, M., 1977, Petrology and petrogenesis of the Ronda high-temperature peridotite intrusion, Southern Spain, Ph.D. Thesis, Massachusetts Institute of Technology, Cambridge, Mass., 220 pp.

Obata, M., 1980, The Ronda peridotite: garnet-, spinel-, and plagioclase-lherzolite facies and the P-T trajectories of a high-temperature mantle intrusion, J. Petrol., 21, 533-572.

Obata, M. and N. Nagahara, 1987, Layering of alpine-type peridotite and the segregation of partial melt in the upper mantle, J. Geophys. Res., (in press).

Okada, H., 1979, Geology of Hokkaido and plate tectonics, Chikyu Monthly, 1, 869-877, (in Japanese).

Okada, H., 1980, Sedimentary environments on and around island arcs; an example of the Japan trench area, Precambrian Research, 12, 115-139.

Okada, H., 1983, Collision orogenesis and sedimentary in Hokkaido, Japan, in Accretion Tectonics in the Circum-Pacific Regions, ed. M. Hashimoto and S. Uyeda, TERRAPUB, Tokyo, 91-105.

Ottonello, G., 1980, Rare earth abundances and distribution in some spinel peridotite xenoliths from Assab (Ethiopia), Geochim. Cosmochim. Acta, 44, 1885-1901.

Ottonello, G., W.G. Ernst and J.L. Joron, 1984a, Rare earth and 3rd transition element geochemistry of peridotitic rocks: I. Peridotites from the Western Alps, J. Petrol., 25, 343-372.

Ottonello, G., J.L. Joron and G.B. Piccardo, 1984b, Rare earth and 3rd transition element geochemistry of peridotitic rocks: II. Ligurian peridotites and associated basalts, J. Petrol., 25, 373-393.

Pallister, J.S. and R.J. Knight, 1981, Rare-earth element geochemistry of the Samail ophiolite near Ibra, Oman, J. Geophys. Res., 86, 2673-2697.

Palme, H. and K.G. Nickel, 1985, Ca/Al rato and composition of the earth's upper mantle, Geochim. Cosmochim. Acta, 49, 2123-2132.

Pearce, J.A. and M.J. Norry, 1979, Petrogenetic implications of Ti, Zr, Y, and Nb variations in volcanic rocks, Contrib. Mineral. Petrol., 69, 33-47.

Presnall, D.C., 1979, Fractional crystallization and partial fusion, in The Evolution of the Igneous Rocks, ed. H.S. Yoder, Princeton University Press, 59-75.

Prinzhofer, A. and C.J. Allegre, 1985, Residual peridotites and the mechanisms of partial melting, Earth Planet. Sci. Lett., 74, 251-265.

Quick, J.E., 1981, Petrology and petrogenesis of the Trinity Peridotite, an upper mantle diapir in the eastern Klamath Mountains, northern California, J. Geophys. Res., 86, 11,837-11,863.

Rajamani, V. and A.J. Naldrett, 1978, Partitioning of Fe, Cu, Ni and Co between sulfide liquid and basaltic melts and the composition of Ni-Cu sulfur deposits, Econ. Geol., 73, 82-93.

Reid, J.B. and G.A. Woods, 1978, Oceanic mantle beneath the southern Rio Grande rift, Earth Planet. Sci. Lett., 41, 303-316.

Ribe, N.M, 1985, The generation and composition of partial melts in the earth's mantle, Earth Planet. Sci. Lett., 73, 361-376.

Richter, F.M. and D. McKenzie, 1984, Dynamical models for melt segregation from a deformable matrix, J. Geol., 92, 729-740.

Richter, F. M., 1986, Simple models for trace element fractionation during melt seggregation, Earth Planet. Sci. Lett., 79, 333-344.

Ringwood, A.E., 1979, Origin of the Earth and Moon, Springer, New York, 295 pp.

Robinson, P. R. Ross, G.L. Nord, J.R. Smyth and H.W. Jaffe, 1977, Exsolution lamellae in augite and pigeonite: fossil indicators of lattice parameters at high temperature and pressure, Amer. Mineral., 62, 857-873.

Ruckmick, J.C. and J.A. Noble, 1959, Origin of the ultramafic complex at Union Bay, southeastern Alaska, Geol. Soc. Amer. Bull., 70, 981-1018.

Scott, D. R. amd D. J. Stevenson, 1984, Magma solitons, Geophys. Res. Lett., 11, 1161-1164.

Scott, D. R. amd D. J. Stevenson, 1986, Magma ascent by porous flow, J. Geophys. Res., 91, 9283-9296.

Shaw, D.M., 1970, Trace element fractionation during anatexis, Geochim. Cosmochim. Acta, 34, 237-243.

Shimizu, N. and C.J. Allegre, 1978, Geochemistry of transition elements in garnet lherzolite nodules in kimberlites, Contrib. Mineral. Petrol., 67, 41-50.

Sinigoi, S., P. Comin-Chiaramonti and A.A. Alberti, 1980, Phase relations in the partial melting of the Baldissero spinel-lherzolite (Ivrea-Verbano zone, western Alps, Italy), Contrib. Mineral. Petrol., 75, 111-121.

Sinigoi, S., P. Comin-Chiaramonti, G. Demarchi and F. Siena, 1983, Differentiation of partial melts in the mantle: evidence from the Balmuccia peridotite, Italy, Contrib. Mineral. Petrol., 82, 351-359.

Sinton, J.M., 1977, Equilibration history of the basal alpine-type peridotite, Red Mountain, New Zealand, J. Petrol., 18, 216-246.

Stockman, H.W., 1982, Noble metals in the Ronda and Josephine Peridotites, Ph.D. Thesis, Massachusetts Institute of Technology, Cambridge, Mass.

Stosch, H.G., 1982, Rare earth element partitioning between minerals from anhydrous spinel peridotite xenoliths, Geochim. Cosmochim. Acta, 46, 793-811.

Stosch, H.G. and G.W. Lugmair, 1986, Trace element and Sr and Nd isotope geochemistry of peridotite xenoliths from the Eifel (W. Germany and their bearing on the evolution of the subcontinental lithosphere, Earth Planet. Sci. Lett., 80, 281-298.

Stosch, H.G. and H.A. Seck, 1980, Geochemistry and mineralogy of two spinel peridotite suites from Dreiser Weiher, West Germany, Geochim. Cosmochim. Acta, 44, 457-470.

Suen, C.J., 1978, Geochemistry of peridotites and associated mafic rocks, Ronda ultramafic complex, Spain, Ph.D. Thesis, Massachusetts Institute of Technology, Cambridge, Mass., 283 pp.

Sun, S.S., R.W. Nesbitt and A.Y. Sharaskin, 1979, Geochemical characteristics of mid-ocean ridge basalts, Earth Planet. Sci. Lett., 44, 119-138.

Takahashi, E., and I. Kushiro, 1983, Melting of a dry peridotite at high pressures and basalt magma genesis, Amer. Mineral., 68, 859-879.

Thompson, J.F.H., S.J. Barnes and J.M. Duke, 1984, The distribution of Ni and Fe between olivine and magmatic sulfides in some natural assemblages, Can. Mineral., 22, 55-66.

Turcotte, D.L. and J.L. Ahern, 1978, A porous flow model for magma migration in the asthenosphere, J. Geophys. Res., 83, 767-772.

Waff, H. S. and J. R. Bulau, 1979, Equilibrium fluid distribution in an ultramafic partial melt under hydrostatic stress conditions, J. Geophys. Res., 84, 6109-6114.

Wager and Deer, 1939, Geological investigations in East Greenland. III the petrology of the Skaergaard intrusion Kangerdlugsnak, East Greenland, Med. om Gromland, 105, 1-352.

Wanke, H., 1981, Constitution of terrestial planets, Phil. Trans. Roy. Soc. Lond. A, 303, 287-310.

Wells, P., 1977, Pyroxene geothermometry in simple and complex systems, Contrib. Mineral. Petrol., 68, 129-139.

Wendlandt, R.F., 1982, Sulfide saturation of basalt and andesite melts at high pressures and temperatures, Amer. Mineral., 67, 877-885.

Wilson, A.H., 1982, The geology of the Great "Dyke", Zimbabwe: the ultramafic rocks, J. Petrol., 23, 240-292.

Wood, B.J. and S. Banno, 1973, Garnet-orthopyroxene and orthopyroxene-clinopyroxene relationships in simple and complex systems, Contrib. Mineral. Petrol., 42, 109-124.

Yoder, H.S., 1976, Generation of Basaltic Melt, National Academy of Sciences, Washington D.C., 265 pp.

Zindler, A. and S. Hart, 1986, Chemical geodynamics, Ann. Rev. Earth Planet. Sci., 14, 493-571.

Appendix I. REE Analytical Technique and Data Quality

Rare earth element abundances were measured in the Horoman peridotites using a radiochemical neutron activation analysis (RNAA) procedure at F. Frey's laboratory at MIT. The purpose of this procedure was to obtain accurate data for samples with very low concentrations of REE. The RNAA procedure involved chemically separating the REE so that the resolution could be considerably enhanced. In this appendix the procedure is outlined, reproducibility and a comparison of data is discussed and analytical problems are expressed.

Procedure

The RNAA procedure used was that developed by Hickey and Chen, and is described briefly in Hickey and Frey (1981). Care was taken in reducing the raw data collected and in estimating errors. Description of the actual procedure used, in some detail, is helpful for understanding of the data reduction and the analytical errors involved.

Sample preparation: Rock powders were weighed on a digital laboratory balance to a precision of five digits beyond the decimal point and the weighed powder was carefully poured into small Suprasil glass vials. The vials were scored with a diamond scribe for labelling of samples. The approximate amount of powder to use was determined by two bracketing conditions. The samples were very depleted in REE so it was desirable to irradiate as much sample as possible, but too much sample was found to be difficult to dissolve. We found that between 200 and 300 mg of sample

was a happy medium and the amount was roughly adjusted between these values, based on the degree of depletion from major elements (i.e., most depleted samples required closer to 300 mg). A basalt sample was used as a standard (actually two standard samples must be prepared) requiring considerably less sample (~70 mg) due to its higher concentration of REE. If too much standard is irradiated, counting quality during analysis is reduced due to disparate activity between samples and standard. A small iron wire was added to each vial after weighing as a flux monitor. The Suprasil vials were sealed using a natural gas-oxygen torch. Care was taken to round off sharp glass tips produced during sealing, lest the vials break during irradiation. Sealed vials were approximately 6 cm long and 5 mm in diameter. The material of the vial is important for its chemical purity, durability, and ease of removing all of the sample powder after irradiation. The samples were irradiated for twelve hours at the high flux position of the MIT nuclear reactor. Plastic vials deteriorate with this much radiation. Eight samples and two standards were irradiated and fit exactly into the irradiation vessel.

Removing sample, adding tracers and dissolution: The irradiated samples were received from the reactor after sufficient cooling time. Lead shielding, radiation badges and other standard radiation safety procedures were followed when handling the radioactive samples. Sample powder was removed by gently breaking the tip of the vial with a pliers

and carefully emptying all the sample into small teflon beakers and rinsing the vials with acetone. Iron wires were removed from the sample and retained for later counting to determine flux variation. To each sample, and one of the standards, two pure tracer radioisotopes were added in dilute HNO_3 solution using pipettes. The two tracer isotopes were ^{144}Ce and ^{169}Yb. Only the ^{144}Ce tracer was added to the other standard. (The tracers are used to determine REE yields of the ion exchange column chemistry done later.) It is important to add precisely the same activity of tracer to each sample and standard, for chemical yields are based on ratios of the tracer isotopes between samples and standards. This was accomplished on a volume basis using pipettes to accurately measure the tracer solutions. The amount of tracer activity added to each sample should be between 0.5-0.8 μCi. This range is a compromise between good counting statistics from tracer peaks (produced by greater activity), and unwanted interference from large tracer peaks upon natural REE peaks and generally high activity (both for reasons of safety and data quality). A mixture of about 10 ml HF and about 1 or 2 ml $HClO_4$ was added to the sample beakers. The covered beakers were heated overnight to digest the rock sample. The samples were then evaporated to dryness and redissolved four times in several ml of 2N HCl.

Ion exchange columns, elutions, solvent extraction:

Ion exchange columns were prepared throughout the

dissolution steps. Fifteen grams of ion exchange resin was weighed for each sample and placed into beakers. The resin was washed three times with 6N HNO_3 to remove foreign cations and then with 2N HNO_3 to equilibrate the resin with the first elute. Resin, wetted with 2N HNO_3, was poured into 0.5 inch diameter ion exchange columns. Levels of columns were adjusted so they all had 20 cm of resin. The first elution consisted of 140 ml of 2N HNO_3 to remove major cations and most of the Cr and other minor cations. The 2N elute was poured into a separatory funnel for each sample and placed in a stand alongside the ion exchange column.

The sample was loaded with just enough 2N HCl to completely dissolve the sample. Loading was done with a syringe, connected to an extender tube to enable direct loading upon the resin surface with a disposable plastic syringe tip that was changed for each sample. The sample was carefully squirted on the surface of the resin and the sample beaker was rinsed with a pre-measured 3 ml of 2N HNO_3 that was also loaded onto the resin. The separatory funnel was quickly connected to the column and the stopcock opened for elution. A collection beaker for the 2N HNO_3 was placed under all of the columns. This effluent was discarded weeks later, after allowing sufficient time for the major element radioactivity to decay. The first elution took ~2 hours. As soon as the 2N eluant had run through the column, the stopcock was closed and the funnel filled with 140 ml of 6N HNO_3 to begin the second elution. This elution also took ~2

hours and the effluent was saved in a clean beaker for it contains the REE, along with Sc and some other minor contaminants. The sample beakers were placed on hotplates and evaporated to dryness overnight.

Polyethylene counting vials were labelled for each sample and marked with a 15 ml volume line. Another set of separatory funnels were prepared for the solvent extraction. 30 ml of tri-n-butyl phosphate (TBP) was measured out, as was 15 ml of 9N HCl. The HCl was placed in a squirt bottle and a portion of it used to dissolve the sample. TBP is an industrial organic solvent that is known to remove Sc and other remaining transition metals from the sample, while leaving behind the REE. The sample and the TBP were poured into the funnel, making certain that the stopcock was closed. After completely rinsing the sample beaker with the acid from the 9N squirt bottle into the funnel, the stopper was placed on the funnel and the sample and TBP thoroughly mixed by vigorously shaking the separatory funnel for several minutes. This process was repeated for all of the samples and standards. The funnels were all placed in racks to allow the organic and inorganic portions to separate (~1 hour).

To separate the sample, the funnel was rinsed with a small amount of 6N HCl, then the stopcock was slowly opened to allow the inorganic sample (at the bottom of the funnel) to drain into the appropriate counting vial. TBP also extracts H_2O to some degree so the original 15 ml of acid

must be supplemented with rinses until the vial is full to the 15 ml mark. Be careful not to allow the TBP to drain through. The samples were now ready to count, using gamma-ray spectroscopy.

Counting: The instrumental neutron activation technique used was very similar to standard INAA procedure used at MIT. Instead of the standard 5-day count with the low energy (LEPs) detector and an 8-day count with the broader spectrum GeLi detector, these two counts were made simultaneously as soon as the samples were ready by switching pairs of samples between the two detectors. Counting times for samples were at least 40K seconds (preferably longer for very depleted samples) and standards were counted for 20K seconds. Another count using the LEPs detector was done after about 15 days and a final count at about thirty days was done for the long half-life REE using the GeLi detector.

Data Reduction and Yield Determination

Data was reduced using the standard TEABAGS program. Generally the program worked excellently but many peaks were plotted (and the data reduced) by hand as a check on the software and to better understand the spectrum. The spectrum consists almost entirely of REE due to the prior chemical separation procedure. The primary analytic problems were due simply to insufficient abundance of certain REE causing poor counting statistics; interference from REE tracer peaks; and problems caused by the different

nature of the REE characteristics of the basalt standards and the peridotite samples.

Radioactive tracers were used to determine the relative yield of the sample REE to the REE of the standard, due to the chemical procedure. The yield is used to correct measured concentration of REE with the assumption that whatever processes affected the tracers will effect the natural REE in the same way. Two tracers were used, ^{144}Ce and ^{169}Yb, to account for any fractionation of the REE during the procedure. ^{169}Yb is produced naturally during irradiation in small amounts. The amount of naturally produced ^{169}Yb for each sample and standard can be calculated using the ratio of ^{169}Yb to ^{175}Yb in the standard which has no ^{169}Yb tracer as a correction factor. (The 177 keV peak was used for ^{169}Yb and the 283 keV peak for ^{175}Yb.) The ratio in this standard times the area of the ^{175}Yb peak for each sample (and the other standard) gives the area of the ^{169}Yb generated during irradiation. Yield is based on tracer ^{169}Yb only, or the difference of the ^{169}Yb measured and the calculated irradiation produced ^{169}Yb. This correction was made for all Yb yield calculations but was found to be unnecessary as "natural" ^{169}Yb was, in all cases, less than a tenth of one percent of the tracer ^{169}Yb. ^{144}Ce is not produced during irradiation so no correction is necessary.

The yield calculation was based on the fact that the same amount of activity of tracer was placed into each

sample and standard prior to the chemical procedure. Any disparity in activity of tracers, between samples and standard discovered during counting, can be attributed to the chemistry. To calculate the yield the 133.5 keV peak (the only major peak) was used for ^{144}Ce, while both the 177 and 198 keV peaks (corrected for "natural" ^{169}Yb) were used for ^{169}Yb. The yield is simply the ratio of the decay time corrected tracer peak areas of the samples to those of the standard (the standard with both tracers was used as the standard). All the calculated yields showed that sample REE were lost relative to the standard. Values for Ce and Yb yields were not identical, implying that some REE fractionation occurred during the chemical process. Actual measured REE abundance for each REE was corrected using a yield factor based on a linear approximation regressed from the Ce and Yb tracer values. This approximation is thought to be valid due to the near linear nature of a plot of ionic radius versus atomic number. Only La is off the straight line, so that some slight error may be introduced for La due to its yield correction factor.

A simple experiment was performed to see where the missing sample REE may have gone. A counting vial was prepared for the 2N HNO_3 effluent (after months of cooling to allow the major elements to decay) to see if any REE were removed with the major elements for one sample (62210). Also a strong HCl elution was performed to scavenge any REE remaining in the ion exchange column for the same sample and

a counting vial was prepared. Very long counts were necessary for these two test samples because the concentrations were so low. Nearly all the Ce tracer was accounted for between the true sample, the 2N HNO_3 effluent and the HCl effluent. Relative to the standard, the sample had 0.977 of the ^{144}Ce, the 2N HNO_3 0.015 and the HCl 0.005. Eu was the only natural REE that could be accurately detected in the acid samples due to its long half-life. Eu concentrations indicated that about one percent of the Eu from the sample was in the HCl (i.e., left in the column) and one-third of one percent was in the 2N HNO_3. Yb tracer yield calculations did not account for all the tracer as well as for Ce. Relative to the standard, the true sample had 0.946 of the ^{169}Yb, the 2N HNO_3 0.009 and the HCl 0.008. Presumably some of the REE were lost to the TBP solution and some lost along the way due to laboratory errors.

The yield factors are believed to be the single largest source of error for this analytical technique. Theoretically, if the counting statistics in the tracer peaks are good and there is no major interference, the yield calculations should produce the same values for a given sample for each counting interval and/or different detector. This was disconcertingly discovered not to be true. The 133.5 keV ^{144}Ce peak is low energy and is interfered with slightly by one of the ^{169}Yb minor peaks so the LEPs detector is necessary to properly resolve it. Both ^{169}Yb peaks (177 and 198 keV) should be relatively interference

free and are about the same size. A careful comparison of these yield calculations for the different counts was made for several irradiations to try to understand the variation. I tried to discover systematics of these yield variations by looking at ratios between yields determined at different counting times. Unfortunately, this did not prove very fruitful as very little systematic behavior existed between different count intervals and different irradiations. The variation between count intervals for the same tracer yield were seldom greater than five percent. This is well outside of the accuracy of a single yield value based on counting statistics propagated through the yield calculation, which was always less than one percent. The precision wasn't actually this bad because one could easily rationalize why some yield calculations were better than others based on the size of the errors and some knowledge of the detector capabilities and interferences. The cause of these variations are still unknown and more study of them should be made to obtain more precise analyses. There may be problems associated with different detector geometry, the relatively large sample size, and the fact that the samples were liquid. The data presented in the thesis are based on a choice of a single set of yield calculations (initial LEPs count for ^{144}Ce and for ^{169}Yb using the 198 keV peak).

Other Analytical Problems

A more technical problem was caused by the fact that the samples and standard had different ambient activity

levels. Ideally, a standard should have concentrations known precisely and have similar concentrations to the samples. A good standard does not exist that meets both these criteria for peridotite samples. The standard chosen was the best compromise possible, as it met the more critical first criterion. Basalt standards have much greater abundances of REE so that during counting the detector dead time is considerably higher than for the peridotite samples. An empirical linear relation exists between a ratio of the areas of the same peak measured at different dead times and a ratio of the total counting time to "live" time. This relation is called the Wyttenbach factor and is usually a very small correction factor that the TEABAGS program does automatically based on input determined empirically for each detector. Since neutron activation is based on ratios of sample to standard this small correction factor is usually cancelled out because the samples and the standard have about the same dead time. For the RNAA analyses discussed here, the Wyttenbach factor became significant due to disparate dead times between samples and standard. It was discovered later that the empirical information for the detectors was given to TEABAGS incorrectly (actually the detectors had been adjusted without changing the input parameters used for the W. factor). The data presented in the thesis was all adjusted using the proper W. factors, so no errors were introduced. Not only is it important to be aware of this type of

technical problems in reducing neutron activation data but it points out the need for more work in obtaining better standards for peridotite analyses. If the general activity of samples and standard are similar (i.e., similar dead times) it wouldn't matter what the W. factor was, for it would cancel. The development of an artificial standard would be ideal. We experimented with an artificial standard by adding volume controlled, pure REE in solution onto aluminum foil and evaporating it. This type of standard is particularly suitable because the foil dissolves easily in HCl acid. Unfortunately this standard was still too concentrated but more work along this line should be done. A basalt standard with relatively low REE (BCR-1) was used in the thesis. Later irradiations, performed mainly on peridotite xenolith samples of Song Yan's from China, used a more depleted basalt sample (AII-92). This standard was better in some respects but apparently created some problems due to the fact that its REE abundances are not known with as great a precision as BCR-1.

High purity iron wires were irradiated with the samples as a neutron flux monitor. Variations in flux between samples and standards must be corrected for. This is also done for standard INAA and correction factors generally prove to be very minor due to very little flux variation. The flux correction turned out to be significant for RNAA, (sometimes as large as 10% but generally around 5%) due mainly to larger flux variations in the reactor itself in

the high flux position compared to the lower flux position used for INAA. The different geometries used in the rabbits containing the samples being irradiated between INAA and RNAA also contributed to the difference in flux variations. These flux variations were corrected for but some small errors may be introduced due to errors in weighing the wires or in counting them. These errors, if they exist for INAA, would be insignificant due to the small magnitude of the flux correction but they may be more important for RNAA flux correction values.

Care must be taken when very long count times are used that some peaks do not overflow the capability of the MCA to count. If single channel values go beyond a certain value, (2^{20}-1 for the Canberra at MIT in 1986) the MCA will continue to count but will not record the previous amount, i.e. it will start over. As long as the peaks do not multiply overflow, this can easily be corrected simply by adding the appropriate "overflow value" to the channels that overflowed. The obvious tell tale sign of an overflown peak is a curious unexpected double peak. Overflow was a problem with the Sm peak for the initial GeLi detector count with the Cr peak during INAA. If the added tracer activity is too great, overflow could be a problem.

A final analytical problem presented by this technique is contamination. Because the samples are so depleted care must be taken to avoid any contamination of even minute amounts of REE. The first irradiation for the Horoman

samples was primarily useless due to La contamination. The powdered samples were sent from Japan but presumably they came in contact with the lanthanum oxide used in preparation of XRF samples. Not only was the La data useless but the huge peaks tended to interfere with other elements reducing their quality as well. Obviously, once the samples are irradiated contamination is unlikely due to the rarity of radioactive REE, the only possible contaminants.

Quality of REE Data

Probably the best way to determine the quality of the REE data is to compare all the independent analyses for each sample. All of the Horoman samples except one, (62131) were analyzed in duplicate by RNAA. Table AI1 shows all of the duplicate analyses of REE using RNAA, as well as poorer quality INAA data, for the Horoman samples. The data in the table are chondrite-normalized using the normalization values of Boynton (1984) and are plotted on a REE diagram (Fig. AI1). Table AI1 includes the accuracy of each data point, which is the two sigma value based on counting statistics, including counting statistic errors for the yield calculation. Table AI1 also includes the approximate relative errors for each REE for RNAA and INAA, as well as the relative precision of the RNAA data. The precision is based simply on the standard deviation of the mean of the five analyses (including the INAA data) of sample 62210 for each REE. This calculation was made at face value assuming that all analyses are of equal and perfect accuracy. This

Table AI1. REE Data Chondrite-Normalized with Errors

IR[1]	La[2]	Ce[2]	Nd[2]	Sm[2]	Eu[2]	Tb[2]	Yb[2]	Lu[2]
62210								
FFQ	---	.48(.20)	1.02(.58)	1.77(.03)	2.01(.04)	2.32(.15)	2.06(.04)	2.20(.06)
GGP	.58(.02)	.63(.16)	1.03(.15)	1.59(.03)	1.81(.04)	2.09(.10)	2.10(.05)	2.30(.06)
GGT	.54(.01)	.52(.12)	.90(.17)	1.46(.03)	1.51(.04)	1.69(.04)	1.76(.03)	1.96(.28)
HHM	.59(.01)	.74(.06)	1.00(.20)	1.44(.02)	1.71(.03)	1.88(.04)	2.03(.03)	2.20(.09)
HHB[3]	.48(.06)	---	---	1.59(.10)	1.61(.09)	---	2.11(.24)	1.86(.31)
62212								
FFQ	---	.54(.15)	.80(.16)	1.75(.03)	1.90(.04)	2.32(.15)	1.87(.03)	2.20(.12)
GGP	.53(.02)	.58(.15)	.95(.18)	1.46(.03)	1.71(.04)	2.00(.13)	1.95(.03)	2.14(.06)
HHB[3]	.45(.03)	---	---	1.49(.07)	1.54(.10)	---	2.06(.19)	1.86(.31)
62213								
FFQ	---	---	.90(.27)	1.46(.03)	1.62(.04)	1.94(.06)	1.91(.05)	2.08(.06)
GGP	.66(.02)	.74(.12)	.97(.20)	1.38(.03)	1.58(.04)	1.77(.06)	1.88(.03)	2.11(.04)
HHB[3]	.45(.05)	---	---	1.28(.10)	1.31(.07)	---	1.67(.19)	1.68(.28)
62131								
GGP	.30(.01)	.36(.11)	---	.67(.02)	.83(.03)	.86(.04)	.91(.08)	1.06(.03)
HHB[3]	.26(.04)	---	---	.56(.07)	.64(.05)	---	1.20(.24)	.87(.28)
62130								
FFQ	---	---	---	.76(.02)	.79(.03)	.95(.04)	.86(.10)	1.06(.06)
GGP	.224(.007)	.22(.07)	.57(.17)	.69(.01)	.79(.03)	.93(.04)	.95(.02)	1.04(.02)
HHB[3]	.19(.03)	---	---	.67(.10)	.69(.07)	---	1.15(.24)	.87(.25)
62128								
FFQ	---	---	---	.074(.003)	.079(.010)	---	.14(.01)	.17(.01)
GGP	.116(.003)	---	---	.062(.003)	.103(.011)	---	.131(.007)	.20(.02)
HHB[3]	.087(.02)	---	---	---	---	---	---	---
62127								
FFQ	---	---	---	.108(.015)	.135(.008)	---	---	---
GGP	.106(.003)	---	---	.097(.005)	.139(.010)	---	.105(.005)	.16(.02)
HHB[3]	.10(.02)	---	---	.11(.03)	---	---	---	---
Acc[4]	3	25	15	2-5	2-12	5	2-5	3-10
Acc[5]	13	--	--	6-27	6-10	--	11-21	16-29
Pre[6]	10	14	6	8	11	13	7	9

[1]Irradiation label
[2]Accuracy based on counting statistics in parentheses following data
[3]INAA irradiation
[4]Relative accuracy for each element from GGP RNAA irradiation
[5]Relative accuracy for each element from HHB INAA irradiation
[6]Relative precision based on mean and standard deviation from five repeat analyses of sample 62210 (including INAA analysis)

Figure AI1. Chondrite-normalized (Boynton, 1984) diagram for all bulk rock REE data collected for the Horoman peridotite samples (see Table AI1 for data, which includes one sigma errors in parentheses), showing the reproducibility of the data. Sample 62210 was analyzed a total of five times, four by RNAA and once by standard INAA. The replication of this sample allows one to have some idea of analytical precision. The other samples were each analyzed at least two times. The analyses used throughout this thesis are from irradiation GGP which is shown by a heavy solid line. This data set is believed to be the most accurate. The heavy dashed line is data from a previous irradiation (FFQ), but different powdered samples were used that were later found to be contaminated with La (La is not plotted for FFQ). Two later irradiations included sample 62210. GGT is shown by the heavy dot-dash line while HHM is shown by the light dashed line. An INAA irradiation is shown by the light solid line and is much less accurate. Some data sets are not complete thus lines connecting data points are only partial. INAA data are particularly sparse (e.g. sample 62128 has just one INAA data point for La, below the GGP line). The lines are generally quite parallel, with the exception of the INAA line, indicating a constant error likely to be due to the yield factor (see text). Some REE from sample 62210 actually show precision better than accuracy from counting statistics based on a single data point. More discussion of error in data is in the text and errors are shown in Table AI1.

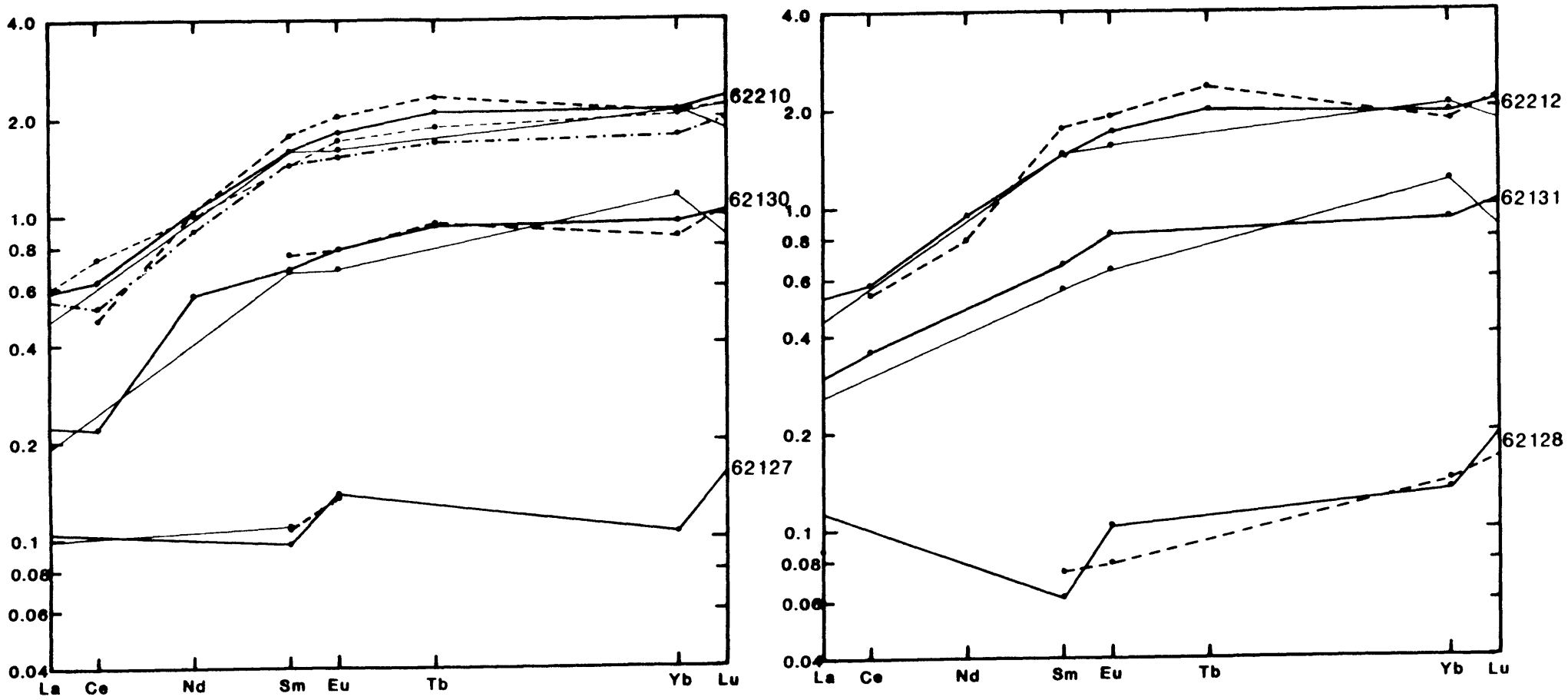
4.0
2.0
1.0
0.8
0.6
0.4
0.2
0.1
0.08
0.06
0.04
La
Ce
Nd
Sm
Eu
Tb
Yb
Lu
62210
62130
62127
62212
62131
62128

Figure AI1

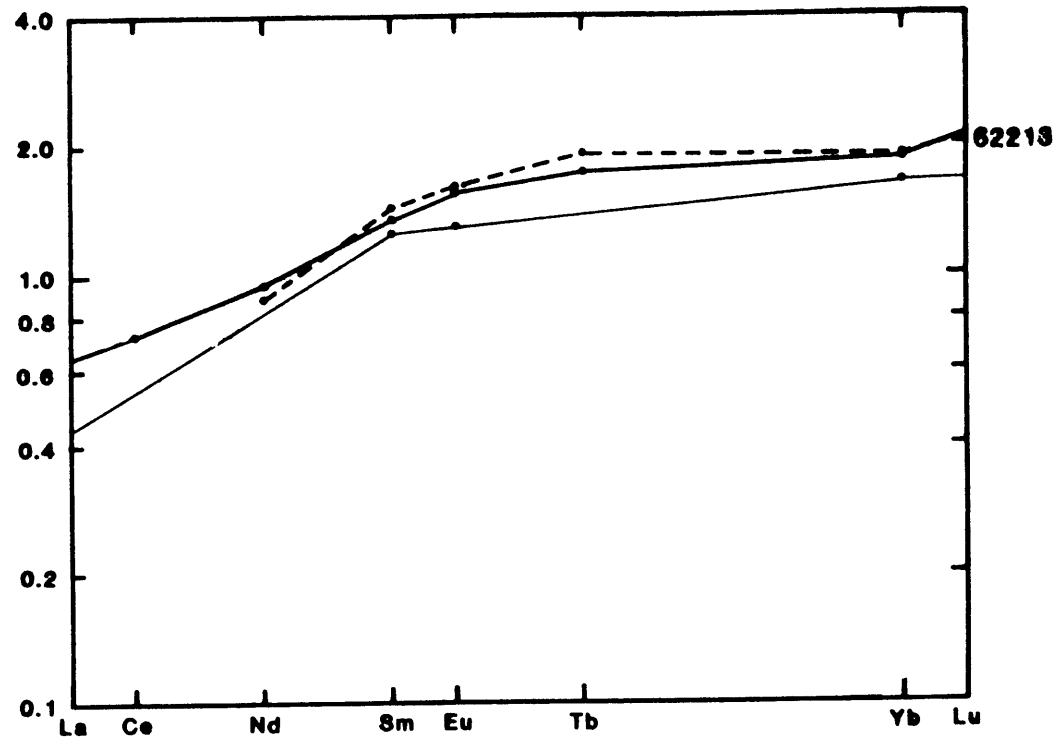

Figure AI1 (cont.)

assumption is clearly false so this approximate precision is an overestimate of the real precision.

Data from irradiation GGP (see Table AI1 and Fig. AI1) was used in this thesis and is considered to be the best quality. Standard INAA data are incomplete and relatively inaccurate but are shown for comparison. Irradiation FFQ data are for samples contaminated by La which reduced the quality of all of the REE data. The FFQ data are generally greater than the GGP data. Several FFQ samples were counted after approximately seven months to test how the contamination affected the data. After this much decay time, the La and any other interfering peaks had decayed away. Only the Yb tracer and Eu have sufficiently long half-lives to still be counted. Both of these abundances had reduced (the Eu to values more commensurate with the GGP values), implying that contamination led to the incorrect, and generally high, abundances initially measured. A different basalt standard (AII-92) was used for irradiation GGT and HHM for which the precision of the known REE concentrations is poorer than for BBC-1 used for irradiation GGP. Only sample 62210 of the Horoman samples were analyzed from these irradiations.

The approximate precision is smaller than the accuracy from a single irradiation for some elements. The general parallel nature of the RNAA REE patterns suggest that the precision is reduced by a constant factor. The yield factor is the likely suspect.

The smooth nature of the REE patterns is a rough indication that the data is of good quality. Five REE element abundances (La, Sm, Eu, Yb and Lu) are high quality data with relative accuracy of ~3% and relative precision based on the duplicate analyses of sample 62210 of less than 10%. The Tb data are poorer quality, while Ce and Nd are poorer yet. The real precision is difficult to quantify, and is not extremely useful without more duplicate analyses, but I think with this technique it could approach the accuracy of individual measurements.

An independent method of exploring precision of analytical data is to compare data from different analytical techniques. RNAA REE data can be compared with INAA data but the precision is not well constrained by this comparison. All of the RNAA data from the GGP irradiation is within the error limits of the INAA data. The INAA data is not very accurate and should really be used only as a rough guide to REE concentrations at the levels of peridotite samples but INAA does not include any of the errors associated with the yield calculation so can be useful. A sample form the Ronda peridotite (R717) was re-analyzed within the same INAA irradiation as the Horoman samples. The variation of the data for this sample and that from Frey, et al (1985) for five REE was less than the uncertainty of those elements quoted in the paper. This implies that the Horoman INAA data is reasonably reliable.

Certainly, the INAA data does nothing to weaken confidence in the RNAA data.

Another analytical technique, isotope dilution (ID), generally has greater accuracy than RNAA. Fortunately, several of Song Yan's peridotite xenolith samples from Hannoba, China were analyzed by both techniques. Horoman sample 62210 was analyzed by RNAA in the same irradiation and using the same technique as the Chinese samples making inferences drawn from the comparison of RNAA with ID valid for Horoman as well. The ID data are just for Sm and Nd for four samples, and Nd is one of the poorest determined elements by RNAA. The ID values for Nd were always well within the RNAA error limits based on counting statistics. The variation in Nd between the two techniques for the four samples was 4%, 7%, 7% and 13%. The ID values for Sm were just about at the RNAA error limits based on counting statistics. The variation in Sm between the two techniques was 0.6%, 5%, 5% and 8%. This simple comparison implies that the real precision of the RNAA data may be very near to the accuracy based on counting statistics from a single irradiation assuming one understands the sources of error involved in this technique.

Appendix II. Least-Squares Linear Regression of Major Elements to Calculate Modes of Horoman Peridotite Samples

As mentioned in the text, point counting of petrographic thin sections, to determine modal proportions of samples from the Horoman peridotite, proved unreliable. Comparisons between modes done by myself and by students of M. Obata on the same samples were disparate. It seemed that a much larger thin section was necessary to perform statistically accurate modes with these coarse-grained rocks, and only small samples were available. Despite the general coarse-grained nature of the samples, other factors made point counting difficult: pervasive disequilibrium texture, inhomogeneous grain-size distribution, non-uniform macroscopic mineral layering, and misidentification of very fine-grained mineral aggregates. In light of these problems, I wished to use the electron microprobe's energy dispersive system and enhanced color graphics to "map" an image for several elements to separate phases, and thus do modal analyses. This proved to be impossible to do accurately, due both to the coarseness of the samples and the fact that the minimum magnification on the electron microprobe was still too small to cover enough of a probe section to be feasible. I decided to perform a least-squares regression analysis utilizing the mineral composition data and the bulk rock chemical data to calculate a mode. The Horoman rocks are well suited for this type of analysis due to their relatively simple major

element chemistry, (i.e. all of the samples consist almost entirely of only five, and in some cases four, phases) and the bulk chemistry is predominantly made up of only five components, with five other more minor components. One should be able to calculate the phase proportions of a sample given that one knows both the sample's bulk composition and the mineral compositions making up the rock. This linear recombination of the phase proportions also has the advantage of removing the effect of various degrees of alteration. Unlike a point-count mode, this calculated mode gives the more useful mineral proportions prior to secondary alteration. The following is a description of the general theory of the least squares linear regression technique used and a detailed description of the actual procedure used in applying this technique to the Horoman peridotite samples. The theory and specifics of the technique was liberally drawn from an excellent paper by Reid and others (1973).

A set of mass balance equations were used in the form

$$s_i = c_{i1}x_1 + c_{i2}x_2 + \ldots c_{im}x_m$$

where c_{ij} represents the amount of the i-th component in the j-th phase, s_i represents the amount of the i-th component in the sample being modelled (i.e. the bulk rock analysis for a particular element i), and x_j represents the amount of the j-th phase required to model the sample. The values of all the x_j's are then calculated to minimize the sum of the squares of the residuals. Units must be chosen to be consistent with the mass balance equations (weight percent

is generally used for geological purposes). If the number of equations is equal to or greater than the number of phases, the set of equations can be solved for the best least-squares estimate of the x_j's. Besides the mass balance equations, an idea of the errors of the chemical analyses (for the s_i's and the c_{ij}'s) and closure requirements for the system are known. These further constraints help to obtain the best solutions for the x_j's (Reid, et al, 1973).

The matrix of c_{ij}'s can incorporate a term enabling the various components to be weighted by using the absolute error of the chemical analyses. Each row of c's is divided by the appropriate error term for the particular s, normalized to any one of the error terms to make them "relative" errors. Covariation between elements should also be included but for most modern instrumental analytical techniques (electron microprobe, XRF, INAA) inter-element correction factors are known and used to reduce the data. The covariations between elements are assumed to be small and are neglected in this study. Error terms can also be incorporated for analytical variance of the c_{ij} terms (Reid, et al, 1973). This was attempted in this study but abandoned, as the information gained was determined not to be useful, particularly since these errors were not really known. Weighting factors are of fundamental importance especially when the errors in the various components used in the regression vary widely. "The mathematical effect of the

weighting factors to most geochemical problems is to assign an importance to each mass balance equation commensurate with the inverse of its absolute error" (Reid, et al, 1973, p. 436).

The other piece of information available, outside of the mass balance equations themselves, is the exact linear constraint that the sum of the x_j's must be unity (or 100% if weight percent is used). This exact linear constraint has a similar effect to adding another equation (Reid, et al, 1973). With this constraint, the sum of the squares of the residuals actually is increased but it is mathematically correct and necessary to include in this type of geochemical computation. Furthermore, without this constraint one really can't accurately compare different models because their x_j's sum to different values. So, the addition of this closure constraint not only gives the estimated mode more physical significance, but allows testing of different models by direct conparison (Reid, et al, 1973).

Errors of the calculated x_j's can be used to assess the significance of the solution. An unbiased estimate of these errors (σ^2 in Reid, et al, 1973) is the sum of the squares of the residuals of the weighted equations divided by the quantity n+r+k-m, where n+r is the number of mass balance equations plus inexact constraints (r=0 in this study), k is the number of exact constraint equations (see Reid, et al, 1973, for the definitions of exact and inexact linear constraints), and m is the number of x_j's or phases. This

value was called "sigma for fit" in the output of the program used for the Horoman linear regression.

A weighted least-squares linear regression program utilizing the principles outlined above was used to determine modal analyses of the seven Horoman peridotite samples from this study. Results of the final best solution is shown in Table 1. A program written by Frank Spear at MIT, (REGRES) and slightly modified by Don Hickmott, was used. I added a subroutine to the program (with considerable help from Tom Juster and Beth Robinson) to apply the closure constraint that the mode must sum to one, using the math outlined in Reid, et al, (1973). The final program used was named REGCLO. The program accepts an input file for each sample in the form of a matrix consisting of the chemical analyses for each phase in the sample, chemical analyses of the bulk rock and weighting factors for each componenent based on relative absolute errors of the bulk rock analyses. The output from the program includes: the best parameter estimates (x_j's or modal proportions in this case) for the particular input data along with standard deviations; a list of the bulk rock component data (s_j's) along with the best-fit model estimates of these s_j's and the residuals between the input data and the model; a list of the input weighting factors used for each component; a value for the residual sum of the squares; and a "sigma for fit" value used to assess the statistical significance of the solution (defined previously).

The data available for the Horoman samples were excellent for this type of regression analysis. For the whole rock XRF data, each sample had been analyzed in triplicate. (Different splits of the same rock powder were analyzed at both M. Rhodes' Univ. of Mass., Amherst, Mass., laboratory and J. Dostal's St. Mary's Univ., Halifax, Nova Scotia, lab; while separately prepared powdered samples from the same rock samples were analyzed at M. Obata's Toyama Univ., Japan, laboratory.) Figure AII1 graphically presents a comparison of these three XRF data sets. The values plotted in the figure are all anhydrous and renormalized to 100%. The same abundances of Na_2O and Cr_2O_3 (INAA) and NiO (XRF) were used for all three data sets. The match of of the three lines is a bit disheartening but except for FeO^*, the Dostal and the UMASS data are near coincident. The patterns in general are near parallel implying that some of the mismatch is due to renormalizing slightly different totals. The FeO^* data from Dostal is suspiciously high. The UMASS data was used in the thesis.

Ten components were used in the least-squares linear regression model. For the mineral data, two sets of independent data were used. Numerous electron microprobe analyses using the JEOL 733 at MIT were made by myself while a compilation of mineral data for most phases on the same samples (not the same probe mount) made by M. Obata at Toyama Univ., Japan was also used. No duplicate analyses were available for olivine. Five, and in some cases four,

Figure AII1. Plot of five major elements (SiO_2, MgO, Al_2O_3, CaO and FeO^*, determined by XRF) versus sample number for three data sets from different laboratories. The data are anhydrous, are plotted in weight percent, and are renormalized to one hundred percent for comparison. The dashed line is data from M. Rhodes' laboratory at UMASS, Amherst, MA and is the data used throughout this thesis. The dot-dash line is data from J. Dostal's laboratory at St. Mary's Univ., Halifax, Nova Scotia from different splits of the same rock powder samples. The solid line is data from M. Obata's laboratory at Toyanama Univ., Japan from different powders of the same samples.

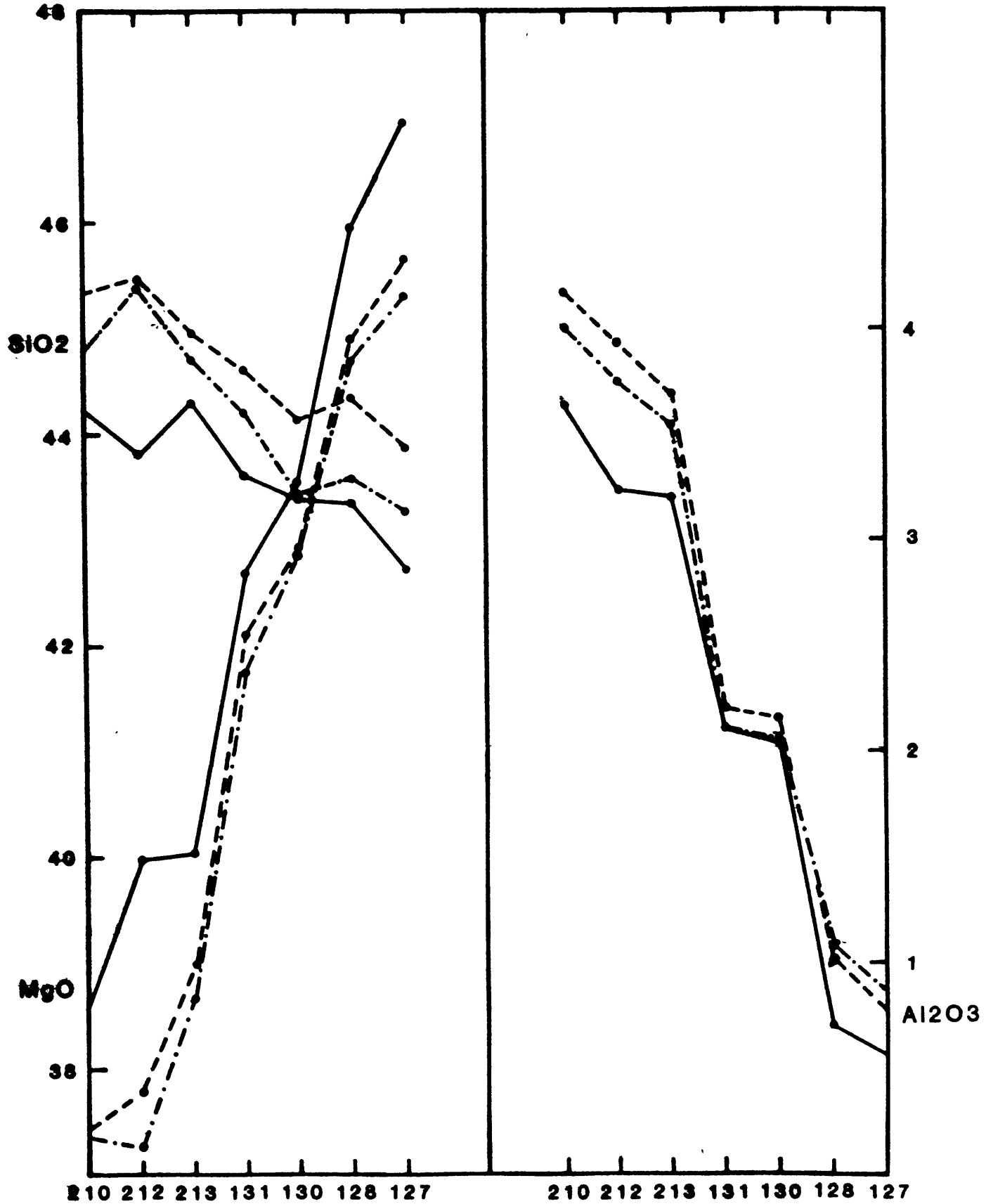
SiO2
MgO
Al2O3
48
46
44
42
40
38
4
3
2
1
210 212 213 131 130 128 127
210 212 213 131 130 128 127

Figure AIII

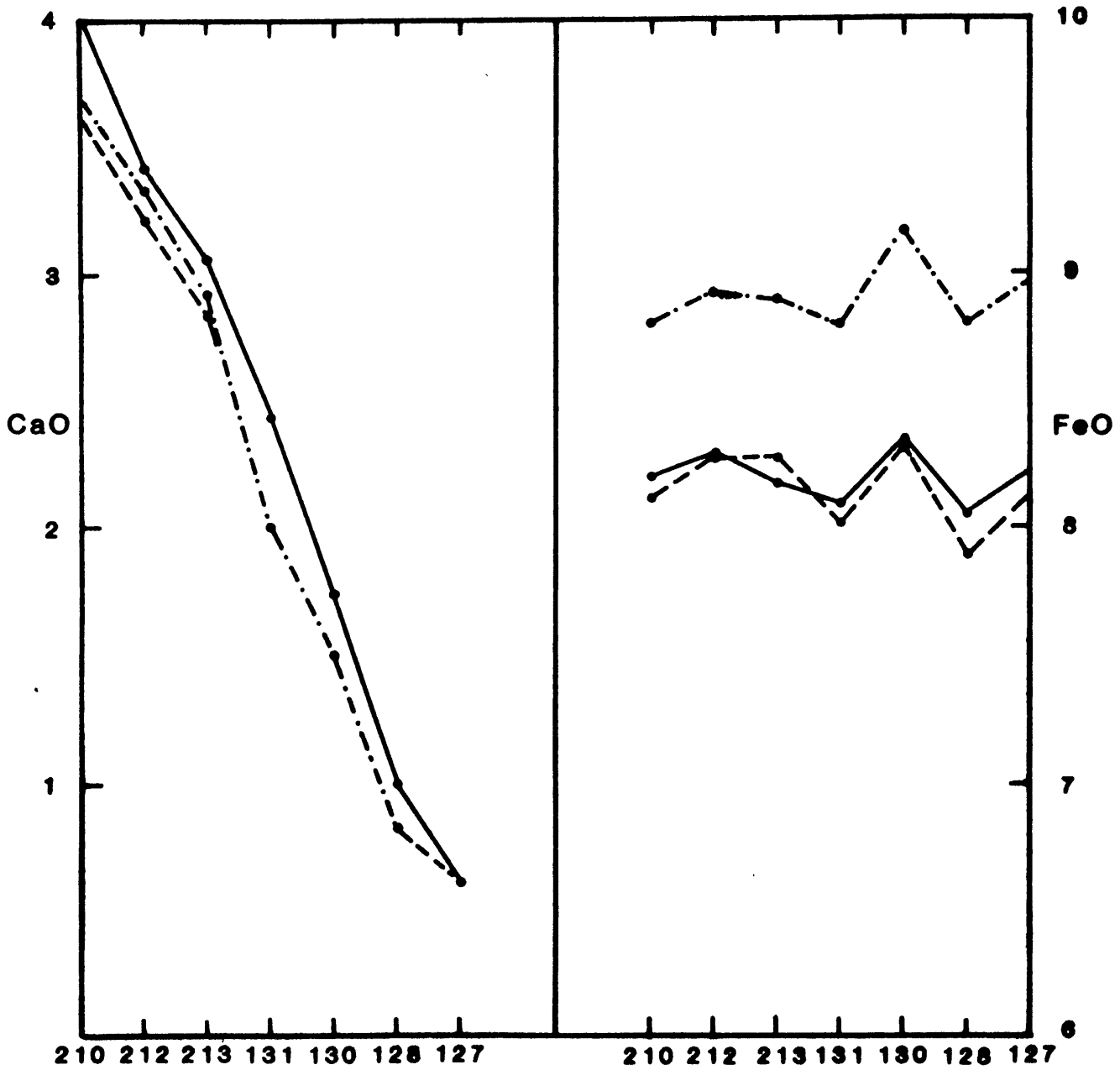

Figure AIII (cont.)

phases (depending upon the presence of plagioclase) were used in the least-squares linear analysis making the solution definitely over-determined.

The first prioity was to compare all this data with the use of the least-squares linear regression program. Using the program and the abundant data we could not only compare the data but use the differences to help improve our model modal estimates. Combinations of input data (unweighted, with weighting factor=1 for all components) were made so that the solutions could be compared on an equal basis. It was clear from the start that something was wrong with the XRF data from St. Mary's University. The residual sum of the squares and the sigma for fit were very large for all the samples for both sets of mineral data when using this bulk rock data. Fortunately, the smallest values for the residual sum of the squares and the sigma for fit were for the combination of MIT mineral data and UMASS XRF data. All this data was collected by myself and so I had all the raw data, plus estimates of error in the analyzes. Therefore, I could weight the bulk rock data and improve the quality of the mineral data by using different individual analyses to average together for the phase compilation that must be used in the regression. Averaging quality analyses together seemed a more valid approach to obtain a single composition for each phase in each sample than choosing a single representative analysis. The input for phase composition must be entered as a single composition, not as a range of

values for each measured component. But any particular composition chosen, (some average of many individual analyses) is only an approximation of the actual correct theoretical (and unknown) composition for that mineral. A variety of problems exist in determining a single mineral composition for each phase to represent a sample. Mineral zoning, exsolution, reequilibration (i.e. neoblasts versus porphyroclasts), variation within electron microprobe counting statistics, variation due to slightly different standardizations for separate probing sessions, and simple differences in quality of the analyses (monitored by oxide totals and mineral stoichiometry) are all problems producing variability between different mineral analyses. These problems were the greatest for the pyroxenes, while the olivine compositions were comparitively very homogeneous within a sample. The regression can be used to improve the composition chosen, by careful observation of the residuals for each component. This may sound like a somewhat arbitrary way to produce better model solutions at the expense of real petrologic information but, if care is taken, it is perfectly legitimate. I followed the rule of only changing mineral compositions based on the prior regression model result, if the change could be made to improve the chosen composition quality. That is, produce better oxide totals and/or better mineral stoichiometries by changing the number of individual analyses to average. Using this rule, the regression becomes only a guide to improving

mineral compositions used in future models, not a justification to make arbitrary changes in oxide components in order to reduce the residuals. These changes most often took the form of discarding poorer quality analyses from the averaged compilation. Not only could observation of the residuals be used to choose which minerals to change (e.g., if the largest residual was Ca, the problem was likely with cpx, not olivine) but also which direction the change should be made based on the sign of the residuals. Further information could be gained from least-squares linear regression models based on the Obata data set for bulk rock and mineral compositions, (with the exception of the bulk rock components NiO, Cr_2O_3 and Na_2O for which MIT/UMASS data was deemed better, olivine analyses, which we did not have from Obata, and a few other missing analyses for which we used MIT data) which generally gave near as good model fits as the unadjusted MIT/UMASS data for both unweighted and weighted results. The Obata data could not be adjusted as I did not possess the raw data making up the mineral compilations, but by carefully comparing the residuals from the Obata mineral data set with the MIT mineral data set (both with the UMASS bulk rock data), I could qualitatively determine how to adjust the MIT mineral compositions with respect to the Obata compositions (still within the rule I set for mineral composition adjustments). In this way I could iteratively improve the model solution using the sum

of the residuals squared and the sigma for fit value given by the computer program.

The adjustments in mineral compositions selected to be used in the model were not made until the original values were weighted. All subsequent models used the weighted solutions. Weighting was based on two sigma variation in 24 repeat analyses, from near the time that the samples were analyzed, of the BHVO-1 sample used as a standard at the UMASS XRF lab (compiled by Michael Baker). For the components Na_2O and Cr_2O_3, INAA statistics from F. Frey's MIT lab were used. The two sigma values were all normalized to the largest value (SiO_2) to provide the weighting factors. A somewhat arbitrary adjustment to the weighting factors was made, based on the fact that the bulk rock compositions are rather bimodal, with SiO_2, MgO, FeO, Al_2O_3 and CaO making up ~99% of the rock and TiO_2, Na_2O, MnO, Cr_2O_3 and NiO making up the remainder. The absolute error for the less abundant components are generally a good deal less, thus giving them very small weighting factors. These weighting factors were enlarged (thus reducing their importance to the model result) to avoid false confidence in this data but the weighting values were still kept considerably less than the more major elements. I think this adjustment is justified base on an argument of relative error as well as the fact that the more minor elements are very poorly known in the mineral data (which otherwise were not included in the weighting factor).

The weighted model solutions were improved for each sample by making the iterative adjustments to the mineral compositions, as described above. It is not certain exactly what statistical parameter, or what value of this parameter, is relavant to geological solutions such as this. The smaller the value of the "sigma for fit", the better the model solution but the unanswered question is how small is small enough? I was able to reduce this statistical parameter to less than 0.1 for all samples except for 62213 (~0.3 for unknown reasons). At these values the actual modal solutions changed very slightly when minor mineral modifications were made. The error values given in Table 1 give some idea of how statistically significant the solutions for each sample were. These errors are considerably smaller than modal statistics through point-counting would be. Table AII1 shows the calculated model modal results for the Obata data to compare with Table 1. The errors are larger reflecting the poorer fits, but generally the results are quite similar. Certainly no changes would be necessary in any interpretations of this work even if the modes expressed in Table 1 were in error to the degree shown by Table AII1. Both of these tables are given in volume percent, as modes should be expressed. The least-squares solution is actually in weight percent. A computer program written by Michael Baker called MINDEN was used to convert weight percent to volume percent utilizing known relations of the densities of end-member components of

Table AII1. Modes of Horoman Peridotites in Volume Percent, From Linear Regression of Major Elements (using Obata mineral analyses)

	Olivine	opx	cpx	spinel	plag
62210	58.3(0.6)	10.1(0.3)	21.1(0.8)	0.54(.06)	9.9(.3)
62212	59.0(0.8)	8.4(0.4)	21.5(1.0)	0.48(.08)	10.6(.4)
62213	62.5(2.1)	7.5(1.6)	20.5(3.1)	0.64(.21)	8.9(.4)
62131	69.9(1.3)	5.9(0.6)	20.2(1.7)	0.49(.11)	3.6(.6)
62130	70.6(0.9)	3.4(0.4)	21.1(1.2)	0.41(.09)	4.5(.4)
62128	72.9(0.6)	2.8(0.3)	23.3(0.8)	0.91(.06)	-
62127	77.7(0.5)	1.7(0.2)	19.9(0.6)	0.70(.04)	-

the minerals in the rocks. The density of the constituent minerals in these samples, with the exception of plagioclase and spinel, are very similar, so the difference between weight percent and volume percent is mainly reflected in these two minerals.